ISSN 0392-3029

LB-AB-13-049-EN-N

ESARDA

European Safeguards Research and Development Association

Bulletin

Nº 49

www.jrc.ec.europa.eu/esarda

June 2013

ISSN 1977-5296

Number 49
June 2013

Editor
Hamid Tagziria

European Commission, Joint Research Centre,
ITU - Nuclear Security Unit
T.P. 800, I-21027 Ispra (VA), Italy
Tel. +39 0332-786324
esarda-bulletin@jrc.ec.europa.eu

ESARDA is an association formed to advance and harmonize research and development for safeguards. The Parties to the association are:
Areva, France ; ATI, Austria; CEA, France;
CNCAN, Romania; EDF, France ; ENEA, Italy;
European Commission; FZJ, Germany;
HAEA, Hungary; IKI, Hungary; IRSN, France
MITyC, Spain; NNL, United Kingdom;
NRI, Czech Republic; NRPA, Norway;
SCK/CEN, Belgium; Sellafield Ltd, United Kingdom
SFOE, Switzerland; SSM, Sweden
Springfields Fuels Limited, United Kingdom
STUK, Finland; UBA, Germany
UKAEA, United Kingdom; URENCO, Germany
VATESI, Lithuania ; WKK, Germany, Oak Ridge National Laboratory (USA)

Editorial Committee
K. Axell (SSM, Sweden)
P. Peerani (EC, JRC, ITU, Italy)
E. Radde (ATI, Austria)
A. Rezniczek (Uba-GmbH, Germany)
B. Richter (FZJ, Germany)
P. Schwalbach (EC, DG ENER)
F. Sevini (EC, JRC, ITU, Italy)
H. Tagziria (EC, JRC, ITU, Italy) (Chairman & Editor)
J. Tushingham (NNL, United Kingdom)

Scientific and technical papers submitted for publication in the peer reviewed section are reviewed by independent authors including members of the Editorial Committee. The bulletin is currently submitted to Thomson-Reuters for evaluation in view of citation.

Manuscripts are to be sent to the Editor (esarda-bulletin@jrc.ec.europa.eu) following the 'instructions for authors' available on http://esarda2.jrc.it/bulletin where the bulletins can also be viewed and downloaded.

Photos or diagrams should be of high quality.

Accepted manuscripts are published free of charge.

N.B. Articles and other material in the ESARDA Bulletin do not necessarily present the views or policies of neither ESARDA nor the European Commission.

ESARDA Bulletin is published jointly by ESARDA and the Joint Research Centre of the European Commission and distributed free of charge to over 1000 registered members, libraries and institutions Worldwide.

The publication is authorized by ESARDA.

© Copyright is reserved, but part of this publication may be reproduced, stored in a retrieval system, or transmitted in any form or by any means, mechanical, photocopy, recording, or otherwise, provided that the source is properly acknowledged.

Cover designed by Jose-Joaquim Blasco (JRC Ispra in Italy),

Printed in Italy

ESARDA
European Safeguards Research and Development Association

Bulletin

Table of Content issue n° 49

Editorial

Dear colleagues,

The ESARDA journal continues its strides to improve its quality and value to its readership and members by consolidating its peer review section while still reflecting an even wider and richer area of activities which are of interest to our communities. I am pleased to present you with Issue 49 which immediately follows a successful 35th ESARDA symposium held in Bruges (Belgium) from 27th to 30 May 2013 which had more than 20 sessions as diverse as (in alphabetical order):

- Arms Control, Non-proliferation and Export Control,
- Containment and Surveillance,
- Implementation of safeguards
- Information Management,
- Neutron Detection,
- Non-Destructive and Destructive Analysis ,
- Novel technologies,
- Nuclear Forensics,
- Post Fukushima NDA techniques for melted fuel debris,
- Safeguards by Design,
- Spent Fuel Verification etc.

The 35th Esarda symposium was marked by a lively panel discussion dedicated to Arms Control and Disarmament Verification (A dialogue on Technical and Transparency Issues) in addition to a sub-working group meeting to discuss technologies (including NDA and novel) and related issues in that thematic area. A special issue of the bulletin dedicated to that thematic area is being considered for 2014. This follows the INMM-Esarda workshop in 2011 on the subjects.

As in previous issues of the journal, the papers of issue 49 resulted from those judged best in each session during Esarda symposium in addition to those independently submitted by their authors who judge their contributions worthy of peer reviewing quality. Every chairman/woman had access to the papers at least two weeks prior to the symposium and was asked to select up to two best papers from his/her session immediately after the work was presented.

Peer reviewing was carried out by independent experts in the field including members of the editorial committee where appropriate. At least two reviewers were used wherever possible. I am grateful to the authors for their contributions and to the reviewers for their great efforts in improving the quality of each paper published. This process for issue 49 has been particularly challenging in view of the large number of papers to review, the tight time schedule to which authors and reviewers alike were subjected to and still responded so well despite their commitments elsewhere. The papers will be published in issue 49 (summer 2013) and issue 50 (autumn 2013) depending on their progress with the review process.

The bulletins can be downloaded from our newly redesigned web site and hard copies are posted to more than 1100 institutions, universities, libraries and individuals, free of charge.

Authors and experts are very much encouraged to:

1. Submit their work anytime during the year to esarda-bulletin@jrc.ec.europa.eu using the ESARDA template (see https://esarda.jrc.ec.europa.eu) and giving the names and e-mail addresses of two potential independent reviewers
2. Cite the work published in the journal in order to increase the visibility, the citation and impact indexes of the journal which is most important to any evaluation process we may undertake.
3. Volunteer as potential reviewers by sending me an e-mail to that effect specifying one's area of expertise.

We would be grateful.

As chairman of the editorial committee and editor of the Esarda bulletin and on behalf of the editorial committee I would like to thank all authors and reviewers who have allowed the new developments and improvements to continue.

Wish you all a very good and well deserved summer break.

Hamid Tagziria,
Editor and Editorial Committee Chairman

https://esarda.jrc.ec.europa.eu
esarda-bulletin@jrc.ec.europa.eu
hamid.tagziria@jrc.ec.europa.eu

Good morning Ladies and Gentlemen, Dear ESARDA friends,

For those who do not know me: my name is Klaas van der Meer and as the President of ESARDA it is a real pleasure for me to welcome you at the 35th ESARDA Symposium here in Bruges.

The sign that is shown here behind me may not be used very often during ESARDA symposia. Nevertheless it symbolises the core business of ESARDA and that is peace.

Where lies the real basis of ESARDA? We can consider ESARDA as part of the process to create the European Union, although it has been established later than the fundament of the EU (1969 versus 1957). The early members of ESARDA originated also mainly, but not exclusively, from the 6 founding members of the EU.

Unlike what many believe nowadays, the EU has not been founded for the sake of creating an single economic space to increase the prosperity for the European citizens. The basic idea for the foundation of the EU/EC, as pointed out eloquently by Jan Techau, director of Carnegie Europe, during the 11 November speech last year for the Flemish Peace Institute, was to establish a peace process in Europe in order to erase the root causes for a future war in Europe after the devastating results of the first and second World War. So the EU is not just about a single market, about getting our money back, about the form and size of imported bananas, it is basically about PEACE and establishing a peace process in Europe in order to prevent another war with maybe even more severe consequences than the previous ones. The single market and everything connected to it are just means to obtain that higher goal of peace.

Jan Techau explained during his 11 November speech last year that this peace process is not a given thing. It has been established but it has to be fed, to be nourished in order to maintain it, keep it going and enhance peace in our and other regions.

This peace process has indeed been very successful. It has been so successful that in Europe we consider peace as a given thing, so obvious that it is not worth worrying about. Many think that what happened for instance in ex-Yugoslavia was an incident, nothing more. When I was flying back to Brussels from Vienna a few months ago I was sitting next to a deputy minister of Montenegro on her way to Brussels for the accession negotiations for the EU. She was an economist, but also her main incentive to become member of the EU was to be part of that bigger peace process in order not to have war in her country, rather than wanting money from participating in the EU.

So the European project is basically a peace process. And here ESARDA comes in smoothly, as part of that bigger European peace process.

Talking about peace is nice but I know I have also quite a few engineers in my audience so they are probably wondering when will I get really to the point: what are we going to do in order to support that peace process? So far no real commitments were discussed. So the question is: what is ESARDA doing to contribute in a practical way to this peace process? Well, in our Terms of Reference we state that the scope of ESARDA is to advance and harmonise (=coordinate) safeguards R&D performed by its members.

To do this we have defined 6 purposes for ESARDA, and I simplified them a little for easier understanding:

1. Improve safeguards
2. Consult all stakeholders in order to be proactive
3. Facilitate collaboration
4. Propose new R&D programmes where necessary
5. Find synergies with other verification regimes and technologies
6. Improve communication with public and other experts

In order to achieve these purposes, ESARDA has several activities that can be divided in internal activities (for members only) and external activities, in which other members of the public can participate.

The internal activities, which are not open to the general public, essentially include:

- activities of the permanent technical and scientific Working Groups, our famous ESARDA Working Groups;
- activities of the “ad-hoc” or temporary Working Groups and Committees;
- activities of the management bodies, the maybe less famous Steering and Executive Committee;
- Internal Meetings of the Association, namely the biannual internal meeting/symposium of the ESARDA members in Luxembourg
- activities in bilateral collaboration with other Organisations.

The external activities are open to the general public. They include:

- organisation of Symposia, more particular the biannual open ESARDA symposium;

- organisation of specialised meetings (Seminars, Workshops etc.), like the joint INMM-ESARDA meetings that take place every three years;
- publication of the ESARDA Bulletin;
- web site at the Joint Research Centre.

So the fact that you are sitting here today, participate in this symposium and listen to the various contributions, means that you participate in one of the in fact main activities of ESARDA that have as ultimate purpose the promotion of peace.

What are the current threats and opportunities for this peace process that relate to ESARDA in the sense: where should we as an organisation put our focus on?

Let's start with the bright side of life: what are the opportunities for peace?

First there is the process of nuclear arms reduction and dismantlement. During this symposium various presentations will be given around that theme, both focussed on the more political aspects and on the technical aspects of verification. The safeguards R&D community can contribute with its technical know-how, but will also have to learn to apply verification methods in an environment different from the usual safeguards environment, both in a political sense and a technical sense.

On the global political agenda there is an increased interest observable for non-proliferation in a broader sense, like for instance the Comprehensive Test Ban and the Fissile Material Cut-off. The advantage of these treaties is that the threshold for accession is lower than for a complete nuclear disarmament but that they provide still a strong political signal. The present superpowers have realised or will realise that the presence of a nuclear arms arsenal will in the long term cause more harm in the sense of more horizontal proliferation than it will do good in the sense of providing security to their territory.

On the European level more attention and more financial means are released for non-proliferation in a narrow and broader sense. The development of European instruments for foreign policy, like Instrument for Stability and CBRN Action Plan provide also extra means for our R&D, as will be pointed out for instance by Saïd Abousahl during his speech on Thursday.

Of course these means are not released without the presence of a need to do this. This brings us to the darker side: the threats for non-proliferation!

There is a perceived or real threat with respect to the use of nuclear material by sub-national groups. Nuclear security (often considered together with CBR security) requires partly know-how that is present in the safeguards community and we should be willing to provide this know-how. ESARDA is a good forum to meet partners with expertise in detection methods of nuclear materials, for instance.

Challenges that remain for the more traditional safeguards are the proliferation issues with the DPRK and Iran. While for the DPRK the safeguards world, in particular the IAEA, can only prepare itself for future verification activities when they become possible, Iran is under IAEA safeguards and the situation is reasonably well-known, except the so-called outstanding issues.

Strongly related to these issues is the increased focus on export control in order to prevent sensitive technology to come in the hands of proliferators. ESARDA has an extensive effort in this with the WG on export control, led by our distinguished ESARDA Secretary Filippo Sevini.

Then there remain some challenges that I would characterise as neither bright nor dark.

The implementation of the AP is progressing and has reached a certain maturity in the EU. ESARDA has provided a strong support to the AP implementation via the IS Working Group. Harmonisation of AP implementation throughout the whole EU and in this way an increased efficiency and effectiveness have resulted to the benefit of both the inspectorates and the operators.

The development of new facilities at the back-end of the fuel cycle and in the future GEN IV reactors with possibly new reprocessing techniques asks for new safeguards approaches. The safeguards world should work proactively and maybe a little faster than we did in case of final repositories, where we discussed about safeguards approaches in working groups for more than 15 years and then realised that a repository was already being built without having decided on the approach.

In a similar framework we should also mention the activities of the IAEA with respect to Safeguards-by-Design and support these. Same thing for the State Level Approach and no doubt that Mr. Whiting of the IAEA will say a few words about it.

I personally advocate the importance of having also an eye on the political part of the proliferation equation, since it is the most important one. At the end a decision to develop nuclear weapons or to refrain from them will be a political decision and the technological aspects will only be in the boundary conditions. I am therefore happy to observe contributions from this area and hope for instance that those who will attend the special panel discussion, an initiative by the VTM Working Group under the aeges of Irmgard Niemeyer, will enjoy participating. A cross-fertilisation between the technical and political scientists is necessary for an effective and efficient verification system.

Ladies and Gentlemen, I have almost reached the end of my text here in front of me. I hope that from this speech, you will remember that peace is the core business of ESARDA and I want to ask you that during your stay here in Bruges, at an evening you have dinner or drink one of the fantastic beers, to think about this and make a toast to "world peace".

With this I would like to open the 35th ESARDA Symposium. I hope you will have a fruitful symposium and I would like to thank you very much for your attention!

Design of a liquid scintillator-based prototype neutron coincidence counter for Nuclear Safeguards

Alice Tomanin[1,2], Paolo Peerani[1], Hamid Tagziria[1], Greet Janssens-Maenhout[2], Peter Schillebeeckx[3], Jan Paepen[3], Anthony Lavietes[4], Romano Plenteda[4], Nicholas Mascarenhas[4], L. Marie Cronholm[4]

1. European Commission - Joint Research Centre - Institute for Transuranium Elements - Nuclear Security Unit, Ispra, Italy
2. University of Ghent, Ghent, Belgium
3. European Commission - Joint Research Centre - Institute for Reference Materials and Measurements - Standards for Nuclear Safety, Security and Safeguards Unit, Geel, Belgium.
4. International Atomic Energy Agency, Vienna, Austria

E-mail: alice.tomanin@jrc.ec.europa.eu

Abstract:

A liquid scintillator-based neutron coincidence counting system designed to address a number of safeguards applications is under development by the IAEA in collaboration with the Joint Research Centre-ITU and Hybrid Instruments LTD.

Liquid scintillators are a promising technology due to their good fast-neutron detection capabilities. The characteristic fast response of scintillators is particularly beneficial for coincidence counting applications, for which a performance level higher than that associated with moderated thermal detectors might be expected. Fast neutron detection requires no thermalization process and therefore, does not incur the resulting neutron detection delays. These features reduce the length of the coincidence gate by three orders of magnitude, reducing practically to negligible values the accidental coincidence rate which dominates the uncertainty in thermal neutron detectors. Recent progress in fast electronic digitizers offers the possibility to perform on-line, real-time pulse shape discrimination (PSD) between gamma and neutron radiation detection, making this technology suitable for nuclear safeguards and security applications.

This paper will describe the experiments and Monte Carlo modelling activities engaged to design a prototype liquid scintillator-based neutron coincidence collar for fresh fuel assembly verification.

The characterization of the system response required accurate calibration measurements in order to determine the operational parameters of the liquid scintillator cell, including gain, pulse shape discrimination and energy thresholds.

Extensive Monte Carlo simulations which are essential for the understanding and characterization of the system's response were also carried out using the MCNPX-PoliMi Monte Carlo code to simulate the radiation transport within the system and to optimize the detector design. The evolution from the different detector configurations we investigated to the characteristic features of the final design will be described.

Keywords: non-destructive assay; neutron detection; coincidence counting; liquid scintillators; Monte Carlo modelling.

1. Introduction

Neutron coincidence counting is a well-known measurement technique commonly used in nuclear safeguards for the verification of the declared quantity of special nuclear material.

The technique relies on the detection of time-correlated neutrons from either spontaneous or neutron induced fissions occurring in a nuclear material containing fissile or fissionable material such as uranium and plutonium. In the presence of a well-known calibration curve, the rate of coincident neutron detection events can be directly related to the mass of such isotopes in the investigated material.

In order to detect neutrons, currently deployed coincidence counters rely on the use of ^{3}He gas, due to its high cross section for thermal neutron captures and low sensitivity for gamma-rays. The recently increased demand for ^{3}He-based neutron detectors, in particular for nuclear security applications, coupled with the limited production of ^{3}He, has made this gas practically unavailable, creating the need to search for alternative neutron detection solutions.

The International Atomic Energy Agency, in collaboration with the Joint Research Centre - Institute for Transuranium Elements and Hybrid Instruments LTD is developing a liquid scintillator-based neutron coincidence counter to replace the current deployed systems for safeguards applications.

The choice of liquid scintillators as a suitable ^{3}He alternative for this particular application was motivated by the very fast response of this detection medium. In addition, improved performance as compared to classical ^{3}He counters is expected with regard to measurement time and related statistics. Fast neutron detection requires no thermalization process and therefore, does not incur the resulting neutron detection delays (i.e., die-away time). These features reduce the length of the coincidence gate by three orders of magnitude, reducing practically to negligible values the accidental coincidence rate which dominates the uncertainty in thermal neutron detectors. Recent

progress in fast electronic digitizers offers the possibility to perform on-line, real-time pulse shape discrimination (PSD) between gamma and neutron radiation detection events, making this technology suitable for nuclear safeguards and security applications.

The characterization of the performance of the system and its design optimization were performed by means of Monte Carlo simulations. Simulations were performed with the MCNPX-PoliMi code [1], a Monte Carlo modelling tool developed to simulate detectors response, combined with a post-processing code developed at the JRC-ITU Ispra. Prior work in post processing for liquid scintillator was taken as reference in the development of the JRC code [2]. Due to the expected non-linearity of the light output function (LOF) of a scintillator, i.e. non-linear transfer of the deposited energy to the light output, each single collision occurring within the effective detection volume has to be evaluated separately. Depending on the incident particle type and the target atom, the energy deposited is converted into scintillation light with the detector-specific light conversion formula. The amount of light produced by subsequent collisions occurring within a specific pulse-rise time are summed to generate pulses which are then processed by the PSD electronics. The post-processor code includes modules to apply the conversion from deposited energy to light and to identify coincident events within multiple detector cells. A validation of the simulations was performed on a small scale coincidence system (composed of two liquid scintillator cells) proving that the modelling reproduces the expected detector response.

2. Liquid scintillator cell characterization

2.1 Measurements set-up

The prototype system is composed of an array of EJ-309 liquid scintillator cells, with cubic geometry of 10 cm width, a multichannel real-time pulse shape discrimination (PSD) system, and a high-speed data acquisition and signal processing system to compute coincidences. The detailed design and electronics setup is discussed by Lavietes et al. [3].

A prototype liquid scintillator cell which has the same geometry and size as the one we foresee to use for the full-scale system was characterized at the JRC-ITU laboratories in Ispra, at the JRC-IRMM in Geel as well as at the PTB facilities in Braunschweig, Germany. Radionuclide gamma sources and monoenergetic neutron beams were used in order to determine the response of the detector to different radiation types and energies. In the following section only the results obtained at JRC-ITU are discussed.

For the coincidence validation measurements, a second EJ-309 liquid scintillator of cylindrical geometry (5 inches diameter and 3 inches length) was used.

2.2 Operating Voltage

The selection of the optimal operating voltage for the detector was primarily based on a study of the detector resolution and linearity of the response to gamma rays. Measurements were performed with a ^{137}Cs, ^{22}Na and ^{232}U source. Figure 2 shows the measured relative FWHM at the Compton edge with respect to the applied voltage for three gamma energies. In addition, an AmBe (α,n) source was used to determine the response for higher energy gamma rays (Compton edge energy 4201 KeV) and to verify the performance of the detector with respect to pulse shape discrimination. As expected, the resolution improves by increasing the high voltage. The best resolution and linearity of the detector response was observed at -1250 V. Measurements with the AmBe neutron source confirmed that this voltage also results in an optimal performance with respect to pulse shape discrimination.

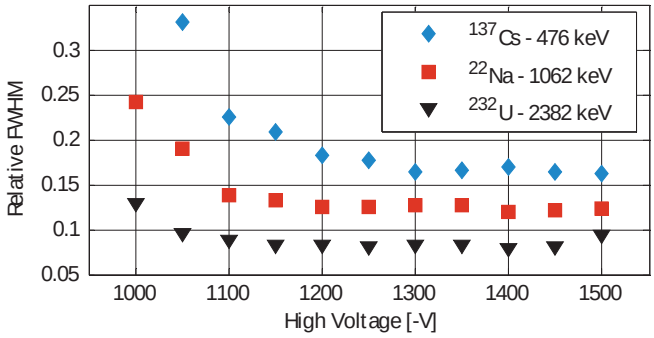

Figure 1. Relative FWHM with respect to applied High Voltage for three different Compton edge energies.

2.3 Pulse Shape Discrimination

The pulse shape discrimination (PSD) electronics implemented in the system is based on a comparison of the peak amplitude to the amplitude in the decay face of the pulse, i.e. the amplitude at 16 ns after the peak. The latter is referred to as discrimination amplitude. This approach allows for real-time discrimination between gamma and neutron detection events.

The performance of the PSD technique for measurements with a ^{252}Cf source is illustrated in Fig. 2. For each detected event the peak amplitude is plotted as a function of the discrimination amplitude. In this plot two clouds of events can be observed. The discrimination between the two clouds is given by a line with two segments, defined by the points A, B and C. Based on this discrimination criterion events due to the detection of a neutron (blue points) can be separated from those resulting from the detection of a gamma ray (red points).

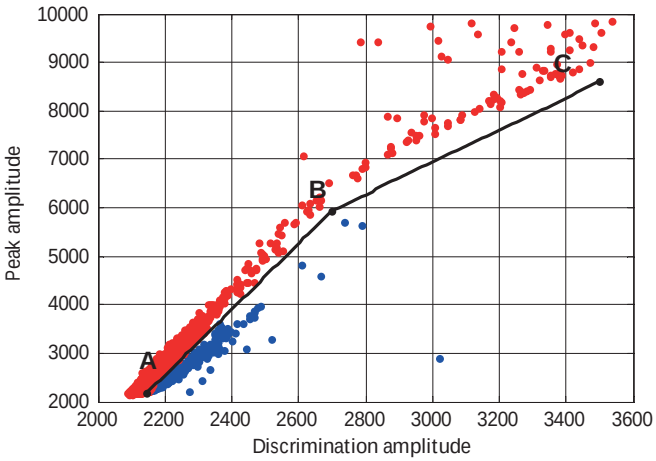

Figure 2. Typical PSD graph for a ^{252}Cf measurements. Gamma pulses are shown in red, neutron pulses in blue. Amplitudes as measured in digitizer units.

Optimization of the PSD was obtained by varying the slope of the A-B discrimination line (i.e. by variation of the x-coordinate of the A point), and analyzing the PSD response of the system in terms of neutron intrinsic efficiency and gamma rejection rate. The gamma rejection rate (GARR), defined as the ratio of misclassified neutrons in the presence of a pure gamma source to the totals detected pulses, can be written as:

$$GARR = \frac{Neutrons}{Neutrons + Gammas}$$

It is well known that the most probable misclassification of neutron and gamma events occurs in the low energy region, therefore the GARR was computed for a measurement with an ^{241}Am source. Background neutrons are included in the total neutron counts for the calculation of the GARR. However, in the low energy region, their contribution is negligible since the most neutron counts are given by misclassified gammas. The intrinsic efficiency values are derived by a measurement with a ^{252}Cf source. For these measurements, the light energy threshold, which will be described in more detail in a following section, was set to 385 electron equivalent keV (keVee, i.e. light generated by an electron depositing 1 keV of energy in the scintillator). Figure 3 represents the resulting Figure of Merit of this analysis. The resulting PSD settings were determined by an optimization of neutron detection efficiency and gamma rejection. For the selected setting, the neutron intrinsic efficiency is 14% and the GARR is 0.05%.

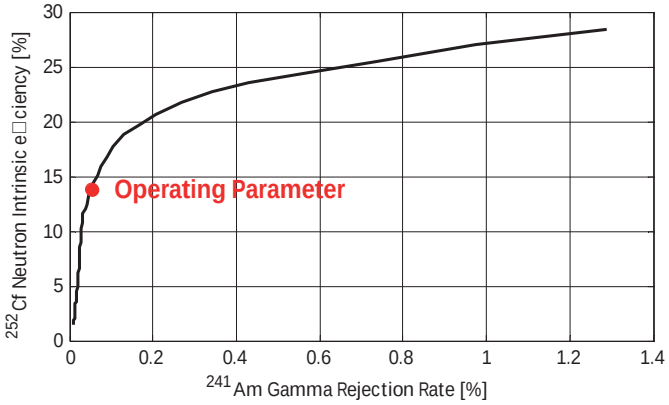

Figure 3. PSD Figure of Merit showing the GARR and the neutron intrinsic efficiency response at the variation of the Ax discrimination parameter. The red circle represents the operating parameter.

2.4 Validation of simulated detector response

The scintillation response of the detector, in terms of light production per incident particle and energy, is required for reliable simulation of the detector's response. Liquid scintillators typically present a linear response for gammas, whereas the light produced by protons and heavier particles varies non-linearly with the energy deposited [4]. The light output function (LOF) for recoil protons (the detection mechanism for neutrons) depends on the liquid type, the cell geometry and the cell–photomultiplier coupling. The LOF for cylindrical EJ-309 liquid scintillator of different diameters has been already reported by Pozzi et al. [5, 6], but the particular geometry of our detector requires a specific derivation of its light response.

The calibration measurements were performed at the PTB laboratories in Braunschweig, Germany, and consisted in time-of-flight measurements using the PTB cyclotron and measurements with quasi-monoenergetic neutron beams

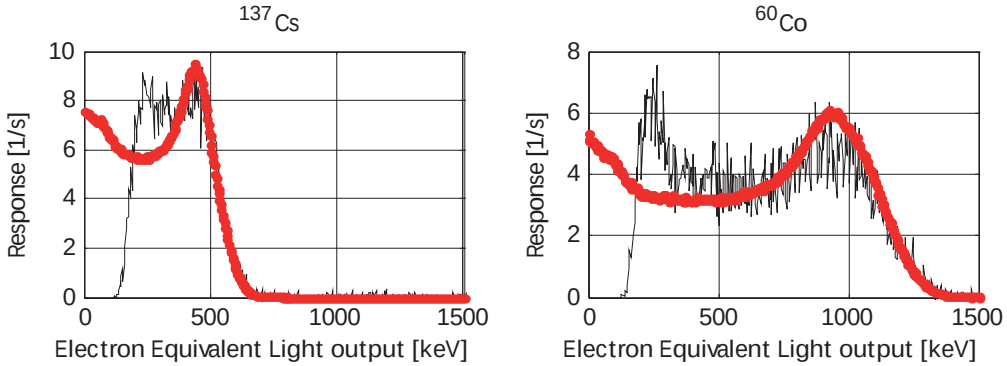

Figure 4. Measured (black line) and simulated (red dots) pulse height spectra for a ^{137}Cs source (left) and a 60Co source (right).

at the PTB Van Der Graaff accelerator. Further measurements were performed at the JRC-IRMM in Geel and at the JRC-ITU in Ispra to verify the experimental LOF against full neutron spectra from AmBe and AmLi sources. The analysis of the data is still in progress. We report here on results obtained with a LOF obtained following a preliminary analysis of the data. A detailed discussion on the results of these experiments together with the experimental response matrix and resulting LOF for electrons and protons will be subject of a separate publication.

The results of the Monte Carlo simulations have been validated by comparing the simulated and experimental response for gamma rays from a ^{137}Cs and ^{60}Co source and for neutrons from a ^{252}Cf spontaneous fission source. The results of the gamma ray measurements were used to determine the conversion factor that relates the observed amplitude to an electron equivalent light output for the data acquisition system.

Figure 4 compares the measured and simulated pulse height spectra for ^{137}Cs and ^{60}Co sources. The positions of the Compton edges observable in the graphs are shifted with respect to the true Compton edges values by the detector resolution. Above a light output of approximately 380 electron equivalent keV there is a good agreement between the shape of the simulated and experimental response. The simulated response, however, is overestimated by at least 15%. This bias is much larger than the uncertainty due to the counting statistics on the detection efficiency, which is about 2%. This bias is probably due to an overestimation of the effective detection volume, i.e. the effective volume of the scintillation liquid. Below a light output of about 380 keV the simulated response is lower compared to the experimental one. This might be due to a background component that is not properly accounted for or due to noise on the detector signal introduced by the electronics.

Fig.5 compares the simulated and experimental response for the detection of neutrons emitted by a ^{252}Cf source as a function of the light output. The figure indicates a good agreement in shape above 600 keV electron equivalent light output.

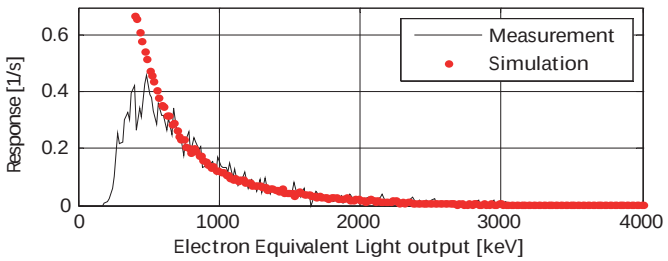

Figure 5. Measured (black line) and simulated (red dots) neutrons pulse height spectra for a Cf_{252} source.

2.5 Energy threshold

A fundamental parameter to use the scintillation detector as part of a counting system for the control of nuclear material is the energy threshold or discrimination level on the light output. This level, which reflects the minimum detectable light output, is an adjustable parameter of the electronic settings.

The pulse height spectrum shown in figures 4 and 5 were taken with the minimum electronic threshold setting. This level was choosen to reduce the noise to an acceptable level compared to the measured signal. The threshold used in the counting experiments corresponds to the minimum light output where the calculated spectrum still agrees with the experimental values.

As can be noted in Figures 4 and 5, the threshold of the electronics used does not result in a sharp edge on the left side of the pulse height spectrum, but it rather presents some broadening effect. This effect is due to a systematic behavior of the acquisition electronics, which introduces a bias in the threshold determination. Further developments in the acquisition electronics are planned in order to address this issue.

In this work, we derived the energy threshold value with a different approach, that is by matching the integral of the simulated response evaluated at different low energy thresholds with the total measured counts. Considering the pulse height spectra for ^{252}Cf reported in figure 5, the value that matches the counts, and thus validates the simulations for the neutron intrinsic efficiency of the detector, was found to be 385 electron equivalent keV, corresponding to a neutron energy of approximately 1.6 MeV. For the investigated detector and for the described setup we observed quite poor performance with respect to neutron detection efficiency at low energies, meaning that the minimum detectable energy is, by default, very high. Further adjustments in the electronic settings can only be applied to increase this threshold. However, this limit is strongly related to the electronics that is used and does not correspond to the lower limit due to the intrinsic detector characteristics. A possible solution to decrease the lower limit is to either use electronics with different dynamic ranges or increase the high voltage and use multiple outputs at different stages of the photo-multiplier tube.

2.6 Validation of coincidence on a two-cell detection system

In order to validate the procedure to simulate coincident events, measurements were carried out with two liquid scintillator cells, a ^{252}Cf source placed at 10 cm from each cell, and increasing thicknesses of lead shielding to study the effect of gamma pile-up. The second cell used for these measurement was a cylindrical 5'' x 3'' EJ-309 scintillator. For the simulation of the cylindrical detector response, the light output function was taken from literature data [5] whereas its energy threshold was set to 155 electron equivalent keV. Fig. 6 shows a part of the experimental set-up.

Results of the validation measurements and simulations are shown in figure 7. While the total count rate is overestimated by about 5-10% in the results (and is explained by the effective scintillator volume overestimation discussed in par. 2.4), the real count rates are underestimated by a factor of about 20%. This inconsistency in system response will be further analyzed in a wider range of neutron energies with coincidence validation experiments using plutonium oxides and AmLi sources to evaluate cross-talk effects.

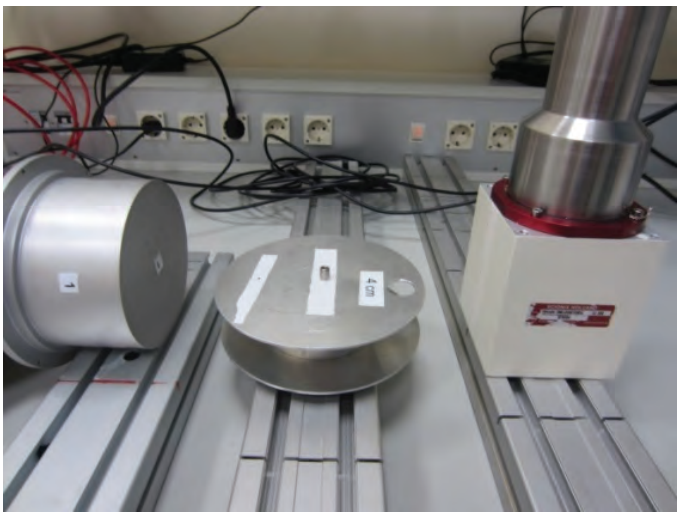

Figure 6. Experimental configuration for the coincidence validation measurements with Cf_{252}. The source to detector distance is 10 cm.

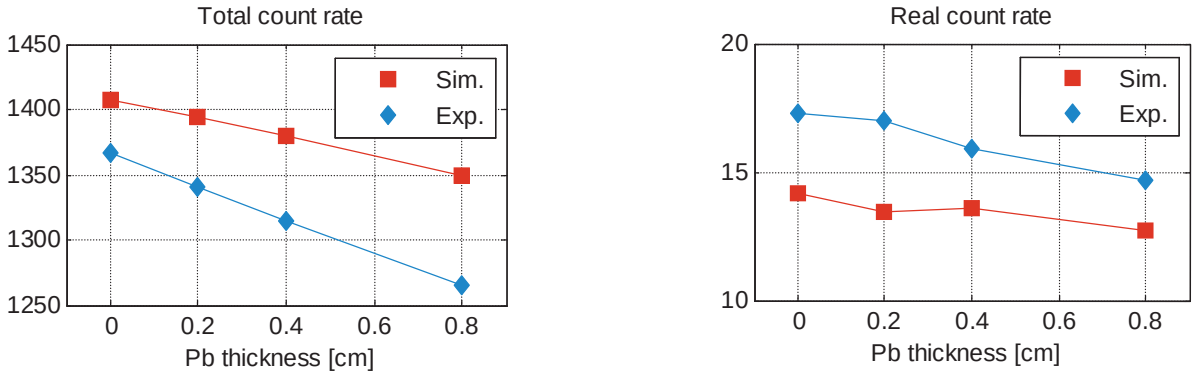

Figure 7. Measured and simulated totals (left) and reals (right) counts rates for the coincidences validation measurements with 252Cf and different lead shielding of different thicknesses. Real count rates are corrected for Accidentals coincidences.

3. Response of the full-system prototype

Figure 8 (left) shows the proposed design of the prototype liquid scintillator based coincidence collar.

It comprises 12 liquid scintillator cells of approximately 1 liter volume each, arranged on three sides of the collar. The fourth side is designed to accommodate an AmLi interrogation source. The cells and source are embedded in a 10 cm thick high density polyethylene (HDPE) wall to moderate the neutrons from the AmLi source. Moderation of the interrogating neutrons will result in decrease of the average energy and consequently in a substantial increase of the average cross section for neutron induced fission in the fuel assembly. A 1 cm HDPE interspace between neighboring cells is foreseen to reduce cross-talk events. The internal cavity accommodating the fuel element is surrounded by a 4 mm layer of lead to reduce the gamma rate at the detectors and by a removable 1 mm thick layer of cadmium used to switch the system to a "fast" configuration when measuring fuel assemblies with neutron poison. The fast configuration significantly reduces the neutron poison effects by absorbing interrogation neutrons below the cadmium cut-off energy of about 0.55 eV.

Extensive MCNPX-PoliMi simulations were performed to characterize the system response and optimize the design. For this study, a typical PWR fuel element has been modeled. The data of the modeled fuel as well as the intensity of the interrogation source were taken from [7]. Figure 8 (right) shows a section of the simulated geometry perpendicular to the fuel element length.

In the next sections the total count rate is denoted by T, the net coincident count rate by R and the count rate due to accidental coincident events by A.

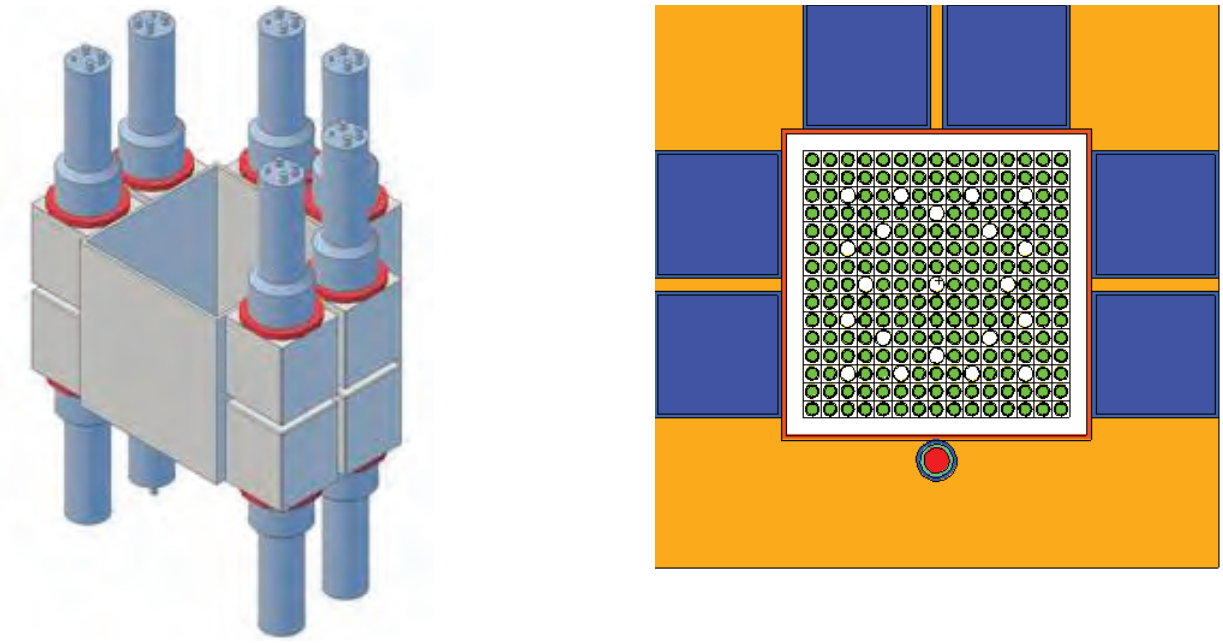

Figure 8. Prototype design of the liquid scintillator based coincidence collar (left, bare configuration without surrounding HDPE) and simulated geometry with MCNPX-PoliMi (right, thermal configuration with surrounding HDPE), containing reference fuel element and AmLi interrogation source.

In thermal neutron coincidence counters, for a given measurement time t, the uncertainty due to counting statistics on the Reals count is dominated by the Accidental count which is, in its turn, driven by the interrogation source:

$$\frac{\sigma}{R} = \frac{\sqrt{2A + R}}{R \cdot \sqrt{t}}$$

This effect leads to poor statistics and thus long measurement times which are necessary in order to achieve the 1% uncertainty due to counting statistics. One intrinsic advantage of liquid scintillators is that the exceptionally short coincidence window given by the detection of fast neutrons leads to smaller accidental rates. To give an example, the coincidence time gates in liquid scintillator is of the order of tens of nanoseconds, whereas tens of microseconds are needed in ^{3}He systems as to account for the neutron thermalization process.

3.1 Background from interrogating neutron source

A first analysis was performed to determine the interrogation source background (no fuel element in the detector) for three different configurations: a bare configuration (no surrounding HDPE); a thermal configuration (10 cm thick HDPE walls on each side of the collar); and a fast configuration (1 mm internal layer of cadmium to prevent interrogation with neutrons with an energy below 0.55 eV). The analyses were performed at different energy thresholds to define the optimal operating condition of the collar. Figure 9 shows the results of the simulation.

The contribution from the AmLi neutron source to coincident count rate results mainly from neutrons which are scattered from one detector to another. In such cases one neutron produces a signal in different detectors. This is also referred to as cross-talk between detectors.

The bare configuration presents steadily higher influences of the interrogation neutrons on the Real count rates. This is given by the absence of HDPE-filled interspace between neighboring detectors, which act both as a support material for the cells, and as a moderator for the neutrons which do not come directly from the fuel element cavity, reducing their probability of being detected by the scintillators.

As a result of this analysis, the bare configuration has been discarded, and two possible operating settings were identified for the following analysis on the thermal and fast configuration:

- 0.5 MeV neutron energy threshold: this operational setting reduces to negligible values the cross-talk effect of the interrogating source neutrons on the count rate of the Reals. This would allow the detector to be calibrated against the count rate of the Reals, as in current 3He system, minimizing the AmLi source driven Accidentals.
- 1 MeV to 1.5 MeV neutron energy threshold: this operational setting reduces to negligible values the influence of the interrogating source neutrons on the count rate of the Totals. We intend to investigate the possibility of calibrating the detector against the count rate of the Totals, which are no longer driven by the AmLi interrogation source, in order to achieve better statistics in shorter measurement time. When using the Totals data, the count rate of the Reals would be used as a control information to confirm the uranium enrichment of the fuel element and verify the absence of any nearby uncorrelated neutron source intended to bias the measurements results in an unattended operational mode.

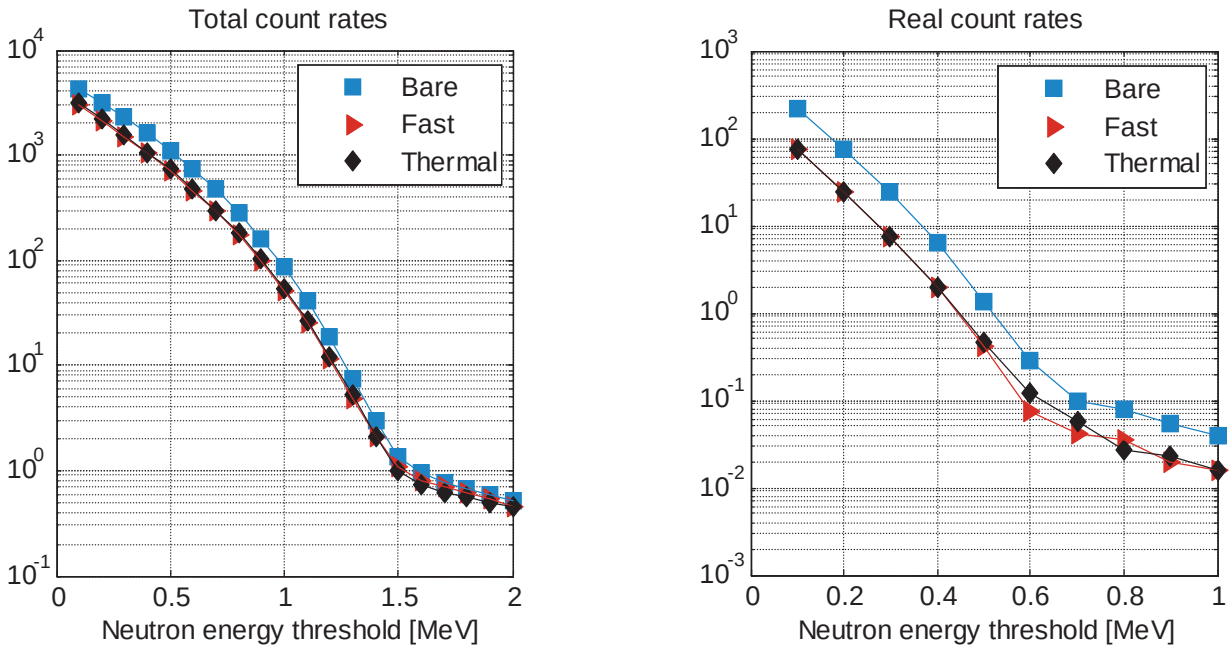

Figure 9. Simulated totals (left) and reals (right) counts rates for the liquid scintillator-based collar in three different configurations: bare, thermal, and fast. The counts are given only by the AmLi interrogation source – no fuel assembly is present. Thresholds are expressed in neutron energy for simplification.

3.2 Prototype response for the verification of a PWR fuel assembly

Table 1 shows results of the simulation performed on the neutron coincidence collar for the fuel assembly interrogation, and for two defined configurations and at three different threshold settings. The enrichment of the fuel is 3.19 wt%. The uncertainties resulting from only counting statistics of all the presented data are below 1%.

Concerning the reals count rates, we observed for both configurations that a neutron energy threshold of 0.5 MeV is sufficient to reduce the influence of AmLi neutrons cross-talk to about 1%.

The resulting count rates are then directly related to the induced fissions in the fuel assembly, and a counting statistics uncertainty of 1% can be achieved in a few minutes.

In absolute values, the AmLi source neutrons detected by the scintillators in both configurations are the same, as it results from figure 9. In the fast configuration, however, the cadmium layer within the cavity reduces the probability of AmLi neutrons to induce fissions in the fuel assembly, and thus the neutron count rates related to induced fissions in the fuel. Consequently, the relative influence of the interrogation source neutrons is higher in the fast configuration, requiring a higher energy threshold of up to 1.5 MeV (neutron energy) to reduce the AmLi contribution to approximately 1% of the Totals count rate. At this threshold, less than 4 minutes measurement would be necessary to obtain the counts of the Totals at less than 1% relative counting statistics uncertainty. In the same measurement time, the counts of the Reals would be determined with a 5% uncertainty, providing a good indication regarding the absence of any uncorrelated sources nearby the collar which would bias the measurement.

Table 1. Simulation of the system response in the proposed configurations and three different threshold settings for a 3.19 wt% enriched fuel element interrogation. Counting statistics uncertainties of the results are below 1%. Thresholds are expressed in neutron energy for simplification.

Threshold	Thermal configuration				Fast configuration			
	T [1/s]	T_{AmLi}	R [1/s]	R_{AmLi}	T [1/s]	T_{AmLi}	R [1/s]	R_{AmLi}
0.5 MeV	1443	20 %	150	0.12 %	634	70 %	23.0	1.07 %
1.0 MeV	578	3 %	39	0.02 %	119	23 %	6.0	0.23 %
1.5 MeV	313	0.13 %	12	0.02 %	51	1.25 %	1.7	0.16 %

3.3 Comparison with ^{3}He-based systems

In the following section we present a comparison of the coincidence collar capabilities with those of a classical ^{3}He thermal coincidence collar.

We simulated the response of two commercially available ^{3}He based system, the JCC73 and the JCC71 models [8], to the same fuel and the same interrogation source intensity simulated in the liquid scintillator analysis. Data were simulated with the MCNP-pta code [9], that postprocesses the coincidence counters response. The results are presented in table 2.

Table 2. Simulation of the response of two typical ^{3}He based neutron coincidence collars in thermal and fast configuration for a 3.19 wt% enriched fuel element interrogation.

Configuration	JCC73			JCC71		
	T[1/s]	R [1/s]	A [1/s]	T[1/s]	R [1/s]	A [1/s]
Thermal	2900	190	538	2100	124	282
Fast	1200	12	92	800	6	41

Table 3 and 4 provide a direct comparison of the achieved counting statistic uncertainty of the two systems for both thermal and fast configuration interrogation at different measurements times. Fast configuration is usually more time-consuming than the thermal configuration, therefore it is the most critical for this analysis.

Table 3. Counting statistics uncertainty related to different measurement times for the ^{3}He based JCC73 and for the liquid scintillator-based coincidence counter, both in thermal configuration. Results for the liquid scintillator- based prototype are reported for the Reals mode (threshold set to 0.5 MeV neutron energy) and for the Totals mode (threshold set to 1.5 MeV neutron energy).

Measurement time	JCC73 σ [%]	LS Reals σ [%]	LS Totals σ [%]
60 s	2.3	1.0	0.7
600 s	0.7	0.3	0.2

Table 4. Counting statistics uncertainty related to different measurement times for the ^{3}He based JCC73 and for the liquid scintillator-based coincidence counter, both in fast configuration. Results for the liquid scintillator- based prototype are reported for the Reals mode (threshold set to 0.5 MeV neutron energy) and for the Totals mode (threshold set to 1.5 MeV neutron energy).

Measurement time	JCC73 σ [%]	LS Reals σ [%]	LS Totals σ [%]
60 s	14.6	2.7	1.8
600 s	4.6	0.9	0.6
1 h	1.9	0.4	0.2
10 h	0.6	0.1	< 0.1

The advantage of fast neutron detection in liquid scintillators is clearly reflected in the results: it shows a consistent saving in measurement and operational time for the prototype system.

4. Conclusions

This paper provides data for the use of liquid scintillators as effective 3He replacement technology for nuclear safeguards applications, given their good neutron detection efficiency and gamma ray rejection capabilities.

We proposed an optimized design for a prototype liquid scintillator-based neutron coincidence collar made of 12 liquid scintillator cells.

Systematic effects, such as stability of the response with respect to high voltage small drifts and environmental changes, have not been evaluated in this paper and are planned for future work.

The capabilities of the system were analyzed by Monte Carlo simulations using MCNPX-PoliMi code, which proved to be an essential tool for simulating the detector response.

The system modelling required accurate characterization of the liquid scintillators cell response in terms of light output production for different incident particles and energies, and these functions needed to be evaluated separately for each cell geometry.

Finally, a comparison of the proposed prototype with existing 3He based systems shows promising fast neutron detection characteristics of the liquid scintillator, which is advantageous in terms of measurement time and related statistics, two very important factors in nuclear safeguards applications.

5. Acknowledgements

The authors would like to thank Raft Nolte (PTB, Braunschweig) for its kind support in the characterization of the detector. The authors would also like to acknowledge professor Padovani (Polytechnic university of Milan, Italy),

professor Pozzi, Jennifer Dolan and Eric Miller(University of Michigan, MI, USA) for their support during the set-up of the simulations and the implementation of the JRC post-processor code.

6. References

[1] E.Padovani, S.A.Pozzi, S.D.Clarke, E.C.Miller, MCNPX-PoliMi User's Manual, C00791 NYCP, Radiation Safety Information Computational Center, Oak Ridge National Laboratory, 2012.

[2] S. Pozzi, E. Padovani, M. Flaska, and S. Clarke (2007). MCNP-PoliMi Post-Processing Code Ver. 1.9. Oak Ridge National Laboratory Internal Report, ORNL/TM-2007/33

[3] Liquid scintillator-based neutron detector development, A. Lavietes, R. Plenteda, N. Mascarenhas, L. M. Cronholm, M. Aspinall, M. J. Joyce, A. Tomanin, P. Peerani, submitted to IEEE Transaction on Nuclear Science, forthcoming 2013.

[4] The theory and practice of scintillation counting, J. B. Birks, Pergamon Press, 1964.

[5] Optimization of a Mixed Multiplicity Counter Using Monte Carlo Simulations and Measurements, A. Enqvist, K. Weinfurther, M. Flaska,S. Pozzi, IEEE Transaction on Nuclear Science, 2010.

[6] Neutron Light Output Response and Resolution Functions in EJ-309 Liquid Scintillation Detectors, A. Enqvist, C. C. Lawrence, B. M. Wieger, S. A. Pozzi, T. N. Massey, Nucl. Instr. Meth. A 715 (2013) p. 79

[7] MCNPX-based determination of UNCC correction factors (Benchmark problems for MCNPX simulation), S. Y. Lee, D. H. Beddingfield, LA-UR-09-03573

[8] Monte Carlo simulation of neutron counters for safeguards applications, M. Looman, P. Peerani, H. Tagziria, Nucl. Inst. Meth. A 598 (2009) p. 542-550.

[9] M.R. Looman, N. Farese, G. Gonano, R. Jaime, B. Pedersen, and P. Schillebeeckx, "Monte Carlo Prediction of the Response of Neutron Counting Instruments", Proceedings of the 21th Annual Symposium on Safeguards and Nuclear Material Management, Seville, Spain, 4 – 6 May 1999, ESARDA Proceedings 29 (1999) pp. 375-381

On the potential of active coincidence counting using a spontaneous fission source to induce fission

Stephen Croft[1], Karen A. Miller[2], and Andrea Favalli[2]

1. Safeguards & Security Technology - Nuclear Security and Isotope Technology Division - One Bethel Valley Road - PO Box 2008, MS-6166 - Oak Ridge, TN 37831-6166, USA.
2. Safeguards Science & Technology Group, NEN-1 - Nuclear Engineering and Nonproliferation Division - Los Alamos National Laboratory - Mailstop E540, Los Alamos, NM 87545, USA

Abstract:

Using the one-group point-model equations as a guide, we compare the active neutron Doubles rate from a multiplying item interrogated with a spontaneous fission neutron source with that of a random neutron source of equal emission rate. We find that, especially for highly multiplying items, ^{252}Cf is likely to provide a viable alternative to the commonly used Am/Li interrogation source. We conclude that detailed design studies and experiments are warranted to develop this concept into practical assay tools.

Keywords: coincidence counting; active interrogation; ^{252}Cf active driver; point-model; collar detector

1. Introduction

Steady state active neutron coincidence counting is a familiar technique applied in nuclear safeguards for the assay of uranium [1]. The usual case is to interrogate the item with the relatively soft spectrum of time-random (α,n) neutrons from Am/Li radionuclide sources. The Am/Li spectrum is continuous extending from zero to about 1.5 MeV with a mean of about 0.5 MeV [2,3] The Am/Li spectrum is considered attractive for the assay of the fissile content of uranium because it does not strongly induce fission in ^{238}U lying as it does mostly below the effective ^{238}U fission threshold energy. The signature of induced fission exploited is traditionally the net neutron coincidence counting rate (usually called the Reals or Doubles rate) measured using shift-register electronics [4]. Genuine coincidences result from the fact that prompt neutron fission neutrons and induced fission chains result in the emission of bursts of neutrons with a common time origin and these can be distinguished from the background of random (α,n) neutrons coming from the Am/Li interrogation sources. On the other hand Am/Li sources typically contain fairly large amounts of α-emitter (in the Ci (1Ci=37GBq) range), have a comparatively high gamma-dose rate per neutron, and are presently difficult to procure. It is therefore natural to ask whether ^{252}Cf spontaneous fission sources might not also be used to good effect. The ^{252}Cf spectrum is spectrally harder but being similar to the spectrum of induced fission neutrons this means that the usual one neutron energy group assumption assumed in the interpretation of coincidence counting measurements should apply with better fidelity – at least in un-moderated assays configurations. In principle one could also try to optimize the coupling of the source to the item including materials to tailor the in-going spectrum to control the ^{238}U fission contribution caused by the external interrogating neutrons. The major challenge to using ^{252}Cf appears to lie in the fact that the correlated neutrons from the source cannot be separated from the induced fission events potentially adding an additional and high source of correlated background. In our analysis we shall conceptually treat the ^{252}Cf as being placed inside the item under study. We do this as a matter of mathematical convenience. However in practice there is will be the potential to optimize the geometry of the interrogation (source, assay item, detector, and moderator/shielding) to decouple as far as possible the correlated neutrons from the interrogation source from the induced fission events in order to minimize the correlated background. Thus, our results will be sufficient to decide if the use of ^{252}Cf is likely to be worthwhile pursuing even though we can anticipate considerable improvement for practical instruments. In this paper we analyze and compare the two scenarios (a fission source vs a random source) within the framework of the well-known one energy-group reactor point-model widely used to invert neutron correlation counting experiments [5].

2. Analysis

The point-model equations traditionally applied in Passive Neutron Coincidence (PNCC) counting using shift-register logic relate the dead time corrected net Totals (or Singles) and Reals (Doubles) rates, T and R to the properties of the item. They take the form [6,7]:

$$T = F \cdot \varepsilon \cdot \nu_{S1} \cdot (1+\alpha) \cdot M_L \tag{1}$$

$$R = F \cdot \varepsilon^2 \cdot f \cdot \left(\frac{\nu_{S2}}{2}\right) \cdot M_L^2 \cdot \left[1+(M_L-1)\cdot(1+\alpha)\cdot\kappa\right] \tag{2}$$

In these expressions:

$F = m \cdot g$ is the spontaneous fission (SF) rate in fis/sec taking place inside the item

$m \equiv m_{eff}$ is the effective mass in grams of the spontaneously fissioning nuclide of interest present

g is the corresponding specific spontaneous fission rate, fis/sec/gram

ε is the neutron detection efficiency, cnt/n, for neutrons emerging from the item

ν_{si} is the i[th] factorial moment of the normalized SF prompt neutron multiplicity emission distribution, $P_s(\nu)$. That is to say, $\nu_1 = \sum_{\nu=1}^{max} \nu \cdot P_{S(\nu)}$ and $\nu_2 = \sum_{\nu=2}^{max} \nu \cdot (\nu - 1) P_{S(\nu)}$, where *max* is the highest value of ν observed following fission

α is the ratio of the random in time neutron to (SF,n) neutron production rates where in the present PNCC context the random in time production includes (α,n)-reactions and delayed-neutrons following fission. If the weak delayed-neutron contribution is negligible then:

$$\alpha = \frac{S_\alpha}{F \cdot \nu_{S1}} = \frac{S_\alpha}{Y_F} \equiv \frac{Y_\alpha}{Y_F} \tag{3}$$

where S_α is the (α,n) production rate in n/sec taking place inside the item and we have introduced the quantity $Y_F = F \cdot \nu_{S1}$ the prompt neutron emission rate, n/sec, arising from SF. In the same spirit we have introduced the notation $Y_\alpha = S_\alpha$ to denote the neutron emission rate, n/sec, arising from (α,n) reactions

f is the signal triggered Gate Utilization Factor (GUF) for Reals coincidence counting according to shift register logic [8]

M_L is the leakage self-multiplication of the item

k is the Ensslin-Krick coefficient and is given by [9]:

$$\kappa = \left[\frac{\nu_{S1}}{(\nu_{I1} - 1)}\right] \cdot \left[\frac{\nu_{I2}}{\nu_{S2}}\right] \tag{4}$$

where ν_{I1} is the mean number of prompt fission neutrons emitted following induced fission and ν_{I2} is the 2[nd] factorial moment of the induced fission prompt neutron multiplicity distribution.

Where details are known about the item then an item specific k-parameter may be calculated, for example, by ratioing the SF and IF moments generated and reported by the general purpose Monte Carlo radiation transport code MCNPX [10]. In practice calibration using similar items to those to be measures usually means that a fixed value of k suffices. In MCNPX (as in real life) the spontaneous fission moments reflect all isotopic contributions. Similarly the induced fission moments must be formed by appropriately averaging over the nuclear data of all of the contributory species that undergo neutron induced fission. However, in practice it is more common to perform the inversion process with a fixed value representative of a class of items and similar to those used for calibration. Provided the variation is not strong across a given class of items and provided the value is used during calibration and during assay any bias is expected to remain modest in comparison to other sources of error associated with using the point-model expressions.

This traditional expression for the Reals (coincidence or Doubles) rate assumes that the probability of parasitic neutron capture, p_c, within the item is negligible compared to the probability of fission, p_f. For Pu items this is often a reasonable approximation and working solely in terms of the leakage multiplication avoids the need to introduce an additional (potentially free) model-parameter. Explicitly, however, we have the following relationships between the leakage self-multiplication and the total self-multiplication M_T [11]:

$$M_L = \frac{1 - p_f - p_c}{1 - p_f \cdot \nu_{I1}} = (1 - p_f - p_c) \cdot M_T \tag{5}$$

where we recognize $p_L = (1 - p_f - p_c)$ as the probability that a neutron inside the item will evade capture and fission and escape so that it might be detected. In the expression for R the quantity of interest inside the square brackets is actually related to the induced fission source term and can be written:

$$p_f \cdot M_T = \frac{M_L - 1}{(\nu_{I1} - 1) - p_c / p_f} \tag{6}$$

which is only being approximated by $\frac{M_L - 1}{(\nu_{I1} - 1)}$, a good approximation when $p_c / p_f \approx 0$, so that the neutron interactions taking place in the item require only a single model parameter to describe in this approximation.

Re-writing the point model expressions term by term we have in terms of the contributory neutron emission rates:

$$T = (\varepsilon \cdot M_L) \cdot [Y_F + Y_\alpha] \tag{7}$$

$$R = (\varepsilon \cdot M_L)^2 \cdot f \cdot \left[Y_F \cdot \left(\frac{1}{\nu_{S1}} \cdot \frac{\nu_{S2}}{2} + \frac{M_L - 1}{(\nu_{I1} - 1) - p_c / p_f} \cdot \frac{\nu_{I2}}{2} \right) \cdot Y_\alpha \cdot \frac{M_L - 1}{(\nu_{I1} - 1) - p_c / p_f} \cdot \frac{\nu_{I2}}{2} \right] \tag{8}$$

Having established these key general relationships let us now completely switch our perspective. Instead of considering these to be expressions for the net passive Totals and Reals due to spontaneous (fission and (α,n)) reactions taking place in the assay item let us use them to describe the net active rates. Y_F and Y_α now represent the strength of the interrogation source, n/s, from the presence of a fission sources and (α,n) source respectively. For convenience we are implicitly assuming that the interrogation source has been placed inside the assay item to avoid the issue of coupling raised earlier. It is worth highlight that the probability of first fission will be different between AmLi and ^{252}Cf owing to the different source spectra, however, for an application source tailoring and source-to-item coupling can be optimized for each situation. Within the fission chain the probability of induced fission will be quite similar for the two sources however, being set by the induced fission neutrons which will also have a similar spatial launch pattern.

Expressed in this way the equations also make it is straightforward to see the difference between an active interrogation of a multiplying item using a pure source of fission neutrons such as ^{252}Cf (defined by Y_F n/s and with $Y_\alpha = 0$) inserted into the item and a pure source of random neutrons, such as is closely approximated by an Am/Li radionuclide source, (defined by Y_α n/s and with $Y_F = 0$) of equal neutron emission rate inserted into the item.

We observe that the overall Totals neutron counting rate (background plus net passive plus net active) will be the same for the two cases, within the framework of the one-group point model we are using, meaning that the Accidentals (or random chance) Reals rate will also be numerically equal. The Accidentals coincidence rate has an expectation value given by the product of the square of the overall Totals counting rate and the coincidence gate width. Accidental events must be subtracted to obtain the genuine Reals rate and this contributes to the final precision. The point we wish to make is that in this regard there is no difference in the Accidentals rate between using the a spontaneous fission source to carry out the interrogation or an (α,n) source under the stated model assumptions.

To proceed we need only, therefore, concentrate on the Reals rate behavior. Let us define R_α and R_F as the net active Reals rates when using a pure (α,n) and a pure spontaneous fission interrogation source respectively. Then we can capture the key functional dependences through the Reals rates per unit interrogating source strength rendered independent of instrumental effects by conversion to unit efficiency and full gating. Algebraically this is captured by the following expressions for q_α and q_F which relate to pure (α,n) and pure SF interrogation respectively:

$$q_\alpha = \frac{1}{Y_\alpha}\frac{R_\alpha / f}{\varepsilon^2} = \left(\frac{\nu_{I2}/2}{(\nu_{I1}-1)-p_c/p_f}\right)\cdot M_L^2\cdot(M_L-1) \qquad (9)$$

And (see equation 7 in [18] for comparison)

$$q_F = \frac{1}{Y_F}\frac{R_F / f}{\varepsilon^2} = M_L^2\cdot\frac{\nu_{S2}/2}{\nu_{S1}} + \left(\frac{\nu_{I2}/2}{(\nu_{I1}-1)-p_c/p_f}\right)\cdot M_L^2\cdot(M_L-1) \qquad (10)$$

The behavior of q_α and q_F express the relative performance of the two interrogation schemes. For equal strength sources we that the difference between the two expressions ($q_\alpha - q_F$) is the term $M_L^2\cdot\frac{\nu_{S2}/2}{\nu_{S1}}$. From an analytical point of view the question is whether this provides additional useful information about the item or simply contributes what amounts to a nuisance signal or noise. The issue is most clearly demonstrated for an item with a leakage self-multiplication close to unity in which case $q_F \to \frac{\nu_{S2}/2}{\nu_{S1}}$, which we recognize as no more than an off-set which can be treated through calibration in principle, for example in the case of a fuel assembly measurement where the geometry is well defined. For highly multiplying items however the intrinsic correlations from the spontaneous fission interrogation source are boosted in proportion to the square of the leakage self-multiplication due to the manifestation of induced fissions.

3. Numerical Example

To illustrate the behavior of q_F with M_2 we take the case of a ^{252}Cf interrogation source for which $\frac{\nu_{S2}/2}{\nu_{S1}} \approx 1.590$ [12]. For simplicity we shall set p_c/p_f to zero and take the induced fission parameters for ^{235}U at 1 MeV (in doing so we are making only a small bias for the sake of illustrative simplicity) making $\frac{\nu_{I2}/2}{(\nu_{I1}-1)} \approx 1.674$ [13]. In this example the ratio of the two terms appearing in q_F is given by:

$$\Lambda = \left[\left(\frac{\nu_{I2}/2}{(\nu_{I1}-1)-p_c/p_f}\right)/\left(\frac{\nu_{S2}/2}{\nu_{S1}}\right)\right]\cdot(M_L-1) \qquad (11)$$

Λ exceeds unity when M_2 exceeds about 1.95 in the current example. This is an indication that for highly multiplying items the use of a ^{252}Cf source is likely to be viable because its inherent correlated neutron rate will be overwhelmed by induced fission chain events. A breakdown of the contributions to q_F is given in Figure 1. For context, from unpublished experimental data, for stacked High Enriched Uranium (HEU) metal plates in 6" (152.4 mm) diameter storage cans, a multiplication of 1.95 equates to a ^{235}U mass of about 17 kg. A situation one can envision for an active well coincidence type assay.

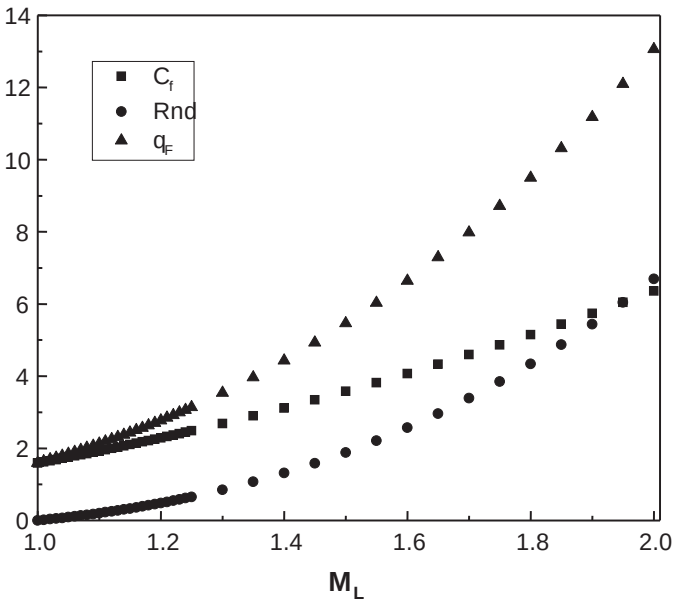

Fig. 1 A plot of q_F vs M_2 for the illustrative example discussed in the text. The M_L^2 (labeled as C_f) and $M_L^2\cdot(M_L-1)$ (labeled as Rnd) contributions are also shown separately. For weakly multiplying items the direct Reals signal from the source dominates but at higher self-multiplications the induced fission is manifest with growing strength.

4. Discussion

In this brief note we have not considered practical considerations such as the engineered coupling of an external source to the item, optimization of the detection geometry and possible spectral tailoring strategies which together could alleviate some of the relative disadvantages of using ^{252}Cf rather than Am/Li as an active interrogation source. However, our analysis is suggestive that more detailed considerations are warranted for some applications.

We note that in the case of UF_6 large volume commercial storage cylinder analysis for enrichment determination some progress has already been made in this area [14]. Multiplication is sensitive to enrichment and the active Reals rate can be related to enrichment through calibration for a given configuration. The extension to active assay of fresh fuel assemblies in an adapted collar design immediately suggests itself, and this application is of great interest given the expansion and evolution of this measurement need [15-17], and an experimental investigation has been recently reported in [19]. There are other potential applications too, for example the assay of sub-critical assemblies designed to generate integral benchmark nuclear data of interest to reactor designers, criticality safety assessments, and safeguards.

We have used the point-model equations [18] here as a guide. Large dense multiplying objects violate the underlying assumptions, for instance the leakage multiplication is not a simple single valued parameter but varies across the items. However it has been established many times [e.g. see 20] that with suitable calibration that coincidence (Doubles) counting is remarkably robust to such violations so that data interpretation using the point-model remains an important practical tool. So, for the present purpose, which is solely to establish a way of thinking about the relative value of ^{252}Cf against the traditional AmLi source for active coincidence counting we feel we are on an adequate footing.

5. Conclusion

Active coincidence counting to assay uranium is an established technique using Am/Li sources. Am/Li sources have many favorable characteristics for this application including a long half-life and a soft energy spectrum which does not cause fast induced fission but they are difficult to obtain. Using the point-model as a guide we have showed that the use of a ^{252}Cf spontaneous fission instead of Am/Li is likely to be viable, particularly for highly multiplying items in which the geometry can be reasonably well controlled and correlations established through calibration. The key finding is that in this regime the inherent coincidence rate coming from the interrogation source, that is the rate one would observe with a benign (or for arguments sake no) item present, is not necessarily prohibitive or even dominant compared to the induced fission signal. Thus meaningful active measurements using ^{252}Cf as the interrogation source, that is measurements which provide good information about the nature of the fissile content of the assay items, seems possible.

6. Acknowledgement

This work was made possible through Action Sheet 14 between The National Nuclear Energy Commission of Brazil (CNEN) and the United States Department of Energy (DOE). We thank Dr. Michael C. Browne for his encouragement. Suggestions made by anonymous reviewers have helped refine this article and we are happy to thank and acknowledge them here.

7. References

[1] T.R. Wenz, H.O. Menlove, G. Walton, J. Baca, Design and calibration of the AWCC for measuring uranium hexafluoride, Los Alamos National laboratory report LA-12992(ISPO-377)(Aug., 1995).

[2] K.W. Geiger and L. Van Der Zwan, The neutron spectra and resulting fluence-kerma conversions for ^{241}Am-Li(α,n) and ^{210}Po-Li(α,n) sources, Health Physics 21(1971)120-123.

[3] H. Tagziria, M.Looman, The ideal neutron spectrum of ^{241}AmLi(α,n)^{10}B sources, Applied Radiation and Isotopes, Vol.70, Issu 10, 2012, pag.2395-2402.

[4] N. Ensslin, W.C. Harker, M.S. Krick, D.G. Langner, M.M. Pickrell and J.E. Stewart, Application guide to neutron multiplicity counting, Los Alamos National laboratory report LA-13422-M(Nov., 1998).

[5] K. Böhnel, The effect of multiplication on the quantitative determination of spontaneously fissioning isotopes by neutron correlation analysis, Nucl. Sci. and Engin. 90(1985)75-82.

[6] L. C.-A. Bourva, S. Croft and M.-S. Lu, Extension to the Point Model for Neutron Coincidence Counting, Proc 25th Annual Meeting ESARDA (European Safeguards Research and Development Association) Symposium on Safeguards and Nuclear Material Management, Stockholm, Sweden, 13-15 May 2003. EUR 20700 EN (2003) Paper P094. ISBN 92-894-5654-X.

[7] I. Pázsit, A. Enqvist and Lénárd Pál, A note on the multiplicity expressions in nuclear safeguards, Nucl. Instrum. and Meths. in Phys. Res. A603(2009)541-544.

[8] S. Croft and L.C.-A. Bourva, The measurement of passive neutron multiplicity counter gate utilization

factors and comparisons with theory, Nucl. Instrum. and Meths. in Phys. Res. A453(2000)553-568.

[9] M.S. Krick, Neutron multiplication corrections for passive thermal neutron well counters, Los Alamos scientific Laboratory report LA-8460-MS(ISPO-89) (July, 1980).

[10] D.B. Pelowitz (Ed.), MCNPX™ user's manual version 2.6.0, April 2008, Los Alamos National Laboratory report LA-CP-07-1473.

[11] S. Croft, A. Favalli, D.K. Hauck, D. Henzlova and P.A. Santi, Feynman variance-to-mean in the context of passive neutron coincidence counting, Nucl. Instrum. and Meths. in Phys. Res. A686(2012)136-144.

[12] M.S. Zucker and N.E. Holden, Parameters for several plutonium nuclides and ^{252}Cf of safeguards interest, Proc. Sixth Annual European Safeguards Research and Development Association Symposium on Safeguards and Nuclear Material Management, Venice, Italy, 14-18 May, 1984. ESARDA 17(1984)341-353.

[13] M.S. Zucker and N.E. Holden, Neutron multiplicity for neutron induced fission of ^{235}U, ^{238}U and ^{239}Pu as a function of neutron energy, IAEA-SM-293/122(1987)329-347.

[14] K.A.Miller, H.O.Menlove, M.T.Swinhoe and J.B.Marlow, Monte Carlo Feasibility Study of an Active Neutron Assay Technique for Full-Volume UF_6 Cylinder Assay Using a Correlated Interrogation Source, Nuclear Instruments and Meths. in Phys. Res. A, vol. 703, 2012).

[15] A. Favalli, S. Croft and M.T. Swinhoe, Perturbation and burnable poison rod corrections for BWR uranium neutron collar, Proc. 33rd ESARDA Annual Meeting, Helia Conference Hotel, Budapest, Hungary, 16-20 May, 2011.

[16] S. Croft, A. Favalli, M.T. Swinhoe and C.D. Rael, State of the art Monte Carlo modeling of active collar measurements and comparison with experiment, Proc. 52nd Annual INMM Meeting, July 2011 Palm Desert, CA, USA.

[17] S. Croft, A. Favalli, and M.T. Swinhoe, The calculation of burnable poison correction factors for PWR fresh fuel active collar measurements, Proc 53rd Annual Institute of Nuclear Materials Management (INMM) Meeting July 15-19 2012 Orlando, FL, USA.

[18] W. Hage and D.M. Cifarelli, "On the Factorial Moments of the Neutron Multiplicity Distribution of Fission Cascades", Nucl. Instr. and Meth., **A236** (1985), 165-177.

[19] H.O.Menlove, S.H.Menlove, and C.D.Rael, The development of a new, neutron, time correlated, interrogation method for measurements of the ^{235}U content in LWR fuel assemblies, Nucl.Instr.and Meth.A, vol.701, 2013, 72-79.

[20] S Croft, LG Evans, MA Schear, and MT Swinhoe, Feasibility of classic multiplicity analysis applied to spent nuclear fuel assemblies, Proc. 52nd Annual INMM Meeting, July 2011 Palm Desert, CA, USA.

Fast neutron coincidences from induced fission as a method for detection of SNM

A. Ocherashvili[a], M. Mosconi[b], J-M. Crochemore[b], A. Beck[a], E. Roesgen[b], V. Mayorov[b], B. Pedersen[b]

a. Physics Department - Nuclear Research Center Negev - P.O. Box 9001, 84190 Beer-Sheva, Israel
b. Institute for Transuranium Elements (ITU) - Joint Research Centre, European Commission - Via E. Fermi 2749, Ispra 21020 (VA), Italy
E-mail: bent.pedersen@jrc.ec.europa.eu

Abstract:

A method for the detection of special nuclear materials (SNM) in shielded containers which is both sensitive and easily applicable under field conditions is presented. The method applies neutron induced fission in SNM by means of an external pulsed neutron source with subsequent detection of the fast prompt fission neutrons. Liquid scintillation detectors surrounding the container under investigation are able to discriminate gamma rays from fast neutrons by the pulse shape discrimination technique (PSD). One advantage of these detectors, besides the ability to do PSD analysis, is that the analogue signal from a detection event is of very short duration (typically a few tens of nanoseconds). This allows the use of very short coincidence gates for multiple detectors for the detection of prompt neutrons from the same fission event while benefiting from a low accidental (background) coincidence rate. These features result in a relatively low detection limit of the fissile mass.

Another principal advantage of this method derives from the fact that the external neutron source is pulsed. By proper time gating the interrogation can be done by either epi-thermal or thermal neutrons. These source neutrons do not appear in the neutron signal following the PSD analysis thus providing a fundamental method for separating the interrogating source neutrons from the response in form of fast fission neutrons.

The paper describes laboratory tests with multiple detectors at the Pulsed Neutron Interrogation Test Assembly (PUNITA) for the purpose of investigating the measurement principle. Results of thermal and epi-thermal neutron interrogations are shown and discussed.

Keywords: security; fission; scintillation; PSD; coincidence;

1. Introduction

A variety of passive and active non-destructive assay (NDA) methods are being investigated for the purpose of detecting special nuclear materials (SNM) in practical applications [1-5]. The prompt emissions in fission events of neutrons and γ-rays are useful signatures for the detection of SNM in shielded containers. One reason for this is the fact that the component of high energy prompt radiation from fission is very penetrating and thus difficult to deliberately shield from detection. Furthermore identifying the detected radiation to be originating from fission events is evidence of the presence of SNM in the object under investigation. To this end it is useful to arrange the detection system to take advantage of the fact that during the fission event multiple prompt γ-rays and neutrons are emitted simultaneously [6-7].

Using an external neutron source to induce fission extends the usefulness of this detection method to apply not only to spontaneous fissile materials but also to materials with a cross-section for neutron induced fission. Pulsing of the external neutron source can provide further advantages to be exploited in the detection method. This includes the fact that by proper timing (gating) of the detection period with respect to the neutron emission from the external source the object can be interrogated by a low energy neutron flux (epi-thermal or thermal neutron flux) only, providing the possibility to distinguish the fast fission neutrons from the low energy source neutrons in an appropriately selected neutron detection system [8].

In the present work we investigate the use of liquid scintillation detectors for the detection of the prompt radiation from fission events. These detectors can distinguish fast neutron interactions from other interactions by means of pulse shape discrimination (PSD).

The intention with this work is to demonstrate the principle of the detection method by means of a detection system which can be scaled up, e.g. by increasing the number of detectors, to handle objects a few cubic metres such as the standard universal load devices (ULDs) used for air traffic cargo. The present work however intends to investigate the feasibility of this technique. Further work is required to optimize the detection system and the PSD algorithms.

2. Experimental setup

The Pulsed Neutron Interrogation Test Assembly (PUNITA) of the Joint Research Centre is designed for experimental studies in non-destructive analysis (NDA) methods for nuclear safeguards and security [9-10]. Figure 1 shows a cross section of PUNITA and a view inside the sample

cavity. The facility is composed of a large graphite liner surrounding a central cavity of volume 50x50x80 cm^3. The (D–T) pulsed neutron generator, the sample under investigation and the scintillation detectors used for coincident detection are located inside the cavity. In total 96 one metre long ^{3}He neutron detectors are embedded in polyethylene modules and shielded by cadmium (fission neutron counters in Figure 1). In the present experiments these detectors are used as reference detectors of the prompt fission neutrons.

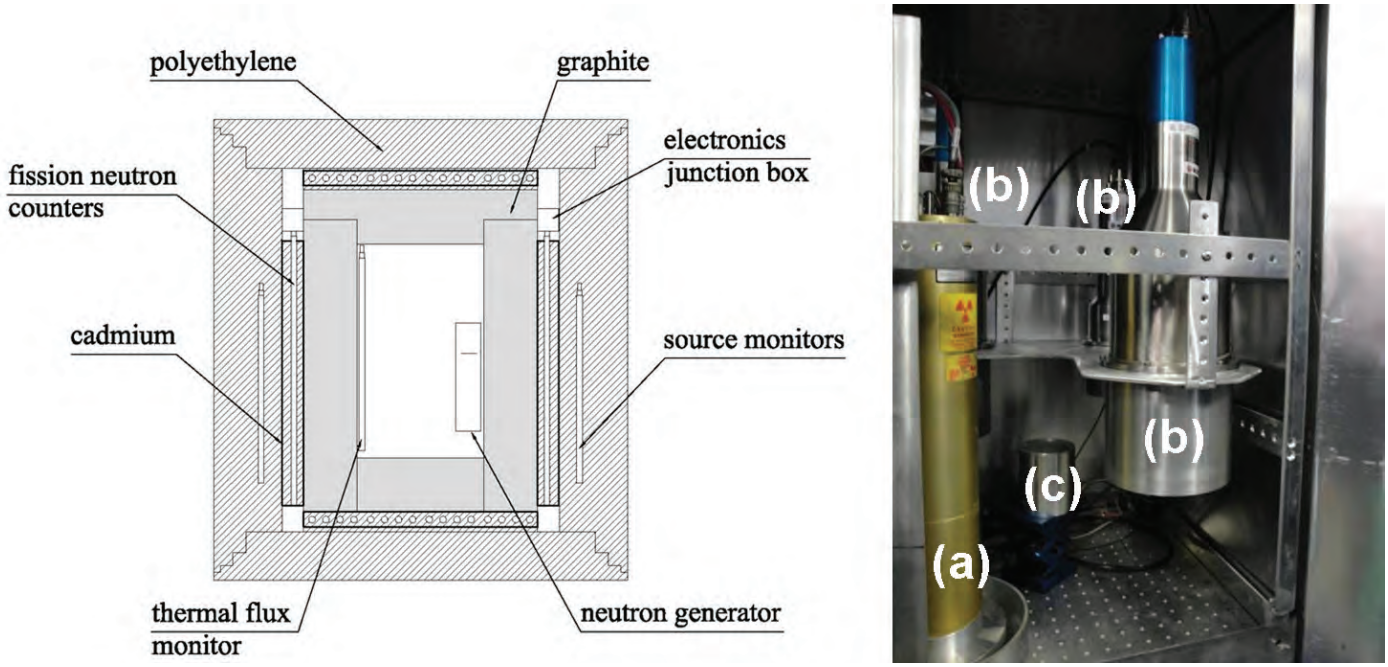

Figure 1: Cross-section of PUNITA showing the permanently mounted neutron detectors and the neutron generator (left picture). The picture shows the sample cavity of PUNITA including neutron generator (a), liquid scintillation detectors (b), and uranium test sample (c).

In Figure 1 is also indicated, as source monitors, bare ^{3}He neutron detectors which are used to normalize detector readings in all experiments to the same total neutron emission from the generator target. The neutron generator (Model A-211 from Thermo Fisher Scientific Inc.) is pulsed at 100 Hz which is chosen based on the average thermal neutron lifetime in the graphite/cavity configuration. The thermal flux generated by source neutrons being thermalized in the graphite peaks at about 250 μs after the 14-MeV neutron burst. The generator is able to produce short and intense bursts of neutrons with no neutron emission between bursts. This fact, together with the very short duty-cycle of one per mille, allow separation of the neutron interrogation into a fast/epi-thermal period from zero to 100 μs, and a thermal period from 250 μs to 9 ms, respectively. In Ref. 8 the neutron field of PUNITA as function of time is explained in detail.

The scintillation liquid used in this work is BC-501A from Saint Gobain Inc [11]. Three detectors are used in the present experiment; two detectors of dimensions 5”x5” and one detector of 3”x3”. The anode output of the photomultiplier is connected directly to a signal digitizer. The digitizer is a four channel LeCroy WaveRunner HRO66 ZI oscilloscope with a 2 GS/s sampling rate and 12-bit ADC.

The performance of the BC-501A scintillation detectors with respect to n/γ discrimination in the PUNITA facility is described in Ref. 8. In this reference the detector response to various reference γ-ray and neutron sources is shown, and a discussion regarding the count rate during a typical pulse cycle of PUNITA is presented. Due to the very fast response of the scintillation detectors the effect of the neutron generator burst can be followed in detail. This is not possible in the ^{3}He proportional counter based “fission neutron counters” surrounding the graphite liner. The charge collection of these detectors is two orders of magnitude slower, and they tend to saturate for as much as 250 μs after the neutron generator burst. Whereas Ref. 9 describes in detail the behaviour of the thermal neutron flux, Figure 2 describes the time behaviour during neutron slowing-down. Figure 2 shows the averaged total (neutron and γ-ray) detection rate in the 3”x3” detector following a neutron generator burst initiated at time zero. Each burst consists typically of 10^6 neutrons, and a typical experiment consists of 3×10^4 bursts. In the time period of 20 to 100 μs after the burst the response decays with a single exponential representing the slowing-down of the fast source neutrons. From 250 μs onwards the response (not shown) is dominated by the decay of the thermal neutron flux.

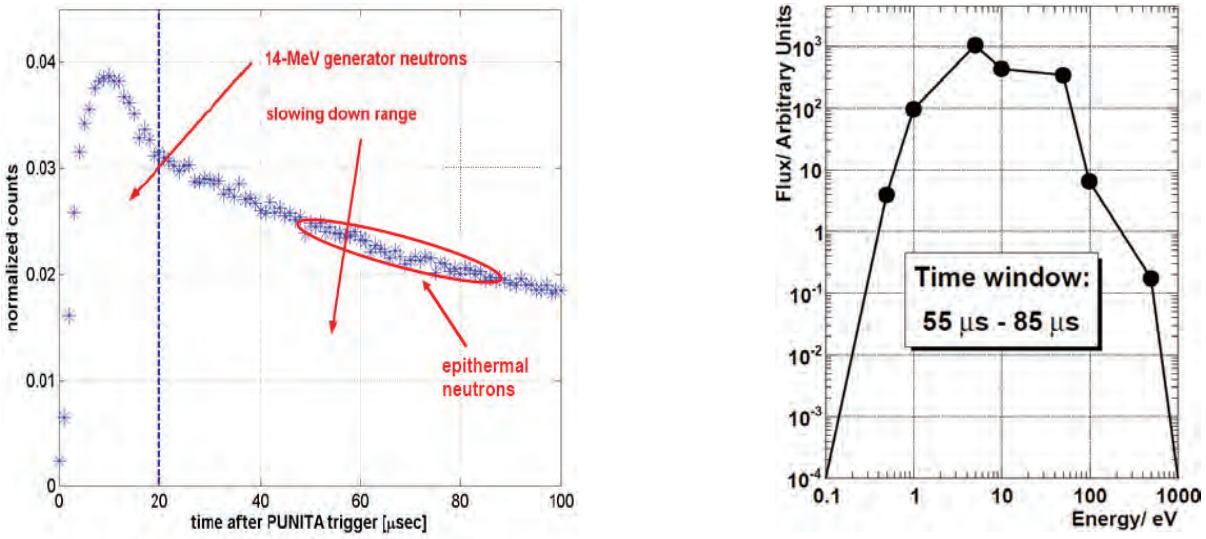

Figure 2: Left side: Total (neutron and γ-ray) response from a BC-501A scintillation detector in PUNITA after a neutron burst at time zero without presence of fissile material. The time interval when epi-thermal neutrons persist is highlighted. Right side: MCNP5 simulation of the neutron energy spectrum of source neutrons in the centre of the empty PUNITA cavity in the time interval 55 μs to 85 μs after the 14-MeV neutron burst.

In Figure 2 the region of 55 – 85 μs is circled and represents a useful region where only source neutrons below 500 keV persist. At this energy (roughly 75 keVee) neutron-proton recoil interactions do not deposit enough energy to be detected, so the detection rate is dominated by γ-ray interactions. The energy spectrum of the source neutrons as calculated by MCNP5 [12] is also shown in Figure 2. The neutron energy is mainly in the range 0.5 eV to 200 eV. This interrogating neutron spectrum is particularly interesting as the energy is too low to produce a "neutron response" in the PSD spectrum thus separating the low-energy source neutrons from the high-energy fission neutrons in the detector response.

In the present work we apply a simplified coincidence scheme which will trigger the storage of events when at least two out of the three detectors have observed a gamma or neutron interaction. At each trigger event all three detector channels are stored for off-line analysis. The trigger scheme of the coincidence detection is shown in Figure 3. Each scintillation detector is coupled to a constant fraction discriminator (CFD, ORTEC 935 Quad 200-MHz Constant-Fraction Discriminator). The walk of each CFD was tested using a ^{60}Co source and their threshold was set to 0.2 V by means of a calibrated amplitude pulse generator. The width of the output pulse was set to 50 ns to impose the requirement that at least two signals must occur within 50 ns to trigger the storage of the event.

The synchronizing digital output signal of the neutron generator is sent through a variable delay to the veto of the CFDs. This feature allows selecting the time period of interrogation with respect to the burst of 14-MeV neutrons from the generator. In this work we investigate two time intervals: the one of Figure 2 (epi-thermal interrogation) and one after 300 μs (thermal neutron interrogation). An ORTEC CO4020 Quad 4-Input Logic Unit is used to implement the two-out-of-three coincidence trigger for the three detectors. The coincidence triggers are summed in a fast OR gate, and used to trigger the storage of the LeCroy waveforms.

Sending a trigger signal to the oscilloscope signifies that a double coincidence event (or triple coincidence event) has occurred. Such a trigger will cause storing of all three detectors channels in the LeCroy internal memory. A waveform of 200 ns duration is stored on each input channel.

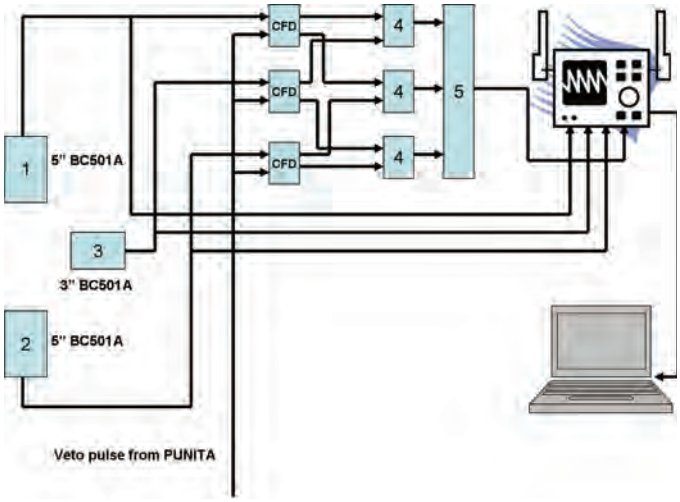

Figure 3: Trigger scheme for the data acquisition. The boxes labeled with 4 are coincidence units and the box labeled as 5 is a fast OR unit.

Tens of thousands 2-fold or 3-fold coincidence events are stored in each experiment for offline analysis. We use MATLAB [13] to perform the PSD analysis (n/γ discrimination) and plot the coincidences according to

their multiplicity (2-fold or 3-fold coincidence events) and kind (gamma-gamma, gamma-neutron, neutron-neutron, etc.).

The BC-501A liquid from Saint Gobain Inc. [11] produces scintillations according to different mechanisms for neutron and gamma ray interactions. The PSD method utilizes the fact that scintillations caused by neutron interactions result in a longer decay component compared to that of gamma interactions. Various techniques can be implemented to yield the discrimination between fast neutrons and gamma ray signals. Most common perhaps is the so-called integration method [14] which has been used extensively in PUNITA [8]. In the present work we apply a variation of this method as illustrated in Figure 4. Analytical expressions obtained by fitting of the scintillation detector anode outputs [15, 16] are used to distinguish the waveforms. The difference between the two signals in Figure 4 (a) appears to be largest at 22.8 ns after the start of the pulse. In practice we use the cumulative sum of the normalized waveform as shown in Figure 4 (b). This figure shows a more pronounced difference between the two pulses. At the level of 90% of the total cumulative sum the difference is 40.8 ns. By implementing a simple algorithm that records the time for reaching the 90% accumulative sum, a speedy and effective distinction between gamma ray and fast neutron detection events is achieved. The obtained discrimination is adequate for the present purpose.

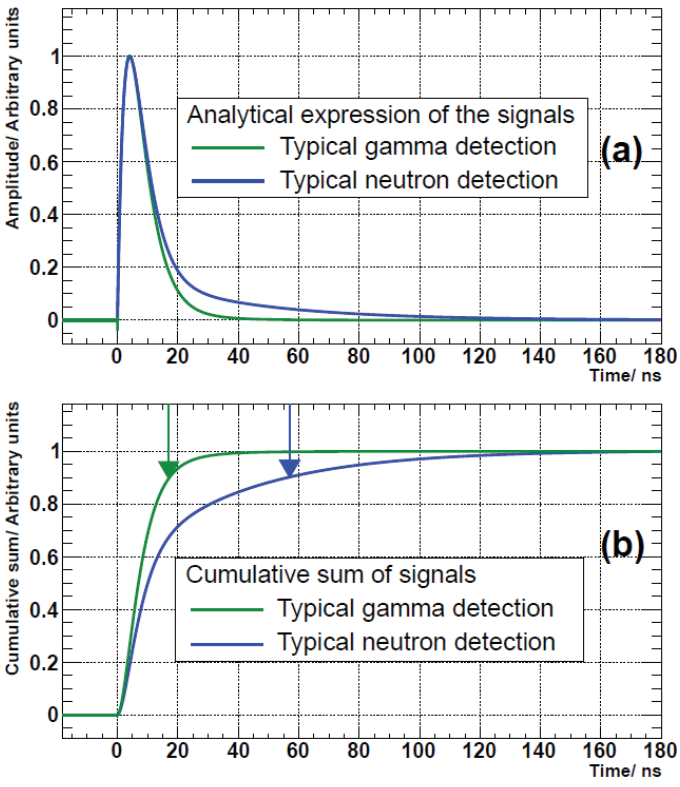

Figure 4: (a) averaged and normalized pulse shape of a gamma and neutron detection event. **(b)** Cumulative sum of pulses in (a), also indicating the time of 90% sum used as PSD signature.

3. Measurements of uranium samples in PUNITA

A series of standard CNNM U_3O_8 sources [17] are used in conjunction with the pulsed neutron interrogation and three BC-501A scintillation detectors. The five CBNM standards are essentially identical in all aspects (total mass, density, geometry, container type) except for the ^{235}U enrichment. The mass of the fissile ^{235}U component is 0.52 g (0.31%), 1.12 g (0.71%), 3.28 g (1.94%), 4.99 g (2.96%) and 7.54 g (4.46%), respectively. Also measurements of an empty CBNM container are included for the purpose of comparison (note: in the following diagrams the empty container is indicated as zero enrichment). The sample is placed in the centre between the three detectors at a distance of 150 mm as seen in the picture of Figure 1.

In the following we show results of interrogation with thermal neutrons (300 μs to 4000 μs after the 14-MeV burst) and epi-thermal neutrons (55 μs to 85 μs after the 14-MeV burst). Each experiment includes 30,000 generator pulses (5 minutes measurements). To facilitate comparison of individual experiments the source monitor readings were used to normalize the response to one generator burst of identical target emission. In order to limit the rate of data storage the total event rate was not recorded but only events with at least a 2-fold coincidence are stored for offline PSD analysis.

3.1 Results of thermal neutron interrogation

By gating the storage of coincidence events to the time period of 300 μs to 4000 μs after the 14-MeV burst only thermal source neutrons persist in the interrogation. Figure 5 shows the normalized rate of detected 2-fold coincidences of the types: (γ-γ), (γ-n) and (n-n) as obtained in the PSD analysis. The large “offset” of coincidence events observed for the empty container is mainly due to mechanisms of the PSD method. Both the standard “integration” method [14] and the method applied in this work (Figure 4) suffer at high counting rates from pile-up events in the long charge integration interval (typically 120 to 200 nanoseconds) i.e. multiple signals adding to the total charge integral thus producing “false” neutron PSD values.

Interestingly however the empty container has systematically less emission suggesting that the difference is due to gamma coincidences originating from uranium.

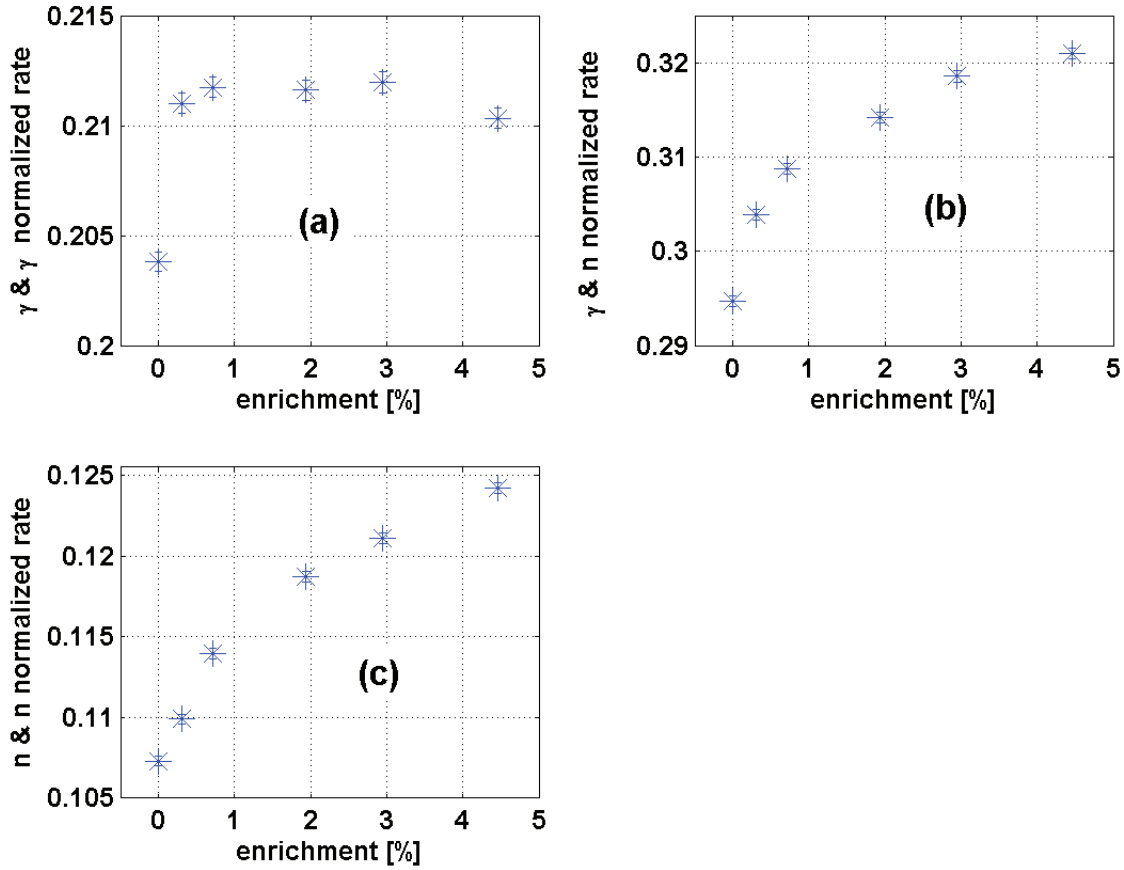

Figure 5: Thermal neutron interrogation producing 2-fold coincidences for different particle composition: γ-γ (a), γ-n (b) and n-n (c) for the five CBNM uranium standards and the empty container (indicated as zero enrichment).

The (γ-γ) 2-fold coincidence rate in Figure 5 (a) shows no dependence on the ^{235}U concentration. This is believed to be due to the gamma emissions from fission events being swamped by a high rate of other γ emitting reactions (e.g. neutron capture) and the high γ detection efficiency.

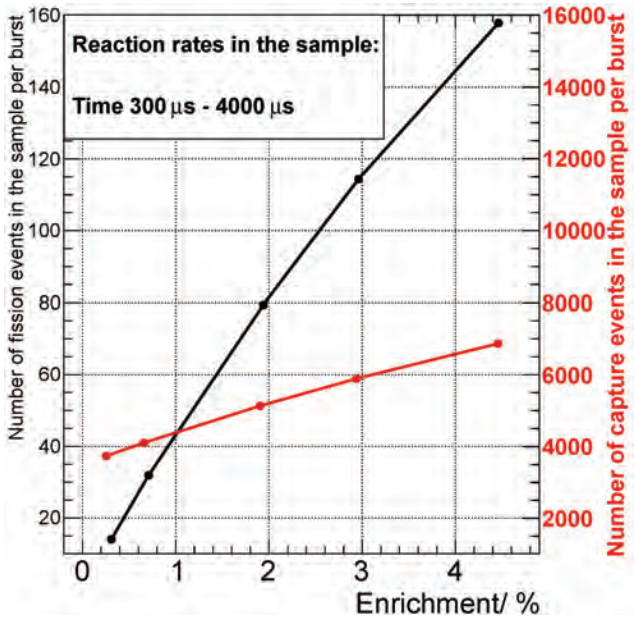

Figure 6: MCNP5 simulations of the rate of neutron capture and neutron induced fission events in the CBNM samples in the time period of PUNITA when only thermal source neutrons persist. The capture reaction rate appears to be much higher and relatively constant compared to the fission rate for the five CBNM standards.

In an attempt to better understand the relative independence of (γ-γ) 2-fold coincidences on ^{235}U enrichment, MCNP5 was used to simulate the thermal neutron capture and thermal neutron fission rate for the five different CBNM samples in the PUNITA facility. The results of the simulations are shown in Figure 6, and seem to indicate that a substantial level of "random" γ-rays from capture may in fact outweigh the enrichment dependent fission γ-rays. To understand this in detail however would require simulation of the detected (γ-γ) 2-fold coincidences, and application of a PSD method less prone to signal pile-up at high counting rates.

The (γ-n) and (n-n) 2-fold coincidences in Figure 5 (b) and (c), do show a clear dependence on the ^{235}U concentration indicating that these coincidences (with a neutron component) originate from induced fission events. The fact that this dependence is not linear is due to the self-attenuation of the thermal neutron flux inside the stronger absorbing (higher ^{235}U concentration) samples.

A similar behaviour is observed from the analysis of 3-fold coincidences but with poorer statistics. Figure 7 shows the different types of 3-fold coincidence events as function of ^{235}U concentration. Again, the pure γ 3-fold coincidences appear independent of the ^{235}U component in contrast to the 3-fold coincidences including neutrons. The statistics on the pure neutron 3-fold coincidences is particularly poor (d).

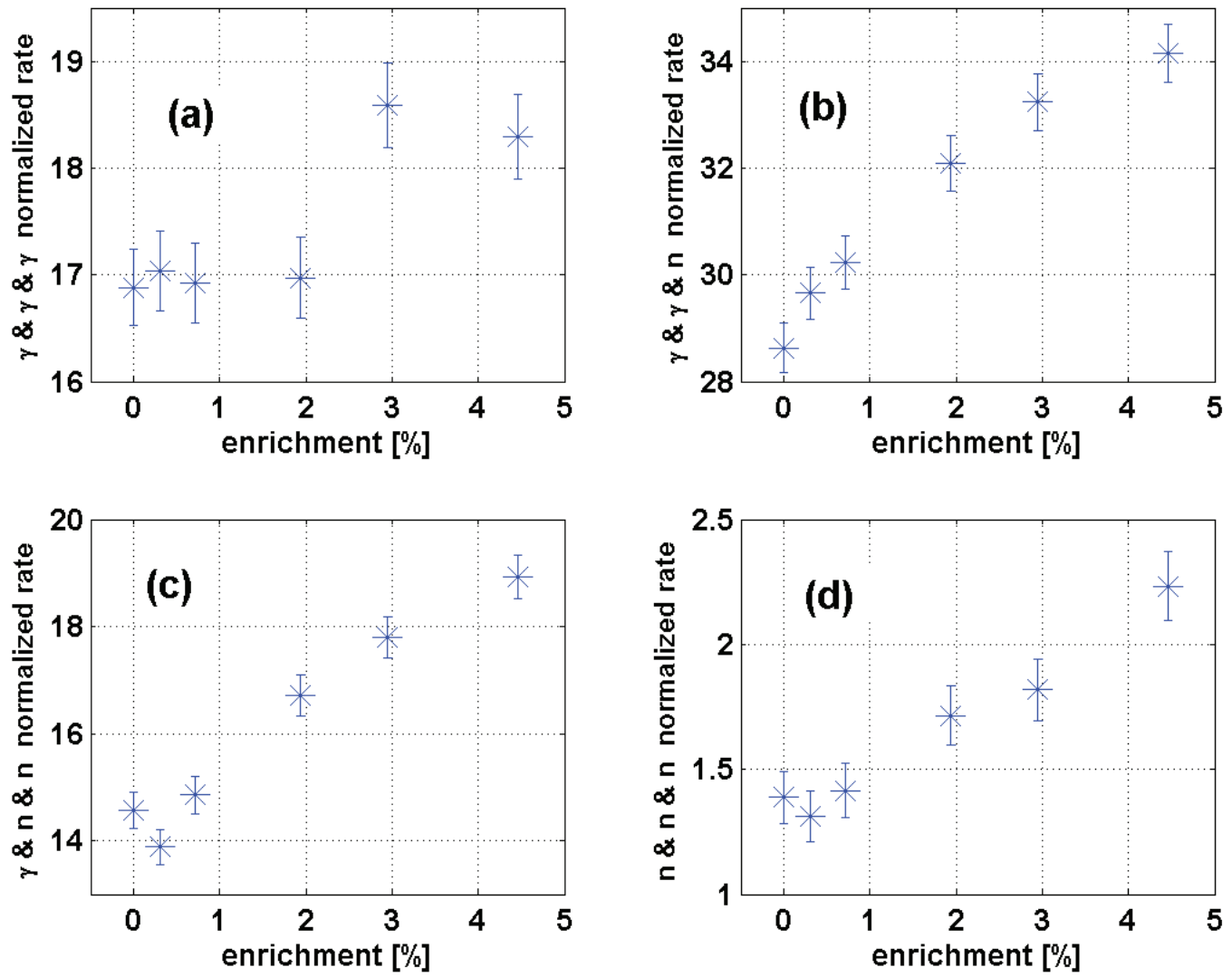

Figure 7: Thermal neutrons interrogations causing 3-fold coincidences of different kinds: γ-γ-g (a), γ-γ-n (b), γ-n-n(c) and n-n-n (d) for the CBNM uranium standards and the empty CBNM container. Zero enrichment signifies empty container.

3.2 Results of epi-thermal neutron interrogation

With the purpose of SNM detection of under practical conditions in mind, it is particularly desirable to detect the prompt fission neutron coincidences (as in Figure 5 and 7), not by means of thermal neutrons, but by epi-thermal neutron interrogation. The reason is the ability of non-thermal neutrons to penetrate most shielding materials. The effect of shielding materials is not dealt with in this work.

The interrogating neutron flux should be of low enough energy not to perturb the detection of fast fission neutrons in the PSD analysis. In this chapter we intend to investigate if meaningful 2 and 3-fold coincidences can be observed. For this purpose the interrogating neutron spectrum achieved 55 μs after the 14-MeV burst (Figure 2) is useful.

Figure 8 shows results of the epi-thermal neutron interrogation of the same set of CBNM samples as for the thermal interrogation. The results show the same trend as in Figure 5 with the exception that the depleted uranium sample (0.31% enrichment) gives a neutron coincidence response even lower than the empty container. A plausible explanation for this effect is perhaps found in the additional complications of epi-thermal interrogation, which is not the case for thermal interrogation, namely the competing neutron capture cross-section in addition to the induced fission cross-section in the resonance region.

The 3-fold coincidence response to epi-thermal interrogation (not shown) has a similar trend as for the thermal interrogation depicted in Figure 6. But also in this case, as in Figure 8, the capture reaction seems to dominate fission for low ^{235}U concentrations.

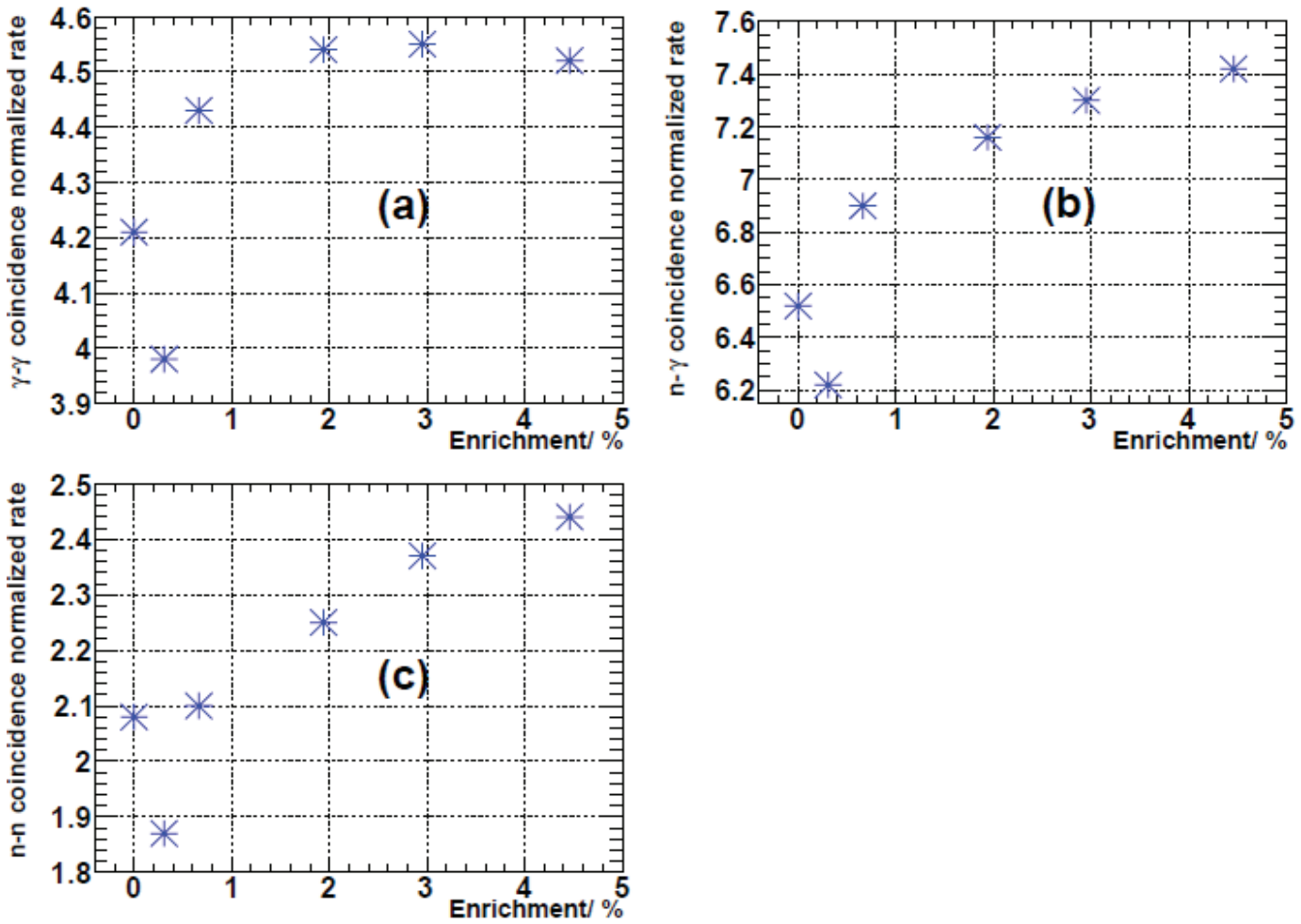

Figure 8: Epi-thermal neutron interrogation producing 2-fold coincidences of different kinds: γ-γ (a), γ-n (b) and n-n(c) for the CBNM uranium standards and the empty CBNM container**.**

Figure 9 shows the neutron capture cross-section data for the only elements in the CBNM samples: ^{235}U, ^{238}U and aluminium, as well as the fission cross-section for the two U isotopes. The interrogating epi-thermal spectrum of Figure 2 is also indicated. Aluminium appears not to play any role in the interrogation of the CBNM samples. The resonance capture in both ^{235}U and ^{238}U seem to play a role in reducing the neutron flux available for inducing fission in the ^{235}U. Fission in ^{238}U is excluded during the epi-thermal interrogation.

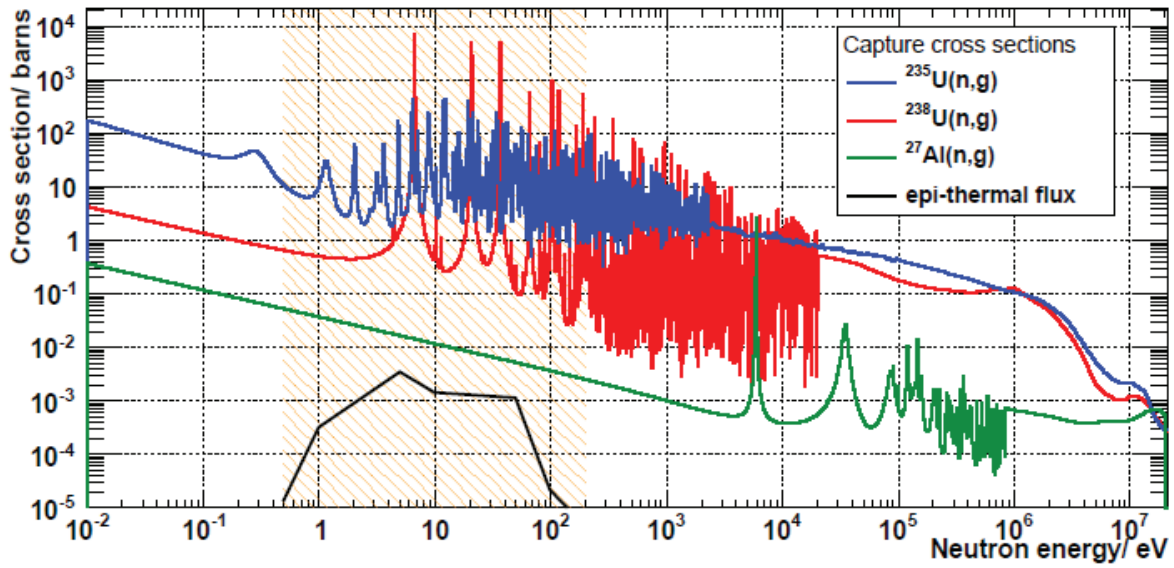

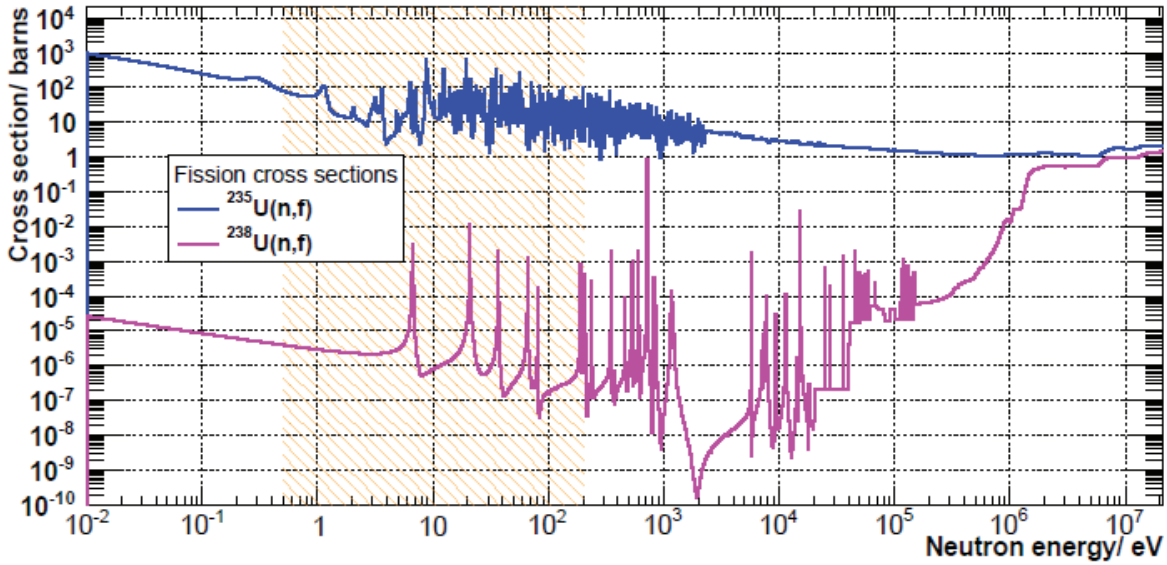

Figure 9: Capture cross-sections for ^{235}U, ^{238}U and aluminium (top), and fission cross-section for ^{235}U and ^{238}U (bottom) as function of neutron energy. In both pictures the energy range of the PUNITA epi-thermal neutron flux is highlighted.

In an attempt to better understand the behavior seen in Figure 8 MCNP5 simulations of the neutron flux inside the CBNM samples during the epi-thermal interrogation were carried out. In Figure 10 the simulated neutron flux in the sample has been divided into total and low-energy flux. The low-energy neutron flux decreases as function of the enrichment due to capture in both U isotopes and fission in ^{235}U, whereas the total (mainly fast flux) increases due to the production of fast fission neutrons. The behaviour of the total (fast) flux seems to agree with the observation of 2-fold (and 3-fold, not shown) coincidences with a neutron component (Figure 8). As for the thermal interrogation, a complete understanding of the detected coincidences would require simulations that include the response of the detectors.

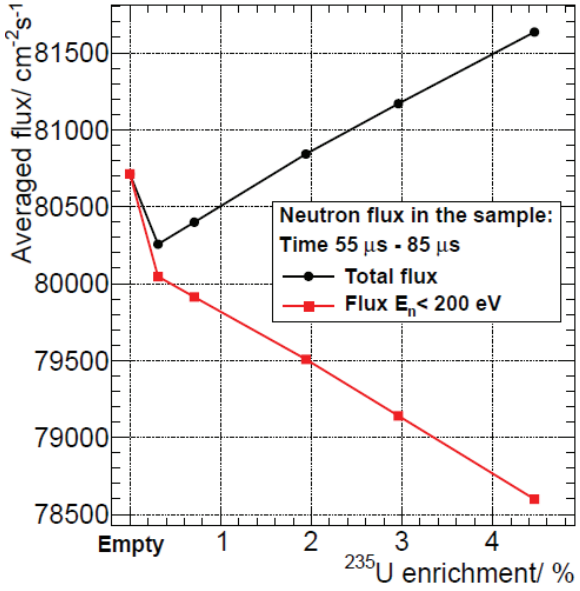

Figure 10: MCNP5 Simulation of the neutron flux inside a CBNM sample of simplified geometry and variable enrichment placed in the centre of the PUNITA cavity at the indicated time following the 14 MeV burst. The low-energy component, responsible for almost all fission events, is shown separately.

4. Conclusions

We have investigated the use of neutron interrogation combined with the detection of neutron coincidence events from induced fission as a method for detection of SNM. As an active method this concerns all kinds of SNM containing fissile isotopes. The detection system consists of multiple liquid scintillation detectors which allows to identify fast neutron interactions by means of the PSD analysis. Due to the fast response of these detectors, very short coincidence gates can be applied for the detection of the coincident prompt fission neutrons. These coincidence events are evidence of fission and consequently proof of the presence of fissile material in the object under investigation. A strong point of this method is the fact that the low energy interrogating neutron flux does not affect the response from the sample in the detection system (when considering neutron coincidence events).

In the present work we investigated the practicality of this detection method by using three detectors in the PUNITA pulsed neutron facility. Results from interrogation with thermal and epi-thermal neutrons were compared. By assaying a series of CBNM standards with variable ^{235}U concentration the neutron coincidence response showed a dependence on the fissile mass which is similar to that achieved by the high efficiency ^{3}He based neutron detection system. Although the data achieved so far are preliminary, this fact gives confidence that the method can work even in an up-scaled configuration.

More experimental work is needed to provide confidence in the method and to determine actual detection limits, to improve the experimental setup (e.g. by applying a higher number of scintillation detectors), and to improve the performance of the PSD algorithm in view of the high counting rates during the neutron interrogation.

The interrogation by epi-thermal neutrons is worthwhile to investigate further as the mpore penetrating neutron source can overcome a larger variety of shielding attempts thus making it potentially interesting for practical applications. The epi-thermal interrogation however will not have as good a detection limit as the thermal interrogation due to the higher ratio of capture to fission reactions in the epi-thermal range. More work is needed to quantify these competing effects both for bare samples and for samples embedded in matrix materials.

5. References

[1] Enqvist A, Flaska M, Dolan J L, Chichester D L, Pozzi S A; *A combined neutron and gamma-ray multiplicity counter based on liquid scintillation detectors;* Nucl. Instr. Meth. A; 652; 2011; p. 48-51.

[2] Jallu F, Loche, F; *Improvement of non-destructive fissile mass assays in α low-level waste drums: A matrix correction method based on neutron capture gamma-rays and a neutron generator;* Nucl. Instr. Meth. B; 266(16); 2008; p. 3674-3690.

[3] Ferrari F, Peerani P; *Performance of an active well coincidence counter for HEU samples; Rad. Meas*.; 45(9); 2010; p. 1034-1043.

[4] Caldwell J T et al; *The Los Alamos second generation system for passive and active neutron assays of drum-size containers*; LA-10774-MS, Los Alamos National Laboratory; 1986.

[5] Chard P M J and Croft S; *Preliminary investigation of active neutron coincidence counting in Differential Die-Away assay*; Proceedings of the 7th Conference on Radioactive Waste Management and Environmental Remediation; Nagoya, Japan; 26-30 September 1999; ICEM '99 CD ROM ISBN 0-7918-1966-3; Session 32; Paper 3.

[6] Pozzi S A, Clarke S D, Flaska,M, Peerani P; *Pulse-height distributions of neutron and gamma rays from plutonium-oxide samples*; Nucl. Instr. Meth. A; 608(2); 2009; p. 310-315.

[7] Clarke S D, Flaska M, Pozzi S A, Peerani P; *Neutron and gamma-ray cross-correlation measurements of plutonium oxide powder*; Nucl. Instr. Meth. A; 604(3) 2009; p. 618-623.

[8] Ocherashvili A, Roesgen E, Beck A, Caspi E N, Mosconi M, Crochemore J M, Pedersen B; *SNM detection by means of thermal neutron interrogation and a liquid scintillatotion detector*; JINST, 7 CO3037, 2012

[9] Favalli A, Pedersen B; *Design and characterisation of a pulsed neutron interrogation facility*; Rad. Prot. Dos.; 126(1-4); 2007; p.74-77.

[10] Favalli A, Mehner H-C, Crochemore J-M, Pedersen B; *Pulsed Neutron Facility for Research in Illicit Trafficking and Nuclear Safeguards*; IEEE Transactions on Nuclear Science; 56(3); 2009; p. 1292-1296.

[11] http://www.detectors.saint-gobain.com/uploadedFiles/SGdetectors/Documents/Product_Data_Sheets/BC501-501A-519-Data-Sheet.pdf

[12] X-5 Monte Carlo Team Diagnostics Applications Group Los Alamos National Laboratory; *MCNP – A general Monte Carlo N-Particle Transport Code, Version 5, Volume I: Overview and Theory;* LA-UR-03-1987; 2003; Los Alamos National Laboratory

[13] MATLAB 7.0 and Statistics Toolbox 7.1, The MathWorks, Inc., Natick, Massachusetts, United States.

[14] http://www.caen.it/csite/CaenProd.jsp?parent=39&idmod=770

[15] Marrone S, Cano-Ott D, Colonna N, Domingo C, Gramegna F, Gonzalez E M, Gunsig F, Heil M, Käppeler F, Mastinu P F, Milazzo P M, Papaevangelou T, Pavlopoulos P, Plag R, Reifarth R, Tagliente G, Tain J L, Wisshak K; *Pulse shape analysis of liquid scintillators for neutron studies*; Nucl. Instr. Meth. A; 490; 2002; p 299-307.

[16] Aspinall M D, D'Mellow B, Mackin R O, Joyce M J, Jarrah Z, Peyton A J;*The empirical charachterization of organic liquid scintillaton detectors by the normalized average of digitized pulse shapes*; Nucl. Instr. Meth. A; 578; 2007; p 261-266.

[17] Carpenter B S, Gramlich J W, Greenberg R R, Machlan L A, DeBievre P, Eschbach H L, Meyer H, Van Andenhove J, Connelly V E, Trahey N M, and Zook A*; Standard Reference materials: Uranium 235 Isotopic Abundance Standard Reference Materials for Gamma Spectrometry Measurements*; National Bureau of Standards Special Publication 260-96; U.S. Government Printing office Washington; 1986.

Development of a reference spent fuel library of 17x17 PWR fuel assemblies

Riccardo Rossa[1,2], Alessandro Borella[1], Klaas van der Meer[1]

1. Studiecentrum voor kernenergie - Centre d'etude de l'energie nucleaire (SCK•CEN)
2. Université libre de Bruxelles (ULB)

Emails: rrossa@sckcen.be, aborella@sckcen.be, kvdmeer@sckcen.be

Abstract:

One of the most common ways to investigate new Non-Destructive Assays (NDA) for the spent fuel assemblies are Monte Carlo simulations. In order to build realistic models the user must define in an accurate way the material compositions and the source terms in the system.

This information can be obtained using burnup codes such as ORIGEN-ARP and ALEPH2.2, developed at SCK•CEN. These software applications allow the user to select the irradiation history of the fuel assembly and to calculate the corresponding isotopic composition and neutron/gamma emissions as a function of time.

In the framework of the development of an innovative NDA for spent fuel verifications, SCK•CEN built an extensive fuel library for 17x17 PWR assemblies, using both ORIGEN-ARP and ALEPH2.2. The parameters considered in the calculations were initial enrichment, discharge burnup, and cooling time. The combination of these variables allows to obtain more than 1500 test cases.

Considering the broad range of the parameters, the fuel library can be used for other purposes apart from spent fuel verifications, for instance for the direct disposal in geological repositories.

In addition to the isotopic composition of the spent fuel, the neutron and photon emissions were also calculated and compared between the two codes. The comparison of the isotopic composition showed a good agreement between the codes for most of the relevant isotopes in the spent fuel. However, specific isotopes as well as neutron and gamma spectra still need to be investigated in detail.

Keywords: Spent Fuel; PWR; ORIGEN-ARP; ALEPH2.2

1. Introduction

Spent fuel is characterized by a very high neutron and gamma emission due to the spontaneous fission of heavy nuclides and radioactive decay of fission products that have been produced during irradiation. The irradiation in the reactor produces numerous fission products and actinides that make the resulting isotopic composition and associated gamma spectra particularly complex [1]. Considering the high neutron and gamma field together with the significant heat coming from the decay of the fission products and actinides, the spent fuel is generally stored under water in a spent fuel pool and it is not directly accessible by the safeguards inspectors. Given the characteristics listed above, the spent fuel can be considered as one of the most difficult materials to verify during an inspection.

Non-destructive assays (NDA) are one of the possible methods to verify the spent fuel and several research projects are trying to improve their current capabilities [2],[3]. One of the ways to investigate new NDA for the spent fuel assemblies are Monte Carlo simulations. In order to build realistic models the user must define in an accurate way the material compositions and the source terms in the system. Therefore an effort was made to define a spent fuel library that serves as reference to benchmark the performances of the measurements methods under investigations.

The goals of this preliminary work are therefore twofold. The first one is to understand how the irradiation history of the fuel influences its isotopic composition (and consequently its neutron and gamma source strength). The second one is to generate automatically several input cards compatible with the MCNPX [4],[5] code that will be used in the study of innovative NDA techniques. To achieve both goals the spent fuel needs to be characterized in terms of isotopic composition, neutron and gamma emission (both source intensity and energy spectrum).

Section 2 of this paper describes the main features of ORIGEN-ARP and ALEPH2.2, the two codes used for the simulations, together with a brief explanation on the models that have been incorporated in both codes.

The third section gives an overview of the main structure of the spent fuel library and of the range of the parameters used to create it (initial enrichment, burnup, and cooling time). This section contains the main results obtained with the ORIGEN-ARP simulations. The neutron emissions are separated into the two main components (α,n reactions and spontaneous fissions) and the total values are plotted against initial enrichment (IE), burnup (BU) and cooling time (CT). In addition, the role of individual isotope is studied to understand how the composition of the spent fuel influences the neutron emissions.

A comparison between the results obtained with ORIGEN-ARP and ALEPH2.2 is carried out in section 4. Both the

neutron emissions and nuclide concentrations calculated by the two codes are evaluated as a function of the burn-up and cooling time.

Section 5 considers some parameters (e.g. boron concentration in the water) that have an impact on the final results of the simulations. The impact is estimated both in terms of neutron emissions and nuclide concentration. This chapter is based on the results of ALEPH2.2 simulations, since with this code the user can completely define the geometry and material composition of the system.

The libraries built with the two codes are compared in section 6 with the spent fuel reference library developed by the Los Alamos National Laboratory (LANL). This comparison considered the data of the total neutron emission and of four neutron emitters (two Cm isotopes and two Pu isotopes) of three corresponding cases (i.e. simulations with the same IE, BU, and CT).

The conclusions at the end of the document summarize the main results coming from the simulations, highlighting the main factors behind the change in the neutron and gamma emission and isotopic composition of the spent fuel.

2. Computational models used for the calculations

The study of the time evolution of the nuclear fuel generally requires the combination of computer codes to model the neutron transport in the reactor and to predict the fuel composition due to the radioactive decay of its isotopes.

Two different codes have been used to perform the simulations: ORIGEN-ARP and ALEPH2.2.

The first code uses a set of pre-compiled averaged cross section values (called ORIGEN-ARP cross section library) as input to the depletion calculation. This procedure avoids the time consuming neutron transport and therefore leads to the strong reduction in the computational time required for the simulations.

The second code uses a statistical approach (Monte Carlo method) for the calculation of the neutron transport and then performs the fuel depletion. By using the Monte Carlo code MCNP(X), ALEPH2.2 retains the great flexibility in the definition of the system (geometry, materials) and in the nuclear data used in the simulation. As a drawback the computational time can be significantly longer than in the case of ORIGEN-ARP.

The simulations with ORIGEN-ARP generally took less than one minute to complete with a regular portable PC. Most of the time was spent by the user in the selection of the input parameters.

The computational time required by the simulations with ALEPH-2.2 strongly depends on the statistics requested by the user (i.e. the parameters of the kcode used as source term) and by the burnup of the assembly. By using a cluster with 16 cpus, the fastest case was the one of 5 GWd/tU and took about 2 hours to complete, whereas the case with 70 GWd/tU took almost 5 days.

2.1 ORIGEN-ARP

The first code used to generate the fuel library is ORIGEN-ARP [6] and it is part of the SCALE package [7] that is developed by Oak Ridge National Laboratory (ORNL).

ORIGEN-ARP employs a graphical user interface (GUI) to select several characteristics of the fuel assembly. The PWR 17x17 (w17x17) case has been chosen considering its worldwide use in the nuclear power plants. The GUI is composed of several menus that are shown subsequently when all parameters in one window have been introduced and validated by the user.

Apart from the type of fuel geometry, the first window (*"Express"*) contains other parameters as follows:

- all results are normalized to 1 ton of uranium;
- the average power is set to 40 MW/tU. This value is taken from [8] and results in a burnup of 14.4 GWd/tU for a cycle of 360 days;
- the moderator density is the default value of 0.723 g/cm^3.

The next section is the *"Composition"* window:

- the abundances of the uranium isotopes are the default values proposed by ORIGEN-ARP depending on the initial enrichment selected in the previous section;
- oxygen was added to the list of isotopes in the fresh fuel in order to model the UO_2 material in the fuel pin. The natural isotopic composition was selected with a concentration of 134500 g/t.

The section *"Neutron"* allows selecting the energy-group structure for the neutron source spectra. The "238-group ENDF5" is the option chosen in the calculation. This group structure extends from 10^{-5} eV up to 20 MeV. This section determines only the division of the energy groups and does not select the data library used by the code for the nuclear data.

At the same way, the photon emissions are treated according to a 74-group library defined by the user. The group structure extends from 10 keV up to 10 MeV.

The most extensive section in the ORIGEN-ARP interface is the *"Cases"* windows, where the user selects the characteristics of the irradiation history. All simulations for the fuel library consider irradiation cycles of maximum 360 days, after which the fuel assembly undergoes a decay period of 30 days. The duration of the last irradiation cycle is adapted to reach the desired level of burnup at the discharge. Following this procedure, the fuel assembly is exposed to the same power level during all cycles in the reactor. After the final unloading from the reactor (i.e. the last irradiation cycle is completed), the ORIGEN-ARP calculation considers 30 cooling

times to compute the isotopic composition and both neutron and gamma emissions.

Other options selected in ORIGEN-ARP are:

- no cutoff is selected for the composition so all the isotopes are reported in the output file;
- output precision is 6 digits for the values of the mass concentrations;
- output precision is 4 digits for the neutron and gamma emission;
- the fuel matrix for the (α,n) evaluation is the UO_2;
- bremsstrahlung is not considered in the model.

2.2 ALEPH2.2

ALEPH is the Monte-Carlo burn-up code being developed by SCK•CEN since 2004 [9]. The code belongs to the category of shells coupling Monte Carlo particle transport codes and deterministic depletion algorithms.

The fuel assembly model considered in ALEPH2.2 tries to be identical to the case considered with ORIGEN-ARP. The geometry is the same as the PWR 17x17 fuel assembly modelled in ORIGEN-ARP (Table D1.A.3 of [6]), with the exception that the active length is reduced to 1 meter. It has been supposed that there is no water gap between neighbouring assemblies and this has been simulated placing reflecting surfaces around the fuel assembly.

The irradiation history is defined in terms of irradiation power (MW), length of the irradiation step (days), and length of the decay step (days, years). All these parameters are chosen to have the same conditions as those used for the ORIGEN-ARP simulations.

Other parameters in the input files are:

- the geometry of the fuel assembly (pin radius and pitch) and the initial composition of the fuel is the same as the ORIGEN-ARP simulations;
- the fuel temperature is 900 K;
- the cladding temperature is 620 K;
- the moderator temperature is 575 K (with a density of 0.723 g/cm^3);
- the water contains 630 ppm of Boron (according to abundances of ^{10}B and ^{11}B). This is the average Boron concentration reported in ORIGEN-ARP (Table D1.A.3 in Ref. [6]); this value is kept constant during the irradiation simulations in ALEPH2.2.
- each irradiation step runs a kcode with 5000 particles and an initial value for k_{eff}=1.16. The k_{eff} of the assembly is calculated taking the average value of 100 cycles, neglecting the first one from the calculations;
- the neutron source is modeled as a Watt fission spectrum with the parameters of the neutron-induced fission of ^{235}U [4].

3. Main characteristics of the fuel library

The reference spent fuel library has been developed using three variables to take into account the most representative irradiation histories of the spent fuel. In particular:

- Initial enrichment (IE): 4 values from 3.5% to 5.0%, with increments of 0.5%
- Discharge burnup (BU): 14 values from 5 up to 70 GWd/tU, with increments of 5 GWd/tU
- Cooling time (CT): 30 values ranging from immediate discharge up to 3 million years

The combination of these parameters allows to obtain 1680 different compositions and source terms.

This fuel library does not consider the element history in the reactor core (location, different length of outages, different power level during irradiation). Future work will refine the results obtained at this stage and investigate these factors.

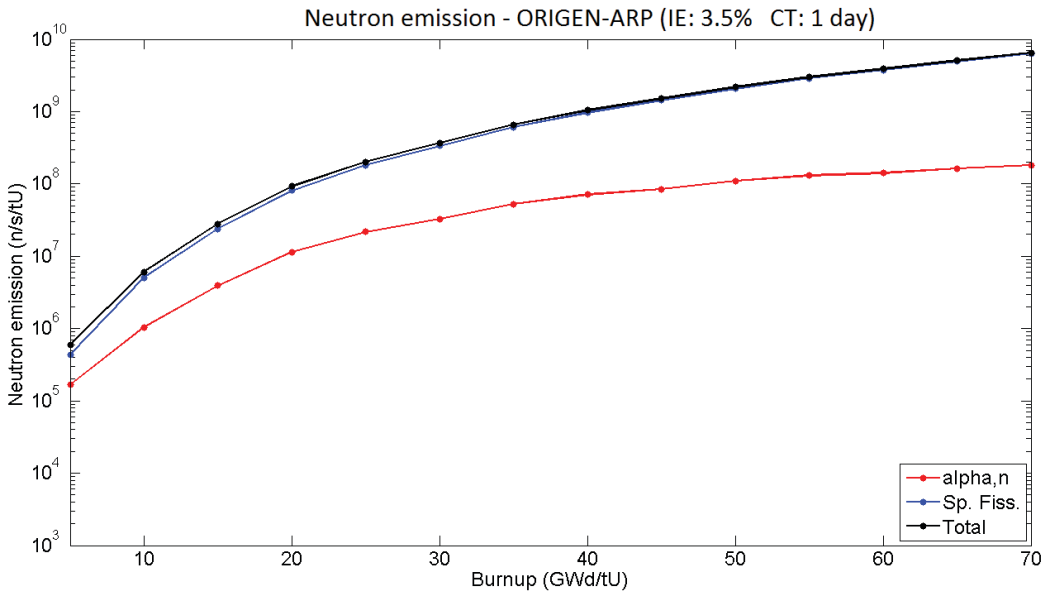

Figure 1: Neutron emission as a function of the burnup for a 17x17 PWR spent fuel assembly with initial enrichment of 3.5% and cooling time of 1 day. The contributions due to (alpha,n) and spontaneous fission reactions as well as the total neutron emission are shown.

Figure 1 shows the neutron emissions as a function of the burnup. The data have been calculated with ORIGEN-ARP, with a fuel of 3.5% initial enrichment and after a cooling time of 1 day. The plot reveals that the spontaneous fission is the main source for the neutron emission after a short cooling time. This fact needs to be evaluated also with higher cooling times.

In order to do so, Figure 2 shows the neutron emission as a function of cooling time for the burnup value of 10 GWd/tU.

The contribution from (α,n) reactions is generally one order of magnitude lower than the term due to spontaneous fission. The only exception is for burnup of 10 GWd/tU with cooling times between 30 and 300 years (Figure 2). For these combinations the two contributions are similar, with cases where the (α,n) reactions have the dominant role on the neutron emission.

Looking at Figure 2, there is a clear increase of the (α,n) contribution around 100 years of cooling time. This is due to the build-up of ^{241}Am from ^{241}Pu (half-life of 14.4 years). The same effect is present also at higher burnup, but it is not visible due to the higher neutron emission that conceals this contribution.

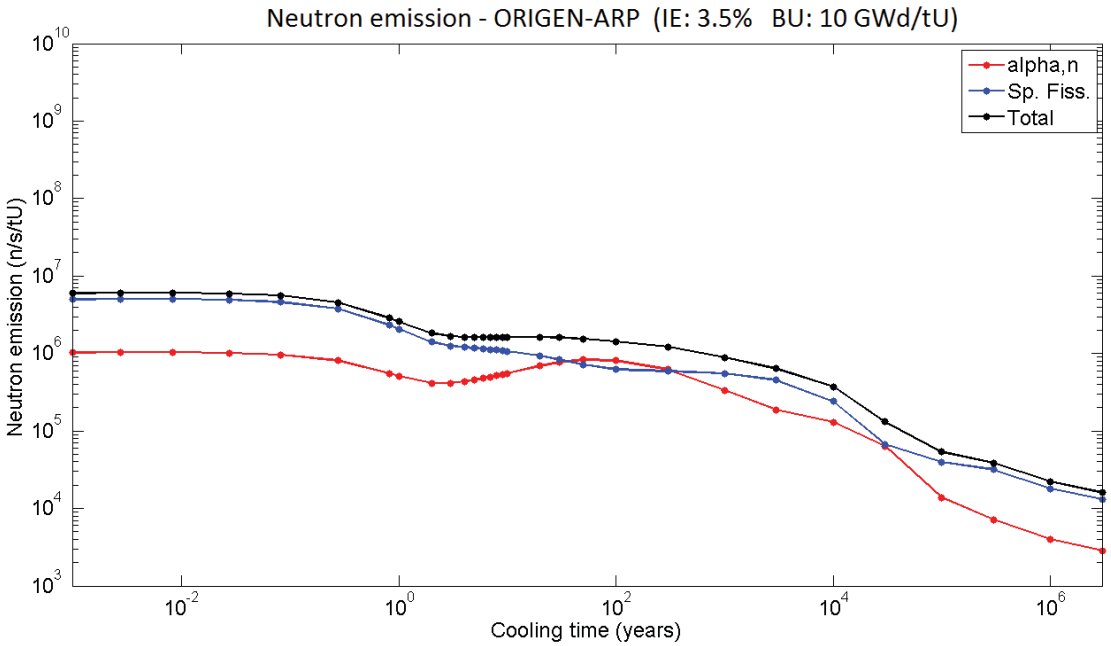

Figure 2: Neutron emission as a function of the cooling time for a 17x17 PWR spent fuel assembly with initial enrichment of 3.5% and discharge burnup of 10 GWd/tU. The contributions due to (alpha,n) and spontaneous fission reactions as well as the total neutron emission are shown.

In order to refine the study it is important to understand the role of each isotope in the total neutron emission. Figures 3 and 4 show the percentage of the total neutron emission due to each isotope as a function of cooling time.

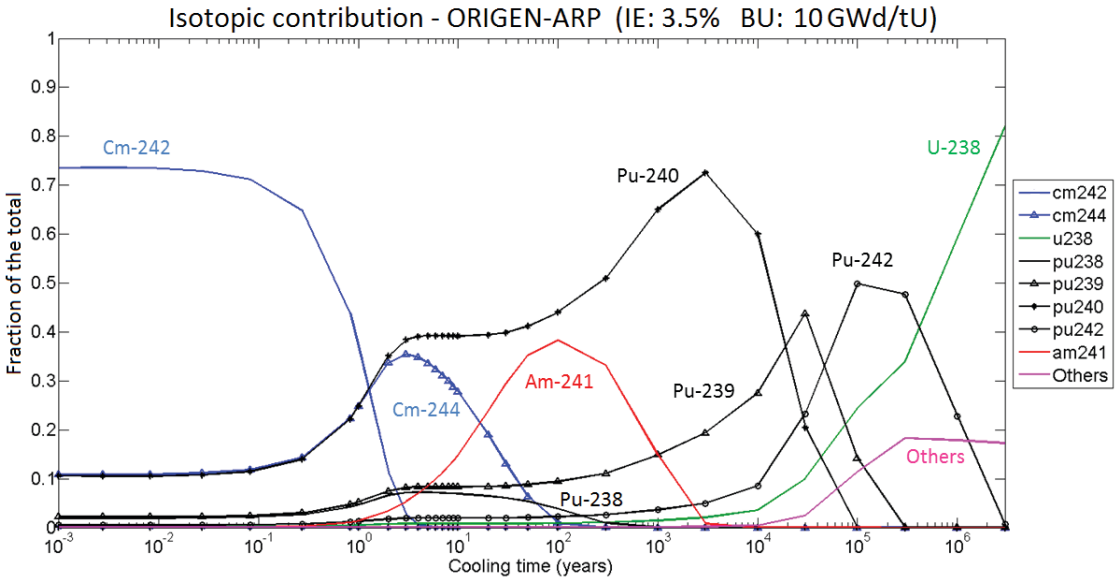

Figure 3: Fraction of the total neutron emission due to a set of isotopes as a function of the burnup for a 17x17 PWR spent fuel assembly with initial enrichment of 3.5% and discharge burnup of 10 GWd/tU. The contributions due to specific isotopes and the sum of all remaining isotopes ('Others') are shown.

Both for Figure 3 and 4 there are 11 isotopes that are responsible for about 99% of the total neutron emission (the value 'Others' is relevant only for cooling times higher than 10000 years).

At low burnup the ^{242}Cm is the main responsible for the neutron emission up to 100 days, a role that is taken then by ^{244}Cm and several plutonium isotopes. Another relevant contribution comes from ^{241}Am (as it has been suggested from the peak in Figure 2). Other curium isotopes are not present at low burnup values because the short irradiation time did not allow the build-up of these high-Z isotopes.

With a burnup of 35 GWd/tU (Figure 4) two isotopes of curium (^{242}Cm and ^{244}Cm) are responsible for basically all neutron emissions up to a few years of cooling time, but opposite to Figure 3 now ^{244}Cm is the main actor. Increasing the cooling time another Cm isotope (^{246}Cm) has an impact on the total neutron emission because the other previous isotopes have short half-lives. Other contributions come from ^{241}Am, ^{240}Pu, and ^{242}Pu.

The latter isotope is the main responsible for the neutron emission in the long term, together with ^{238}U, and a list of other isotopes (indicated as 'Others'). One must bear in mind that the magnitude of the emission for high cooling times is very low compared to the value at the discharge and this is the reason why many isotopes have a non-negligible role for long cooling times.

Increasing the burnup to 60 GWd/tU there are small differences to the case of 35 GWd/tU. ^{244}Cm takes an even higher contribution for the short cooling times, as well as ^{246}Cm for intermediate values. At very high cooling time ^{248}Cm appears to be important along with ^{242}Pu and ^{238}U.

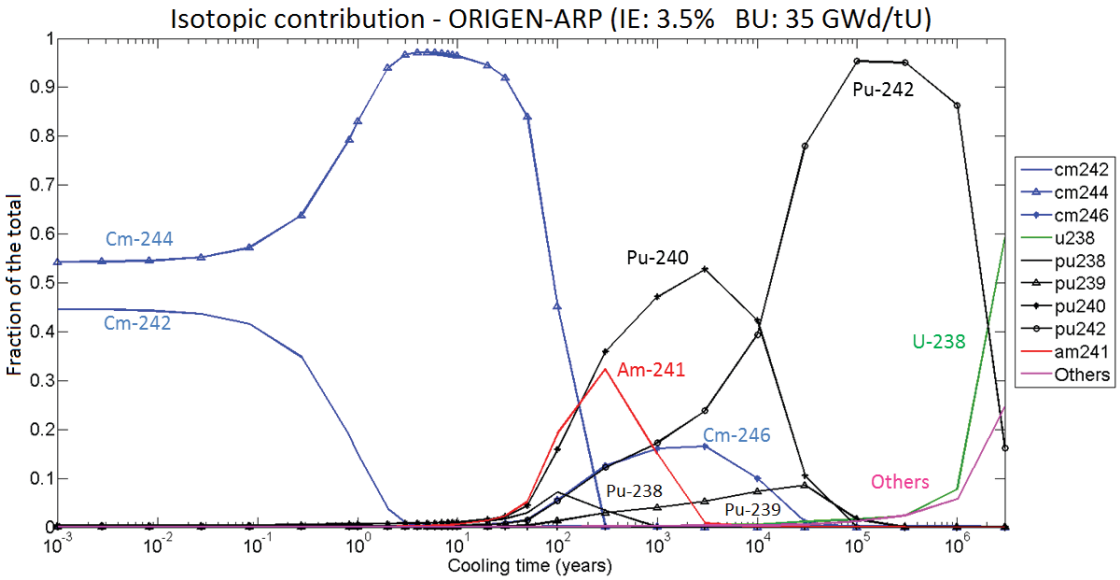

Figure 4: Fraction of the total neutron emission due to single isotopes as a function of the burnup for a 17x17 PWR spent fuel assembly with initial enrichment of 3.5% and discharge burnup of 35 GWd/tU. The contributions due to specific isotopes and the sum of all remaining isotopes ('Others') are shown.

The analysis so far focused on the influence of burnup (BU) and cooling time (CT) on the neutron emissions. Since the initial enrichment (IE) plays also a role, the next part investigates this variable. Figure 5 shows the ratios of the total neutron emission as a function of the burnup for the enrichments considered in the simulations.

By looking at the magnitude of the difference between the enrichment values, it seems that this variable plays a minor role in the determination of the neutron emission compared to burnup and cooling time. In fact, while by changing the burnup the neutron flux value varies of more than one order of magnitude, the maximum difference with the initial enrichment is of less than a factor 3.

The origin of the peak observed in Figure 5 can be explained by looking at Figure 6. This plot shows the ratio of the total neutron emissions after a cooling time of 10 years. In addition to the curve 'Total' (that is the same of the curve '3.5/5.0' of Figure 5) also the ratios for specific isotopes are added. The curve related to the single isotopes is calculated taking the ratio between the neutron emission due to this isotope at 3.5% initial enrichment and the total neutron emission at 5.0%

It is clear that the shape of the curve 'Total' is determined by the one of ^{244}Cm at burnup higher than 30 GWd/tU, while at lower burnup mainly ^{239}Pu, ^{240}Pu, and ^{241}Am determine the shape of the curve.

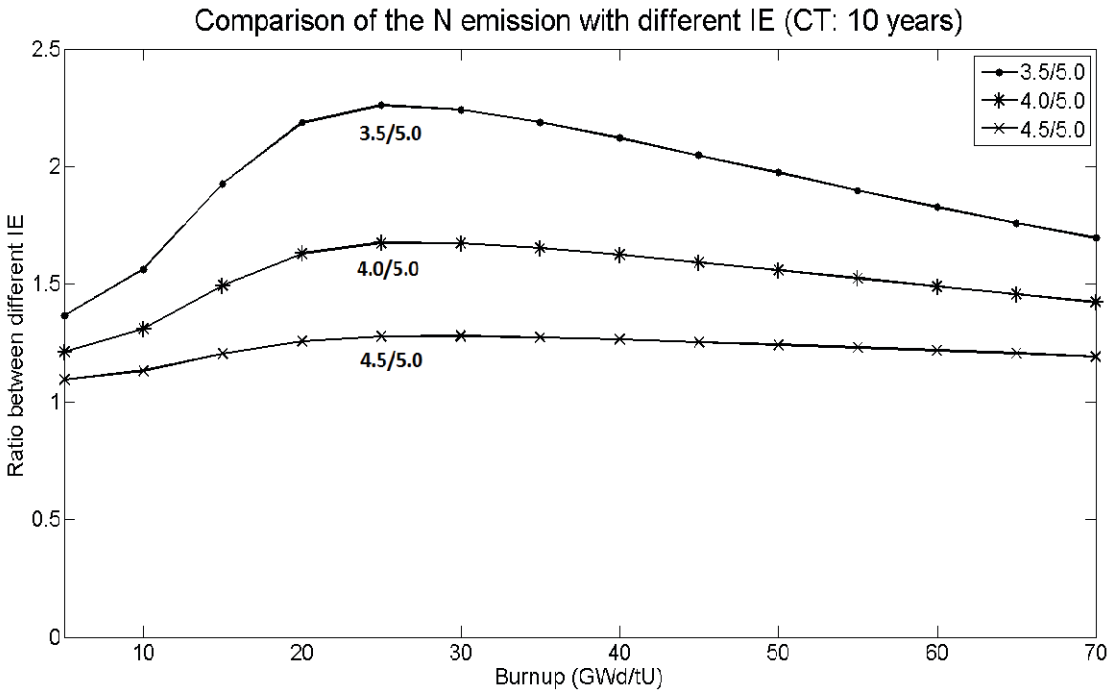

Figure 5: Ratio of total neutron emissions for different enrichments as a function of the burnup for a 17x17 PWR spent fuel assembly with cooling time of 10 years. The initial enrichments used for the ratio are indicated close to the corresponding curve.

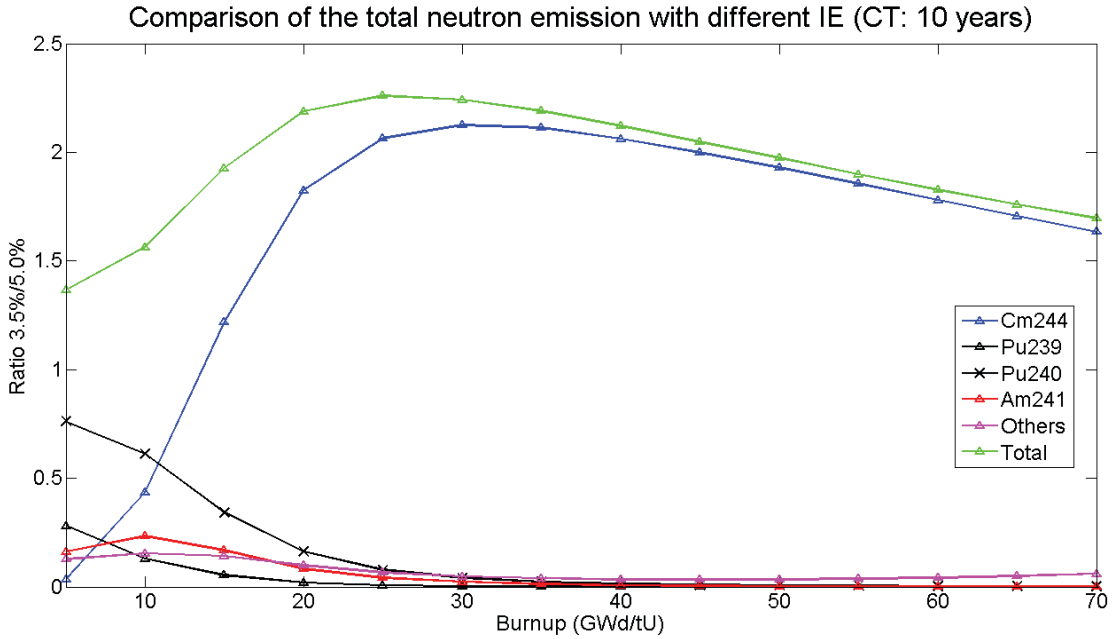

Figure 6: Total neutron emission with different initial enrichments – role of selected isotopes (CT: 10 years). The green curve ('Total') is the same of Figure 5 ('3.5/5.0'). The curves relative to single isotopes are calculated taking the ratio between the neutron emission due to the specific isotopes in the case of fuel with 3.5% initial enrichment and the total neutron emission at 5.0% initial enrichment.

4. Comparison of the two codes

The next step is to compare the two codes used to generate the spent fuel library. The set of simulations in the codes used the same values of:

- IE, BU, and CT;
- average power during irradiation;
- radius of the fuel pin, cladding, and pitch between neighbouring pins;
- boron concentration in the water.

The impact of the boron concentration, the water gap between the assemblies, and the data library on the final results will be investigated in the next section.

Each code applies a different normalization unit for the calculated data (t_U for ORIGEN-ARP and cm^3 for ALEPH2.2). In order to compare the two codes it is necessary to renormalize one of the two to have the same measurement unit in all simulations.

Figure 7 compares the results of ORIGEN-ARP and the ones coming from ALEPH2.2 in relative terms. The fuel used in these simulations had an initial enrichment of 3.5%. ORIGEN-ARP always yields a lower value of emissions compared to ALEPH2.2. The ratio of the values coming from the two codes remains rather constant around 0.95 with the burnup. The only exception is at 100 years of cooling time, where there seems to be a decreasing trend for burnup higher than 40 GWd/tU.

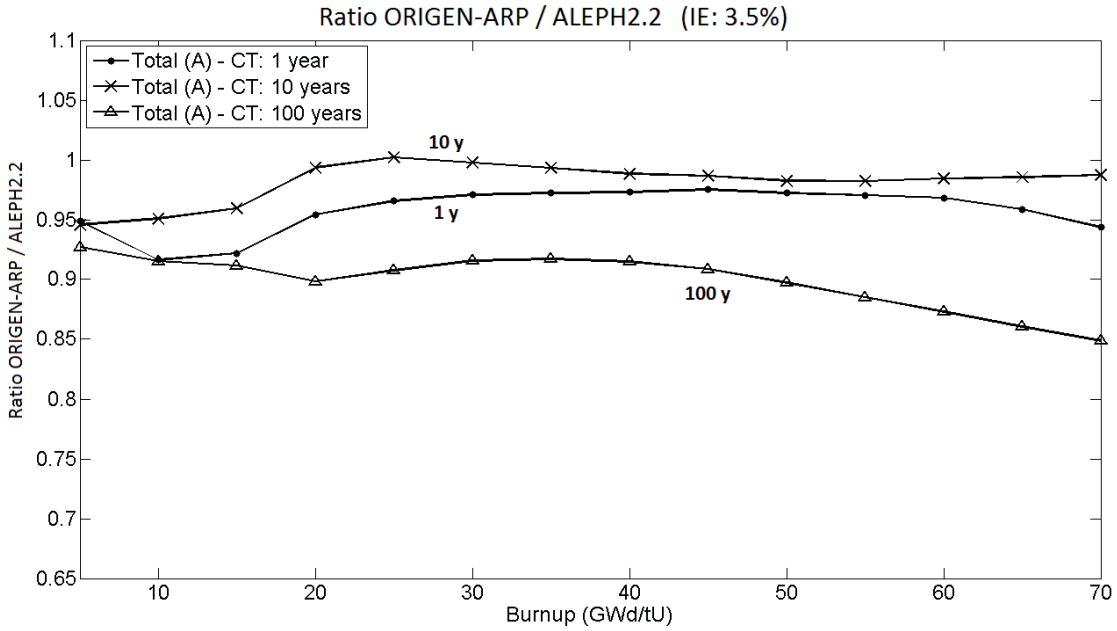

Figure 7: Ratio of the total neutron emission as a function of the burnup. The plot shows the ratio between the total neutron emission calculated by ORIGEN-ARP and ALEPH2.2 for fuel with a 3.5% initial enrichment and 1, 10, and 100 years of cooling time.

A comparison of the nuclides concentrations obtained by the two codes has been made in order to understand the reason of the difference in the neutron emissions. The following table shows the ratio between the concentrations of selected nuclides as a function of the burnup. The isotopic compositions are calculated at direct discharge.

Table 1 shows that the mass concentrations of the main neutron emitters calculated by ORIGEN-ARP are usually lower compared to the results obtained with ALEPH2.2.

The fact that ^{242}Cm and ^{244}Cm are responsible for over 90% of the neutron emission up to few years of cooling time, explains the lower neutron emission calculated with ORIGEN-ARP. The values in the table follow the same trend independently from the initial enrichment of the fuel.

Isotope / BU (GWd/tU)	cm242	cm244	cm246	cm248	u235	u238	pu238	pu239	pu240	pu241	pu242	am241
5	0.862	1.126	0.875	0.870	0.996	1.000	1.101	1.012	1.024	1.046	1.091	1.052
10	0.828	1.005	0.740	0.697	0.991	1.000	1.046	1.000	0.997	1.063	1.071	1.049
15	0.840	0.978	0.698	0.645	0.987	1.001	1.023	0.995	0.976	1.068	1.079	1.079
20	0.857	1.007	0.732	0.669	0.981	1.001	1.004	1.000	0.990	0.993	1.054	1.076
25	0.845	1.007	0.737	0.693	0.976	1.001	0.985	1.001	0.991	0.990	1.018	1.057
30	0.838	0.998	0.724	0.696	0.970	1.002	0.966	1.004	0.988	0.991	1.003	1.054
35	0.841	0.990	0.720	0.685	0.965	1.002	0.949	1.005	0.995	0.969	0.996	1.073
40	0.845	0.982	0.704	0.683	0.960	1.002	0.932	1.006	0.995	0.971	0.983	1.080
45	0.846	0.979	0.690	0.675	0.956	1.003	0.916	1.009	0.994	0.970	0.976	1.082
50	0.851	0.973	0.682	0.662	0.954	1.004	0.901	1.008	0.997	0.961	0.973	1.106
55	0.858	0.971	0.672	0.653	0.953	1.004	0.885	1.009	0.998	0.963	0.965	1.118
60	0.861	0.972	0.663	0.646	0.954	1.005	0.871	1.014	0.995	0.965	0.961	1.120
65	0.866	0.972	0.657	0.637	0.958	1.006	0.857	1.013	0.998	0.963	0.958	1.145
70	0.873	0.973	0.650	0.628	0.963	1.006	0.844	1.015	0.999	0.965	0.955	1.160

Table 1: Ratio between the nuclide concentrations obtained with ORIGEN-ARP and ALEPH2.2 as a function of the burnup. The fuel had 3.5 % initial enrichment and the concentrations were taken at direct discharge from the reactor.

5. Impact of other parameters on the results

5.1 Boron concentration

Simulations with ALEPH2.2 considered cases with water without boron and with a boron concentration of 630 ppm (the same as the ORIGEN-ARP cases). In this section the impact of boron on the neutron emissions is discussed.

The neutron emissions as a function of the burnup obtained with and without boron follow the same trend as in Figure 1. The trend of the curves is very similar, but the neutron emissions are higher when boron in present. The magnitude of the boron impact can be seen in Figure 8 where the ratio between corresponding values of burnup is shown. By looking at the ratio, one can estimate that the influence of boron is within 10% of the total neutron emission.

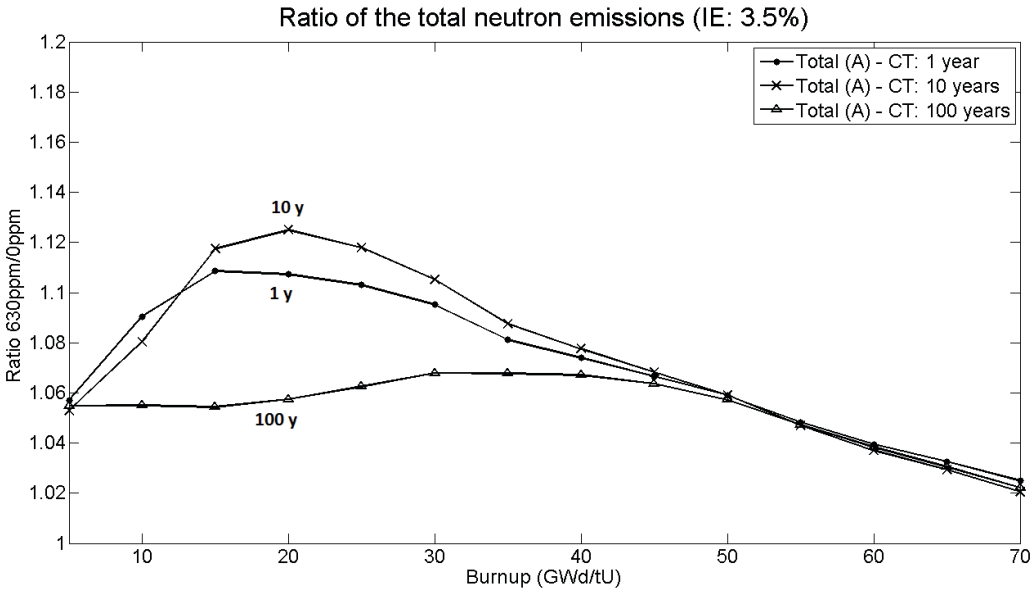

Figure 8: Influence of the boron concentration as a function of the burnup – ratio of the neutron emission. The fuel had 3.5 % initial enrichment and the ratio has been calculated for 1, 10, and 100 years of cooling time.

The presence of boron modifies the energy spectrum of the neutron flux during irradiation in the reactor. This is because boron is an absorber of thermal neutrons and therefore the contribution of epithermal neutrons to the spectrum becomes higher when boron is present in the moderator.

This induces an increase of the resonance captures and a higher production of actinides. Figure 9 shows the ratio between the mass concentration of ^{242}Cm, ^{244}Cm, and ^{240}Pu calculated with and without boron. The fuel had an initial enrichment of 3.5% and a cooling time of 10 years. Considering that the isotopes in Figure 9 are the main neutron emitters, this explains the higher neutron emission observed in the simulations with 630 ppm of boron.

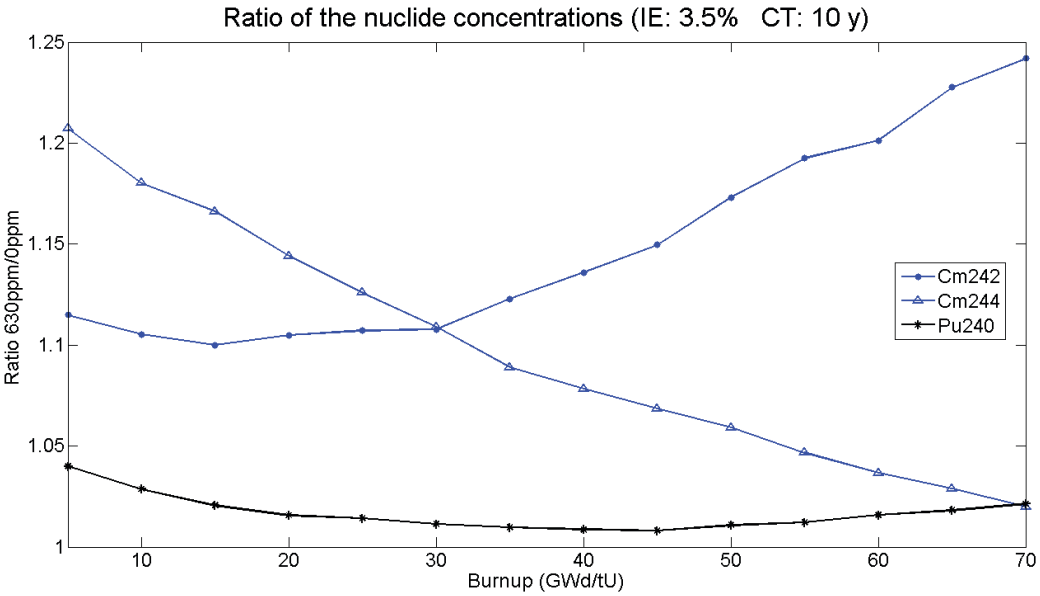

Figure 9: Influence of the boron concentration as a function of the burnup. The plot shows the ratio of the nuclide concentrations calculated with ALEPH2.2 considering fuel with 3.5% initial enrichment and 10 years of cooling time.

5.2 Water spacing between fuel assemblies

One important characteristic about the geometry of the fuel assembly is the distance between two neighbouring fuel assemblies during the irradiation in the reactor. This parameter depends on the type of fuel assembly and likely also on the particular configuration of the reactor (e.g. number of fuel assemblies in the core).

A set of simulations has been run to quantify the impact of the spacing between fuel assemblies on the concentration of the nuclides and consequently on the neutron and gamma emissions from the spent fuel. The only parameter changing in the simulations was the water spacing between the fuel assemblies (from 0 up to 10 mm). Other characteristics were:

- The initial enrichment of the fuel was 3.5%
- The discharge burnups were 10, 35, and 60 GWd/tU
- The water in the reactor had a constant boron concentration of 630 ppm.

Figure 10 shows the total neutron emission as a function of the water spacing and discharge burnup. The ratio has been calculated normalizing all values to the neutron flux without water gap between the assemblies. From the plot it is evident that the water around the assembly influences significantly the neutron emissions. Already with a water gap of 4 mm (i.e. 2 mm for each side) the total emission is altered by 5% However, this difference decreases with increasing burnup.

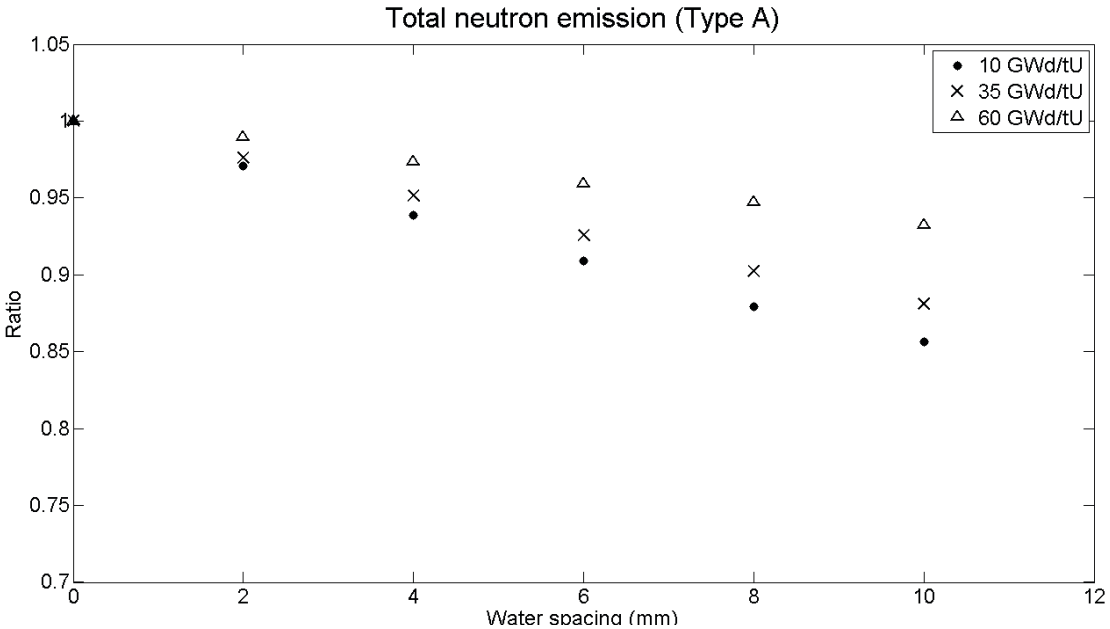

Figure 10: Total neutron emission as a function of the water spacing. The values are normalized to the case without gap between the assemblies. The fuel had 3.5% initial enrichment and the values refer to direct discharge from the reactor.

No water gap has been placed in the default simulations and this is motivated by the fact that operators try to keep uniform conditions over the whole core cross section. Therefore the pitch between outer rows of neighbouring fuel assemblies should be similar (if not equal) to the pitch of the rods within one single assembly.

5.3 Nuclear data library used in the codes

Another important parameter in the simulations is the set of data library that is used. The data libraries available in ALEPH2.2 are the ENDF/B-VII.1 [10] and JEFF-3.1.2 [11] libraries. Both libraries contain full data sets which include neutron transport data (cross sections and secondary particle emission data), radioactive decay data (which are used by the depletion module for the neutron source calculation), and fission product yields data (which are also used by the depletion module). The choice of the library influences the results because of the different values for the evaluated nuclear data (e.g. nuclides cross sections) adopted in each data set.

Figure 11 shows the ratio of the neutron emissions at discharge calculated using the different libraries as a function of the burnup. The difference in the results is within 10%, with the simulations using the ENDF data library always overestimating the neutron emission compared to the calculations with the JEFF library.

ALEPH2.2 calculates the spontaneous fission neutron source in two ways: the first one generates the Watt fission spectrum of the neutrons for nuclides undergoing spontaneous fission, with the parameters taken from ORIGEN-S [9] ('Type A' curve in Figure 11); the second one calculates the source using the information stored in radioactive decay data library (ENDF/B or JEFF, 'Type B' curve in Figure 11). Usually, the two methods give close results, but a trend is observed for high burnup with the 'Type B'

calculations. The trend observed with the calculations arises because ALEPH2.2 recognizes a different set of isotopes contributing to the neutron emission from spontaneous fissions depending on the data library that is used in the calculation. The impact of the nuclides that are missing according to some data library (e.g. ^{252}Cf is not used if the data library is ENDF/B-VII.1) is not negligible and it is the reason of the trend shown in Figure 11.

It is important to mention that ALEPH is still in the development phase and there are interactions with the development team to investigate this issue.

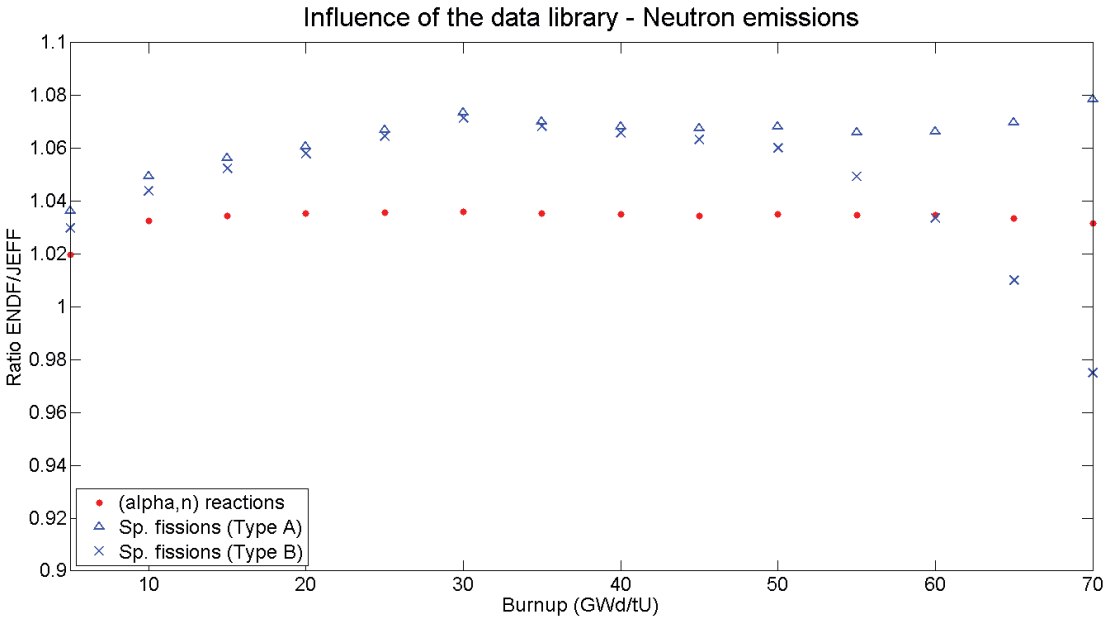

Figure 11: Ratio of the neutron emission calculated with ALEPH2.2 using different nuclear data libraries. The fuel had 3.5% initial enrichment and the values refer to direct discharge from the reactor. The contributions due to (α,n) reactions and spontaneous fission are shown.

Table 2 shows the ratio between the nuclide concentrations calculated with the two libraries available in ALEPH2.2. The values refer to the fuel with initial enrichment of 3.5% and directly after discharge.

As shown in the comparison between the two codes, also in the case of different data libraries the highest discrepancy is found for curium isotopes (^{244}Cm and ^{246}Cm). The selection of the data library influences most of isotopic concentration within 5% but also for ^{238}Pu the disagreement is higher and it increases with the burnup.

Isotope / BU (GWd/tU)	cm242	cm244	cm246	u235	u238	pu238	pu239	pu240	pu241	pu242	am241
5	1.053	1.195	1.179	1.000	1.000	1.018	1.006	1.013	1.020	1.025	1.031
10	1.042	1.159	1.172	1.000	1.000	1.017	1.001	1.007	1.015	1.016	1.020
15	1.037	1.147	1.166	1.000	0.999	1.021	1.001	1.004	1.011	1.011	1.017
20	1.036	1.138	1.156	1.000	0.999	1.025	1.002	0.998	1.013	1.012	1.018
25	1.035	1.130	1.155	1.001	0.999	1.033	1.001	0.996	1.011	1.010	1.018
30	1.034	1.124	1.159	1.001	0.999	1.041	1.000	0.995	1.008	1.010	1.017
35	1.032	1.108	1.156	1.001	0.998	1.050	0.999	0.993	1.007	1.010	1.016
40	1.031	1.097	1.154	1.001	0.998	1.059	0.998	0.991	1.008	1.009	1.015
45	1.029	1.089	1.153	1.001	0.998	1.069	0.998	0.988	1.006	1.008	1.015
50	1.029	1.084	1.145	1.002	0.997	1.080	0.998	0.985	1.009	1.007	1.015
55	1.028	1.074	1.138	1.002	0.997	1.092	0.997	0.983	1.007	1.008	1.015
60	1.027	1.066	1.134	1.001	0.997	1.104	0.994	0.985	1.000	1.008	1.012
65	1.026	1.058	1.128	1.000	0.996	1.117	0.992	0.984	0.997	1.007	1.010
70	1.023	1.051	1.123	0.999	0.996	1.130	0.990	0.983	0.996	1.005	1.006

Table 2: Ratio between the nuclide concentrations obtained with the two libraries (ENDF/JEFF) as a function of the burnup. The fuel had 3.5% initial enrichment and the values refer to direct discharge from the reactor.

6. Comparison with the LANL reference spent fuel library

In the framework of the Next Generation Safeguards Initiative (NGSI), the Los Alamos National Laboratory developed several reference spent fuel libraries [12], [13].

Since the geometry of the fuel assembly is the same as the one chosen for our case, it is possible to compare the results of the neutron emissions obtained with their calculations. However, of all the libraries developed by LANL, only the first one is relevant for the comparison since it assumed a uniform composition and irradiation conditions for the complete fuel assembly.

There are three combinations of initial enrichment, burnup, and cooling time that are coincident between our library and their case:

- Case 1 - IE: 4% BU: 30 GWd/tU CT: 5 years
- Case 2 - IE: 4% BU: 45 GWd/tU CT: 5 years
- Case 3 - IE: 5% BU: 60 GWd/tU CT: 5 years

The comparison focused on the neutron emissions of the main contributors and on the total neutron emissions.

The next table shows the ratio between the values calculated by Los Alamos (LA) and with ALEPH2.2 (ALE) or ORIGEN-ARP (ORI). They contain also the ratio between the values obtained with ORIGEN-ARP and ALEPH2.2 (column ORI/ALE).

IE:	4.00%	BU:	30 GWD/tU		CT:	5 years			
Nuclide	ORI/ALE			LA/ALE			LA/ORI		
	(α,n)	Sp. Fiss.	Total	(α,n)	Sp. Fiss.	Total	(α,n)	Sp. Fiss.	Total
pu238	0.8101	0.9642	0.8314	0.8098	0.9483	0.8290	0.9996	0.9835	0.9970
pu239	0.8288	0.9720	0.8289	0.8473	0.9737	0.8474	1.0223	1.0017	1.0223
pu240	0.8150	0.9963	0.9704	0.8350	1.0020	0.9781	1.0245	1.0057	1.0080
pu242	0.8628	1.0182	1.0180	0.8776	1.0163	1.0161	1.0171	0.9981	0.9981
am241	0.8039	0.9981	0.8040	0.8374	1.0191	0.8375	1.0417	1.0210	1.0417
cm242	0.8193	1.0119	0.9751	0.8377	1.0142	0.9805	1.0224	1.0022	1.0055
cm244	0.8556	1.0044	1.0032	1.1653	1.3454	1.3439	1.3619	1.3394	1.3396
cm246	–	0.7414	0.7414	–	1.5552	1.5552	2.1419	2.0976	2.0976
Total	0.8202	1.0036	0.9968	0.8954	1.3368	1.3205	1.0918	1.3320	1.3247

IE:	4.00%	BU:	45 GWD/tU		CT:	5 years			
Nuclide	ORI/ALE			LA/ALE			LA/ORI		
	(α,n)	Sp. Fiss.	Total	(α,n)	Sp. Fiss.	Total	(α,n)	Sp. Fiss.	Total
pu238	0.7745	0.9219	0.7949	0.8058	0.9347	0.8236	1.0404	1.0138	1.0361
pu239	0.8317	0.9753	0.8317	0.8553	0.9740	0.8554	1.0284	0.9987	1.0284
pu240	0.8218	1.0044	0.9783	0.8390	0.9971	0.9745	1.0209	0.9927	0.9961
pu242	0.8377	0.9886	0.9884	0.8738	1.0023	1.0022	1.0432	1.0139	1.0139
am241	0.7897	0.9803	0.7898	0.8422	1.0152	0.8423	1.0665	1.0356	1.0664
cm242	0.7987	0.9864	0.9505	0.8768	1.0511	1.0178	1.0978	1.0657	1.0708
cm244	0.8387	0.9845	0.9833	1.1283	1.2898	1.2885	1.3454	1.3100	1.3103
cm246	0.5935	0.7145	0.7145	1.2754	1.4891	1.4891	2.1489	2.0843	2.0843
Total	0.8077	0.9826	0.9795	0.9546	1.2880	1.2819	1.1819	1.3108	1.3088

IE:	4.00%	BU:	45 GWD/tU		CT:	5 years			
Nuclide	ORI/ALE			LA/ALE			LA/ORI		
	(α,n)	Sp. Fiss.	Total	(α,n)	Sp. Fiss.	Total	(α,n)	Sp. Fiss.	Total
pu238	0.7619	0.9071	0.7820	0.8037	0.9239	0.8203	1.0549	1.0186	1.0491
pu239	0.8314	0.9750	0.8315	0.8595	0.9699	0.8595	1.0337	0.9948	1.0337
pu240	0.8230	1.0059	0.9798	5.9134	0.0000	0.8451	7.1853	0.0000	0.8625
pu242	0.8308	0.9805	0.9803	0.8767	0.9969	0.9968	1.0552	1.0168	1.0168
am241	0.7887	0.9788	0.7888	0.8472	1.0117	0.8472	1.0741	1.0336	1.0741
cm242	0.8020	0.9905	0.9545	0.8840	1.0508	1.0189	1.1023	1.0609	1.0675
cm244	0.8375	0.9833	0.9820	1.1116	1.2598	1.2585	1.3273	1.2812	1.2816
cm246	0.5893	0.7095	0.7095	1.2601	1.4586	1.4585	2.1382	2.0557	2.0557
Total	0.8049	0.9798	0.9771	0.9659	1.2569	1.2523	1.2000	1.2828	1.2818

Table 3: Comparison between the neutron emission due to specific isotopes (as well as the total values) reported in the LANL reference spent fuel library, and the ones calculated with ALEPH2.2 (LA/ALE) and ORIGEN-ARP (LA/ORI). The data from the comparison between ORIGEN-ARP and ALEPH are also reported (ORI/ALE). The values of initial enrichment, burnup, and cooling time are shown at the top of each table.

The agreement with the LANL fuel library is very good for ^{240}Pu and ^{242}Pu (all values within 5%), while there are different results with the other isotopes. The LANL fuel library generally has higher values (≈15–30%) compared to the ones calculated with ORIGEN-ARP and ALEPH2.2 and this induces higher total neutron emissions as well.

From information available on the report on the LANL spent fuel library we can highlight some similarities and differences that can explain in part the discrepancy in the results:

- The boron concentration in the water was 660 ppm for the LANL simulations whereas we used a concentration of 630 ppm.
- The fuel, moderator, and cladding temperatures are the same for both libraries.
- The only geometric parameters that change are the length (365.76 cm for LANL, 100 cm for ALEPH cases) and the pellet radius (0.41 cm for LANL, 0.4025 cm for ALEPH).
- There are four radial subdivisions for the fuel pellet modelled by LANL.
- The average power during irradiation is 38 MW/tU instead of 40 MW/tU used in our cases.
- The simulations done by LANL considered irradiation cycles of 420.3 days, apart from the last irradiation cycle that is reduced to 312.3 days.
- Each irradiation cycle of the LANL library determines an additional burnup of about 15 GWd/tU to the fuel assembly.
- The nuclear data library used by the LANL cases was the ENDF/B-VII.0, whereas the ORIGEN-ARP cases used data from ENDF/B-VI.2 and the ALEPH simulations from the ENDF/B-VII.1 data set.

Apart from the factors included in the previous list, the difference in the results can be determined also by other characteristics that are not contained in the LANL report.

7. Conclusions

A reference spent fuel library has been built using the software ORIGEN-ARP and ALEPH2.2 to provide some insights of the different isotopes relevant for neutron emission. A comparison of the two codes has been performed to check their consistency and the reasons of possible discrepancies.

The neutron emission increases with increasing burnup, whereas there is an opposite trend with initial enrichment and cooling time. Apart from very low burnup values, the spontaneous fissions are the main contribution to the total neutron emission, with (α,n) reactions accounting for the remaining.

By looking at the role played by individual isotopes, it is clear that the main contributors are the curium isotopes (^{242}Cm and ^{244}Cm are very important up to 100 years of cooling time, while ^{246}Cm and ^{248}Cm arise at high burnup). At low burnup and also at high cooling times there are significant contributions from plutonium isotopes (especially ^{240}Pu and ^{242}Pu). As a general consideration, there are always less than 10 isotopes that combined are responsible for about 99% of the total neutron emissions. Only for cooling times higher than 10000 years more isotopes have relevant contributions.

The build-up of several actinides (such as the Cm isotopes) explains the trend of the neutron emission with initial enrichment, burnup, and cooling time of the spent fuel. In fact, decreasing the initial enrichment or increasing the burnup will lead to a higher fluence level, a higher production of actinides and therefore to a higher neutron emission.

Comparing the two codes used in the simulations, the general agreement is rather satisfactory since the total neutron emission values are within 15%. This is due to a different concentration of actinides calculated by the two codes and possibly also to approximations applied in both models.

The boron added to the water during irradiation in the reactor core is also playing a role, although reduced compared to the main variables associated to the irradiation of the spent fuel (IE, BU, CT).

The presence of boron determines the hardening of the neutron energy spectrum during the irradiation in the reactor. This induces an increase of the resonance captures and a higher production of actinides. The results show that the addition of 630ppm of boron increases the total neutron emission of about 10%. Other important parameters that affect the calculated composition of the spent fuel are the water spacing between neighbouring fuel assemblies during the irradiation in the reactor (decrease of the total neutron emission of roughly 1% for each mm of gap) and the nuclear data library that is used in the calculations (10% on the total neutron emission).

The library has been compared with one reference spent fuel library made by LANL. There are three comparable cases (i.e. same IE, BU, and CT) and the comparison showed good agreement (difference lower than 5%) for some plutonium isotopes, but a larger discrepancy for the curium isotopes (≈30%).

8. Acknowledgements

This work is sponsored by GDF SUEZ in the framework of the cooperation agreement CO-90-07-2124 between SCK•CEN and GDF SUEZ.

9. References

[1] International Atomic Energy Agency (IAEA), *"Spent Fuel Reprocessing Options"*. IAEA-TECDOC-1587. August 2008

[2] International Atomic Energy Agency (IAEA), *"Addressing Verification Challenges. Proceedings of an International Safeguards Symposium"*. Vienna, 16-20 October 2006

[3] S. J. Tobin et al., *"Next Generation Safeguards Initiative research to determine the Pu mass in spent fuel assemblies: Purpose, approach, constraints, implementation, and calibration"*. Nuclear Instruments and Methods in Physics Research A 652 (2011) 73-75. September 2010

[4] Oak Ridge National Laboratory (ORNL), *"RSICC COMPUTER CODE COLLECTION – MCNP5/MCNPX"*. CCC-740. June 2011

[5] D.B. Pelowitz et al., *"MCNPX User's Manual, Version 2.7.0"*. LA-CP-11-00438. April 2011

[6] I. Gauld, S. Bowman, J. Horwedel. *"Origen-ARP: automatic rapid processing for spent fuel depletion, decay, and source term analysis."* ORNL/TM-2005/39. January 2009

[7] Oak Ridge National Laboratory (ORNL), *"SCALE: A Modular Code System for Performing Standardized Computer Analyses for Licensing Evaluation"*. ORNL/TM-2005/39. January 2009

[8] A. Borella et al., *"Spent Fuel Measurements with the Fork Detector at the Nuclear Power Plant of Doel", 33rd ESARDA Symposium, Budapest, May 2011*

[9] A. Stankovskiy, G. van den Eynde. *"ALEPH 2.2 A Monte Carlo Burn-up Code"*. SCK•CEN-R-5267. September 2012

[10] M.B. Chadwick et al., *"ENDF/B-VII.1 Nuclear Data for Science and Technology: Cross Sections, Covariances, Fission Product Yields and Decay Data"*, Nuclear Data Sheets Volume 112, Issue 12. December 2011

[11] Nuclear Energy Agency (NEA), *"The JEFF-3.1.1 Nuclear Data Library"*, JEFF Report 22, OECD/NEA, Paris (2009), and *"The JEFF-3.1 Nuclear Data Library"*, JEFF Report 21, OECD/NEA, Paris (2006)

[12] J. Richard, *"Summary of Summer Work: Analysis of the Neutron Source Term of a Spent Fuel Assembly"*, LA-UR-10-00075. September 2009

[13] H. R. Trellue et al., *"Description of the Spent Nuclear Fuel Used in the Next Generation Safeguards Initiative to Determine Plutonium Mass in Spent Fuel"*, LA-UR-11-00300. December 2010

Production of monodisperse uranium particles for nuclear safeguards applications

Alexander Knott, Martin Dürr

Forschungszentrum Jülich - IEK-6: Nuclear Waste Management and Reactor Safety - 52425 Juelich (Germany)
E-mail: a.knott@fz-juelich.de, ma.duerr@fz-juelich.de

Abstract:

Particle analysis of nuclear materials is a powerful tool in nuclear safeguards and nuclear forensic studies. For the analysis, quality control and reference material samples are required for instrument and method validation as well as the assurance of the quality of reported results. The availability of uranium- and plutonium-containing particles with well-defined properties such as size, density, elemental and/or isotopic composition is limited.

The potential of particle production processes starting with monodisperse aerosols prepared from dilute uranium/plutonium solution has already been demonstrated. Monodisperse uranium and plutonium particles with known elemental contents can be produced using a Vibrating Orifice Aerosol Generator (VOAG). The production of these particles is a two-step process: 1) generation of uniform aerosol particles, and 2) drying, calcining and collection of particles.

This paper describes an experimental set-up for particle generation and issues associated with the overall particle production process, its current status and future plans for production of the various nuclear materials needed.

Keywords: Environmental Sampling; Destructive Assay; Isotopic Measurements; Nuclear Forensic; LG-SIMS

1. Introduction

Environmental sampling is administered in States as part of the Safeguards Agreements with the International Atomic Energy Agency (IAEA) and provides a tool to strengthen the effectiveness and improve the efficiency of the safeguards system. It is a powerful measure to investigate the completeness of a State's compliance with its safeguards agreements; Environmental sampling is also part of IAEA's legal authority stemming from the Model Additional Protocol (INFCIRC/540). Generally, environmental swipe sampling has been implemented by the IAEA by collecting swipe samples from within nuclear facilities. The swipe samples are investigated specifically for the presence of undeclared nuclear materials and activities. It is fundamentally based upon the fact that every industrial process releases traces such as particulates into the environment. These signatures are representative for a facility's activities and may be found even decades after a specific process has been discontinued.

Swipe samples returned from inspections are initially screened for traces of nuclear activities such as fission and activation products using radiometric methods. Analyses using bulk techniques provide more detailed information on the presence, concentration and isotopic composition of uranium, plutonium and other safeguards relevant information. They provide, however, only average results for the entire sample.

Complementary to the bulk analytical efforts, particle analysis has emerged as an important analytical tool for nuclear safeguards verification activities as well as forensic investigations over the past decade. Particle analysis refers to the characterization of discrete micro- and sub-micrometer-sized particles, and properties such as their microcrystallography, morphology, elemental and isotopic composition are determined. For the measurement of these properties a variety of instrumental techniques are employed such as Scanning Electron Microscopy (SEM), with or without energy dispersive and/or wavelength dispersive X-ray Fluorescence Spectrometers (EDX/WDX), or Thermal Ionization and Secondary Ion Mass Spectrometry (TIMS and SIMS).

SIMS is used in safeguards and forensic investigations to identify, for example, uranium-containing particles at the same time analyzing them for their isotopic composition. Evaluation and calibration of SIMS and other instrumental methods requires reference and Quality Control (QC) materials. Ideally, such particles should resemble those analyzed from inspection samples. However, one needs to concede to the fact that a wide variety of particles exist on collected swipe samples and that reference material (RM) can be synthesized only in limited types and characteristics. For reference particles, it would be desirable to be able to tailor the particle properties according to the need of analytical procedures to be applied in particle analysis.

Different approaches to produce QC particles have been used in the past. At the VTT Technical Research Centre in Finland, particles were produced from certified reference materials using a device called the atomizer as a particle generator. [1] These particles have a well characterized isotopic composition, but cover a wide range of sizes and densities. At the Institute for Reference Materials and Measurement (IRMM) in Belgium, particles were produced

by hydrolyzing uranium hexafluoride in a controlled environment [2]. Uranium oxyfluoride and oxide particles of various sizes and compositions were produced in these experiments, the particles closely matching material found in enrichment facilities or facilities handling uranium hexafluoride. Special glass micrometer sized particles with varying amounts of uranium and uranium isotopics were produced at the IRMM [3], as were uranium oxide particles produced at Harwell for QC purposes [4]. Monodisperse particles were produced and investigated at the Joint Research Centre's Institute for Transuranium Elements in Karlsruhe, Germany. Using a Vibrating Orifice Aerosol Generator (VOAG) a study was carried out to produce particles of well-defined size, density, geometry and elemental contents [5] [6] [7].

This paper describes a setup under development for the production of monodisperse particles using a VOAG with the goal to establish a robust and stable production process. This paper presents the current status and results obtained by the first test-runs.

2. Particles for Quality Control and Quality Assurance

For particles to be suitable for quality control and quality assurance, certain properties need to be fulfilled. As with any reference material, the degree of homogeneity within and between the samples needs to be ensured and verified. For particles, this means that they should have uniform properties throughout the whole batch to the furthest degree possible. With a batch of uniform particles, identical test particles can be provided to the various users of analytical methods. In principle, the property of every individual particle needs to be known, which is verified by characterizing single particles based on a statistical sampling scheme. A number of techniques and procedures to identify and to analyze individual particles exist. If morphology and size distribution are not homogenous throughout the whole batch they may not be suitable as reference materials (RM`s). In order to calibrate a highly sensitive machine, like the Large Geometry Secondary Ion Mass Spectrometer (LG-SIMS), uniformity in characteristics is the most important feature. In particular, a known amount of uranium in each particle would greatly serve the purpose of a particle reference material. In the case of SIMS analysis, the production process also needs to ensure that the isotopic composition is uniformly distributed throughout the whole batch.

In light of the current techniques available for particle analysis in safeguards, reference particles should be uniform in

- uranium (respective plutonium) content,
- isotope ratios,
- size,
- chemical composition,
- morphology.

An additional requirement besides uniformity is the possibility to tailor the properties listed above so that these reference particles can provide quality assurance and quality control for the various analytical procedures. Currently it is envisioned to produce particles with various isotopic signatures. At first, particles only containing uranium shall be produced until the production process is fully understood and under good control. Different enrichment levels are preferred, especially from 0.5, 5, <20% ^{235}U enrichment with different isotopic compositions. At first, the production process will use certified reference materials (CRM`s) from different suppliers like NIST, IRMM, CEA, etc. available in different forms as precursor material; mostly these are nitrate solutions. In natural uranium (NU) the isotopes ^{235}U and ^{238}U are the major components. Then again there are the less abundant isotopes like ^{234}U and ^{236}U which are called minor isotopes. For nuclear safeguards analysis, the measurement of the major ratio of ^{235}U/^{238}U is of key interest. Since the implementation of the new LG-SIMS, which is able to reduce isobaric interferences much more effectively, the measurement of minor ratios has become routine. The ^{236}U/^{238}U ratio provides additional information. This ratio covers a wide range from 10^{-11} for NU up to 10^{-2} for re-enriched uranium and is therefore a strong indicator in nuclear safeguards and non-proliferation applications [8] [9]. Nowadays, the variety of RM suitable for these specific nuclear safeguards analysis methods is very limited, especially those with tailor-made isotopic content of the minor isotopes. Another important parameter for safeguards applications is the enrichment in ^{235}U (0.5 - 20%, or even higher) and on the minor isotopes of uranium, plutonium and its fission products. Another field of application is its use as a reference material for age-determination. Age dating offers valuable information about the collected materials; it may even provide insight information into its composition, last date of purification and enrichment history. Calculating the decay of the radioactive nuclides provides the authorities with the ability to calculate the production date or age [10] [11]. So far, there are no reference materials available for particle age-dating methods.

The aim of this project is the "in-house" production of monodisperse particles which can be used as RM or CRM eventually, especially for mass spectrometry like SIMS, LA-MC-ICP-MS, TIMS, etc. Within the next 12 months we are expecting to be able to produce monodisperse particles with reproducible results.

3. Particle Production Process

Production of solid aerosol particles is a two-step process. First, a stream of identical droplets is generated as a solution passes through a vibrating orifice, and second, drying, calcination of the droplets and collection of dry particles.

The generation of monodisperse particles is based on the following principle: A syringe pump feeds a liquid solution through a small orifice at a predetermined and constant rate. A piezoelectric ceramic driven by an oscillating voltage potential causes the orifice to vibrate at a constant frequency, producing a uniform droplet stream. The droplet stream is introduced into the centre of a turbulent air jet, dispersing droplets and preventing coagulation. The dispersed droplets mix with a larger volume of clean, dry air, which evaporates any volatile portion of the droplets.

Because each disturbance cycle of the orifice produces only one droplet, the precise size of the droplet can be deduced from the operating parameters. The two key parameters determining the droplet diameter are liquid feed rate (f) and oscillating frequency (ν).

$$\text{Ø}_{Droplet} = \left(\frac{6 \times f}{\pi \times \nu}\right)^{1/3} \quad (1)$$

For each orifice, an optimal frequency range with a compatible liquid feed rate has to be defined in which it produces monodisperse aerosol particles. This frequency range and liquid feed range is restricted, because only within a certain range of feed rate and vibrating frequency can the generator uphold a steady droplet stream. Control of droplet diameter via the parameters *f*,ν is also limited, because of the power law of eq. (1). Effectively, the initial volume of a droplet formed by the aerosol generator is dominated by the diameter of the orifice. As a droplet consists of a volatile (solvent) and a non-volatile (solute) component, its volume changes rapidly after formation. If a portion of the primary droplet is volatile, the final particle size depends on the volumetric concentration (c) of the non-volatile portion.

The particle diameter can be calculated using equation (2). [12]

$$\text{Ø}_{Particle} = \left(\frac{1}{c} + 1\right)^{1/3} * \text{Ø}_{Droplet} \quad (2)$$

c = Volumetric amount of the soluble part of the solution
I = Correctional-term for all the non-volatile impurities

Therefore, the main parameter for controlling particle size is through the concentration of non-volatile components in the feed solution. After drying and dispersing, the particles are treated thermally to convert them from dried metal nitrates to the corresponding oxides. Only then do we expect the particles to be stable, i.e. to maintain their integrity, which is necessary to conserve the properties across the batch and during extended periods of time. It is estimated from previous experience with neodymium at the Forschungszentrum Juelich [13] that an additional loss of 80 Vol.-% for the calcination is realistic.

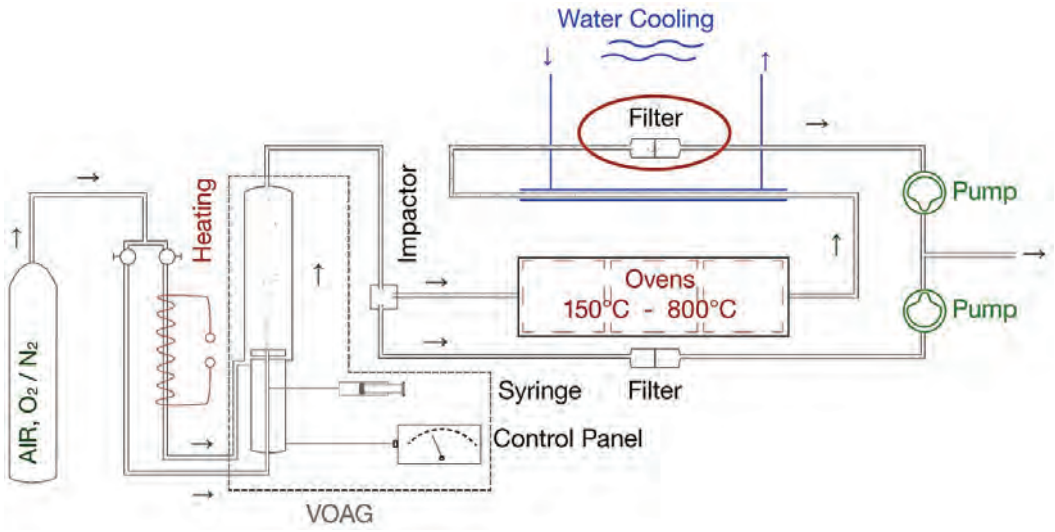

Figure 1: Layout of the setup.

The heat treatment is accomplished 'in-stream', i.e. by heating the carrier air stream in which the particles are immersed. The calcination of the particles is performed by passing the particles through a four-zone furnace where temperatures gradually rise from 150°C to 800°C converting the particles to their oxides.

The chemical form of the final particles is determined from the feed solution and the heat treatment. Starting from certified uranium oxides (mostly U_3O_8) diluted aerosol solutions are prepared by dissolving the uranium oxides with nitric acid – see equation (3). After diluting the solution to a concentration of a few 100 µg U/g an aliquot is combined with an alcohol and water mixture– in our case a 1:1 ratio of ethanol and water.

$$U_3O_8 + 8\ HNO_3 \rightarrow 3\ UO_2(NO_3)_2 + 2\ NO_2 + 4\ H_2O \quad (3)$$

Thermal treatment leads to degradation of the nitrates to the corresponding nitrous-gases, mostly N_2O_5 and NO – see equation (4).

$$UO_2(NO_3)_2 + \Delta_{Thermal} \rightarrow UO_3 + NO_x \quad (4)$$

After calcination the particles have to be cooled down near room-temperature and are collected on Nuclepore track-etched polycarbonate-membrane filters (Whatman™", diameter of 25 mm and an average pore-size of 0.6 μm). Dilution and dispersion air-streams of the system are separately controlled by membrane pumps. Both air-streams are filtered to remove the majority of particles before entering the membrane pumps in order to reduce the amount of particle contamination of equipment. A schematic diagram of the experimental setup is shown in Figure 1.

4. Results and Discussion of the First Test-Runs

Test runs were performed, in order to demonstrate that it is possible to produce monodisperse particles of specific diameter (e.g. 1 μm). In addition, the question of reproducibility was studied, which is of major importance because the amount of uranium per particle has to be under control. This can only be achieved if parameters like the density, geometry/diameter remains stable throughout production of the batch. The aim of these measurements was therefore the assessment of three important parameters: evaluating the morphology with SEM-measurements, amount of particles being produced and the distribution of those particles over an area of 500x500 μm.

4.1 'Cold-Test' with Nd Particles

Based on several test experiments the initial parameters to operate the VOAG have been evaluated and are shown in Table 1. For test production runs using neodymium as a substitute for uranium, the generated particles were collected on standard glass, high-grade steel planchets as well as Nuclepore-filters.

Dispersion stream	0.012 L/min
Dilution stream	30 L/min
Frequency	72.34 kHz
Run-time	2 & 5 min
Concentration	0.84 mmol/L
Liquid-Feed Rate	$1.39 \cdot 10^{-4}$ L/min
Syringe Pump Run Speed	$4.2 \cdot 10^{-4}$ cm/s

Table 1: Parameters for the generation of the neodymium particles.

As an aerosol solution, a 1:1 mixture of high purity water and high purity ethanol (EtOH; Merck, analytical grade) was used and the concentration of neodymium(III)nitrate hexahydrate (99.998 % $Nd(NO_3)_3 \cdot 6H_2O$, Alfa Aesar, Germany) of the mixture was adjusted to 0.84 mmol/L. To collect the calcinated particles, track-etched polycarbonate membrane filters were used (Whatman™, Nuclepore filters with 0.6 μm pore size and a diameter of 25 mm).

An Aerodynamic Particle Spectrometer (APS) and Optical Particle Sizer (OPS) by TSI[1] were used to determine the size of the generated neodymium particles. The APS and OPS measurements were performed online during the production test run.

4.2 Scanning Electron Microscopy (SEM)

Two different SEM instruments were used to characterize the morphology of the neodymium particles. In Juelich, a FEI Quanta 200 scanning electron microscope (SEM) was used to determine the particle morphology, geometry, size and average diameter. The SEM is also equipped with three separate detectors, a secondary electron detector (SE), an energy-dispersive X-Ray detector (EDX) and a backscatter electron detector (BSE). Particles collected on glass plates and Nuclepore filters were measured directly. A voltage of 20.0 kV was used to record the images. The elemental composition of single particles was measured by its specific X-Ray spectrum.

In Seibersdorf, a Philips XL30 with WDX 600 and an Oxford Microscope and an EDAX was used. This SEM was operated at reduced pressures ($P = 1.1 \cdot 10^{-5}$ Pa) and a very low accelerating voltage of V= 9kV. The results were compared with known peaks of the following elements: Fe (Kα), Si (Kα), Cr (Kα), Fe (Kβ), C (Kα), O (Kα), Nd (Kα) und Nd (Kβ).

4.3 Size and Morphology of Nd Test-Particles

Online and offline measurements of the generated neodymium oxide particles using the OPS, APS and SEM were in general agreement indicating a typical size of the particles of 4.2 - 5.0 μm. This is in good agreement with the calculated size using equation (2). But a difference in the average diameter of about 25% is suggested by the results obtained from the APS and OPS measurements. The discrepancy between the APS and OPS measurements showed that the aerodynamic and the optical diameter could be measured accurately. But it also illustrated that both the aerodynamic and the optical diameter are not necessarily the same as the effective physical diameter. Nevertheless, SEM measurements confirmed the accuracy of the APS measurements, which can be performed online during production runs. APS provides an opportunity to measure the diameter online and with high accuracy. The average diameter of the neodymium particles of 4.7 μm is confirmed on the measurement of ten random particles by SEM. The standard deviation of the average particle diameter is less than 5% indicating an acceptable uniformity of the generated particles.

The SEM measurements showed that all particles were spherical in shape except those collected on the Nuclepore-filter membranes. The latter were not only

[1] http://www.tsi.com/Particle-Sizers/

deformed but also slightly smaller in size. All particles showed a coronal-like pattern around their impact site on the collection medium. This indicates that the particles were not completely dry before impacting on the target. Figure 2 shows the geometry and morphology of two particles collected on different substrates. The left image shows a wet neodymium particle impacted on a glass-planchet with a very distinctive splash-pattern, and the right image a particle collected on a stainless steel target.

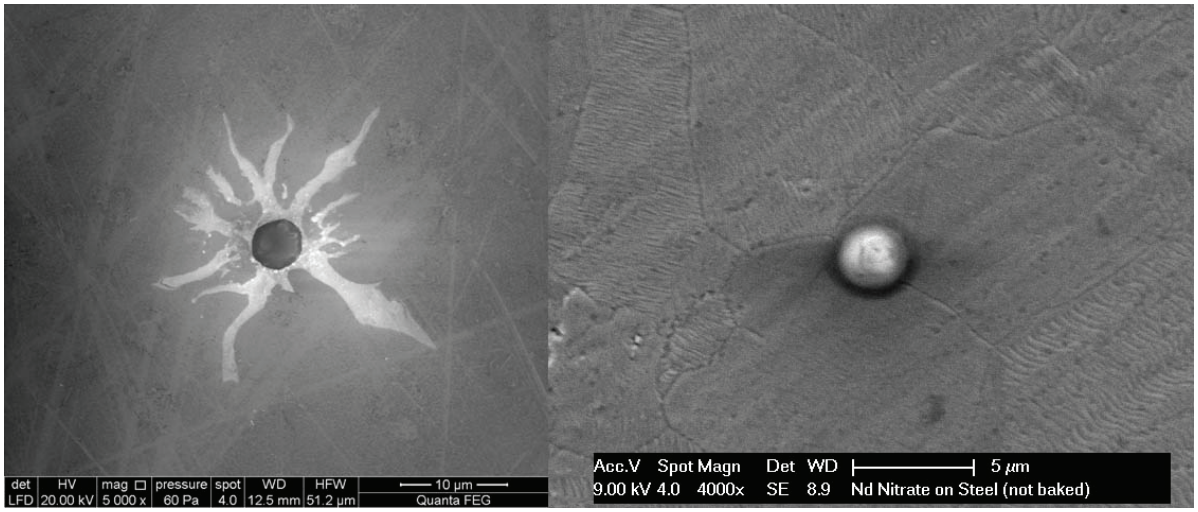

Figure 2: Left: $Nd(NO_3)_3 \bullet 6H_2O$ sphere on a glass-target and Right: $Nd(NO_3)_3 \bullet 6H_2O$ sphere on a steel-target.

Online measurements with the APS and OPS were also used to measure the amount of particles being produced. These measurements were performed right before impacting on the specific targets. The results can be seen in Table 2 – they were achieved with the parameters of Table 1. The results also show a big discrepancy between the amount of particles before the Nuclepore Filter and the glass and steel targets. This is due to the fact that the Nuclepore Filter is integrated into the sample unit which is integrated in the dilution air stream, whereas the glass and steel targets were just damped with a hose. This clearly indicates the effects of different geometries on the air currents inside the apparatus. It has to be noted that different volumes of the dilution air stream had a huge impact on the amount of particles being detected.

Before glass filter	600 particles/min
Before steel filter	620 particles/min
Before Nuclepore filter	200 particles/min

Table 2: Particle density before targets measured with the APS.

One of the first conclusions could be drawn from the online measurements with the APS and OPS. We were able to measure the amount of particles reaching the targets and could compare those numbers with the amount of particles being produced. Clearly, it showed that the dependency of the internal air currents (both dilution and dispersion air) to small differences to the setup as well as to some parameters like the liquid feed rate and the vibration frequency of the orifice - see chapter 3 last paragraph. Clear indications for those effects are the values recorded in Table 2; they just depict the optimal values being recorded. SEM images taken over an area of 500x500 µm could also confirm that the amount of particles reaching the target varied drastically depending on changes to the frequency of the orifice vibration as well as to changes to the sampling-setup.

Another obvious difference could be observed between the particles which were damped on the targets and those which impacted on the Nuclepore filters. Particles collected on glass and steel-planchets were less skewed when compared with those impacted directly on Nuclepore filters. SEM images also suggest that most particles were not completely dry prior to impacting. This issue will be addressed by using preheated air in the dispersion air stream

SEM images over an area of 500x500 µm were made to investigate the distribution of particles over a larger area. It could be observed that very few agglomerations occurred and that all particles were of uniform size.

5. Conclusion

A Vibrating Orifice Aerosol Generator was installed and preliminary studies on the production of uniform particles were carried out. SEM images of the particles confirmed a well-defined size, geometry and production of discrete particles with a very low degree of coagulation.

Further optimization of the experimental set-up and adjustments of the experimental parameters will be performed over the next few months. First runs with nuclear materials are planned in the second half of 2013, with the main

objective of "in-house" production of monodisperse particles which can be a used as Quality Control materials for particle analytical techniques such as SIMS, LA-MC-ICP-MS, and TIMS.

6. Acknowledgements

The authors thank Nicole Erdmann (JRC-ITU) for her advice on the aerosol production using the VOAG instrument, and Martina Klinkenberg (Forschungszentrum Juelich) and Ernesto Chineo (IAEA) for their support with the SEM measurements.

The authors also acknowledge contributions by the IAEA, and thank Stephan Vogt (IAEA) and Cheol-Su Kim (IAEA) for valuable support to this paper.

A. Knott acknowledges support under Special Service Agreement contract with the IAEA. This work was partly funded under Task A1961 of the German Support Programme to the IAEA.

7. References

[1] Hokkinen, J.; Taper, U. & Ziliacus, R.*; Production of Plutonium Particles*; Internal VTT Report; 2011; p 1-12.

[2] Kips, R.; Leenaers, A.; Gabriele, T.; Betti, M.; Van den Berghe, S.; Wellum, R. & Taylor, P.; *Characterization of Uranium Particles Produced by Hydrolysis of UF6 Using SEM and SIMS*; Microscopy and Microanalysis; 2007; 13; p 156-164.

[3] Raptis, K.; Ingelbrecht, C.; Wellum, R.; Alonso, A.; Bolle, W. D. & Perrin, R.; *The preparation of uranium-doped glass reference materials for environmental measurements*; Nuclear Instruments and Methods in Physics Research Section A: Accelerators, Spectrometers, Detectors and Associated Equipment; 2002; 480; p 40-43.

[4] Pidduck, A. & Donohue, D.; *Micro-Analytical Characterization of Uranium Particles in Support of Environmental Sampling for Safeguards*; INMM Proceeding 47th Annual Meeting; 2004; p 1-8.

[5] Erdmann, N.; Betti, M.; Stetzer, O.; Tamborini, G.; Kratz, J.; Trautmann, N. & van Geel, J.*; Production of monodisperse uranium oxide particles and their characterization by scanning electron microscopy and secondary ion mass spectrometry*; Spectrochimica Acta Part B: Atomic Spectroscopy; 2000; 55; p 1565-1575.

[6] Stetzer, B. O.; *Spaltspuranalyse von Uranoxidpartikeln*; Dissertation; Johannes Gutenberg-Universität; Mainz; 2001.

[7] Ranebo, Y.; Niagolova, N.; Erdmann, N.; Eriksson, M.; Tamborini, G. &Betti, M.; *Production and Characterization of Monodisperse Plutonium, Uranium, and Mixed Uranium–Plutonium Particles for Nuclear Safeguard Applications*; Analytical Chemistry; 2010; 82; p 4055-4062.

[8] Richter, S.; Eykens, R.; Kühn, H.; Aregbe, Y.; Verbruggen, A. & Weyer, S., *New average values for the n(238U)/n(235U) isotope ratios of natural uranium standards*; International Journal of Mass Spectrometry; 2010; 295; p 94-97.

[9] Richter, S.; Alonso, A.; Bolle, W. D.; Kühn, H.; Verbruggen, A.; Wellum, R. & Taylor, P.; *Re-certification of a series of uranium isotope reference materials: IRMM-183, IRMM-184, IRMM-185, IRMM-186 and IRMM-187*; Int. J. Mass Spectrom.; 2005; 247; p 37-39.

[10] Stanley, F. E.; *A beginner's guide to uranium chronometry in nuclear forensics and safeguards*; Journal of Analytical Atomic Spectrometry; The Royal Society of Chemistry; 2012; *27;* p 1821-1830.

[11] Varga, Z.; Wallenius, M.; Mayer, K. & Hrnecek, E.; *Alternative method for the production date determination of impure uranium ore concentrate samples;* Journal of Radioanalytical and Nuclear Chemistry; 2011; 290; p 485-492.

[12] Berglund, R. N. & Liu, B. Y. H.; *Generation of monodisperse aerosol standards;* Environmental Science & Technology; 1973; 7; p 147-153.

[13] Daniels, H.; Neumeier, S.; Bukaemskiy, A.; Modolo, G. & Bosbach, D.; *Fabrication of oxidic uranium-neodymium microspheres by internal gelation*; Progress in Nuclear Energy; 2012; 57; p 106-110.

Investigation on the long-term stability of IRMM-1027 series of Large-Sized Dried (LSD) spikes

Renáta Buják[a], Jeroen Bauwens[a], Rožle Jakopič[a], Maarten de Groote[b], Ludwig Cardon[b], Yetunde Aregbe[a]

[a.] Institute for Reference Materials and Measurements (JRC-IRMM) - Joint Research Centre, European Commission - Retieseweg 111, 2440 Geel, Belgium

[b.] Faculty of Engineering and Architecture, Department of Materials Science & Engineering, Centre for Polymer and Materials Technologies (CPMT), Ghent University - Technologiepark 903, 9052 Zwijnaarde, Belgium

E-mail: renata.bujak@ec.europa.eu, yetunde.aregebe@ec.europa.eu

Abstract:

The IRMM-1027 is a certified reference material for nuclear material control and accountancy. Each individual spike contains about 50 mg uranium (m(^{235}U)/m(U) ~ 20%) and about 1.8 mg plutonium (m(^{239}Pu)/m(Pu) ~ 98%) in dried form. They are used for the determination of U and Pu content of spent fuel solutions with isotope dilution mass spectrometry (IDMS) by plant operators and safeguards authorities. The dried uranyl and plutonium nitrates are embedded in an organic substance, which provides a stable layer at the bottom of the vial and preserves the integrity of the spike during storage and transport. Cellulose acetate butyrate (CAB) with 19 wt% butyryl content has been applied on the IRMM-1027 spikes for the last decade. However, the cellulose matrix containing the spike material tends to flake off after about two years. In order to prolong the shelf life of the spikes, JRC-IRMM has been investigating CABs with higher butyryl contents – 35 wt% and 52 wt% –, to optimize the chemical stability and to achieve a longer lasting layer. Empirical tests have shown that the higher the butyryl content, chemically the more stable and the more resistant the CAB is. Accordingly, future series of LSD spikes will be prepared with CAB containing 35 wt% butyryl, which should remain intact for at least 4 years. Furthermore, JRC-IRMM together with CPMT is investigating the chemical and mechanical properties of the three different CABs to further improve understanding on their stability and durability.

Keywords: LSD spike; certified reference material; nuclear material accountancy; CAB; deterioration

1. Introduction

The IRMM-1027 series of LSD spikes are used for the determination of U and Pu content of spent fuel solutions by isotope dilution mass spectrometry (IDMS) at safeguards laboratories and nuclear facilities worldwide. The ratio of U:Pu=25:1 in the LSD spikes is designed according to the customers' specifications. The uncertainty that is introduced by the reference material is fit for safeguards purposes, and allows the laboratories to achieve IDMS measurement results with uncertainties below the respective target value of 0.28%, expressed as relative combined standard uncertainty [1].

Cellulose acetate butyrate is a cellulose derivative with various amounts of hydroxyl, acetyl and butyryl groups. The mechanical and chemical properties of the CAB matrix are crucial for the stability of the organic layer and consequently influence the shelf-life of LSD spikes. CAB-19 (CAB with 19 wt% butyryl content) was applied for the first time in 2002 to replace the previously used tetrahydrofuran (THF) as a protective organic matrix of the dried uranyl and plutonium nitrates [2]. The advantages of CAB compared to THF are: easier preparation and handling in a glove-box, shorter drying period, and more easily dissolves in hot nitric acid. The chemical preparation of CAB-19 has been further improved [3] and it was demonstrated that the IRMM-1027 spikes have a shelf-life of two years. However, after this period the spikes start to crack, chip and flake off due to the deterioration of the CAB matrix. Therefore, JRC-IRMM has been testing CAB-35 and CAB-52 with 35 wt% and 52 wt% butyryl content on the spikes to assess the long-term stability and robustness of the three different organic substances. The stability of the CAB is affected by several factors such as: radiation [4]; acid residuals, humidity, and temperature [5]; physical shocks during transportation and mechanical stress in the thin layer [6]. Consequently, JRC-IRMM and CPMT are investigating the chemical and mechanical properties of the pure CAB layers – without nuclear material – before and after ageing, irradiation and transport tests in order to find the best suitable matrix for future LSD spikes.

2. Long-term stability of LSD spikes

The processing of LSD spikes is presented on the following flow chart (Figure 1).

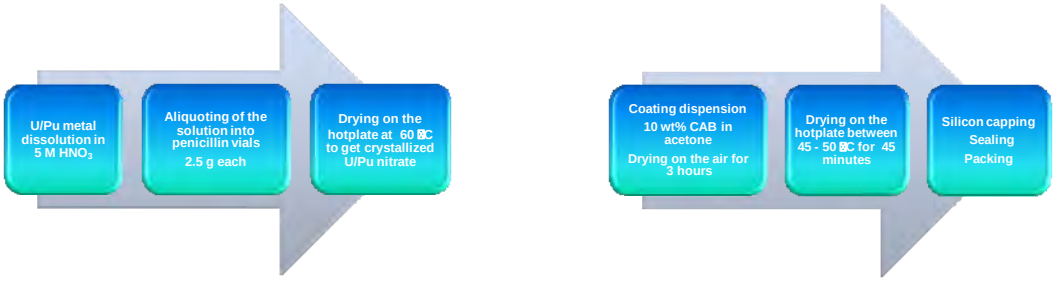

Figure 1: Preparation steps involved in LSD processing

The aliquoting of the U/Pu nitrate solution is done by an automated system [7] while the drying and the CAB addition on the individual spikes are carried out manually in separate glove boxes. First, the nitrate solution containing the U and Pu is evaporated until complete dryness. As uranyl nitrate is hygroscopic and CAB is sensitive for moisture uptake, humidity control is essential in the glove boxes (~ 20-25% relative humidity). Then, the dried uranyl and plutonium nitrates are treated with a solution of CAB in acetone. Finally, the vials are capped and sealed in plastic bags.

At JRC-IRMM, empirical tests were carried out to compare the three types of CAB together with the actual LSD spike sample. The preparation procedure for CAB-19, -35, and -52 was the same and the vials were stored and observed for two years. The outcome is shown on Figure 2. The vial containing the CAB-19 (No. 964) has a brownish colour and some cracks, while the spikes containing CAB-35 (No. 922) and CAB-52 (No. 586) are still intact. This is a good indication that CAB with higher butyryl content is more durable and provides a longer shelf-life for the spike material.

Figure 2: LSD spikes with CAB-19, CAB-35 and CAB-52 at the age of 2 years

These empirical tests are still on-going and visual observation is done regularly. The longest demonstrated shelf-life has been observed for test vials from the IRMM-1027M series that were covered with CAB-35 and have been intact already for four years. The CAB-52 was tested on the IRMM-1027L series and have not shown any flaking or cracking for two years. As a result of the successful test with CAB-35, it was decided to use it for the next series of LSD spikes IRMM-1027O. This would allow extending the shelf life on the IRMM-1027O certificate to three years. Furthermore, extensive studies have confirmed that the CAB-19 [2] and the CAB-35 [8] have no impact on the IDMS measurements and on the chemical treatment of spikes for the end users.

3. CAB: properties, stability and degradation behaviour

CAB is built up from repeating anhydroglucose units (monomers). Each monomer has three hydroxyl groups that can be esterified. The extent of esterification is expressed as mass percent (wt%) of butyryl group (see Figure 3). Its general features can be summarized as stiffness, moderate heat resistance, and moderate impact resistance. Some of the detrimental properties include a relatively narrow window between the melt flow temperature and the decomposition temperature due to the relative liability of the polysaccharide backbone at high temperatures [9].

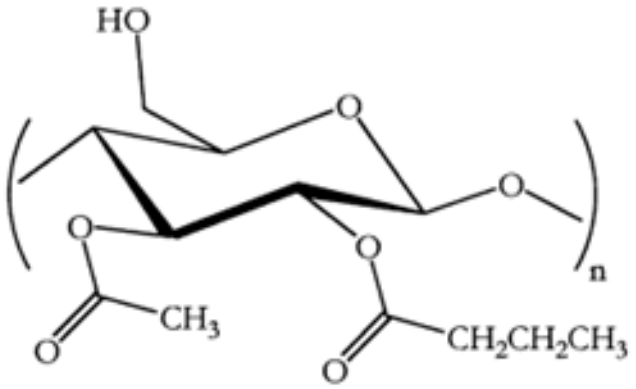

Figure 3: Cellulose acetate butyrate [9]

The chemical and mechanical stability of CAB are crucial for the long-term stability of the LSD spikes. There are several parameters which may influence the performance of the CAB layer. While it is possible to predict the sites of chemical attack in reactions such as hydrolysis or attack by acids, it is more difficult to predict the degradation pattern due to heat, light and radiation.

The drying temperature and the ambient humidity can be controlled during the spike preparation, however there are other parameters that cannot be fully controlled and could have a detrimental effect on the CAB matrix. These are the *radiation* coming from the spike material itself, natural *light*, *temperature* changes and *mechanical shocks* during transport and their combined effects.

The nuclides of Pu and U emit high energy alpha particles which are able to break bonds and create radicals or ions in the cellulose matrix. The calculated absorbed dose in the thin film is about 2×10^5 Gy which causes moderate or severe effects on cellulose acetate [4]. The detrimental effect of radiation appeared on the samples as fissures, discoloration and releasing off gas as well as changes in the tensile strength [10]. However, there is still lack of evidence to draw detailed conclusions concerning the radiation effect on the cellulose acetate butyrate. Therefore, JRC-IRMM in co-operation with the Ghent University, designed an irradiation experiment with X-rays simulating the long-term effect of radiation on CAB for one, two and three years. 100×100 μm samples of each CAB type will be irradiated. The effect of radiation will be observed visually. The density, which is related to the degradation of the CAB, will be monitored via the Compton scatter peak intensities.

The packing of radioactive material is carried out in two phases: the packing of the inner package and of the container. The IRMM-1027 LSD spikes are first sealed in plastic bags, then put in a plastic Type A container for radioactive materials, and finally they are transported in large sealed containers. For the transport of IRMM-1027 LSD spikes, currently the "EMMA package" is used according to relevant regulations [11]. Concerning the package material specifications and the fact that the transport of radioactive material does not take longer than one week, the units of IRMM-1027 are never exposed to a temperature range outside of 4 to 40°C. Although the spikes are well packed, shocks and temperature changes could cause deterioration of the CAB. Therefore, further investigation underpinned by experimental data is planned. Preliminary test results of the different types of CABs on the chemical and mechanical properties carried out by CPMT confirm JRC-IRMM's empirical observations that so far, the CAB-35 seems to be the best candidate to be applied on IRMM-1027 LSD spikes, thus it guarantees their longer shelf-life in the future.

Likewise, additional data are required about the ageing of the CAB layers due to heat, UV light and humidity, in order to identify the most influencing parameters for the deterioration of the organic matrix.

4. Outlook

The shelf-life of LSD spikes covered with CAB-19 is about two years and there is a need from our end users to prolong it. JRC-IRMM has already optimized the chemical preparation of the CAB layer and has carried out empirical studies to test CAB with 35 and 52 wt% butyryl content as well. The studies have shown that the CAB with 35 wt% butyryl content is more stable and durable; therefore it is more suitable for the future LSD spikes. Consequently, the IRMM-1027O series are covered with CAB-35.

Furthermore, additional studies will be carried out on how the ageing: light, heat, and humidity; radiation; and shocks during transport are affecting the durability of the three types of CAB.

5. Acknowledgement

The authors would like to thank to Prof. László Vincze from the Ghent University for his ideas in the irradiation tests.

6. References

[1] International Atomic Energy Agency; *International Target Values 2010 for Measurement Uncertainties in Safeguarding Nuclear Materials – IAEA/STR – 368;* Vienna; November 2010

[2] Surugaya N, Hiyami T, Verbruggen A, Wellum R; *Preparation, certification and validation of a stable solid spike of uranium and plutonium coated with cellulose derivative for the measurement of uranium and plutonium content in dissolved nuclear fuel by isotope dilution mass spectrometry; Analytical Sciences;* 24; 2008, p 247-252

[3] Bauwens J, Jakopič R, Wellum R, Verbruggen A, Aregbe Y, Richter S, Eykens R, Kehoe F, Kühn H; *Consideration on the development of large-sized dried spikes; 34th ESARDA Symposium;* Budapest; May 2011

[4] Hanks C L, Hamman D J; *Radiation Effects Design Handbook, Section 3. Electrical Insulating Materials and Capacitors*; Radiation Effects Information Centre; Columbus; July 1971

[5] Allen N S, Edge M, Horie C V Eds; *Polymers in Conservation*; The Royal Society of Chemistry; Cambridge; 1992

[6] Perera D Y; *On adhesion and stress in organic coatings, Progress in Organic Chemistry;* 28; 1996, p 21-23

[7] Verbruggen A, Bauwens J, Van De Steene N, Jakobsson U, Eykens R, Wellum R, Aregbe Y; *An automated system for the preparation of Large Size Dried (LSD) Spikes; ATALANTE 2008*; Montpellier; May 19-22, 2008; P7_05

[8] Jakopič R, Verbruggen A, Eykens R, Kehoe F, Kühn H, Kushigeta Y, Jacobsson U, Bauwens J, Richter S, Wellum R, Aregbe Y; *An inter-calibration campaign using various selected Pu spike isotopic reference materials; J Radioanal Nucl Chem;* 286; 2010; p 449-454

[9] Edgar K J, Buchanan C M, Debenham J S, Rundquist P A, Seiler B D, Shelton M C, Tindall D; *Advances in cellulose ester performance and application; Progress in Polymer Science*; 26; 2001; p 1605-1688

[10] Winogradoff N N; *X-Ray Irradiation of Cellulose Acetate; Nature*; 165; 1950; p 72

[11] International Atomic Energy Agency; *Regulations for the Safe Transport of Radioactive Material, 1996 Edition, "Requirements", IAEA Safety Standards Series No. TS-R-1 (ST-1, Revised)*; IAEA, Vienna; 2000

"I agree that ESARDA may print my name/contact data/photograph/article in the ESARDA Bulletin/Symposium proceedings or any other ESARDA publications and when necessary for any other purposes connected with ESARDA activities."

Comparative assessment of the Pu content of MOX samples by different techniques

R. Buda[1], R. Carlos-Marquez[1], E. Dahms[1], F. d'Amati[1], L. Emblico[1], J. Horta-Domenech[1], A. LeTerrier[1], K. Lützenkirchen[1], S. Millet[1], S. Morel[1], A. Mühleisen[1], A. Nicholl[1], V. Piron[1], D. Poublan[1], M. Ramos-Pascual[1], A. M. Sanchez-Hernandez[1], F. Sarli[1], P. Schwalbach[2], A. Terrasi[2], P. van Belle[1], M. Vargas-Zuniga[1], J. Zsigrai[1*], E. Zuleger[1]

1. Institute for Transuranium Elements, Joint Research Centre, European Commission, Karlsruhe, Germany
2. Directorate General for Energy, European Commission, Luxembourg

* E-mail: jozsef.zsigrai@ec.europa.eu

Abstract:

The isotopic composition and concentration of Pu in eight "high-burn-up" mixed-oxide (MOX) fuel samples have been determined by destructive and non-destructive techniques. In addition, the U concentration and U isotopic composition was also available from the destructive techniques. The applied non-destructive techniques were gamma spectrometry, calorimetry and neutron coincidence counting, while the destructive techniques were titration, alpha spectrometry and thermal ionization mass spectrometry combined with isotope dilution. The current study describes the measurements and compares the results obtained by the mentioned techniques. Some lessons learned for the improvement of the non-destructive assay are also discussed.

Keywords: High burn-up MOX, NDA, U and Pu assay

1. Introduction

In order to determine the Pu content of mixed-oxide (MOX) samples from fuel fabrication plants, safeguards inspectors usually send the samples to an analytical laboratory. The very precise measurement results obtained by destructive analysis (DA) techniques in the analytical laboratory are essential for safeguarding the fuel fabrication plants. However, the transport of the nuclear samples is usually quite expensive and time consuming. With all this, more than a year may pass before the analytical results are available

For this reason it would be advantageous to perform some of the measurements on-site, possibly without generating radioactive waste, to have a quick assessment of the Pu content of the verified materials before they are shipped to a laboratory for more detailed analysis. Non-destructive (NDA) measurement techniques make this possible.

Previous studies done several years ago (see, e.g., [1], [2], [3] and [4]) have compared the Pu concentrations obtained either by calorimetry (CAL) or neutron coincidence counting (NCC) in various samples to the results of destructive techniques. They have shown that under ideal conditions the accuracy of CAL and NCC come close to that of the DA options.

In this work we investigated the performance of gamma spectrometry, CAL and NCC. Gamma spectrometry was used for determining the Pu isotopic composition, and both CAL and NCC were used to measure the Pu concentration. The results of the non-destructive techniques were compared to DA results from potentiometric titration and isotope dilution mass spectrometry (IDMS). IDMS values were taken as the Pu reference values for the study.

2. Determining the isotopic composition

Many of the techniques used for measuring the U and Pu content of the samples require the knowledge of the isotopic composition in order to be able to convert the measured signal to total Pu (or U) concentration. In addition, the isotopic composition itself is an important piece of information in the safeguards verification of nuclear activities.

In this work the non-destructive determination of the Pu isotopic composition of the investigated MOX samples was done by gamma spectrometry. The destructive option for measuring isotopic composition was thermal ionisation mass spectrometry (TIMS) combined with alpha spectrometry. The destructive analysis provided both the U and Pu isotopic composition.

Two high-resolution gamma spectrometers based on liquid-nitrogen-cooled planar HPGe detectors were deployed. We call the two spectrometers "external" and "internal". The detectors were connected to analog NIM electronics. In this setup, the resolution measured using 2 microseconds shaping time was 512 ev at 122 keV for the "internal" spectrometer, while for the "external" spectrometer it was 541 eV. For both detectors we have selected the counting time in such a way, to achieve a total of at least 5 x 10^7 counts in the energy range up to 300 keV.

The "external" gamma spectrometer was based on a stand-alone HPGe detector Canberra GL0210R having 200 m^2 active area and 10 mm thickness, inside its own lead shielding. For the gamma measurements outside the glovebox, the sample-to-detector distance was adjustable and there was a choice of absorbers between the detector and the source. We used 0.5 mm of Sn foil in front of the samples and we chose the source-to-detector distance in such a way that the dead-time was around 1-2 % and the total count-rate was around 500-1000 counts per second (cps).

The "internal" gamma spectrometer was integrated with a neutron coincidence counter attached to a glove-box, so that a gamma measurement could be done simultaneously with a neutron measurement. This was the so-called "N-Gamma counter" or "OSL counter" ([5]-[7]), which includes a Canberra GL0310R HPGe detector having 300 m^2 active area and 10 mm thickness. The detector was viewing the samples through a 1 cm diameter and 1.5 cm long lead collimator. In most cases, the Cd sleeve into which the samples where placed provided just the right filtering of the low-energy gammas from ^{241}Am. In addition, by means of a cylindrical Al placeholder placed into the Cd-sleeve, the pellet samples could be positioned inside the counter very accurately. The dead time was between 2-5 % and the total count rate was about 700-2000 cps. However, for one powder sample (see sample 17891 below) which contained almost 2 g of Pu, the filtering by the Cd sleeve was not sufficient so the count rate and dead time were quite high (4000 cps and 12 %, respectively).

The gamma spectra from the two spectrometers were evaluated using the computer code MGA v9.7 [8], [9].

As ^{242}Pu cannot be directly measured by gamma spectrometry it has to be estimated based on an isotopic correlation. In particular, we have used the following correlation [10], [11]

$$\frac{^{242}Pu}{^{239}Pu} = C_0\left[\frac{^{238}Pu}{^{239}Pu}\right]^{C_1}\left[\frac{^{240}Pu}{^{239}Pu}\right]^{C_2} \quad (1)$$

According to the algorithm of [10], we have chosen C_0=1.333, C_1=0.330 and C_2=1.700.

To evaluate Equation (1), we have used the features available in MGA. Namely, the MGA code uses an equation which has a total of 10 parameters for determining the ^{242}Pu/^{239}Pu ratio [9]. The values of those parameters can be set in the MGA setup file. Equation (1) can be obtained from the MGA equation by setting the first three MGA parameters to their chosen values, and the remaining seven parameters to zero.

The investigated MOX samples contained "high-burn-up" Pu, with relatively high ^{242}Pu (7%) and low ^{239}Pu (~55%) fraction. This presents a challenge for gamma spectrometry and in particular for the MGA code, because it relies on the presence of the ^{239}Pu gamma peaks, and because the estimation of the ^{242}Pu fractions is more significant than for low burn-up Pu. Nevertheless, the obtained results show that MGA V9.7 is able to cope with this situation.

Table 1: Isotopic composition of Pu in the investigated MOX samples measured by the combination of TIMS and alpha spectrometry

Sample internal Id	^{238}Pu [%]	Relative uncert. [%]	^{239}Pu [%]	Relative uncert. [%]	^{240}Pu [%]	Relative uncert. [%]	^{241}Pu [%]	Relative uncert. [%]	^{241}Pu [%]	Relative uncert. [%]
17891	2.549	0.77	54.691	0.011	26.642	0.039	8.050	0.16	8.068	0.16
17897	2.259	0.77	55.750	0.011	26.489	0.039	7.992	0.16	7.511	0.16
17903	2.482	0.77	55.273	0.011	26.568	0.039	7.824	0.16	7.853	0.16
17909	2.440	0.77	55.579	0.011	26.502	0.039	7.707	0.16	7.773	0.16
17915	2.105	0.77	56.430	0.011	26.515	0.039	7.696	0.16	7.254	0.16
17921	2.170	0.77	56.245	0.011	26.635	0.039	7.554	0.16	7.396	0.16
17927	2.328	0.77	54.329	0.011	28.584	0.039	6.981	0.16	7.778	0.16
17933	2.224	0.77	56.518	0.011	26.356	0.039	7.533	0.16	7.370	0.16

Table 2: The sample form, total sample weight, and the ^{241}Am/Pu ratio in the investigated MOX samples measured by the two gamma spectrometers. (Note: net weight for pellets is measured while net weight for powders is from declaration)

Sample internal Id	Sample form	Net weight [g]	External		Internal	
			^{241}Am/Pu [%]	Relative uncert. [%]	^{241}Am/Pu [%]	Relative uncert. [%]
17891	Powder	8.2	2.951	1.69	3.002	1.84
17897	Pellet	6.47925	3.370	1.22	3.359	1.27
17903	Pellet	6.35146	3.005	1.19	2.983	1.36
17909	Pellet	6.49535	2.978	1.68	2.930	1.14
17915	Powder	4.4	2.810	1.06	2.778	1.10
17921	Pellet	6.50995	2.628	1.17	2.592	1.25
17927	Powder	5.7	1.652	1.43	1.647	1.12
17933	Pellet	8.42318	2.658	1.61	2.695	1.32

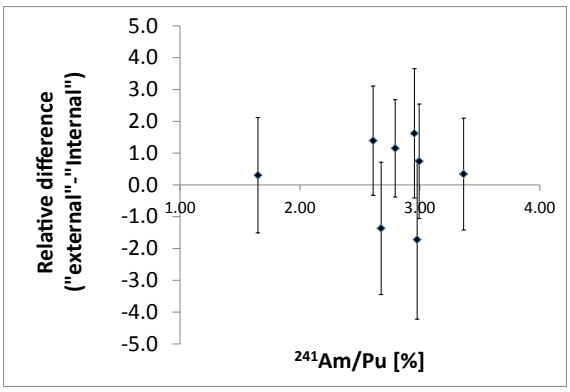

Figure 1 The relative difference of the ^{241}Am/Pu ratio obtained from the two gamma spectrometers, as a function of the ^{241}Am/Pu ratio. The error bars represent the combined uncertainty calculated from the uncertainties reported by MGA for the two spectrometers.

In Figure 1 we can see that the ^{241}Am/Pu ratios determined from the spectra taken by the two gamma spectrometers agree within the uncertainties reported by MGA.

Taking the TIMS results as reference, the performance of the two gamma spectrometers is compared in Table 3 and Table 4 as well as in Figure 2. The Pu isotope abundances calculated from the gamma spectra taken by the two detectors agree very well. Furthermore, for both spectrometers, the bias between the values from gamma spectrometry and values from TIMS is less than the combined uncertainty obtained from the uncertainty reported by MGA and the uncertainty of the TIMS (+alpha) measurement. Nevertheless, the numbers in Table 5, show that the average biases from the "internal" gamma spectrometer have consistently larger bias against TIMS, than the results from the "external" gamma spectrometer, even though they overlap within their standard deviations.

Table 3: Relative bias (%) of the MGA results obtained from the "external" spectrometer against TIMS (+alpha) results. The uncertainty is the combined uncertainty calculated from the uncertainty reported by MGA and the uncertainty of the TIMS (+alpha) measurement.

Sample internal Id	^{238}Pu	Relative uncert. [%]	^{239}Pu	Relative uncert. [%]	^{240}Pu	Relative uncert. [%]	^{241}Pu	Relative uncert. [%]	^{241}Pu	Relative uncert. [%]
17891	0.81	1.85	1.01	1.57	-0.19	1.76	-0.68	1.68	-5.85	10.00
17897	0.96	1.44	0.65	1.08	-0.03	1.27	-0.02	1.21	-5.00	10.00
17903	0.23	1.41	1.72	1.07	-1.19	1.23	-0.12	1.18	-8.06	10.00
17909	1.71	1.84	0.85	1.52	-0.36	1.75	0.58	1.66	-5.94	10.00
17915	0.38	1.31	1.47	0.95	-0.97	1.11	-0.59	1.06	-7.39	10.00
17921	2.18	1.40	0.20	1.05	0.13	1.21	1.04	1.16	-3.69	10.00
17927	-0.04	1.61	-0.02	1.37	-1.39	1.44	-1.02	1.42	6.19	10.00
17933	1.48	1.78	0.55	1.43	0.09	1.67	0.38	1.59	-5.39	10.00

Table 4: Relative bias (%) of the MGA results obtained from the "internal" spectrometer against TIMS (+alpha) results. The uncertainty is the combined uncertainty calculated from the uncertainty reported by MGA and the uncertainty of the TIMS (+alpha) measurement.

Sample internal Id	^{238}Pu	Relative uncert. [%]	^{239}Pu	Relative uncert. [%]	^{240}Pu	Relative uncert. [%]	^{241}Pu	Relative uncert. [%]	^{241}Pu	Relative uncert. [%]
17891	0.87	1.99	1.55	1.78	-0.93	1.87	-0.19	1.83	-7.54	10.00
17897	1.74	1.48	0.49	1.19	-0.09	1.31	0.78	1.26	-4.66	10.00
17903	0.72	1.56	1.15	1.29	-0.64	1.38	0.33	1.35	-6.47	10.00
17909	1.06	1.37	1.22	1.08	-0.60	1.17	-0.17	1.14	-6.87	10.00
17915	0.80	1.34	1.58	0.99	-1.30	1.14	0.12	1.09	-7.88	10.00
17921	1.43	1.47	0.80	1.18	-0.41	1.28	0.36	1.25	-5.39	10.00
17927	-0.53	1.35	0.79	1.05	-2.16	1.13	-1.31	1.10	3.76	10.00
17933	2.66	1.52	0.03	1.23	0.44	1.35	1.30	1.31	-3.95	10.00

Table 5: Pu isotopic fractions average bias between gamma spectrometry and TIMS for the two gamma spectrometers

	Pu 238		Pu 239		Pu 240		Pu 241		Pu 242	
	Avg. bias	St. dev.	Avg. bias	St. dev.	Avg. bias	St. dev.	Avg. bias	St. dev.	Avg. bias	St. dev.
"External"	0.97	0.77	0.81	0.59	-0.49	0.61	-0.06	0.70	-4.39	4.49
"Internal"	1.09	0.92	0.95	0.53	-0.71	0.79	0.15	0.77	-4.88	3.75

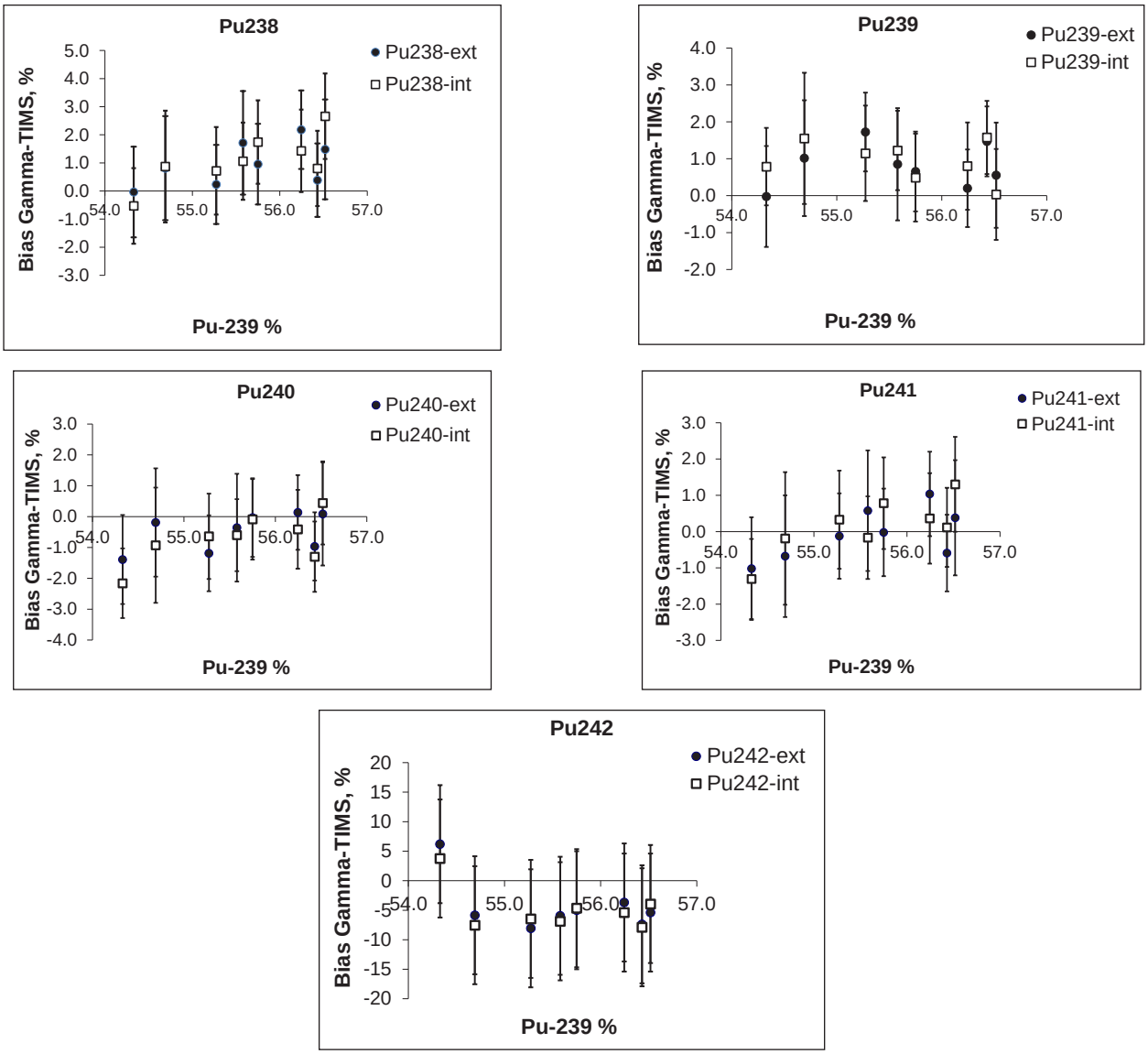

Figure 2: The relative difference of the Pu isotopic composition between gamma spectrometry and TIMS as a function of ^{239}Pu isotopic fraction. The error bars represent the combined uncertainty obtained from the uncertainty reported by MGA and the uncertainties of the TIMS (+alpha) measurement.

3. Determining the U and Pu concentration

3.1 Calorimetry

Calorimetry provides a very precise non-destructive option for measuring the Pu content of small solid samples (powders and pellets), provided that chemical reactions are negligible. The decay heat of these samples can be measured to a precision better than 0.4-0.5%. The decay heat is directly proportional to the mass of the decaying isotopes. Different Pu isotopes have different decay heat; therefore, one needs to know the isotopic composition of Pu in order to convert the measured heat to Pu mass. In addition, ^{241}Am, which is a decay product of ^{241}Pu, has a very high specific decay heat, so the ^{241}Am/Pu ratio as also required in order to calculate the proportion of the heat from ^{241}Am. If accurate information on the Pu isotopic composition is available (e.g. from TIMS and alpha spectrometry), then the Pu mass can be evaluated from the measured decay heat to an accuracy better than 1 %. If only isotopics from gamma spectrometry are available, the accuracy of the Pu mass measurement by calorimetry is around 1-2 %.

Each of the eight MOX samples were received in brass transport containers packed together in a single double bag. In our laboratory the whole package was introduced into a glove-box, where the samples were separated, but kept in their original transport containers.

In order to determine the Pu concentration from the calorimetric measurements, a measure of the total sample mass is needed as well. The weighing uncertainties directly translate to the uncertainty of the Pu concentration. The weight of each pellet has been measured on an analytical balance. For weight measurement the pellets were taken

out from their transport containers, inside the glove-box. The containers of the powder samples were not opened during the NDA measurements, therefore their declared weight was taken for calculating the Pu concentration.

For the calorimetric measurements the MOX samples were kept in their original transport containers. As the calorimeter available in our laboratory is currently not attached to a glove-box, the samples had to be bagged-out from the glove-box for the calorimetric measurements. They were bagged-out inside their containers one-by-one, in very small double bags. The double-bags needed to be very small in order that the samples could fit into the measurement cell of the calorimeter. We used a TAM III calorimeter from TA Instruments. In order to reach thermal equilibrium, the samples were left in the calorimeter for 2-3 days.

3.2 Neutron coincidence counting (NCC)

The neutron-gamma counter ("OSL counter") was also used for measuring the total and time-correlated neutron radiation of the samples, by means of neutron coincidence counting. The rate of time correlated neutrons is proportional to the effective ^{240}Pu mass. To convert ^{240}Pu effective to total Pu mass, the Pu isotopic composition is required.

Furthermore, to relate the measured signal to the effective ^{240}Pu mass, the neutron counter has to be calibrated. For calibration one could use standards similar to the measured samples. However, due to the great variety of samples, with varying isotopic composition, geometrical form, matrix composition etc. this approach can become impractical, as a very large number of calibration standards would be needed. An alternative, followed in the present work, is to use Monte Carlo modelling to calculate correction factors which relate the calibration done with a physical standard to a calibration applicable to the configuration of the measured samples [7]. At the time of writing this article, the evaluation of the data from the neutron measurements is still in progress, and it is not presented here.

3.3 Isotope dilution mass spectrometry (IDMS)

In this work the reference destructive analysis technique used for the quantification of U and Pu concentration is Isotope Dilution Mass Spectrometry (IDMS) [12]. The MOX samples were spiked with ^{233}U and ^{242}Pu. Accurate weighing in the spiking procedure is a must for precise results in IDMS, so it has to be carried out to the best practices. The so-called "double weighing reverse pipetting method" [12], was our procedure of choice due to its proven higher precision over other methods.

After the spiking, a column separation was carried out to collect the U and Pu fractions, which were subsequently analysed by thermal ionization mass spectrometry and, for the Pu fractions, by alpha spectrometry. The separation was carried out with UTEVA (®Eichrom) resin, conditioned in 6M HNO_3. Before separation, H_2O_2 was added to the samples, so that Pu was converted into its tetravalent state. For the reaction to be effective, at least 45 minutes are required. Then 1 mL of sample is loaded on the column. 6M HNO_3 is used to wash the columns after loading, to remove fission products and Am. Subsequently, the Pu fraction is stripped from the column with a solution of Hydroxylamine and Ascorbic acid in 2M HNO_3 and collected for analysis.

As ^{238}U is usually present in these samples by a factor of 100 to even 1000 higher than Pu, even a small percentage of contamination can generate a high background at m/z ratio 238. The chromatographic separation does not guarantee a 100 % separation of plutonium from uranium. In order to solve the problem of the isobaric interference of ^{238}Pu with ^{238}U in the mass spectrometer, the ^{238}Pu to $^{239/240}$Pu ratio was measured by alpha spectrometry.

Before collecting the U fractions, the columns were washed with 6mL of the Pu stripping solution, to reduce as much as possible the presence of Pu leftovers in the U fraction. U was then stripped from the columns by means of an ammonium oxalate solution.

3.4 Titration

The uranium content of the MOX samples was also determined using potentiometric indirect titration following a modified Davies and Gray methodology [13]. The samples were dissolved in 8M nitric acid and later adjusted to reach concentrations around 40 mg U/g solution suitable for titration. The determination of the U mass fraction in MOX samples is possible for a U/Pu ratio higher than 2.5.

The plutonium content in the dissolved samples, having at least 10 mg Pu/g solution, was determined using potentiometric back titration [14]. A minimum amount of 0.5 g of solid sample or 10 ml of liquid sample (HNO_3 solution) are required.

4. Results

The relative differences of the Pu concentration obtained by the applied techniques with respect to IDMS are shown in Table 6 and in Figure 3. The NDA options presented here are the combination of calorimetry with gamma spectrometry and the combination of calorimetry with operator-declared isotopics.

The NCC results are not evaluated in this paper, as the calibration of the neutron counter by Monte Carlo modelling is in progress and will be presented elsewhere.

The uncertainty of the Pu concentration measured by calorimetry is the combined uncertainty obtained from the uncertainty of the heat measurement, the uncertainties of the Pu isotopic fractions and the uncertainties of the nuclear data (half live and specific heat of the Pu isotopes and ^{241}Am). The uncertainties of the weight measurements are not included.

Table 6: Relative (percent) differences of the Pu concentration obtained by various techniques with respect to IDMS. The uncertainties of the differences combine the uncertainty of the NDA and DA measurements.

Sample Id	Sample form	Calorimetry + isotopics from gamma		Calorimetry + declared isotopics		Titration		Declared	
		Value	Abs. Unc.	Value	Abs. Unc.	Value	Abs. Unc.	Value	Abs. Unc.
17891	powder	1.40	1.28	0.80	1.01	0.23	0.16	1.83	0.09
17897	pellet	-0.15	0.93	-0.49	0.96	0.06	0.16	0.32	0.18
17903	pellet	-0.46	0.94	-0.68	1.00	0.09	0.16	-0.74	0.13
17909	pellet	-0.87	1.26	0.03	1.00	0.33	0.16	-0.35	0.12
17915	powder	0.86	0.85	0.42	0.98	-0.33	0.16	-0.16	0.19
17921	pellet	-1.27	0.91	-0.50	0.98	-0.11	0.16	-0.11	0.11
17927	powder	1.16	1.13	0.15	1.05	0.25	0.16	0.85	0.17
17933	pellet	-0.55	1.20	-0.14	1.00	0.16	0.21	-1.79	0.13
Average		**0.01**	**1.06**	**-0.05**	**1.00**	**0.09**	**0.17**	**-0.02**	**0.14**
Average of abs. values		**0.84**		**0.40**		**0.20**		**0.77**	
Standard deviation		**0.99**		**0.51**		**0.22**		**1.07**	

One of the powder samples (sample id. 17891) contained almost 2 g of Pu so the heat output of the sample was quite high and it was on the edge of the usual range of applicability of the calorimeter available in ITU. In addition, as for all powder samples, the weight of the powder was taken from the declaration. Consequently, the bias for this sample is larger than for the other samples, as it can be seen from Table 6 and Figure 3. Therefore, repeated measurements with smaller, precisely weighed amounts of powder were done. The measurements on the subsamples provided better agreement with the IDMS results. Nevertheless, here we present the original data from the full sample, as it can represent a realistic situation which might be encountered in potential future field measurements.

Combining calorimetry with the isotopic composition declared by the operator gives a result which is even closer to the reference values from IDMS, than the combination with gamma spectrometry. Since the consistency of the operator-declared isotopic composition can be verified by gamma spectrometry, the combination of calorimetry with the operator-declared isotopic composition could be also a viable option for the safeguards verification of the Pu content of MOX fuel.

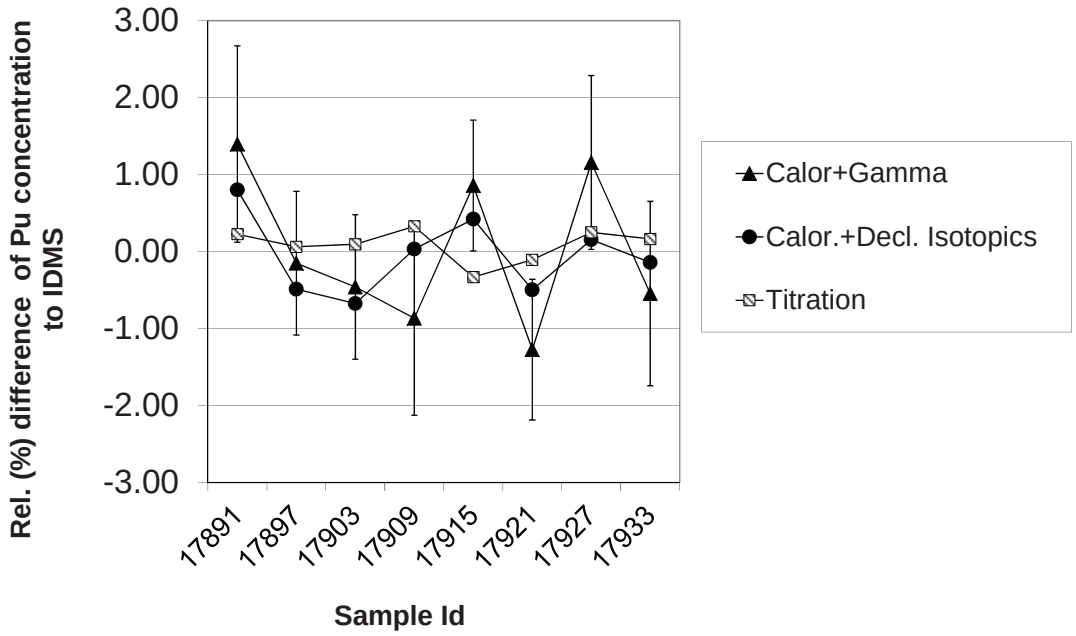

Figure 3: Relative differences of the Pu concentration obtained by various techniques with respect to IDMS. The error bars (1s) for the combination of calorimetry and gamma spectrometry only are shown. They include the uncertainty of the NDA and DA measurement.

We observed that the combination of calorimetry with isotopic composition determined by TIMS and alpha spectrometry (not shown in Figure 3 and Table 6) agrees less well with IDMS than the combination with operator-declared isotopics. The reason for this is a negative bias of about 1.2 % which we observed in our alpha-spectrometric measurement of the ^{238}Pu to $^{239/240}$Pu ratio. This translates directly to a bias in ^{238}Pu abundance, which has a strong impact on the accuracy of the Pu mass calculated from the calorimetric measurements. The bias in the alpha-spectrometric measurements was due to relatively poor resolution of the spectrometer and inappropriate peak area evaluation in the alpha-spectrometric software. In measurements of future samples we intend to reduce this bias through the use of a better spectrometer and better alpha-spectrometric software which enables proper peak fitting.

5. Conclusions

The results in Table 6 and Figure 3 show that calorimetry combined with isotopic composition from gamma spectrometry provides a fairly accurate measurement option for Pu concentration, with an accuracy of about 1%, in a fully non-destructive way.

It is interesting to note that, on average, the non-destructive measurement options show a better agreement with IDMS, than the declared concentrations. For the powder samples this might be due to the fact that more than one year has passed between the time of the declaration and of the measurements in ITU. During this time the samples could have either lost or gained some moisture, affecting their weight and consequently the Pu concentration at the time of the measurement. Another reason might be a potential inhomogeneity of the verified batch. However, we do not have enough information either to confirm or reject these hypotheses.

The planned step forward is to re-evaluate all the above described measurements based on the so-called “CANEGA” approach [15], which combines three non-destructive techniques, to simultaneously determine the Pu mass and the Pu isotopic composition, including ^{242}Pu abundance, without any prior knowledge of the type of Pu under assay. The term “CANEGA” stands for CAlorimetry, NEeutron coincidence counting and GAmma spectrometry. The combination of these three techniques may improve the accuracy of the non-destructive measurement of Pu isotopic composition, and consequently also the accuracy of the non-destructive measurement of the Pu concentration [15].

6. References

[1] K. Mayer, H. Ottmar, O. Cromboom, K. Casteleyn, *Analysis of MOX Samples using Chemical and Radiometric Methods - A Method Comparison,* Proceedings of the 21st ESARDA Annual Meeting, Symposium on safeguards and nuclear material management, Seville 1999, p605-608

[2] H. Ottmar, S. Abousahl, P. van Belle, A. Morgenstern, M.-C. Vincent, Plutonium Assay by Calorimetry – An Experimental Case Study for Reactor-Grade Plutonium Materials, Proceedings of ESARDA Symposium, Stockhom, 2003,

[3] P. van Belle and H. Ottmar, An Analysis of the Measurement Uncertainty in Determining the Plutonium Content in Small Samples by Neutron Coincidence Counting, Proceedings of ESARDA Symposium, Bruges, 2001, p496-508

[4] H. Menlove, R. Wellum, M. Ougier, K. Mayer, *Performance Tests Of The High Accuracy Combined Neutron/Gamma Detector (Osl-Counter)*, Proceedings ESARDA, Rome 1993, p363-369

[5] D. Davidson, J. Verplancke, P. Vermeulen, H. Menlove, H.G. Wagner, B. Brandalise, *A New-High-Accuracy Combined Neutron/Gamma Counter For In-Glove-Box Measurements Of Puo2 And MOX Safeguards Samples (OSL-Counter)*, Proceedings ESARDA Symposium, Rome 1993, p585-588

[6] Menlove, H., Davidson, D., Verplancke, J.; Vermeulen, P., Wagner, H.G.; Wellum, R. Brandelise, B. Mayer, K., *Design and performance of a new high accuracy combined small sample neutron/gamma detector,* LA-UR--93-2670; CONF-930749—26, 34th annual meeting of the Institute of Nuclear Materials Management, Scottsdale, 1993

[7] H.Ottmar, A.Schubert, T.R.Wenz, H.O.Menlove, G.W.Eccleston, U.Blohm-Hieber, M.T.Swinhoe, *A Consistent Calibration Approach for Neutron-Coincidence Counting of Small $Pu0_2$ and MOX Samples,* Proceedings of the ESARDA Symposium on safeguards and nuclear material management, Montpellier 1997, p335-344

[8] R. Gunnink*, MGA: A Gamma-Ray Spectrum Analysis Code for Determining Plutonium Isotopic Abundances*, UCRL-LR-103220, 1990

[9] MGA user manual, Canberra Industries, Inc, 2008

[10] S. Abousahl, P. Van Belle, H. Eberle, H. Ottmar, *Performance Of Isotope Correlations For The Estimate Of ^{242}Pu, Proceedings of the Symposium on International Safeguards*, IAEA-SM-367/5/04/P, Vienna, 2001

[11] G. Bignan, W. Ruhter, H. Ottmar, A. Schubert, C. Zimmerman, *Plutonium Isotopic Determination By Gamma Spectometry: Recommendations for the*

^{242}*Pu content evaluation using a new algorithm*, ESARDA BulletiN, No. 28, January 1998, p1-6

[12] P. van Belle and E. Zuleger, ITU Procedure for the Verification of Large Scale U/Pu Dried Spikes, ITU Technical Note, Report No: JRC-ITU-TPW-2009/22

[13] ASTM Standard C 1267 – 06, Standard Test Method for Uranium by Iron (II) Reduction in Phosphoric Acid Followed by Chromium (VI) Titration in the Presence of Vanadium, 2006

[14] German standard, DIN 25704, Determination of the plutonium content in sulphuric acid and nitric acid solutions; potentiometric titration method with potassium dichromate, 1993

[15] S. Abousahl, P. van Belle, H. Ottmar, *Combined calorimetry/neutron coincidence counting/gamma spectrometry (CANEGA) measurements for plutonium mass and isotopic assay*, Nuclear Instruments and Methods in Physics Research A 543 (2005) p608–618

Change in impurities observed during the refining and conversion processes

George Healey[a], Peter Button[b]

a. 77 Annie Cresent, Ajax, Ontario, Canada L1T 3Z4
b. Canadian Nuclear Safety Commission, 280 Slater St., Ottawa, Ontario, Canada K1P 5S9
E-mail: george.healey@sympatico.ca, peter.button@cnsc-ccsn.gc.ca

Abstract:

In 2009 the Canadian Safeguards Support Program undertook a sampling campaign to follow a batch of UOC feed material through the refining and conversion processes at Cameco Corporation's Blind River and Port Hope facilities. A total of 59 samples were taken in three categories as follows; sixteen UOC samples, twenty-two samples during the conversion of UOC to UO_3, and twenty-one samples during the conversion of UO_3 to UF_6. Samples were analyzed for trace element content by ICP-MS, uranium and lead isotope ratios by MC-ICP-MS and hydrogen and oxygen isotope ratios by IRMS techniques.

The analytical results have been examined to find the extent to which trace element levels and isotopic compositions change at the various processing steps. Both national forensics organisations and IAEA safeguards are interested in characterising these materials.

Initial results were presented at the ESARDA 2011 meeting in Budapest, but the data was incomplete and the results from different laboratories were inconsistent. This paper will provide an update on our findings.

Keywords: UOC; uranium; impurities; forensics; traceability; isotopic

1. Introduction

The principal objective of this work is to be able to identify the origins of Uranium Ore Concentrates (UOCs) and the down-stream uranium products leading to UF_6. Characterisation of these materials is of interest to the IAEA where it may assist in validating declarations. Establishing the origins of these materials is also of great interest to national forensics programs. The findings of this report may also impact how sampling should be carried out at bulk facilities.

This program was conducted as a joint IAEA task; samples were also shared with the IAEA (Seibersdorf Analytical Laboratories, SAL) and JRC-ITU. As reported before, we faced certain challenges in reconciling the various data sets provided by the laboratories.

Firstly, for each of the four sources of UOC available for this study, aspects of geochemistry/mineralogy, mining practice and milling processes are examined to evaluate their influence on the trace element spectrum of product UOC. Secondly, an examination is made of changes that take place in the trace element spectrum as a blended feed of the subject UOCs are converted to final product UF_6. Thirdly, we briefly review some of the isotopic data that has been collected as a part of this work.

2. Collection of Samples and Analytical Results

Canada hosts uranium mines, a refinery and conversion facility. Collectively, they provide the possibility of tracking the same material from ore through to UF_6; though in this case, we only collected samples from Uranium Ore Concentrate (UOC) through to UF_6.

Samples were collected at Cameco's Blind River refinery in November 2009 and at Cameco's Port Hope conversion facility in February 2010. The location of these two facilities is shown in Fig. 1.

Figure 1: Refinery and Conversion facilities in Canada.

Upon receipt at Blind River, each lot is routinely analysed to determine its U and trace element content. Based on the analytical results and on production requirements, drums of UOC are selected from specific lots to provide sufficient feed for 24 hours, one day, of digestion. The number of drums selected from each lot, referred to as a blend, is controlled so as to provide a reasonably uniform total trace element input to digestion. Nevertheless, the solvent extraction process can tolerate considerable variation in trace element values thus the composition of blends can vary from day to day.

Figure 2 shows the blend of UOCs (UOC origin and quantity of each contributing to the blend) associated with our sampling campaign; we sampled this blend as it passed through the refining and conversion processes. For the purposes of this study, the trace element content of the digester output was calculated as a weighted average of the blends loaded into the digester over a three day period of November 9, 10 and 11, 2009. The blending of UOCs of different origin essentially eliminates any possibility of relating subsequent conversion intermediates and final product to a specific UOC input.

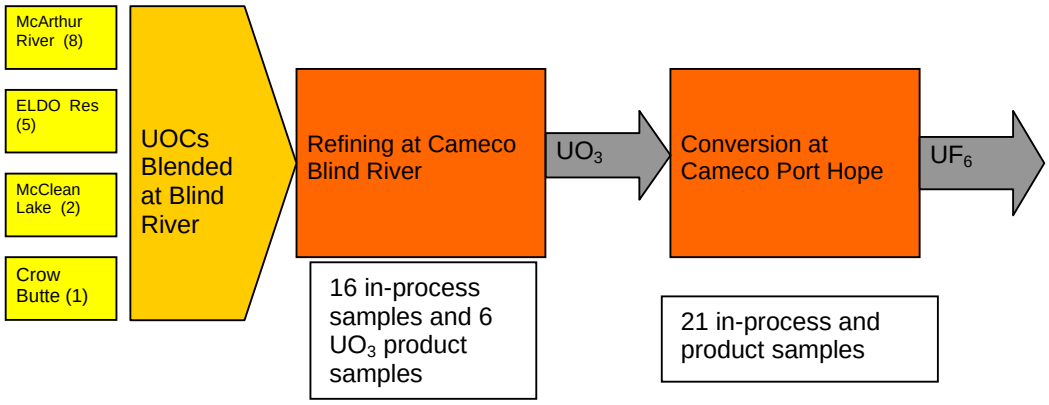

Figure 2: Major processes: blending, refining and conversion. The proportional contribution of each UOC to the blend is shown in brackets.

Considerable effort was expended during the sampling campaigns to ensure that samples would be taken from the same material as it progressed through the refining and conversion processes. Once collected, samples were then carefully homogenised before splitting to ensure that the samples distributed to the various laboratories would be consistent.

Samples were distributed to the following laboratories for analysis:

– Queen's University Facility for Isotope Research (QFIR), Kingston, Canada
– Seibersdorf Analytical Laboratory (SAL), Vienna, Austria
– Institute for Transuranium Elements (ITU), Karlsruhe, Germany

Cameco also provided process control and quality control analyses and historical analytical data as well as TE analyses for UO_2 and UF_4 samples that would not routinely be done. Cameco data was used as 'reference values' against which to assess the TE data provided by the three participating laboratories. For the most part, SAL trace element values are presented in this study. The reason for using SAL values was that SAL values were in good agreement with the Cameco reference data where that data was available. Out of the 67 element TE data set reported by the laboratories, SAL appeared to have analysis issues with just one element. ITU had difficulty with 7 elements and QFIR had difficulty with 13 elements. For the study, the ITU and QFIR trace element values were only used in cases where SAL values were not available, e.g., for the liquid samples from Blind River.

The variability in reported values for TEs was a surprise finding of the study. The question therefore arises as to what conclusions about TE behaviour during conversion processes would have been made if TE values had only been available from one lab rather than from three (and without the availability of 'referee values'). There appears to have been a limited review of results before reporting. This results in the reporting of values with very small measurement uncertainties, indicating high measurement precision, yet values that were sometimes inaccurate by factors of 10 to 200. It is understood that the elemental analysis of such complex mixtures such as these is problematic for laboratories. Some of the differences observed can be associated with different sample preparation procedures and different corrections for interference effects.

3. Elemental Impurities in UOCs

The Blind River refinery receives UOC from various sources with different milling practices. The sources of UOC involved with this sampling campaign were:

– McArthur River mine – processed at Key Lake Mill – UOC as U_3O_8
– Eldo Resources – processed at Rabbit Lake Mill – UOC as $UO_4 \bullet 2H_2O$
– McClean Lake mine – processed at McClean Lake Mill – UOC as U_3O_8
– Crow Butte – ISL – processed at Crow Butte Central plant – UOC as $UO_4 \bullet 2H_2O$

Impurities in the UOCs result from the source material, mining practices and milling processes. The results reported in 2011 [1] are mostly still valid, but here we offer some explanation for their Trace Element's (TE) behavior.

Comments are also provided as to which trace elements could be considered as 'marker elements' to distinguish between the UOCs available for this study. Within a spectrum of trace elements in UOC, a marker element is one which by virtue of presence and magnitude could be used to conclude that one UOC has a different origin than another. Trace elements originally present in ore and which survive mill processing are considered to be more reliable than those introduced by mill chemical processes. The proposed marker elements were selected from the available 67 element data set. Only elements present at a concentration of 1 ppm or greater were considered for suitability as markers.

The 67 element data set included the rare earth elements. A developing technique of considerable interest involves the determination of rare earth element patterns to link materials to sources. Examination of the rare earth element patterns is not addressed in this paper.

In the sections which follow, we provide analytical results to the same precision as the laboratory. This level of precision is not indicative of accuracy; however it does serve to maintain a link with the value retained in our database.

3.1 McArthur River UOC

McArthur River is a high-grade underground uranium mine. The average ore grade is 15-16% U_3O_8, the principal uranium minerals being pitchblende and coffinite. Due to the high U content, special procedures are necessary for radiological health and safety.

Ore is mined by the "raise bore" method. The raise bore technique requires tunnels (levels) to be driven above and below the ore body. A pilot hole is drilled between levels. When the pilot drill breaks through into the lower level, the drill bit is removed and a larger cutting bit, a reamer head, is attached to the drill string. As the reamer head is retracted toward the upper level, the cuttings drop to the lower level floor and are subsequently transported to an underground grinding station. The cuttings are wet ground to create a slurry which is then pumped to surface.

For mining purposes, reamed out holes (raises) are backfilled with Portland cement-based concrete. To extract as much ore as possible, the raises overlap, thus some of the backfill concrete placed in one hole is removed as the next hole is drilled. Material shipped to Key Lake consists of ore, concrete, and waste rock in slurry form.

At Key Lake, the slurry is blended (down blended) to a concentration of 4% U_3O_8. Low-grade U ore and other mineralized waste from previous open pit mining operations is prepared (ground) for use as down blend material. After downblending, leaching, solvent extraction, precipitation and calcining, the final product is U_3O_8. Note that it is already a blended product due to the down blending. Other impurities may be found due to the introduction of Portland cement in the mining process.

The consequence of the addition of so much dilution of the mined ore is that the trace element spectrum of McArthur River/Key Lake origin UOC will be more representative of the dilution material than of the ore. The use of H_2SO_4 and sulphate chemicals will result in S contamination in UOC.

For samples analyzed, the average total TE content of McArthur River UOC is 10935.6 ppm. The total average S level is 8872.8 ppm and the total Mo is 1231.3 ppm. These two elements constitute 92.4% of the total TE content. Subtracting S and Mo from the total leaves 831.5 ppm for all of the other trace elements. Thus, except for the high values for S and Mo, McArthur River UOC is high quality (high purity) material. Elements which unambiguously distinguish the McArthur River UOC from the other three UOCs (marker elements) would be S, W, B, and Ca. However, the S values were the result of temporary production problems and are subject to process changes. The Ca values could also be influenced by blending changes. The W and B values derive from the ore and would be more difficult to change. Thus, W and B are considered to be the more reliable markers for McArthur River UOC with respect to this set of four UOC sources.

3.2 Comments concerning sampling at a mine/mill

The situation at McArthur River illustrates an interesting point about sampling. A sample of the high grade uranium bearing stratum, i.e., the high grade ore without dilution, would have a particular TE spectrum in terms of element presence and magnitude which we will call TE spectrum A. A sample taken from the output of the underground crushing circuit would consist of high grade ore diluted with waste rock and cement. The crusher output would still be called ore, but it would be medium grade and have a particular TE spectrum, spectrum B, due to the presence of diluting species. TE spectrum A and B would be different. A sample taken from the output of the surface crushing plant would consist of the underground crusher output plus a large amount of dilutive species such as waste rock and very low grade uranium ores. The surface crusher output would still be called ore but, comparatively, it would be low grade ore and would have a particular TE spectrum, spectrum C, due to the presence of the diluting species. TE spectrum C would be different than spectra A or B. The output from the surface crusher is what is fed into the leaching circuit at the mill at which point the terms ore and mill feed are synonymous. The TE spectrum of UOC product is determined by the TE spectrum of the mill feed, TE spectrum C, influenced by process chemistry. Comparison of the TE spectrum of UOC to TE spectra A or B would lead to erroneous conclusions. Clearly, in taking or requesting an 'ore' sample, it would be important to

know in considerable detail exactly where the sample was taken and what ore processing might have taken place. It is suggested that for ore vs. UOC comparison purposes samples be taken from mill feed.

3.3 Eldo Resources (Rabbit Lake) UOC

Formerly an open pit mining operation, ore is currently extracted from the underground Eagle Point deposit. Eagle Point is an underground hard rock mine where low-grade ore (0.6-0.7 % U_3O_8) is mined by conventional vertical blast hole stoping methods. Because the ore is low-grade it can be mined and processed by conventional methods. Mined ore is transported to the surface for processing at the Rabbit Lake mill. Processing at the mill consists of grinding, H_2SO_4 leaching, decantation, solvent extraction, gypsum precipitation, and precipitation of UOC as uranium peroxide (UO_4•$2H_2O$). Wear of the grinding balls will add Fe. Use of alloy steel balls could contribute Si, V, Cr, and Mn.

The average total TE content is 23832.5 ppm (just over 2%). 34 elements are present at a level of 1 ppm or greater. Seven elements are present at levels greater than 1000 ppm: Al, Ca, Fe, Mg, Mo, S, and Si. Of these, Ca, Mg, and S are probably present due mainly to process chemistry. Al, Fe, Mo, and Si would be ore-related as carryover through solvent extraction; similarly for the high levels of P and K. The very high Al value probably reflects the presence of Illite, a complex alumino silicate clay mineral, in the ore zones.

13 elements could be considered to be markers for Rabbit Lake UOC, Al, Cr, Cu, Fe, Ga, Mg, Mn, P, Pb, Sc, Si, Ti and V. There is a notable presence of rare earth elements exemplified by 6 ppm Y and 3.5 ppm Sc.

3.4 McClean Lake UOC

Mining at McClean Lake ceased in 2010 and the McClean Lake mill (JEB mill) shut down in June 2010. At McClean Lake, ore deposits were originally found near the surface and were exploited by open pit mining methods. These deposits are located about 8 km northeast of the Rabbit Lake mine. Ore supply to the mill in 2009 and until shutdown was mainly from the Sue E deposit together with a small amount from the Sue A and Sue B deposits. The average grade mill feed in 2009 was 0.97% U_3O_8. Upon receipt at the mill, ore is finely ground, slurried with water, and pumped to the leaching circuit. In the leaching process, sulphuric acid and hydrogen peroxide are added to the slurry to dissolve the uranium from the ore. After solvent extraction purification, uranium is precipitated as ADU and calcined to U_3O_8.

The average total TE content is 5318.5 ppm, just over 0.5%. 26 elements were present at a level of 1 ppm or greater. Two elements are present at levels greater than 1000 ppm, Na and S with Mo present at an average level of 975.9 ppm. The presence of the high levels of Na and S are due mainly to process chemistry. Rare earth element values at McClean Lake are more comparable to those at McArthur River than at Rabbit Lake.

Ni, Th, Zn, and Zr – are potential markers for McClean Lake UOC. All four elements originate from ore, none are process-related.

3.5 Crow Butte UOC

Crow Butte is a solution mining or in-situ recovery (ISR) operation located in Nebraska, USA. At Crow Butte, a sodium bicarbonate leach solution with O_2 injection passes through the porous ore zone where mineral dissolution takes place and is then pumped to the surface via production wells.

Product solution passes through resin filled ion exchange columns. Uranium and trace elements transfer from the product solution to the resin. Loaded resin is stripped with an aqueous solution of sodium bicarbonate ($NaHCO_3$) and salt (NaCl). Uranium is present in the strip solution as uranyl carbonate, $UO_2(CO_3)_3$. Following further chemical processing, uranyl peroxide, (UO_4•$2H_2O$) is precipitated, thickened, dewatered, washed, and dried and drummed.

Coffinite is the main uranium mineral species. The origin of the uranium is in-situ rhyolitic ash material. The most common minerals in the sandstone are quartz, plagioclase (calcium alumino silicate), K-feldspar, coffinite, pyrite, calcite, illite/smectite and tyuyamunite [$Ca(UO_2)2(VO_4)2$•nH_2O]. Garnet, magnetite, marcasite, and illmenite ($FeTiO_3$) are present. Vanadium mineralization is present.

The average total TE content is just under 1.5%. 25 elements are present at a level of 1 ppm or greater. Five elements are present at levels greater than 1000 ppm: Na, V, Ca, Zr and S. The high Na level is a result of process chemistry. All other trace elements originate from the ore.

The high level of V is a result of the presence in the ore body of tyuyamunite and possibly unspecified species in volcanic ash. The high level of Ca could have numerous mineral sources principal among which would be calcite. The high Zr value probably originates from garnet, particularly taking into account the notable Hf value of 11.3 ppm. The high S value would originate from the pyrite content of the ore. The total for the five trace elements in excess of 1000 ppm is 12864.4 ppm (90.95% of the TE total). There is notable presence of yttrium (7.9 ppm) which, considering the level of P (233.3 ppm), might indicate the presence of xenotime (YPO_4) in the ore.

Four elements – Hf, Na, V, and Zr – are potential markers for Crow Butte UOC. Sodium is process-related; Hf, V, and Zr originate from ore.

4. Refining and Conversion Processes

Samples for TE analysis supplied to the three participating laboratories for this study were taken at the processing steps listed below.

– Receipt of UOCs - TEs measured
– Blending of UOCs - TEs not measured
– Digestion – TEs both measured and estimated by calculation
– Purification (solvent extraction) - TEs measured
– Concentration (boildown) (HNO_3 > UNH) - TEs measured
– Denitration (UNH > UO_3) – TEs measured
– Shipment of product UO_3 and receipt at Port Hope – TEs measured
– UO_3 preparation – TEs measured
– UO_2 production – TEs measured
– UF_4 hydrate production – TEs measured
– UF_4 dehydration - TEs measured
– UF_6 production -TEs measured

Cameco does not routinely sample and analyse each process step listed above but does routinely perform TE analysis of UOC receipts, product UO_3 and UF_6 for process control and specification purposes. Routine analysis done by Cameco is for fewer elements and with higher detection limits than for the analyses done for this study.

The first conversion activity at Blind River is to prepare a feed solution for the solvent extraction purification process. Receipts of UOC (lots) from different sources have different TE contents. It is desirable to supply a feed of reasonably uniform composition to solvent. In addition to UOC, steel shot and other scrap metal together with UO_3 dust recovered from the denitration dust collectors is used as a blend component. Once the drums in a blend are dumped into the feed hoppers and transferred to the digester the UOCs essentially lose their identity. Any product characteristics are derived from the blend and subsequent processes.

Digestion converts solid UOC, plus additions, into a liquid feed solution for solvent extraction. UOC is continuously fed into the digester where it is converted to uranyl nitrate. UOC is not the only material entering the digestion system. For operational purposes iron is added either as grit blast or as a solution from scrap recovery. Process chemicals such as phosphoric acid may also be added as well as recycled sumpage.

Following digestion the solution is fed to the solvent extraction circuit to produce purified uranyl nitrate referred to as “OK Liquor”. The purified uranyl nitrate (OK Liquor) is concentrated to produce uranyl nitrate hexahydrate (UNH). The concentrated UNH is then fed to the denitration pots for thermal decomposition to UO_3, the final product of Blind River.

At the Port Hope facility, pulverised UO_3 is fed into fluid bed reactors where UO_3 is reduced to UO_2.

UF_4 production is a two-stage operation. The first stage is reaction of UO_2 with HF in aqueous solution to produce uranium tetrafluoride hydrate ($UF_4 \bullet 2.5H_2O$). Dried and pulverised UF_4 is then fed to the UF_6 flame reactors to produce the final product.

5. Trace Element Changes During Refining and Conversion.

The following charts (Fig 3 to Fig 14) display the changes in a selection of TEs during the refining and conversion processes. The charts use SAL TE values. The reference level (100%) is the value calculated based on the blending information and the reported values for the individual UOCs. Note the scale on left (green) covers the full 100% and the scale on the right (blue) is set to accommodate the much lower values encountered later in processing. As expected, the effect of solvent extraction is to substantially reduce TE values in the digester input feed. Reduction factors are different for different elements and range from 1 to 1700.

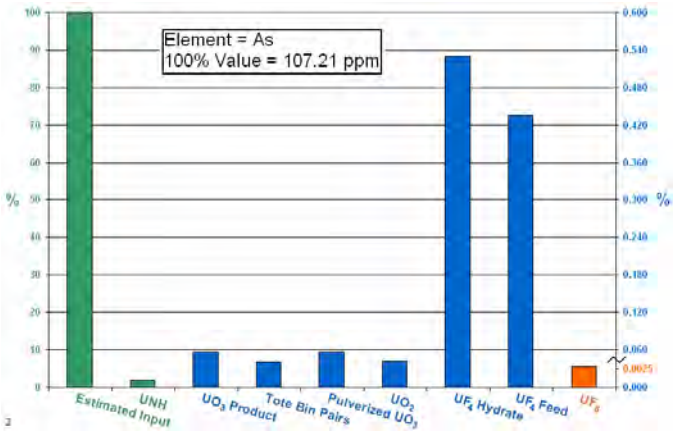

Fig 3: Arsenic returns in UF_4 production, but removed in final product (below detection limit)

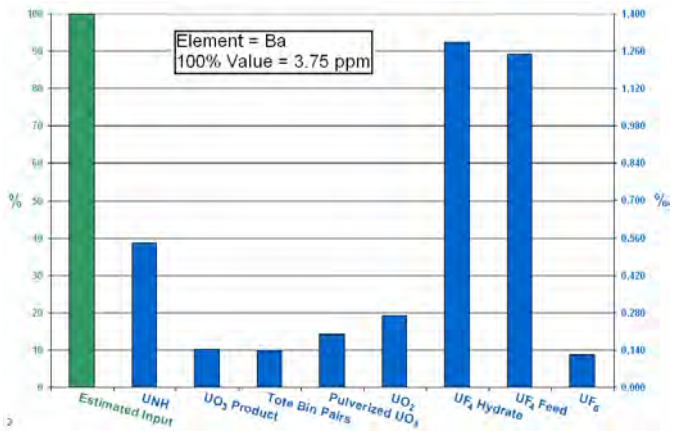

Fig 4: Ba increases during UF_4 production, but reduced in final product.

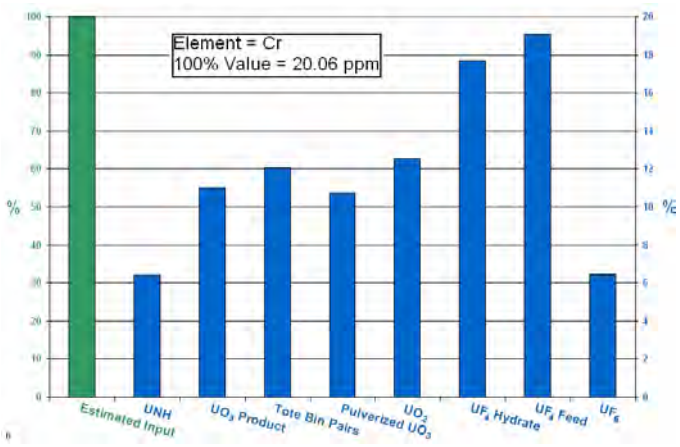

Fig 5: Cr increases after UNH – evidence of corrosion

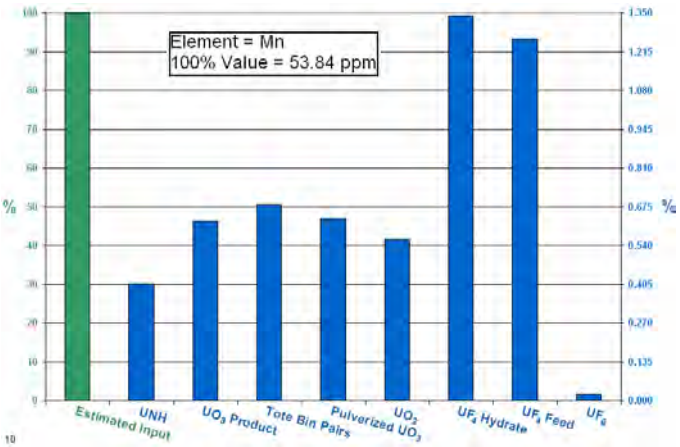

Fig 8: Evidence of corrosion during UF_4 production

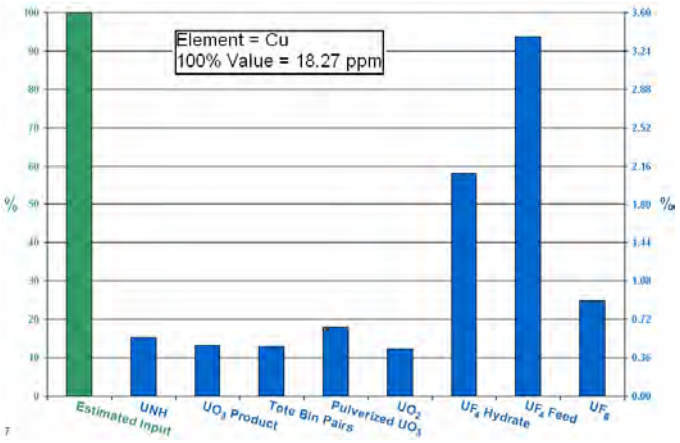

Fig 6: Cu increases in UF_4 production

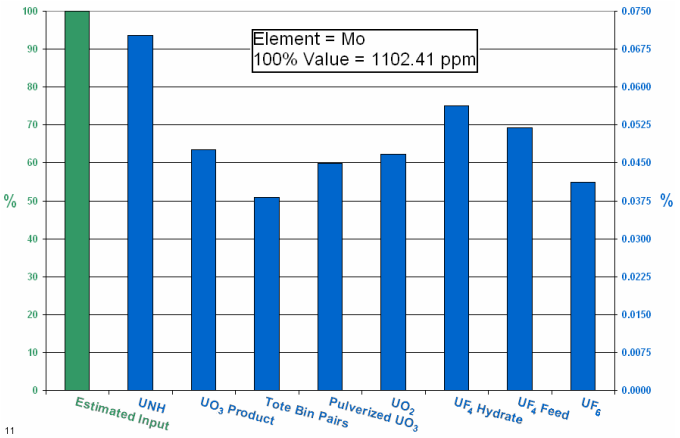

Fig 9: Mo is difficult to remove completely

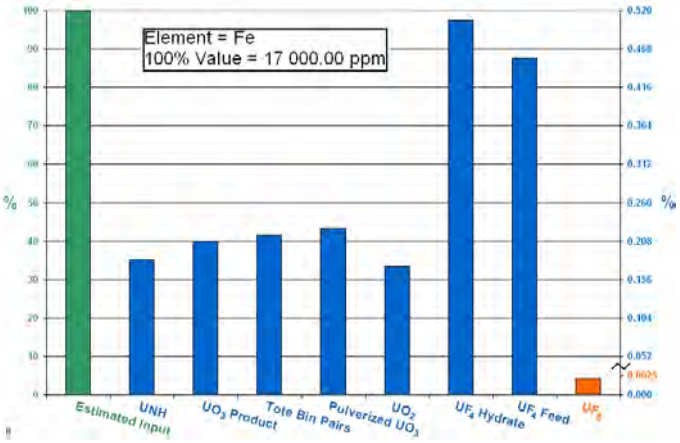

Fig. 7: Evidence of corrosion in UF_4 production. Note iron may be added in digestion.

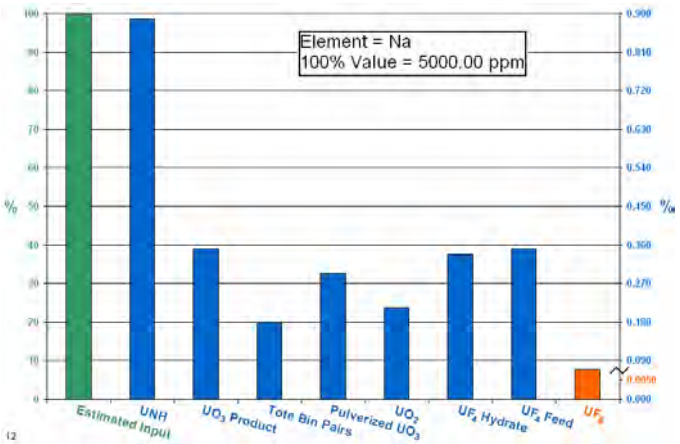

Fig 10: Na removed to below the detection limit

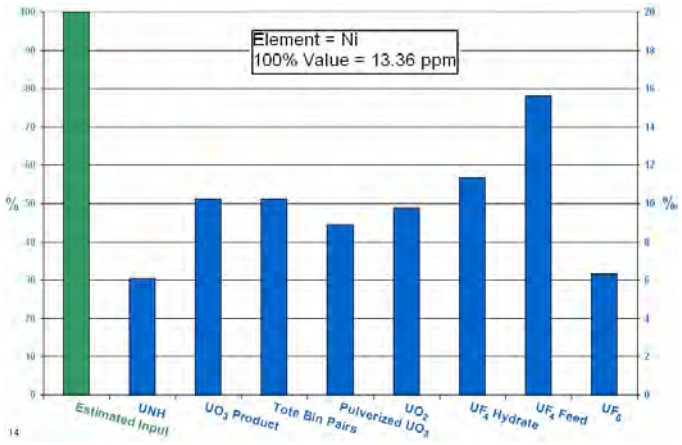

Fig 11: Difficult to remove Ni completely

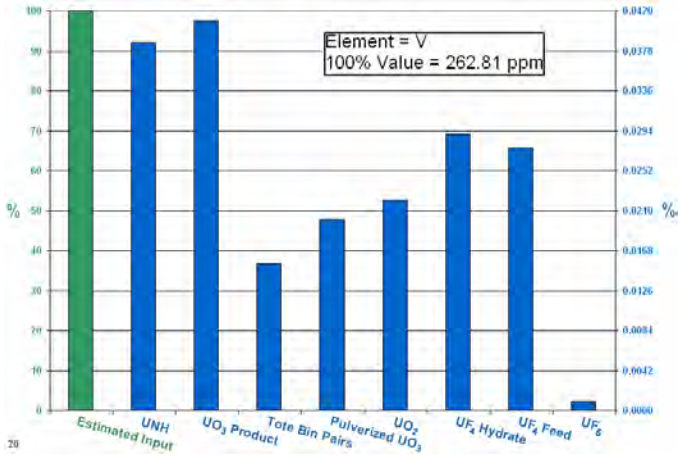

Fig 12: V is common in ores

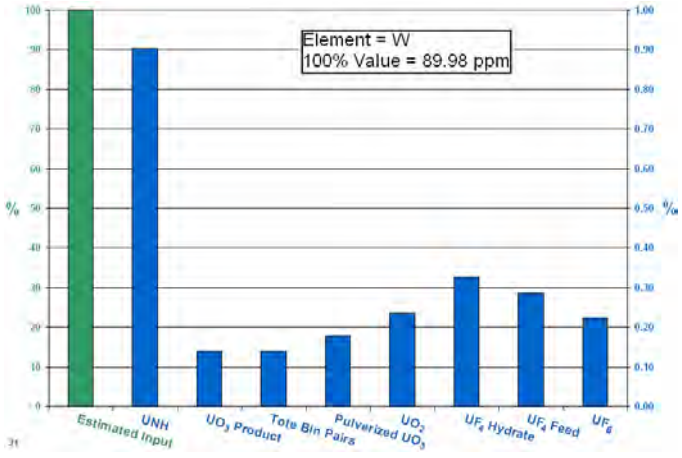

Fig 13: Tungsten is often found in ores

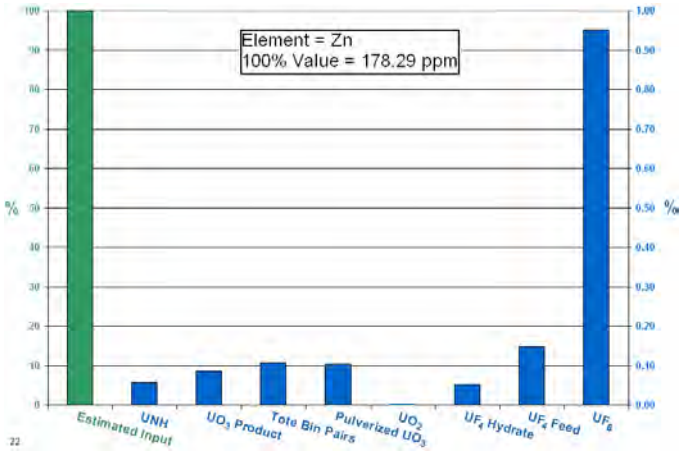

Fig 14: Where did the Zn come from?

6. Overview of Trace Element Behaviour During Conversion

The behaviour of trace elements during the conversion of UOC to UF_6 follows, for the most part, an expected pattern. Impure UOC is dissolved in nitric acid to produce an impure uranyl nitrate solution. The trace element content of the UOC does not change during dissolution but other chemicals are added to the dissolution process with the net effect of increasing the total trace element load. Dissolver solution undergoes solvent extraction where most (>99.5%) of the trace element load is rejected to rafinate. Purified uranyl nitrate solution is then concentrated via evaporation followed by thermal decomposition (denitration) to UO_3. Very little change in trace element concentration takes place during evaporation and denitration. UO_3 undergoes mechanical preparation for hydrogen reduction to UO_2. Only minor changes in trace element content occur during the preparation and reduction stages. UO_2 is dissolved in hydrofluoric acid to produce UF_4 hydrate. Trace elements are introduced via the use of recycle acid so the trace element content of the UF_4 hydrate is higher than for feed UO_2. The use of recycle acid is the major recontamination source in the UO_3 through UF_6 conversion stages. Drying and dehydration of UF_4 hydrate result in only marginal changes in the trace element content of dried UF_4. Dried UF_4 is reacted with F_2 in flame reactors to produce UF_6. Fluorination creates non-volatile fluorides which drop out as ash; thus, the trace element load decreases during UF_6 production.

7. Uranium Isotopic Data

7.1 Uranium Isotope Ratios

Uranium isotope ratios were reported by SAL, ITU, and QFIR, specifically the U234/U238 ratio and the U235/U238 ratio. Isotopic analysis was carried out on the samples from the 16 lots of UOC received at Blind River from four mills. Additionally, samples were taken from the 10 process steps during the conversion of UOC to UF_6, some of

which had parallel process lines. A total of 113 U isotopic ratio measurements were available. A consequence of the number of UOC sources and lots and the number and duality of process steps is that the number of samples taken for each was small, often two to three. In general the number of samples taken was insufficient for robust statistical analysis and conclusions. For ease of presentation and discussion, the isotopic ratios are given as whole numbers rounded to 5 digits. A multiplier of 10^{-7} and 10^{-9} applies to all U235/U238 and U234/U238 ratios respectively.

7.2 U235/U238 Isotopic Ratios

The average value of the U235/U238 isotopic ratio for all 113 available values, regardless of the laboratory, material source, material type, or conversion activity is 72541×10^{-7} with one standard deviation (sigma) of 17×10^{-7} and a relative standard deviation (RSD) of 0.02%. The RSD of 0.02% falls just below the lower value of a range of 0.03-0.05% used by SAL as the measurement uncertainty for U235/U238 isotopic ratio measurements. This data shows that, within measurement uncertainties, the influence of mining methods, milling practices and chemical processes during conversion of UOC to UF_6 on the U235/U238 ratio is negligible. Consequently, the U235/U238 ratio could not be used to differentiate between UOC feedstocks or conversion products.

7.3 U234/U238 Isotopic Ratios – UOC

There are significant differences in the U234/U238 isotopic ratios for the four uranium ore concentrates used in this study. There is a wide range of values between a maximum of 54993×10^{-9} and minimum of 53030×10^{-9}, a range of 3.6%.

Taking McArthur River UOC as a reference, the isotopic ratio for ELDO UOC is 2.49% lower, for McClean Lake UOC 1.33% lower, and for Crow Butte UOC 3.13% lower. These differences are higher than the range of 0.2-0.5% used by SAL as the measurement uncertainty for U234/U238 isotopic ratio measurements. The U234/U238 isotopic ratio for all 37 values is 54246×10^{-9} with one sigma of 686×10^{-9} and an RSD of 1.26%. The differences are not a result of inter-laboratory analytical differences. The differences between lab averages for UOC using the McArthur River average value as a reference are 0.22% for ITU and 0.06% for QFIR, thus at and below measurement uncertainty.

7.4 U234/U238 Isotopic Ratios – Conversion

Differences in isotopic ratios between conversion process stages are either within or below the SAL measurement uncertainty range for U234/U238 isotopic measurements (0.2-0.5%). The differences were calculated based on the difference between the isotopic ratio average of process stages and the calculated average weighted value for the U234/U238 isotopic ratio of the input to the digestion system. UOC, grit blast, and UO_3 recycle were included in the calculation.

Although no significant changes occur in the U234/U238 isotopic ratio during conversion stages, there appears to be an indication that changes do take place but on a very small, minor scale. It was found that the isotopic ratios of conversion stages are higher than isotopic ratios for the digestion stage calculated input. The pattern of indicated change is that from the input isotopic ratio into the digestion stage, isotopic ratio values increase through to the UO_3 pulverisation stage. Isotopic ratio values then drop during UO_2 production and drop further during the UF_4 and UF_6 production stages and appear to essentially return to very near the input to digestion values.

The pattern of isotopic ratio increase from the input baseline and then decline through UO_2-UF_6 to near baseline is unusual. The increase is unusual because there is no source of additional U234 to cause an increase in the U234/U238 ratio. Further, there is no loss mechanism during the conversion stages showing a decrease in the U234/U238 ratio to account for the decreased isotopic ratio values.

One possibility to explain the higher isotopic ratio values for the digester through pulverised UO_3 stages vs. the digester input values would be that the input values are too low. If the Crow Butte UOC is eliminated from the weighted average input calculation, the input average becomes essentially the same value as for the UO_3 isotopic ratio averages. There is no reason to suspect that the Crow Butte UOC was not included in the digester input. Even so, this would not explain the decreased values from UO_2 through UF_6. Another possibility is that the pattern is a measurement (instrument) effect of unknown cause.

8. Summary and Conclusions

- The trace element spectrum of feed to a mill depends on the mineralogy of the ore body plus, as applicable, the mineralogy of dilutive species accompanying the ore through mining practice or for other processing purposes. Mining and mill feed preparation practices were different for each of the four UOC sources. The associated mills each had different UOC production methods in terms of process chemistry. These differences combine to give UOC from a mine-mill combination a unique trace element character.
- Mining and mill feed preparation practices can change over time. Mill chemical processing can also change with time.
- UOC from each source was blended at Blind River and dissolved together with additional liquid and solid process chemicals and recycle streams. Solvent extraction

was effective to the degree that it was not possible to relate the trace element content of the product UO_3 to any contribution by any specific UOC input.

- Conversion of UO_3 to UO_2 results in only marginal changes in trace element values. The processes are mainly mechanical operations with hydrogen reduction of UO_3 to UO_2. No process chemicals (other than hydrogen) are involved.
- Conversion of UO_2 to hydrated and dehydrated UF_4 results in a notable increase (126 ppm net total) in trace element values. A limited number of elements, iron, potassium, sodium, phosphorus account for most (88%) of this increase. The increase in iron is a result of corrosion product originating from the drum drying operation. Potassium originates from the use of KOH cleaning solutions. The origin of the increased sodium and phosphorus values is not known.
- Conversion of dehydrated UF_4 to UF_6 results in a notable decrease (171 ppm total) in trace element values. A limited number of elements: iron, sodium, phosphorus account for most of this decrease. hus, three of the elements mainly responsible for increases in the trace element levels in UF_4 are also mainly responsible for the decrease during UF_4-UF_6 conversion.
- Although a sophisticated analytical technique, ICP-MS can have difficulty with numerous elements. Drawing conclusions based on one set of ICP-MS trace element results from a single laboratory requires some caution.
- Before using a set of ICP-MS trace element values from any laboratory, all of the values should be carefully examined vs. available specifications or historical values and the origin and type of sample. There should be a positive answer to the question “does this value make sense?” Consideration should be given to the possibility that questionable and/or unusual values might have safeguards implications.
- The U235/U238 isotopic ratio is not influenced, within measurement uncertainties, by ore source, mining methods, milling practices, or chemical conversion processes. The U235/U238 isotopic ratio could not be used to differentiate between sources of UOC.
- The U234/U238 isotopic ratio was significantly different for each of the four uranium ore concentrates used in this study. A wide range of U234/U238 isotopic ratio values was found for each UOC source. The U234/U238 isotopic ratio has potential could be used to differentiate between sources of UOC. The wide range of ratio values might be an issue in some cases.

9. Acknowledgements

This paper draws on a larger study carried out under IAEA Task A1796, which was funded through the Canadian Safeguards Support Program.

Chemical analysis was provided by:

Queen’s University facility for Isotope Research (QFIR)

The IAEA’s Safeguards Analytical Laboratory (SAL)

and JRC’s ITU laboratory

We are grateful for the assistance provided by Cameco, whose assistance with sampling made this work possible. We are also grateful to Cameco technical staff who contributed to our technical understanding of uranium refining processes.

The analytical results provided here represent a snap-shot at a given time and were collected for scientific purposes. They should not be used as the basis for any commercial representation.

10. 10. References

[1] Button, P; Healey, G; Chipley, D; *Tracing Origins of uranium products, ESARDA Symposium 2011*.

Images Objects vs. Pixels: A comparison of new methods from both domains

Sven Nussbaum[1], Julia Tueshaus[1], Irmgard Niemeyer[2]

1. University of Bonn, Geographic Institute, Center for Remote Sensing of Land Surfaces (ZFL), 53113 Bonn, Germany, sven.nussbaum@uni-bonn.de, julia.tueshaus@uni-bonn.de
2. Forschungszentrum Juelich GmbH, Institute of Energy and Climate Research, IEK-6: Nuclear Waste Management and Nuclear Safety, 52425 Juelich, Germany, i.niemeyer@fz-juelich.de

Abstract:

Under the Additional Protocol of the Non-Proliferation Treaty (NPT) complementing the safeguards agreements between States and the International Atomic Energy Agency (IAEA), commercial satellite imagery is an important source of information within the "information driven safeguards" approach of the IAEA. The new Geospatial Exploitation System (GES) creates a huge demand for spatial information and new tools to analyze this data. The IAEA faces the challenge of a steadily increasing number of nuclear facilities worldwide and therefore (semi-) automated and computer driven methodologies can add a big value in the verification process. Another challenge of the IAEA is to stay on-top of new technologies and to use them effectively and efficiently within the safeguards verification process. In the last decade several new pixel-based and object-based approaches for image analysis and for change detection have evolved and this paper aims at evaluating and testing some of them in the field of safeguards. New pixel-based classification algorithms like the support vector machines or time series analysis have been widely used in the field of land cover change analysis, but haven't been applied in the verification process. New developed object-based change detection approaches and optimized workflows have been developed and should now be tested in the field of safeguards. The aim of this paper is to apply and evaluate some of these methods using the example of different nuclear sites, and to compare their suitability in the context of information-driven-safeguards.

Keywords: satellite imagery, change detection, time series analysis, object based image analysis

1. Introduction

"Spatial is special" or *"Think spatial!"* these mottos seem to have arrived in the International Atomic Energy Agency (IAEA). In concert with the paradigm change from traditional to information-driven safeguards, geoinformation has a significantly increased importance in the safeguards analysis process. One key reason for this development is the implementation of the new Geospatial Exploitation System (GES). With the GES geoinformation (GI) like satellite imagery or site plans of nuclear facilities are available for a broad range of inspectors, analysts or country officers. As soon as this wider audience will gain access to that kind of information, they will recognize how valuable it is, and the request for geoinformation will continue to grow.

The increased demand for spatial information goes hand in hand with a steadily rising number of nuclear facilities under (integrated) safeguards worldwide. Here, computer-driven processing algorithms and tools become essential for automating the analysis of the vast amount of safeguards-related data as much as is reasonably possible. In particular, algorithms for pre-processing satellite imagery acquired by new sensors or geoprocessing models that generate additional safeguards relevant information, could add a big value in the safeguards verification process, for examples see Nussbaum & Niemeyer [1], Niemeyer et al. [2] or Listner & Niemeyer [3]

With the improving spatial resolution and the amount of details visible on remote sensing data, also new algorithms for analysing very high resolution satellite imagery with regard to safeguards verification are needed. Object-based approaches show promises against pixel-based one as they try to imitate the image understanding of an image analyst, see e.g., Listner & Niemeyer [4,5], or Nussbaum & Menz [6]. An image analyst can easily identify image regions along with their colour, shape, texture and context, and categorize them into objects of interest, such as buildings, streets, forests etc. Computer-driven object-based image analysis is an approximation to human perception. Using specific object features (e.g. colour, shape, texture or context) of defined object classes through rule bases, each object can be assigned to an object class. The selection of the optimum features can either be performed automatically by applying statistics to a set of samples for each class or interactively by integrating knowledge on the object classes in the recognition process. Object-based image analysis approaches are far from being able to perform an image interpretation on its own, however, they offer some time and cost effective procedures for object recognition and feature extraction, especially when using very high resolution satellite imagery.

This development towards object-based methodologies follows a trend recognized by Blaschke [7, p.12] already in 2010. He concluded from a comprehensive literature review that OBIA represents a significant trend in remote

sensing and GI science. With this new trend also the availability of new tools in the area of OBIA has increased. This paper presents a workflow which enlarges the possibilities of OBIA with adapted tools in the area of segmentation und feature analysis. By including these tools the analysis process itself can be made more straightforward and time saving.

However, also advanced pixel-based approaches for image classification, such as support vector machines algorithms, see e.g. Mountrakis et al. [8], are still worth considering. As far as low or medium resolution satellite data is concerned, time series analysis (TSA), see e.g. Lambin & Linderman [9] could be another possible source for (mostly free) valuable safeguards relevant information. TSA analysis is applied to a huge sequence of satellite images acquired over the same area of interest in order to detect trends and changes over time.

This paper aims at discussing some workflows, novel algorithms and methods to be applied in the field of safeguards verification. A comprehensive evaluation or detailed case studies have not been performed yet, thus the quality of the tools will be assessed visually. Moreover, their user-friendliness and easiness and the time exposure will be discussed. In summary, the authors are confident that these novel tools can produce safeguards relevant information and support the verification process.

2. Image Classification

The aim of image classification is to determine areas or objects of interest in an (semi)-automated way. Objects of interest can be, e.g., buildings, pipelines or other safeguards relevant structures in a satellite scene. While discussing both the object-based and the pixel-based approach, the paper focuses on the improvement of segmentation and feature analysis in the OBIA workflow.

Digital image processing in remote sensing usually follows a certain workflow (see Figure 1). The first general step is usually the pre-processing of the imagery. This step is necessary for both pixel- and object-based image analysis and includes geometric correction and/or atmospheric/radiometric correction. Since pre-processing does not differ for either domain, it will not be further discussed here.

In OBIA, the step following the pre-processing is the generation of image objects. This can be done using a variety of existing segmentation methods. The given study uses the so-called multi-resolution segmentation implemented in the software eCognition 8.7, which has proven to achieve reasonable results, see Marpu et al. [10].

Segmentation has always been one of the most crucial parts, as it bears the problem of correct parameterization in order the retrieve meaningful objects that are close to real-world objects. So as to cover all objects with their varying sizes and relations, a hierarchical network of objects with different object levels representing smaller, mid-scale and bigger real world objects is needed.

One parameter is the so called *scale parameter* and it determines (simply said) the size of the resulting image objects. In most studies scale parameters have been found using a time consuming and unreliable trial-and error approach. Dragut et al. [11] proposed a statistical method in order to determine the best scale parameters for the multiresolution image segmentation. The estimation of scale parameter (ESP) tool builds on the idea of local variance of object heterogeneity within a scene.

The ESP runs as a process in eCognition and generates multiple hierarchically linked images object levels. The local variance is calculated for each scale level and plotted against the corresponding scale. The peaks in the graph at which the local variance changes indicate the most appropriate scale levels based on the data properties of the scene [11].

Once the image objects have been generated, the next step in OBIA is the definition of the rule sets for classification. The advantage in OBIA of having much more possible feature at hand (colour, shape, texture or context) to classify can turn into a disadvantage in the sense of finding the correct features to use for classification. How to choose the best features from the list of over hundreds possible feature descriptions in eCognition? Which features are the typical ones for this or that class, which are the ones the separates the classes' best? Nussbaum et al. [12] proposed a statistical tool SEaTH in order to calculate the *Separability* for each class combination for any number of features. The tool also determines the *Threshold* where classes can be separated best. The implementation of this tool in eCognition can be downloaded at: www.treatymonitoring.de/tools

From a users' perspective these tools are easy to handle and they make the OBIA workflow fast and more straightforward (see Figure 1).

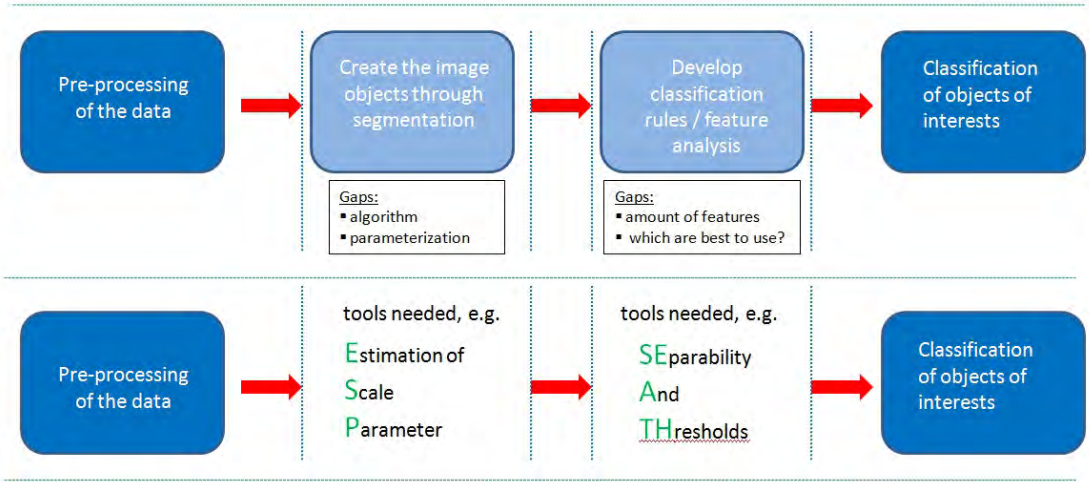

Figure 1: OBIA workflow using additional tools to fill the existing gaps.

Figure 2 a) shows as test area a nuclear facility. A subset of a QuickBird image from August 2005 to be used as test image shows a small part of the facility with buildings, streets and background (soil) which represent the target classes of interest. According to the OBIA workflow the image was loaded into eCognition and then segmented by using the ESP tool [11]. Figure 2 b) shows the interface of the ESP tool; here, the grey circles indicate peaks of local variance, i. e. possible good scale parameter settings for segmentation. The multi-resolution segmentation generated three hierarchical object levels using the local maxima of the scale parameter at 80, 150 and 220.

After segmentation the samples for the classes *buildings, streets* and *soil* where defined in eCognition. These samples where used in the SEaTH tool [12] to determine the best features and thresholds for separating the classes of interest. Figure 2c) shows the interface of SEaTH, which highlights as a result the best features and thresholds to choose. Based on the SEaTH output the class descriptions were implemented, followed by the classification process itself. The result of the classification is shown in Figure 2d).

Figure 2: OBIA workflow and comparison of object-based and pixel based classification. a) Test image: subset of QuickBird image over a nuclear facility, copyright DigitalGlobe; b) ESP interface and results; c) SEaTH interface and class features; d) result of OBIA classification; e) result of support-vector machine pixel-based classification.

A brief visual validation showed that all the big buildings were detected and that the streets seemed to be a little over-classified.

In comparison, the support vector machine (SVM) classifier implemented in the ENVI software package was applied for pixel-based classification. After loading the image and the definition of class samples to calibrate the algorithm, the classificatory runs fully automatically. The result of this is shown in Figure 2 e). The known salt-and-pepper effect for pixel-based algorithms using high-resolution imagery is still visible in the results. However, the main streets show more realistic shape compared to the OBIA street class, and the majority of the big buildings have been identified. The SVM misses 4 buildings compared to the OBIA. This is probable due to the fact that these four buildings are darker compared to the others and are thus not considered for the SVM building class which is solely based on the spectral features.

OBIA can be a powerful tool in the context of non-proliferation analysis. The typical image analysis within the IAEA is conducted by imagery analysts who visually analyse the images, look for changes or verify the completeness of the member state declarations. Generally, this is a very effective and, given the large experiences of the analyst, a very accurate method. However, this is time-consuming for large areas or unfamiliar terrain. OBIA can thus be an additional tool to support the analysts. OBIA procedures could be used for example to pre-select areas of interest (AoIs) or to identify objects of interest (OoIs). In particular man-made structures with specific geometry can be extracted and identified much easier based on image objects rather than just using pixels, because OBIA allows the description of these object by using multiple features including shape and texture. This also applies for buildings and structures within the nuclear fuel cycle, where the specific functions of the installations cause their shape to some extent.

At large mining sites for instance, regions which have significantly changed may represent AoIs, while trucks or other heavy equipment indicating activities on that site could be OoIs. Looking for a specially shaped building visually in an urban area or in a complex environment with probable more industrial areas and settlements is a challenging task. Again, OBIA could help to pre-process the images and present the analyst with a selection of possible OoIs, such as buildings. The processing time of the OBIA analysis has increased significantly in the last years and by using the proposed tools (ESP & SEATH) the workflow can be streamlined. Once a comprehensive OBIA workflow within one software framework, e.g. within the Geospatial Exploitation System (GES) of the IAEA, is implemented than processing time is only a matter of hardware equipment and can be optimised.

Besides the positive impacts of OBIA for the analysis capabilities of the IAEA it has to be mentioned that OBIA can only be a tool among others to support but never replace the analyst. The interpretation of the OBIA results and the validation of the overall analysis always need a human analyst.

3. Change detection - Time series analysis using medium resolution imagery

One major focus in the development of change detection (CD) methods for safeguards applications was the implementation of object-based techniques focussing on the change between two acquisition times [3]. Since 1972, satellite sensors with low to medium spatial resolution were launched in order to continuously acquire surface data. Therefore the analysis of large image series is possible. Since the Landsat archive was opened to public in 2008, images with moderate-temporal and moderate spatial resolutions (up to 15m) have become freely available. Accordingly, time-series analysis (TSA) of remote sensing data has advanced. Instead of comparing two images from two different dates, TSA analyses plenty images (up to hundreds) acquired over the same area. The idea is to study the change of every pixel in the time series through time and see how each pixel evolves. With this development, trends over time, seasonal or abrupt changes can be made visible, see Verbesselt et al. [13]. Because many images are needed, most studies use freely available medium resolution imagery like Landsat, for examples see Dubovyk et al. [14, 15].

But how could TSA using medium resolution satellite imagery be applied for safeguards verification? One scenario in which TSA could play a role is the detection of construction activities at former clandestine sites. As long as sites were clandestine, usually no commercial operator of VHR sensors would task this particular region for image acquisition, thus the operator might not have any data from the start of construction in the archive. Maybe, the construction started before the first VHR satellite was launched at all. Given the absence of data for the start of construction, this particular point in time could be narrowed down by using a semi-automatic TSA trend analysis. We used a former clandestine underground site for investigation.

Figure 3: Google earth imagery ©,

Figure 3 shows a Google Earth time-series. VHR imagery before 2004 were neither available from Google Earth nor from the Digital Globe Archive. Our study focused on the two buildings and the construction activities like streets between 2000 and 2004. This site was chosen despite the fact the national government claimed that at that time there were no nuclear activities at the particular site.

For the given site all available and cloud-free Landsat-7 imagery between 2000 and 2004 were used. This paper only shows the results for 2002, as this is the year when the construction activities were detected. For the year 2002 16 images could be downloaded from http://earthexplorer.usgs.gov/. For pre-processing the data, a relative radiometric correction was applied to the images using the IR-MAD algorithm; see Canty & Nielsen [16].

We used TSA to automatically generate a trend profile for our Area of Interest (AoI) for the Landsat series. If a strong trend existed, the area of the trend was masked out, and a temporal profile for that area was generated. In this temporal profile the peaks or troughs of the curve determined the dates of maximum change and could be directly linked to the date of the images. Therefore an image analyst could simply focus on these dates and visually check the change (e.g. construction start) at the AoI.

Using the Earth Trends Modeler software[1] a trend from these 16 images was calculated. The single pixel values per band were plotted against time and the trend was calculated by a linear regression per pixel over time with range between -1 and 1. This means if a pixel value in that given band has steadily increased over time a positive trend is recognized and the trend values approximates 1. If a pixel value has steadily decreased over time it approximates -1 as a trend values. In our case we choose band 3 as our major indicator, because the spectral difference between built-up area and surrounding

[1] Copyright by IDRISI ©

background maximizes in this band, see Figure 4. However, any other band, band combination or index could be used and this will be part of our future research activities.

The trend image shown in Figure 5 indicates huge changes within our AOI (strong positive trend) in 2002, indicated by red pixels. In order to highlight only significant changes, a threshold of three standard deviations from the mean trend value was applied. These pixel represent the significant change areas and were selected (Figure 6a). By superimposing the change areas, on a Landsat scene for visualisation purposes (Figure 6b), it turned out that the change areas automatically generated by the threshold also covers the two buildings. A temporal profile for the change area was generated (Figure 6c), showing the mean of all pixels at the 16 image acquisition times.

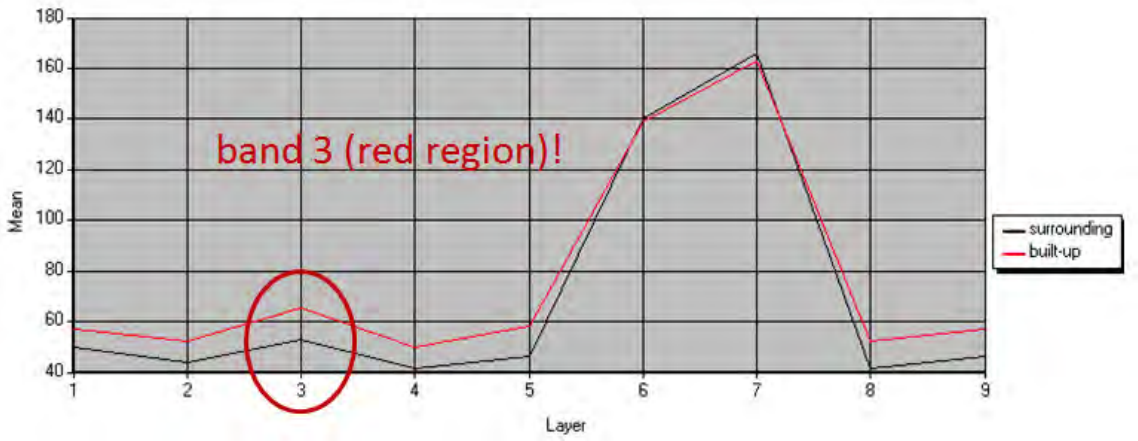

Figure 4: Third band is a major indicator for change in the trend analysis

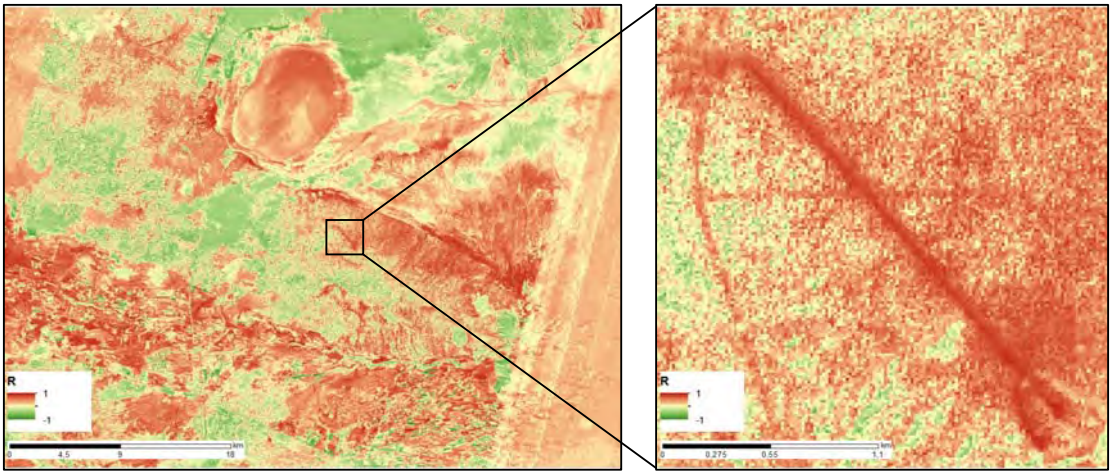

Figure 5: Trend image of the Landsat scene (left) and our AoI (right) at the former clandestine site for the year 2002

The temporal profile clearly shows that there was a big change signal between 25 March 2002 and 05 May 2002. The image analyst can now focus on these time period and visually check the images. Both images are shown in Figure 7. It is obvious that the construction activities start in between these two dates. Thus, in this case study we were able to narrow down the construction start date to a time-frame of 40 days accuracy.

This example of a posterior analysis has shown that TSA can generate safeguards relevant information in order to enhance/specify the picture of a state in the context of the state level approach of the IAEA. The method is also able to detect undeclared activities in a larger area. However, the larger the unknown area the more changes may occur. Depending on the region also seasonal changes in vegetation can have an effect on the change signal. Therefore the manual interpretation part of the results by an imagery analyst is essential.

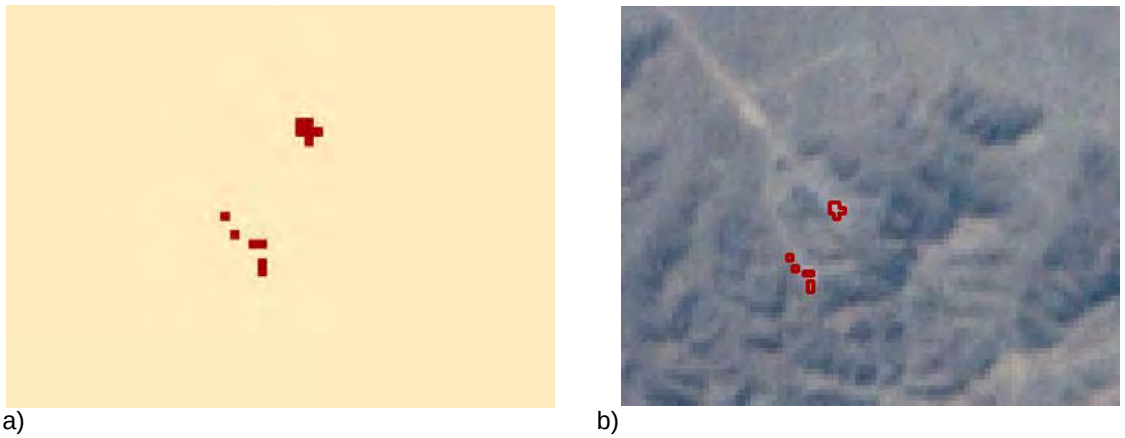

a) b)

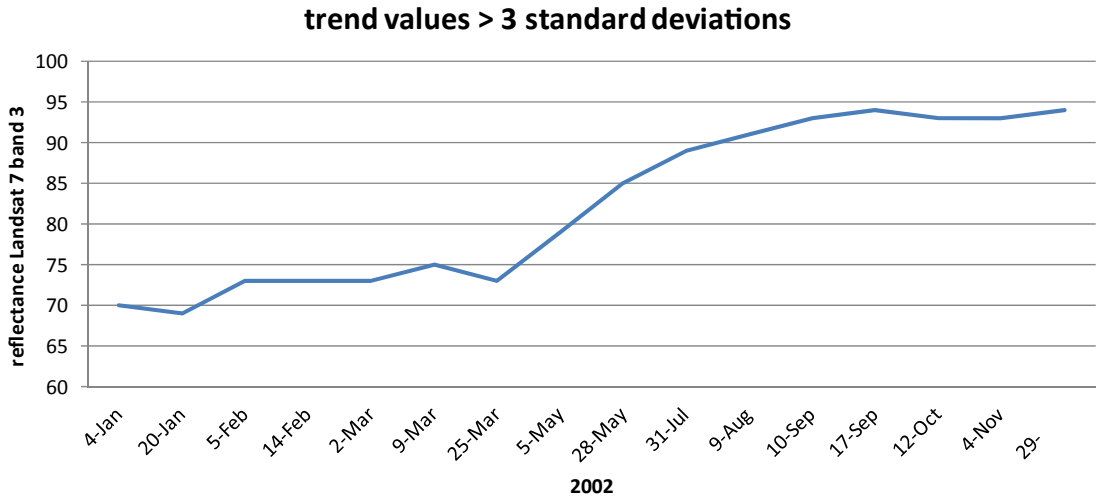

c)

Figure 6: Change areas of significant change (a,b) and temporal profile for the change areas (c).

Figure 7: Visual comparison of the detected construction start by the methodology.

4. Conclusions

In order to cope with the challenges of information driven safeguards and geoinformation the IAEA needs to stay on top of new technologies. Thus it is very valuable to consider new analysing techniques or tools. It is also important to investigate in existing techniques which have not been applied to safeguards yet. In chapter 3 novel tools for streamlining the OBIA workflow have been applied and implemented. It could be shown that these simplify the OBIA workflow and close some of the gaps which still existed. These gaps where segmentation and feature analysis. When using the tools ESP and SEaTH in combination it makes the analysis process much faster, easier and

straightforward. A comprehensive validation, however, is out of the scope of this paper. The tools used have not been integrated into one single software package, thus results still need to be manually transferred between different programmes. In principle, OBIA is not far from being operationally useable; however, a much more user-friendly implementation is required to be applicable by the IAEA imagery analysts. As soon as the OBIA workflow could be implemented in the IAEA software portfolio, e.g. as a tool in the new Geospatial Exploitation System (GES), the imagery analysts would benefit from the concept of image objects. A library of object descriptions (special infrastructure or vehicles, etc.) could be developed and then steadily further developed.

Testing and applying new pixel-based and more robust classifiers like the support-vector machine algorithm leads to comparable results, but here also a more extensive validation should be carried out. Shortcomings in terms of misclassification also demonstrate the advantage of the OBIA approach, which in our example considered a shape and a spectral feature to identify the buildings. Nevertheless new pixel-based classifier like the SVM should still be considered when analysing high-resolution imagery since they enhance and become more powerful too.

Concerning change detection, time series analysis has shown to be a valuable tool in the field of safeguards. With our methodology it is possible to (semi-) automatically narrow down construction activities of sites based on medium resolution imagery. This can be very helpful in the case when there are no high resolution images available because the activities where clandestine. It can also be applied to sites where construction or other activities happened in the past, during a time when no commercial high-resolution sensors where available at all. For the future, this methodology will be further investigated and applied to different case studies. It will be tested which bands, band combinations or indices can improve the change signal. Nevertheless, for our case study, the results were reliable and generated safeguards relevant information.

4.1 Privacy regulations and protection of personal data

"I agree that ESARDA may print my name/contact data/photograph/article in the ESARDA Bulletin/Symposium proceedings or any other ESARDA publications and when necessary for any other purposes connected with ESARDA activities."

4.2 Copyright

The author agrees that submission of an article automatically authorises ESARDA to publish the work/article in whole or in part in all ESARDA publications – the bulletin, meeting proceedings, and on the website.

The author declares that their work/article is original and not a violation or infringement of any existing copyright.

5. References

[1] Nussbaum, S. & I. Niemeyer: *Geographic Information Systems (GIS) – from Visualization to Analysis,* Proceedings 53rd Annual Meeting INMM 2012, Orlando Florida, USA. (2012)

[2] Niemeyer, I., Listner C. & S. Nussbaum: *Object-based Image Analysis Using Very High-resolution Satellite Data,* Journal of Nuclear Management (JNMM), No. 4, 2012, Special Issue: Science for Verification. (2012); p. 100-109

[3] Listner C. & I. Niemeyer: *Object-based Change Detection Using Very High-resolution Satellite Data*, 33rd ESARDA Annual Meeting, Budapest, (2011), p. 16-20

[4] Listner, C. & I. Niemeyer: *Advanced Object-based Change Detection Using Very High-Resolution Remote Sensing Imagery,* Proceedings of the IEEE Geoscience and Remote Sensing Society, Munich; (2012)

[5] Listner, C. & I. Niemeyer: *Object-based Change Detection,* Photogrammetrie, Fernerkundung, Geoinformation, 4, (2011), p. 233 - 245

[6] Nussbaum, S. & G. Menz: *Object-Based Image Analysis and Treaty Verification: New Approaches in Remote Sensing - Applied to Nuclear Facilities in Iran*. Springer - Verlag, Berlin. (2008)

[7] Blaschke, T.: *Object based image analysis for remote sensing,* ISPRS Journal of Photogrammetry and Remote Sensing 65, (2010), p. 2-16

[8] Mountrakis, G., Jungho I. & C. Ogole: *Support vector machines in remote sensing: A review,* ISPRS Journal of Photogrammetry and Remote Sensing 66, No.3, (2011), p. 247–259

[9] Lambin, E.F. & M. Linderman: *Time series of remote sensing data for land change science*, IEEE Transactions on Geoscience and Remote Sensing 44, No.7, (2006): p. 1926–1928

[10] Marpu, P.R., Neubert, M., Herold, H. & I. Niemeyer (2010): *Enhanced Evaluation of Image Segmentation Results*, Journal of Spatial Science 55(1), p. 55-68

[11] Dragut, L., Tiede, D. and S.R. Levik: *ESP: a tool to estimate scale parameter for multiresolution image segmentation of remotely sensed data*, International Journal of Geographical Information Science Vol. 24, No. 6, (2010), p.859–871

[12] Nussbaum, S., Niemeyer, I. & M.J. Canty: *SEaTH - A new tool for automated feature extraction in the*

context of object-oriented image analysis. Proc. AGIT – Obia, Salzburg, (2006), ISPRS; Volume No. XXXVI – 4/C42; ISSN (2006): p. 1682-1777

[13] Verbesselt, J., Hyndman R., Newnham G. & D. Culvenor: *Detecting trend and seasonal changes in satellite image time series*, Remote Sensing of Environment 114, No. 1 (2010), p. 106–115

[14] Dubovyk, O., Tüshaus, J., Khamzina, A. & G. Menz: *Monitoring of Vegetation Trends with MERIS Time Series in Arid Irrigated Drylands of Central Asia*. Proceedings of the Sentinel-3 OLCI/SLSTR and MERIS/(A)ATSR Workshop', 15–19 October 2012, Frascati, Italy, (2012)

[15] Dubovyk O., Menz, G. & Khamzina, A.: *Trend analysis of MODIS time-series using different vegetation indices for monitoring of cropland degradation and abandonment in Central Asia,* IGARSS 2012 – IEEE International Geoscience and Remote Sensing Symposium: Remote Sensing for a Dynamic Earth, (2012).

[16] Canty J.M. & A. Nielsen: *Automatic radiometric normalization of multitemporal satellite imagery with the iteratively re-weighted MAD transformation*, Remote Sensing of Environment, Vol.112/3, (2008), p. 1025-1036.

Proliferation resistance features of reprocessed uranium in Light Water Reactor fresh fuel

K. Abbas, G.G.M. Cojazzi, G. Mercurio, P. Peerani, G. Renda

European Commission, Joint Research Centre - Institute for Transuranium Elements
Unit E08 - Nuclear Security - T.P. 210 - Via E. Fermi, 2749 - 21027 Ispra, Italy
kamel.abbas@jrc.ec.europa.eu

Abstract:

The introduction of reprocessed uranium in fresh Light Water Reactor fuel as a measure against proliferation has been recently put forward in the non-proliferation discussion. In particular, the use of reprocessed uranium implies the presence of the ^{232}U radioisotope, and this can make the possible diversion of the fresh fuel and further uranium re-enrichment more complicated.

This work attempts to further evaluate a composition of a proliferation resistant UO_2 fuel made of a mixture of fresh and reprocessed uranium, therefore implying, inter alia, the presence of ^{232}U and ^{236}U in the resulting fuel. A new UO_2 fuel half-made of fresh uranium with the other half of reprocessed UO_2 is proposed and assessed via simulation. $^{232}U/^{208}Tl$ emits a high energy γ-ray of 2.6 MeV enhancing its detectability and any attempt to further enrich the mixture to weapon grade using, for example, centrifugation process could be hindered as the enrichment of ^{232}U will rise faster than that of ^{235}U. Moreover, the high-energy α particles emitted by ^{232}U and ^{236}U might tend to dissociate UF_6 molecules, potentially complicating the centrifugation process. In terms of radiological emissions, the calculations have shown that the dose rate at 1 m from a fuel assembly made of the proposed mixture is of the same order of magnitude of that of the fuel made of non-reprocessed uranium, though the dose rate doubled.

Keywords: ^{232}U, ^{236}U, proliferation resistance, safeguards, nuclear fuel cycle

1. Introduction

While some countries are currently considering introducing nuclear power, others are in the process of expanding their existing capacity. Nuclear power could help these countries to move towards a secure low carbon emission electrical energy supply. Following the recent devastating accident at Fukushima, most countries operating nuclear reactors are reviewing and reinforcing their safety and regulatory procedures rather than relinquishing this source of energy. For example, in Japan, following a political decision, all the nuclear power plants in the country were shut down. However, after a year and after thorough safety assessments, there is a new political orientation foreseeing the resumption of nuclear power production as it remains one of the best options to satisfy the energy needs of the country.

Presently, there are about 500 commercial power reactors operating or under construction worldwide and most of them require enriched uranium as fuel. The possible future nuclear expansion raises concerns over the risk of diversion of nuclear materials through the expected growth in exports or transfers of nuclear fuel. Moreover, recent revelations of possible clandestine nuclear programs have caused an increase in international efforts against the proliferation of weapons of mass destruction. In this context, new approaches are needed to prevent such threats. Research and development efforts on new proliferation resistant nuclear fuels are an example of activities in support of the reduction of these threats.

According to the IAEA [1]: “Proliferation Resistance is defined as that characteristic of a nuclear energy system that impedes the diversion or undeclared production of nuclear material, or misuse of technology, by States intent on acquiring nuclear weapons or other nuclear explosive devices. The degree of proliferation resistance results from a combination of, inter alia, technical design features operational modalities, institutional arrangements and safeguards measures. These can be classified as intrinsic features and extrinsic measures. Intrinsic features result from technical design and include features that facilitate the implementation of extrinsic measures including safeguards.

This paper will mainly focus on intrinsic features. In particular, it attempts to evaluate a composition of a proliferation resistant UO_2 fuel made of a mixture of fresh and reprocessed uranium. The concept of introducing reprocessed uranium in fresh fuel has been suggested and investigated by several authors [2 - 6], including its effect on proliferation resistance. In this paper, we focus on UO_2 fuel for Light Water Reactors (LWR). Reprocessed uranium contains, in addition to ^{238}U and ^{235}U, several other uranium isotopes of interest, in particular ^{232}U and ^{236}U. In section 2, the main features of ^{232}U are summarised. In section 3, the concept of reutilisation of reprocessed uranium is presented, including an example of proliferation resistant fuel with reprocessed uranium. Section 4 illustrates some of the advantages of using reprocessed uranium from a proliferation resistance and safeguards point of view with a particular emphasis on detectability.

2. ^{232}U characteristics and production

^{232}U is a pure α emitter with a half-life of 69.85 y and two main α-ray emissions at 5.32 and 5.26 MeV, with intensities of 69% and 31% respectively. Figure 1 shows the main ^{232}U decay pathways. The relevant pathway with regard to this study is the one leading to ^{208}Tl (3.65 min) which emits a high energy 2.6 MeV γ-ray (branching ratio > 99%).

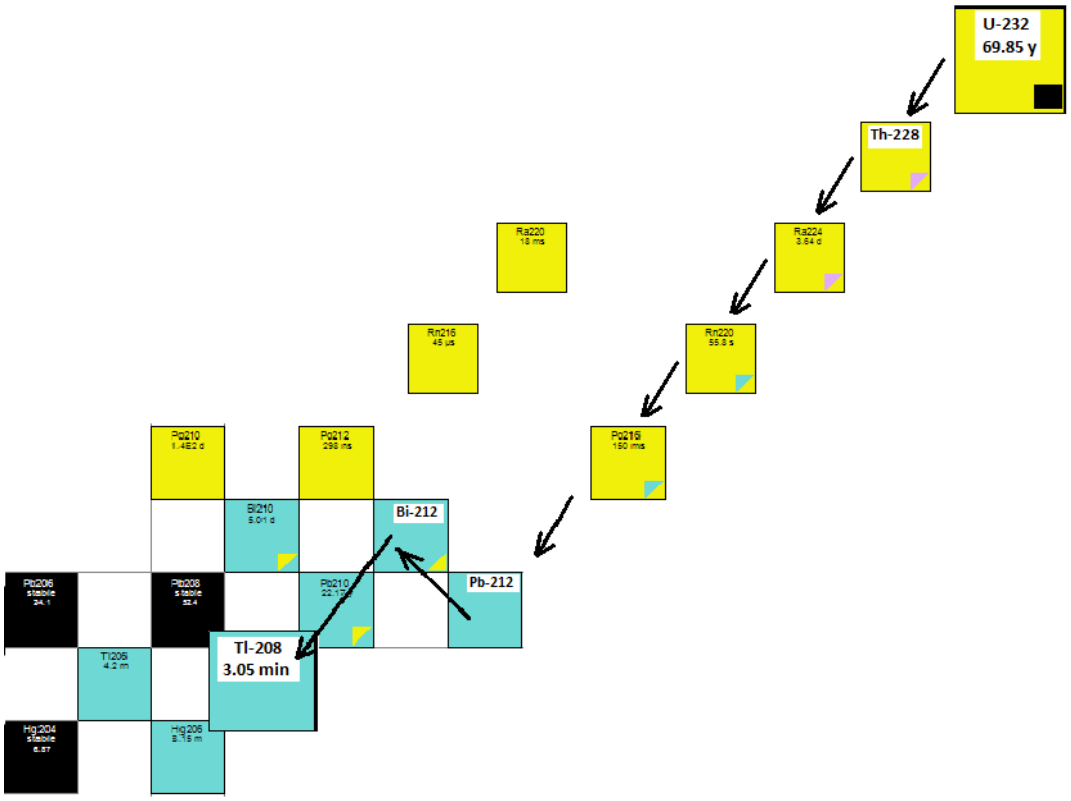

Figure 1: Decay pathway of ^{232}U to ^{208}Tl.

Figure 2 shows the build-up of ^{208}Tl from ^{232}U and other daughters such as ^{228}Th and ^{224}Ra. Several years of ^{232}U decay are needed to build up ^{208}Tl. This period could fit within the typical cooling times of spent fuel before reprocessing or disposal. Figure 3 presents measured and simulated γ-ray spectra of a sample of 20 months old 3.7 MBq ^{232}U. While the measured γ-ray spectrum measured in this work was acquired with a calibrated High Purity Germanium Detector (HPGe) of 50 % relative efficiency, the simulated spectrum was calculated using Nucleonica [7]. Qualitatively the two γ-ray spectra are in good agreement, demonstrating the reliability of the Nucleonica simulation tool used in this analysis. In both spectra, the 2.6 MeV γ-ray peak is well resolved.

There are several nuclear reactions leading to ^{232}U in the nuclear fuel cycle (uranium or thorium fuels) such as:

^{237}Np(n,2n)^{236}Np – β –^{236}Pu – α – ^{232}U

^{234}U(n,2n)^{233}U – ^{233}U(n,2n)^{232}U

^{232}Th(n,2n)^{231}Th – β – ^{231}Pa(n, γ)^{232}Pa – β – ^{232}U

^{230}Th(n,γ)^{231}Th – β – ^{231}Pa(n, γ)^{232}Pa – β – ^{232}U

^{235}U – α – ^{231}Th – β – ^{231}Pa(n, γ)^{232}Pa – β – ^{232}U

^{236}Pu – α – ^{232}U

The production of ^{232}U rises with the cooling time of the irradiated fuel due to the α decay of ^{236}Pu. ^{236}Pu is produced in small quantities from the decay of ^{236}Np, an activation product of (n,2n) and (γ,n) reactions on ^{237}Np during the reactor irradiation cycle.

For an indication of the uranium composition in a typical Pressurised Water Reactor (PWR) spent fuel, the ORIGEN depletion code contained in the SCALE software package [8] was used. Simulations performed in this work indicate that typically irradiated fuel (UO_2, 3-4% initial enrichment, burn up 40 GWd/t, 3 y irradiation) would contain several other uranium isotopes of interest in addition to ^{238}U and ^{235}U after a standard cooling time (~ 5 y),. These include ^{232}U, ^{233}U, ^{234}U and ^{236}U of approximate concentrations of 1.0×10^{-7}, 3.2×10^{-7}, 1.8×10^{-2} and 5.0×10^{-1} % of the total mass of uranium, respectively. The high energy 2.6 MeV γ-ray emitted by the ^{208}Tl daughter makes ^{232}U easily detectable and difficult to shield. Table 1 shows the results of ORIGEN calculations simulating the uranium isotopic composition of 1 ton of 3.5% enriched UO_2 fuel irradiated to 40 GWd/tU over three, one year long cycles and then cooled for 5 years. The ^{208}Tl radioisotope content is also included.

Table 1: Uranium isotopic composition in 1 ton of UO_2 fuel enriched at 3.5%, irradiated to 40 GWd/tU during 3 cycles of 1 year each and after 5 years of decay. ^{208}Tl radioisotope content is also included.

Uranium radioisotopes	Mass (g)	Concentration (mass %)
^{232}U	9.76×10^{-4}	1.03×10^{-7}
^{233}U	3.04×10^{-3}	3.21×10^{-7}
^{234}U	1.74×10^{2}	1.84×10^{-2}
^{235}U	7.35×10^{3}	7.76×10^{-1}
^{236}U	4.71×10^{3}	4.97×10^{-1}
^{238}U	9.35×10^{5}	98.7
^{208}Tl	1.91×10^{-11}	2.00×10^{-15}

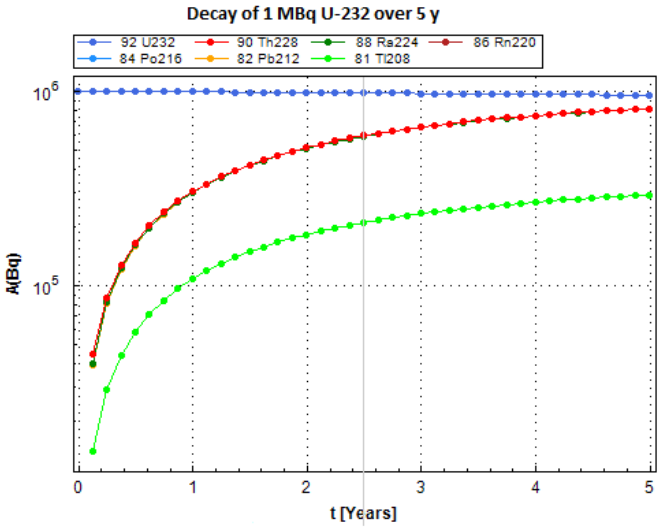

Figure 2: ^{232}U decay and build-up of ^{208}Tl and other daughters calculated with Nucleonica [8].

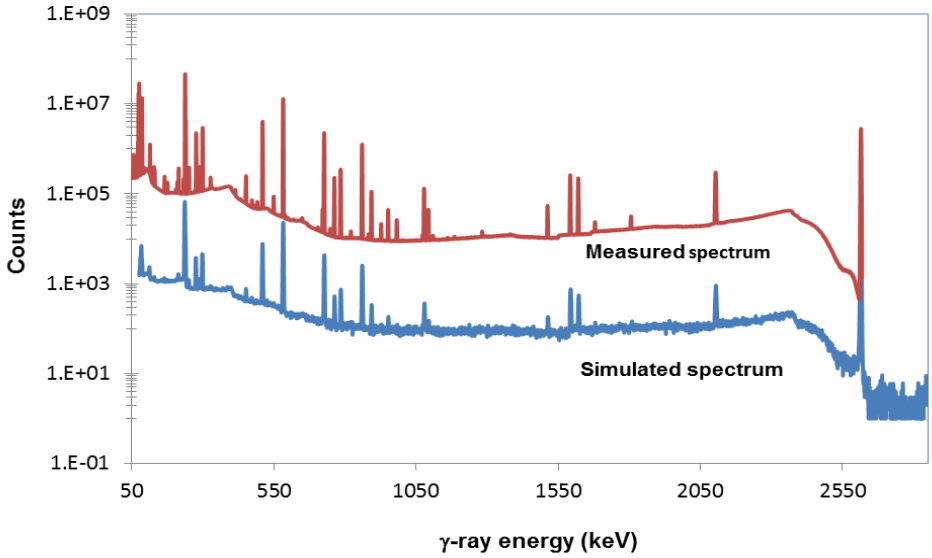

Figure 3: Measured (top spectrum) and simulated (bottom spectrum) γ-ray spectra of a sample of 20-month-old ^{232}U with an activity of 3.7 MBq. The measured γ-ray spectrum was acquired with an HPGe detector of 50% relative efficiency.

3. Re-utilization of reprocessed uranium for fabrication of proliferation resistant nuclear fuel.

As mentioned above, the possible expansion of nuclear energy will face new challenges to ensure a safe and sustainable use of this source of energy. The LWR is a proven technology and many countries are building or planning to build such reactor types (e.g. China and other emerging countries). As the number of nuclear power plants increases, it is expected that the amount of nuclear material transported all over the world will also increase. Consequently, the threat of nuclear material diversion would rise if new safeguards and security measures are not undertaken.

From the standpoint of the nuclear fuel cycle, uranium enrichment and fuel fabrication stages imply the use of sensitive technologies needing tight controls. According to some investigators, even the possibility of a sub-national terrorist group building an enrichment facility should not be ruled out [9]. In this case, low enriched uranium (LEU, enrichment < 20%) could be stolen from shipments for further enrichment to the levels needed for proliferation purposes. Furthermore, it is worth mentioning that enrichment from LEU to HEU requires less separative work than enrichment from natural uranium to LEU.

Reprocessed uranium contains ^{232}U and ^{236}U radioisotopes that deserve some attention from the point of view of its re-utilisation for manufacturing proliferation resistant fuel. ^{232}U and ^{236}U present safety issues for the nuclear industry if their concentrations lead to dose limits exceeding e.g. those of fresh MOX fuel [4]. It is worth mentioning that as these two uranium isotopes are produced during fuel irradiation, their analysis in spent fuel is useful as it can provide forensic information on the fuel irradiation conditions and history.

The presence of large amounts of ^{232}U in the uranium isotopic composition might require heavy biological shielding during fuel handling activities. The main source of radiation dose is the high energy γ-ray of ^{208}Tl. In this case, remote handling of such material would be necessary to prevent exceeding radiation exposure limits to the operators. A high content of ^{236}U in the reactor core fuel can also represent an issue for the reactor's operation as this isotope is a high neutron capturer and its concentration in the reactor core needs to be controlled. In particular, any excess neutron absorption has to be addressed and compensated to ensure the needed fission rate.

This paper proposes to manufacture nuclear fuel composed of fresh and reprocessed uranium with the latter containing ^{232}U, which constitutes an intrinsic barrier against nuclear proliferation [9]. The proposed composition of new UO_2 fuel is half-made of fresh UO_2 and the other half with reprocessed UO_2. ^{232}U and ^{236}U concentrations in the resulting fuel are on the same order of magnitude as typical irradiated UO_2 nuclear fuel while the enrichment of ^{235}U is adjusted to a typical LWR fuel enrichment level (3 – 4%). An example of the uranium composition in a proposed UO_2 fuel is presented in Table 2.

Based on a scenario simulated with ORIGEN, this fuel is obtained by mixing the reprocessed uranium from 1 ton of irradiated UO_2 (40 GWd/tU, 3 years irradiation, 5 years cooling) with 1 ton of fresh 6% UO_2 resulting in an overall enrichment for the new fuel of 3.46 %. Based on ORIGEN calculations, if the proposed fuel is irradiated in the same conditions (40 GWd/tU, 3 years irradiation) and allowed for 5 years cooling, it would have the uranium composition presented in Table 2. As previously mentioned, the concentrations of ^{232}U (5. X 10^{-8}% and 2. X 10^{-7}%) and ^{236}U (0.3% and 0.7%) in the proposed fresh and irradiated fuel remain of the same order of magnitude with respect to those of irradiated fuel made of fresh uranium only (^{232}U: 1. X 10^{-7}% and ^{236}U: 0.5%).

Figures 4, 5 and 6 present simulated γ-ray spectra of reprocessed uranium from spent UO_2 fuel (no reprocessed uranium), uranium in the fresh proposed UO_2 fresh fuel (3.46% enriched, made of mixture of fresh UO_2 (6% enriched) and reprocessed uranium) and reprocessed uranium from irradiated proposed UO_2 fuel (40 GWd/tU, 3 years irradiation and 5 years cooling), respectively. In the three γ-ray spectra, the γ-ray peaks of ^{208}Tl are well resolved, constituting a precise fuel signature at high γ-ray energy.

Table 2: Uranium isotopic composition in an example of new 3.46% enriched UO_2 fuel. The proposed fuel is composed of reprocessed uranium (separated from 1 t UO_2 irradiated fuel) mixed with 1 t of fresh 6% enriched UO_2. The irradiations conditions refer to a burn-up of 40 GWd/tU, with a 3 years irradiation followed by 5 years cooling.

Uranium radioisotopes	Concentration in spent UO_2 fuel (mass %)	Concentration in the proposed 3.5% enrichment UO_2 fuel (mass %)	Concentration in the irradiated proposed 3.5% enrichment UO_2 fuel (mass %)
^{232}U	1.03 X 10^{-7}	5.01 X 10^{-8}	2.16 X 10^{-7}
^{233}U	3.21 X 10^{-7}	1.56 X 10^{-7}	4.45 X 10^{-7}
^{234}U	1.84 X 10^{-2}	3.64 X 10^{-2}	2.04 X 10^{-2}
^{235}U	7.76 X 10^{-1}	3.46	5.89 X 10^{-1}
^{236}U	4.97 X 10^{-1}	2.56 X 10^{-1}	7.08 X 10^{-1}
^{238}U	98.7	96.2	98.7
^{208}Tl	2.00 X 10^{-15}	9.83 X 10^{-16}	4.28 X 10^{-15}

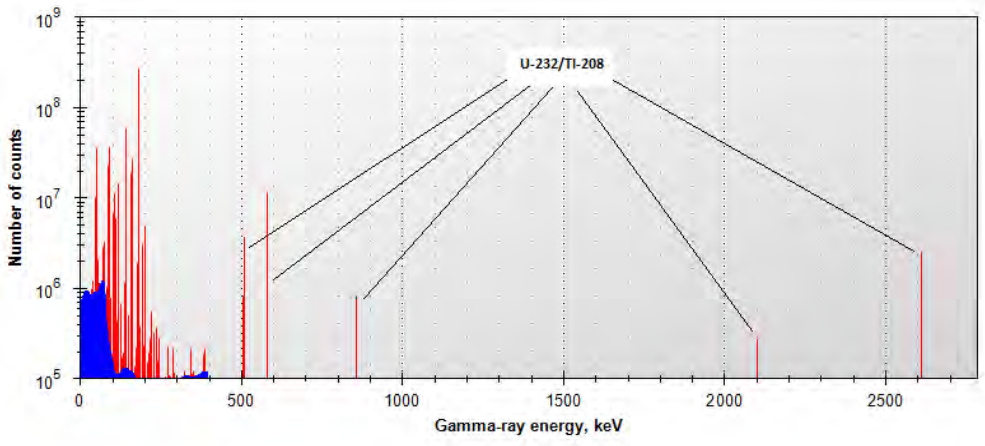

Figure 4: Nucleonica simulated γ-ray spectrum of reprocessed uranium from spent UO_2 (3.5% enriched) irradiated for 3 years followed with 5 years cooling. Only contributions of uranium nuclides and ^{208}Tl are simulated for clarity.

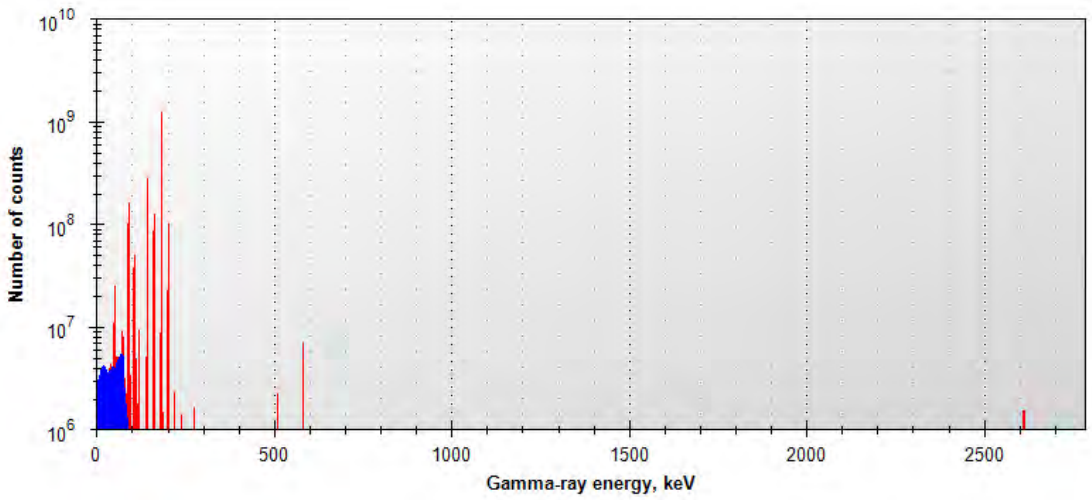

Figure 5: Nucleonica simulated γ-ray spectrum of a proposed fresh UO_2 fuel (3.46% enriched). This fuel is made of reprocessed fuel mixed with fresh 6% enriched UO_2 fuel. Only contributions of uranium radioisotopes and ^{208}Tl are simulated for clarity.

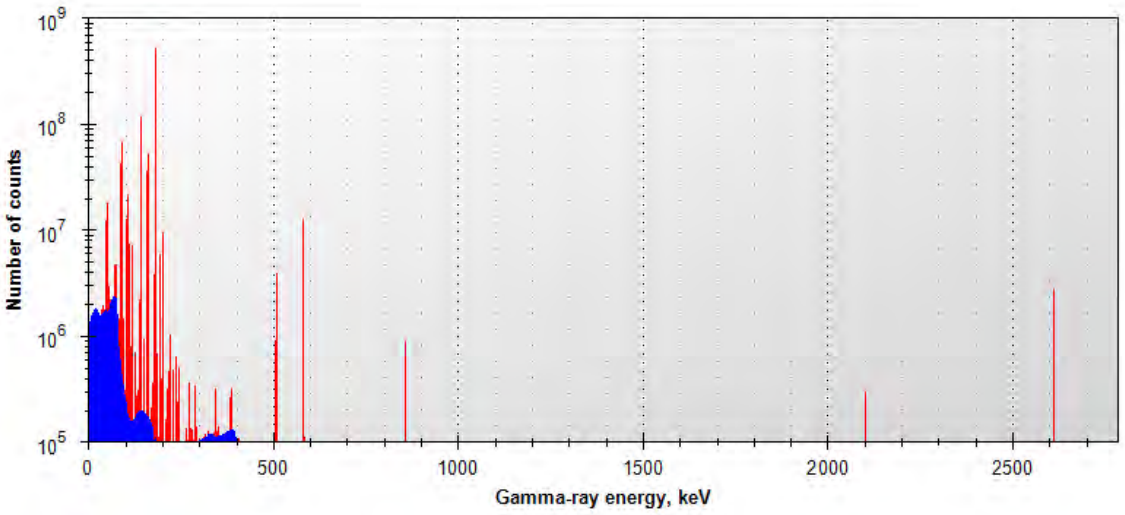

Figure 6: Nucleonica simulated γ-ray spectrum of reprocessed uranium from irradiated fuel as in figure 5. Only contributions of uranium radioisotopes and ^{208}Tl are simulated for clarity.

4. Some advantages of using reprocessed uranium for new UO_2 proliferation resistant fuel

The proposed nuclear fuel is based on the use of reprocessed uranium and can represent a significant saving of natural uranium resources. The use of reprocessed uranium in the conception of new and more proliferation resistant fuel as proposed in this work would also contribute to the decrease of the stock of high enriched uranium, where available, another aspect of the fight against nuclear proliferation [6].

The presence of ^{232}U at moderate concentrations in the proposed fuel is advantageous as the highly penetrating γ-ray emitted by the ^{208}Tl daughter results in enhanced fuel detectability. From the point of view of a reactor core's neutron balance, the impact of ^{232}U is negligible due to its very low concentration. However, the presence of a significant concentration of ^{236}U would affect the reactor's neutronics, and it might reduce achievable burn up. In the case of VVER-1000 fuel, Smirnov et al. reported that the ^{235}U enrichment should be increased to overcome the issue of the ^{236}U content[4].

The high-energy γ-ray emitted by $^{232}U/^{208}Tl$ constitutes an advantage in terms of fuel detectability. Indeed, masking the presence of $^{232}U/^{208}Tl$ would require considerable shielding, potentially discouraging diversion attempts for use in an undeclared activity. This would also be beneficial for discouraging nuclear material smuggling attempts, thus providing barriers to both state and non-state actors.

Figure 7 shows the Nucleonica simulated γ-ray spectra of the proposed uranium fuel composition when an illustrative 20 cm lead shielding is used. From the figure, it is evident that detection of proposed fuel remains possible even with shielding (γ-ray peaks of ^{208}Tl well resolved), but for fuel without ^{232}U (no high-energy γ-ray peaks), a drastic attenuation of γ-radiation below 1.5 MeV would occur, making material concealment possible. On the other hand, the presence of $^{232}U/^{208}Tl$ has the disadvantage of making any manipulation of the material more complex due to higher radiation doses. Therefore, the activity of such material should be kept below certain limits to ensure doses tooperators and safety risks are "as low was reasonably achievable."[4, 5].

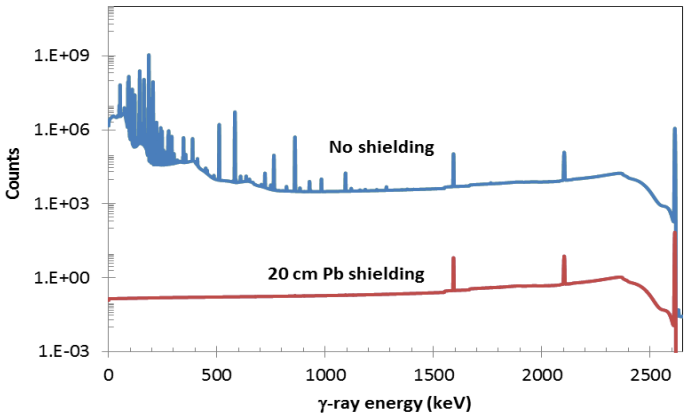

Figure 7: Simulated γ-ray spectra of the proposed uranium fuel composition. The spectra are simulated with (bottom) and without (top) 20 cm of lead shielding showing the drastic attenuation of γ-radiation below 1.5 MeV.

The handling, transport and storage of fuel have to be addressed for any development of new nuclear fuel in terms of assessing the fuel dose rate. For the fuel composition assessed in the example above, according to simulations performed with Nucleonica, the dose rate at 1 m of 500 kg of 3.5% enriched uranium fuel (about 1 fuel assembly of PWR fuel) is about half (~ 33 μSv/h) that of the same assembly made of the fuel proposed in this work (3.46% enriched made of mixture of fresh and reprocessed uranium). Therefore, the proposed fuel composition does not increase the dose rate in a significant way (estimated to be ~ 66 μSv/h at 1 m from a fresh assembly). These considerations can also be extended to radiation protection issues. On the other hand, the proposed fuel composition would not contribute to proliferation resistance in terms of radiation barrier. As already seen, it can enhance proliferation resistance by making the material easier to detect. In particular, the capability to remotely detect the material enables the implementation of techniques for item tracking and process monitoring, increasing the possibility of detecting diversion of fuel from the facility and therefore, improving the system's safeguardability [10].

Still from a safeguardability point of view, it is worth mentioning that the presence of ^{232}U and daughters in the proposed mixture does not mask the 186 keV γ-peak from ^{235}U. Indeed, as shown in Figure 8, neither ^{232}U nor its daughters produce significant γ-lines in the range of 150-220 keV, which are the range of interest for ^{235}U identification. In this figure we show simulated γ-spectra in high resolution germanium detectors, the absence of interfering lines between ^{232}U and ^{235}U would make the use of low resolution NaI spectrometers still possible, as frequently used nowadays for un-irradiated uranium.

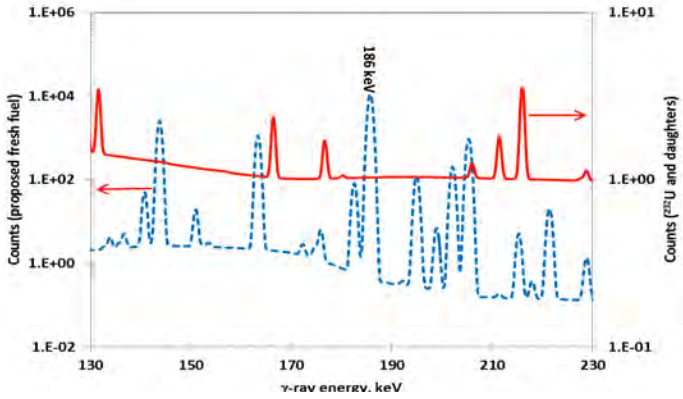

Figure 8: Simulated γ-ray spectra in the energy range 130-230 keV of the proposed uranium fuel (dashed line) and of ^{232}U including its daughters (continued line) showing no γ-peak interferences between ^{232}U and ^{235}U.

In addition, any attempt to re-enrich the proposed uranium to weapon grade using, for example, centrifugation processes would become problematic as the ^{232}U concentration would raise faster than that of ^{235}U, thus worsening the radiation conditions inenrichment facilities [4, 5]. This might have a strong impact on material handling.

Moreover, in the context of 20% enriched uranium doped with ^{232}U, [9] shows that the α-particles emitted by ^{232}U and ^{236}U could dissociate UF_6 molecules inducing uncontrolled release of fluorine and causing enrichment to fail, possibly discouraging a potential proliferator. Given the large difference in the ^{232}U concentration, the quantification of these effects for the mixture proposed in this paper is currently under investigation.

Although a proliferation analysis of the entire nuclear fuel cycle utilizing the proposed fuel is out of the scope of this paper, it is worthwhile to highlight the fact that the use of reprocessed uranium for fresh LWR fuel implies the existence of either a closed fuel cycle within the country or some kind of arrangement with supplier countries. Reprocessing is considered to be a very sensitive technology in terms of nuclear proliferation resistance, and the existence of this fuel cycle capability might enable proliferation routes that need to be carefully analysed. From a proliferation resistance point of view, the second option, i.e. an arrangement with supplier countries would certainly present fewer concerns than the first one.

5. Conclusions

This paper proposed a proliferation resistant UO_2 fuel concept using reprocessed uranium. Based on ORIGEN code calculations, it is shown that for a mixture half-made of fresh uranium enriched at 6% and the other half of reprocessed uranium resulting in new ("fresh") UO_2 fuel enriched at about 3.46%, the concentrations of ^{232}U and ^{236}U remain of the same order of magnitude compared to spent fuel originally made of fresh uranium. Other similar and

consistent scenarios could be obtained by mixing different proportions of reprocessed uranium with uranium of varying enrichment level.

The presence of both ^{232}U and ^{236}U radioisotopes in reactor fuel were considered to be complications in the nuclear fuel cycle as ^{232}U rises the radiation field of the fresh fuel and ^{236}U is a strong neutron absorber that needs to be compensated by using higher enrichment levels. In this work, the proposed UO_2 fuel makes benefit of moderate concentrations of those uranium radioisotopes (^{232}U and ^{236}U) to enhance the proliferation resistance and safeguardability of the nuclear material, improving its detectability in particular. In fact, fresh fuel containing ^{232}U is difficult to hide as it emits γ-radiation of high energy.

Moreover, any attempt to enrich (via centrifugation) uranium from LEU to HEU for proliferation purposes would be complicated, as the concentration of ^{232}U will increase faster than ^{235}U. The possible dissociation of UF_6 molecules in the terminal phase of the enrichment process due to the high level of α-particles is under investigation.

The authors are further investigating the proposed fuel as well as fuel composed of fresh and recycled uranium with plutonium, and the use of multi-recycled uranium.

6. Acknowledgements

The work presented in this paper is part of JRC Institutional Activity on Nuclear Safeguards and Security within the 7th EURATOM Framework Programme, and has been carried out as joint collaboration of the Actions Information Analysis for Nuclear Security (IANUS) and Nuclear Simulations (NUSIM).The authors are grateful to Patricia Mortreau and Riccardo Rossa for the helpful discussions. Thanks are also due to the anonymous reviewer for the technical review and the useful suggestions. The careful revision of the paper by Lance K. Kim and his suggestions are also acknowledged.

7. References

[1] IAEA, *Proliferation Resistance Fundamentals for Future Nuclear Energy Systems*, IAEA, STR-332, Vienna, (2002).

[2] V. I. Volk and A.V. Khaperskaya; Recycling of uranium from spent RBMK fuel in the nuclear fuel cycle; *Atomic Energy*, Vol. 109, No. 1 (2010).

[3] A. Yu. Smirnov, G. A. Sulaberidze, P. N. Alekseev, A. A. Dudnikov, V. A. Nevinitsa, V. N. Proselkov, and A. V. Chibinyaev; Evolution of Isotopic Composition of Reprocessed Uranium during the Multiple Recycling in Light Water Reactors with Natural Uranium Feed, *Physics of Atomic Nuclei*, Vol. 75, No. 13, pp. 1616-1625, (2012).

[4] A. Yu. Smirnov, V. A. Apse, V. D. Borisevich, V.B. Glebov, G.A. Sulaberidze, A.N. Shmelev, A.A. Dudnikov, E.A. Ivanov, V.A. Nevinitsa and N.N. Ponomarev-Stepnoi; Introduction of recycled uranium into fuel composition of light-water reactors as a protective measure against proliferation; *11th Workshop on separation phenomena in liquids and gases*, Saint Petersburg, Russia, June 13-12 (2010).

[5] P. N. Alekseev, E. A. Ivanova, V. A. Nevinitsaa, N. N. Ponomarev_Stepnoia, A. N. Rumyantseva, V. M. Shmeleva, V. D. Borisevichb, A. Yu. Smirnovb, and G. A. Sulaberidzeb; The Concept of the Use of Recycled Uranium for Increasing the Degree of Security of Export Deliveries of Fuel for Light Water Reactors; *Physics of Atomic Nuclei*, Vol. 73, No. 14, pp. 2264–2270 (2010).

[6] IAEA, Use of Reprocessed Uranium, *Proceedings of the Technical Committee Meeting*, IAEA, TECDOC-CD-1630, Vienna, August (2007).

[7] Nucleonica GmbH, Radiations, Nucleonica Nuclear Science Portal (www.nucleonica.com), Version 3.0.11, Karlsruhe (2011).

[8] SCALE: A Comprehensive Modeling and Simulation Suite for Nuclear Safety Analysis and Design, ORNL/TM-2005/39, version 6.1, Oak Ridge National Laboratory, Oak Ridge, Tennessee, June 2011. Available from Radiation Safety Information Computational Center at Oak Ridge National Laboratory as CCC-785.

[9] E. F. Kryuchkov, V. A. Apse, V. A.Yufereva, V. B. Glebov, and A. N. Shmelev; *Evaluation of Self-Protection of 20% Uranium Denatured with ^{232}U Against Unauthorized Re-enrichment*; Moscow Engineering Physics Institute (State University), Kashirskoe shosse, 31, 115409, Moscow, Russia (2008).

[10] G.G.M. Cojazzi, G. Renda, F. Sevini, Proliferation Resistance Characteristics of Advanced Nuclear Energy Systems: a Safeguardability Point of View, *ESARDA Bulletin No. 39, Special Issue on Proliferation Resistance*, October (2008). Available at: http://esarda2.jrc.it/bulletin/bulletin_39/index.html

Application of the PR&PP Methodology to the MYRRHA research facility

Riccardo Rossa, Klaas van der Meer, Alessandro Borella

StudieCentrum voor Kernenergie - Centre d'etude de l'Energie Nucleaire - Boeretang 200, Mol 2400 Belgium
E-mail: rrossa@sckcen.be, kvdmeer@sckcen.be, aborella@sckcen.be

Abstract:

In the past years two publications offered the initial points for the assessment of the proliferation resistance of the MYRRHA (Multi-purpose hYbrid Research Reactor for High-tech Applications) facility [1]. The first document [2] applied the TOPS methodology (Technological Opportunities to Increase the Resistance of Global Civilian Nuclear Power Systems) both to the MYRRHA facility and to the BR2 reactor, the material testing reactor operating at SCK•CEN [3]. The second paper [4] provided an initial study according to the PR&PP methodology.

This article presents an overview of the PR&PP methodology to MYRRHA. Thanks to the deeper level of detail of the design a complete study with this methodology has been performed, to identify the challenges to the system and how the system can respond to them.

The misuse threat has been analyzed both for MYRRHA and for the BR2, by applying the PR&PP methodology to both facilities. The comparison carried out with the TOPS methodology [2] considered the diversion threat; therefore this article extends the comparison focusing on the misuse threat.

The PR&PP methodology was also used to investigate possible design variations for MYRRHA and make some suggestions to the MYRRHA design team by applying the Safeguards-by-Design concept.

Keywords: PR&PP; MYRRHA; proliferation resistance; Safeguards-by-Design; TOPS

1. Introduction

In the framework of the European Research Area of Experimental Reactors, MYRRHA is envisaged as one of the major three research reactors which will be developed in Europe, along with the Jules Horowitz Reactor (in Cadarache, France) and the PALLAS facility (in Petten, the Netherlands).

This reactor is currently being designed at SCK•CEN, the Belgian Nuclear Research Center and is planned to be built on the same technical domain. This research center hosts the BR2, a material testing reactor.

A previous publication [2] compared these two installations with the TOPS methodology and found that MYRRHA would be more vulnerable for State-supported diversion of nuclear material, while BR2 is more vulnerable for diversion by non-State actors.

To extend the study performed in [4] this article analyzes in detail the MYRRHA facility with the PR&PP methodology. Since new detailed design information is available now, this study can focus on the identification of the acquisition pathways, suggesting design variations in order to increase the proliferation resistance of the overall system.

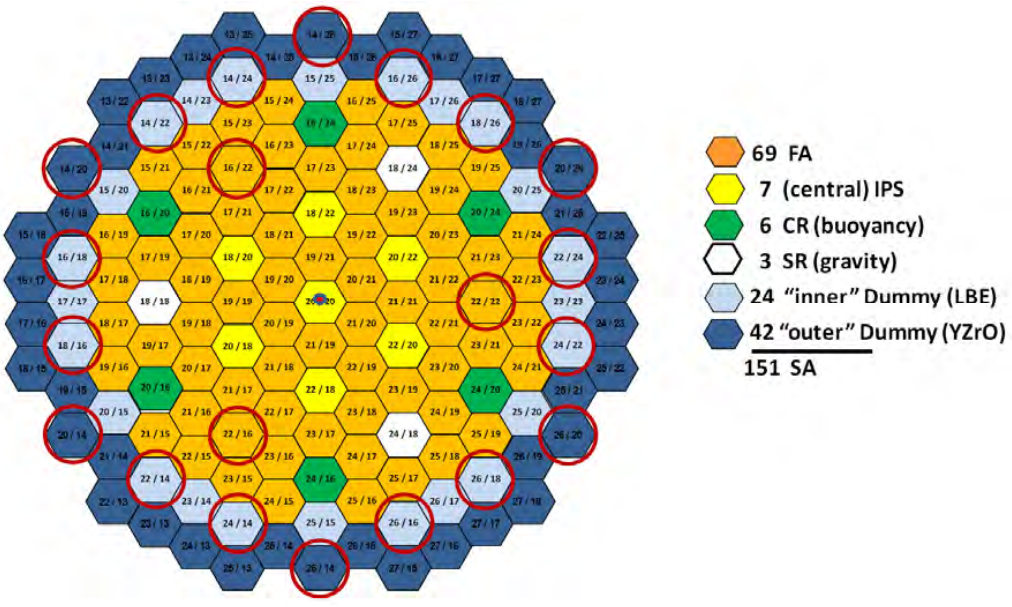

Figure 1: cross section of the critical configuration.FA: Fuel Assembly; IPS: In-Pile Section; CR: Control Rod; SR: Safety Rod

2. Description of the MYRRHA facility

MYRRHA consists of an Accelerator Driven System (ADS) with the capability to operate both in sub-critical and critical mode. According to the present information (August 2011, [5],[6]), MYRRHA will be a large power research reactor (100 MW_{th}) with a fast neutron spectrum. The multiplying core will be loaded with Mixed-Oxide fuel (MOX fuel) and cooled by liquid lead-bismuth eutectic. Figure 1 shows the cross section of the reference configuration.

The most relevant features for proliferation resistance assessment of the reactor are:

- high power level (100 MW_{th});
- Lead-Bismuth Eutectic (LBE) will be used as spallation source and coolant. Due to its opaqueness and oxygen-free atmosphere it is considered a Difficult-to-Access (DtA) area;
- 69 Fuel Assemblies (FA) occupy the central region of the structure;
- 7 In-Pile Sections (IPS, 1 central and 6 radials) are used for experiments and material testing;
- 66 items, called Reflector Assemblies (RA), surround the fuel assemblies and partially shield the outer structures from the intense neutron field. 42 assemblies are structural identical to fuel assemblies but with YZrO pins instead of fuel rods;
- additional fuel will be stored under LBE inside four In-Vessel Fuel Storages (IVFS), placed around the reactor core.

The average neutron flux expected in the reactor core will be in the range of 10^{15} n/cm^2/s, while in the In-Vessel Fuel Storages the value should decrease of about two orders of magnitude [6].

Considering the single fuel element, MOX fuel is the favorite choice because of its better neutronic properties in the fast energy spectrum compared with the traditional UO_2 fuel [7].

The preliminary choice for the fuel of the critical configuration is reactor grade Pu (RG-Pu), with a Pu enrichment of 34.5 wt.%, in order to obtain the desired compact core and high neutron flux [8].

Considering the sub-critical configuration, it will contain 72 fuel assemblies with an enrichment of 30% of RG-Pu. Since the plutonium content is lower than in the case of the critical core, and considering that the most recent design information concerns the critical configuration, only this one has been used in the analysis.

The Pu enrichment is however still under investigation and may change as the design develops.

Another relevant information for the analysis is the path of the nuclear material (e.g. fuel assembly) once it enters the facility. Figure 2 shows all the locations (e.g. storage areas, reactor core) and the relative transportations within the facility.

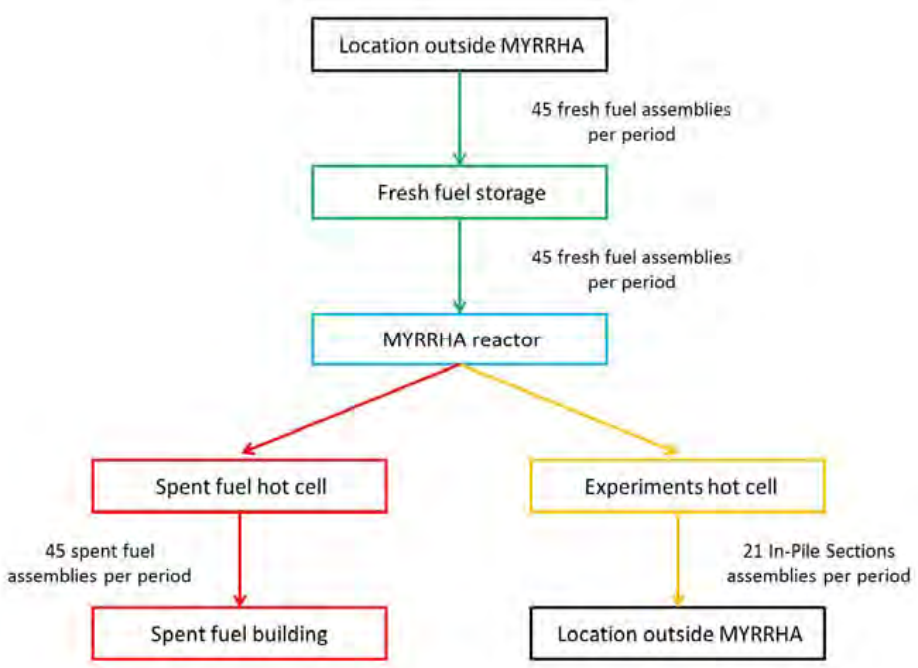

Figure 2: Material flow during one period of irradiation (420 days). Arrows indicate transfers of material between two locations.

3. Description of a generic safeguards approach for MYRRHA

A generic safeguards approach for MYRRHA is described here that has been used as a basis for the evaluation by the PR&PP methodology.

The basis of the safeguards will be Nuclear Material Accountancy, supplemented by Containment and Surveillance (C/S) measures. C/S measures will be used to have a clear follow-up of the MOX fuel in the reactor for the preservation of the Continuity of Knowledge. Either cameras or seals will be applied to the spent fuel, since it will be stored for a long period without the necessity to manipulate it. Present safeguards approaches apply cameras to spent fuel storages. With regards to fresh fuel, seals will most probably only be applied during transport to the facility, unless they remain attached until the fuel is actually transferred to the reactor. Cameras will be placed at strategic locations to follow the transfers of fresh fuel assemblies from the fresh fuel storage to the reactor and the transfers of spent fuel assemblies from the reactor to the spent fuel storage. NDA measurements will be applied to fresh fuel assemblies with a high probability to detect even smaller diversions. NDA measurements on spent fuel assemblies will have a lower probability to detect diversions, certainly via partial defects.

Due to the inert atmosphere in the reactor building - as it is envisaged in the current design - the transfer of the fuel assemblies will be highly automated. Also the fuel manipulation in the pressure vessel (from interim storage to reactor core and vice versa) will be highly automated. Authenticated transfer of these data to the Inspectorates is envisaged so that the Inspectorates are able to follow the fuel assemblies when they are under the PbBi coolant in the reactor core or interim storage.

In case wet storage for spent fuel assemblies will be chosen, the assemblies have to be completely free of PbBi before they go into the spent fuel storage pool. This additional manipulation requires an additional inspection, probably with help of one or several cameras.

To verify that the facility is not misused for unreported plutonium production, power monitoring of the reactor could be a solution. However, such a power monitor for liquid metal in a large pool is not standard safeguards equipment and should be developed.

Given the generic description of the MYRRHA safeguards approach, specific issues like joint IAEA-Euratom inspections have not been considered in this paper.

4. Description of the PR&PP Methodology

The PR&PP methodology has been developed in the framework of the Generation Four International Forum [9, 10]. This methodology can assess both the proliferation resistance and the physical protection robustness of a nuclear facility.

The analysis can be divided into three main steps. The first step is the threat definition (with the identification of the possible actor strategies), while the second one is the evaluation of the system response to these threats, with the identification of the elements and of the targets inside the system.

The second section ends with the identification of the acquisition pathways and the estimation of the measures for each pathway.

The final part of the evaluation allows the comparison of the different pathways and the presentation of the results. Summarizing, the PR&PP methodology is based on the following steps:

- **Challenges**
  - definition of the threat space
- **System response**
  - system element identification
  - target identification and categorization
  - pathway identification and analysis
  - estimation of measures
- **Outcomes**
  - pathway comparison
  - system assessment and results

To analyze the system the PR&PP methodology defines a set of six parameters (or measures):

- *Proliferation Technical Difficulty (TD)* is the difficulty to successfully acquire a nuclear weapon due to the need for technical sophistication (knowledge and infrastructure).
- *Proliferation Cost (PC)* is the cost (personnel and investments) required for the acquisition of a nuclear weapon. In case of the misuse of existing installations, only the additional costs for proliferation are taken into account, not the regular operation costs.
- *Proliferation Time (PT)* is the time between the first act to acquire a nuclear weapon and its final construction.
- *Fissile Material Type (MT)* is the categorization of applicability of fissile material in a nuclear weapon.
- *Detection Probability (DP)* is the probability to detect misuse or diversion in a certain pathway.
- *Detection Resource Efficiency (DE)* is the efficiency in the use of staffing, equipment, and funding to apply international safeguards to the facility. For this study the DE is defined as the additional resource needed to apply safeguards, considering current expenses devoted to the Host State.

In addition to the proposed scale for the "Proliferation Time" and "Fissile Material Type" metrics [9], a percentage scale has been applied to all metrics. This scale represents the difficulty of each scenario. The higher the value, the more effort is assumed for the proliferator (Table 1).

In the scale, the range of values has been refined for some metrics (e.g. the 25–75% range is now described by five values). This is done because when applying the original division often the same linguistic value was used for several scenarios. Using a higher number of bins resulted in the introduction of intermediate linguistic values, such as "Low to Medium" or "Medium to High".

Considering that MYRRHA will be a research reactor, the definition for the last measure has been adapted to better reflect the characteristics of the system.

The metric "Detection Resource Efficiency" has been evaluated considering the complete system, since safeguards equipment has to be applied to the facility as a whole and not only for specific scenarios.

As a consequence, this last metric (DE) can be used to compare different design variations, and assess the repercussion that each variation can have to the total cost of safeguarding the facility.

Evaluating the cost of safeguards equipment however is not an easy task because of the difficulties to gather all information on the cost of the equipment and on the inspector resources that the equipment requires.

The calculation of the additional cost to safeguard MYRRHA started from the current expenses that the Department of Safeguards devotes to the Host State.

For each design variation (e.g. type of spent fuel storage), it is necessary to assess the resources needed for the implementation of safeguards (e.g. number of Person Day of Inspection, PDI).

At the end of the analysis it is possible to compare the resources requested for each variation and therefore identify the best solution for the cost reduction of safeguards measures.

Measure	Metric scales bin		Proliferation Resistance
Proliferation Technical Difficulty	0 – 5 %		Very Low
	5 – 15 %		Very Low to Low
	15 – 30 %		Low
	30 – 40 %		Low to Medium
Proliferation Cost	40 – 60 %		Medium
	60 – 70 %		Medium to High
	70 – 85 %		High
Detection Probability	85 – 95 %		High to Very High
	95 – 100 %		Very High
Proliferation Time	0 – 3 months	1 – 20 %	Very Low
	3 m – 1 year	20 – 40 %	Low
	1 – 10 y	40 – 60 %	Medium
	10 – 30 y	60 – 80 %	High
	> 30 y	80 – 100 %	Very High
Fissile Material Type	HEU	1 – 20 %	Very Low
	WG Pu	20 – 40 %	Low
	RG Pu	40 – 60 %	Medium
	DB Pu	60 – 80 %	High
	LEU	80 – 100 %	Very High
Detection Resource Efficiency	Comparative metric between different design variations		

Table 1: Evaluation scales used in the analysis.

5. Evaluation of MYRRHA

5.1 Challenges

Possible threats to the system can be both concealed and overt diversion of material, both concealed and overt misuse of the facility, or the use of a clandestine facility alone.

Since Belgium will be the host state of MYRRHA, and since it is an active participant of the International Community, both overt diversion and misuse are not credible and have been excluded from the analysis. The building of a clandestine replica is not realistic, considering the dimensions and complexity of the facility.

The considered challenges (or threats) to the facility are:

- *Concealed diversion of nuclear material from declared flows or inventories;*
- *Concealed misuse of the declared facility for the unreported plutonium production*.

For an easier assessment of the system, it has been assumed that it has been divided into three Material Balance Areas (MBA):

- **BM01**: considers the fresh fuel and contains the fresh fuel storage area;
- **BM02**: includes the reactor vessel, containing both the MYRRHA core and the four IVFS;
- **BM03**: covers the path of the spent fuel from the reactor vessel to the spent fuel building.
- Diversion of nuclear material can happen both during transportations and during storage periods.

Misuse of the facility for the unreported plutonium production can occur both inside the reactor core and inside the IVFS.

5.2 System response

5.2.1 System element identification

The next step of the analysis is the identification of the system elements that are relevant for the diversion and for the misuse.

Figure 2 is a schematic representation of the MYRRHA facility considering the transportations of nuclear material and the places where the material will be stored. The figure uses different colors to identify the division of the system in the three MBA defined in the paragraph above. The first MBA (BM01) is represented in green, the BM02 is depicted in blue, while the last one is in red and yellow.

5.2.2 Target identification and categorization

The most relevant material for diversion is the fuel itself, and either fresh or irradiated assemblies are attractive due to the high plutonium percentage. Calculations [11] show that the material type does not change during the irradiation, being always reactor grade plutonium. The diversion can concern both a single assembly and a transport cask which will contain more than one fuel assembly.

The fuel inventory is distributed over the three MBAs defined before, as follows:

- **BM01**: the fresh fuel storage will contain 45 assemblies, the inventory for one year of operation.
- **BM02**: a total amount of 381 kg of Pu is estimated inside the core [6], equal to about 48 Significant Quantities (SQ). According to this calculation, each fuel assembly will contain on average 5.5 kg of Pu.
- Additional 45 fresh fuel assemblies will be stored inside the In-Vessel Fuel Storage (IVFS), to allow refueling for three cycles (about one year of normal operation), together with a maximum of 90 spent fuel assemblies (45 fuel assemblies will exit the reactor core each year, and then will stay another year in the storage to cool down). The four IVFS will contain a maximum of 90 fuel assemblies (either fresh or irradiated), adding other 62 SQ (500 kg of Pu).
- **BM03**: the inventory of the spent fuel storage will increase during the years, adding 45 spent assemblies (31 SQ, 250 kg of Pu) every year.

For the unreported plutonium production natural or depleted uranium targets will have to be constructed.

The breeding capability has been estimated with the Binford study [12], accounting for the different flux levels inside the core and in the IVFS. Calculations [13] show that the production capability is quite high, but the flux level inside the core is too high to produce weapons-grade Pu (WG-Pu), which can be produced only in the IVFS.

Depending on the irradiation strategy, the uranium that has to be inserted to produce one SQ can vary from 500 kg (core irradiation) to 35 tons (IVFS irradiation).

5.2.3 Pathway identification

Several diversion strategies have been identified:

- *RE*: replacement of a full cask with an empty cask.
- *SB*: send back a full cask instead of an empty one.
- *RD*: replacement with a dummy assembly.
- *S*: switch between a fresh and a spent fuel assembly. Fresh fuel is then diverted, while spent fuel is loaded again in the core.
- *PS*: insertion of a fresh fuel assembly in a position where an already-irradiated assembly is declared. Fuel assembly undergoes less irradiation cycles.
- *PR*: insertion of a fuel assembly in the position of a reflector assembly. Fuel assembly is then diverted as a reflector assembly
- *HW*: introduction of a spent fuel assembly in the waste hot-cell. Fuel is then diverted as waste.

- *HE*: introduction of a spent fuel assembly in the experiments hot-cell. Fuel is then diverted as material that underwent an irradiation experiment.

The simple diversion without replacement (either of an assembly or a cask) has been considered too easy to detect and therefore has not been considered in the analysis.

A total of 42 diversion pathways have been identified and evaluated in detail in [13].

Irradiation for the unreported plutonium production can occur in several locations:

- Inside the core, in the position of fuel assemblies (FA);
- Inside the core, in the position of reflector assemblies (RA);
- Inside the core, in the position of In-Pile Sections (IPS);
- Inside the In-Vessel Fuel Storage (IVFS).

Further information on the targets and on the irradiation strategies can be found in [13].

5.2.4 Estimation of measures

The proliferation resistance measures have been evaluated according to the analysts' judgment, together with the reference documents for the methodology [9, 10].

A generic proliferation strategy can be divided in the segments of:

- **Acquisition**: activities carried out to acquire nuclear material in any form.
- **Processing**: activities carried out to convert the nuclear material obtained in the acquisition stage into material ready for use in a nuclear weapon.
- **Fabrication**: activities carried out to manufacture and assemble a nuclear explosive device.

Separate values of each metric are first indicated for the acquisition stage and for the processing stage of the proliferation action (Table 2 gives an example, complete analyses in [13]).

Pathway type	Insertion in the waste hot-cell.		
Pathway description: spent fuel is introduced in the waste hot cell after unloading from IVFS. Fuel assembly inserted in cask. Use heavy truck and trailer to move cask. Fool or disable camera. Compromise the inventory measurement record.			
	Value	**Acquisition Basis**	**Processing Basis**
Proliferation Technical Difficulty	**High**	*Low.* Need to remove the spent fuel via the experiment hot cell. Use of elevators and trailer to move the cask.	*High.* Spent fuel will require reprocessing to extract Pu in a usable form. Radiation shielding must be used.
Proliferation Cost	**Low to Medium**	*Very Low to Low.* Cleaning process is needed and may not be foreseen in the facility.	*Low to Medium.* Clandestine reprocessing facility is required. For this, assume $10M - $100M.
Proliferation Time	**Medium**	*Very Low to Low.* Depends on the time between the decision of the diversion and the next scheduled refueling.	*Medium.* Reprocessing time would be of the order of months, but constructing a facility could take years.
Detection Probability	**Medium to High**	*Medium to High.* This parameter depends on the level of C/S of the waste hot cell and on the level of verifications foreseen for waste.	*Not considered.*

Table 2: Example of estimation of measures for a complete diversion pathway.

Subsequently, the two measures are combined to form a unique value for each metric. The values reported in Table 3 take the maximum of the single values attributed for the acquisition and processing stages.

The fabrication segment has not been taken into account because it requires specific classified information about the design of nuclear explosives.

The following table summarizes the main results from the diversion analysis. Since some diversion pathways show similar characteristics, they have been grouped to reduce their number. The complete list takes into account both the simple diversion (of either one fuel assembly or one fuel cask) and the replacement of the same items with a dummy assembly or an empty cask. In the summary table only the replacement cases were considered because they have been judged as the limiting case for the safeguards verification.

The "Material Type" is not reported in Table 3 because it does not change in all scenarios, while the "Detection Resource Efficiency" will be used later in the analysis.

Target	Strategy	Diversion point	TD	PC	PT	DP
Cask of fresh fuel	RE; SB	During transportation in MBA BM01	2	2	10	98
Fresh fuel assembly	RD	During transfer or storage in BM01	8	2	10	95
	RD	During transfer in BM02	10	2	10	98
	S	During core reshuffling	30	5	10	75
Spent fuel assembly	PR	During core reshuffling	30	5	10	75
	PS	During core reshuffling	50	30	40	75
	RD	During transfer in BM02	75	30	40	98
	HW; HE	During transfer from the IVFS	75	30	40	70
	RD	During hot-cell manipulations	75	30	40	90
	RD	During transfer to BM03	75	30	40	80
	RD	During storage in BM03	75	30	40	98
Cask of spent fuel	RE; SB	During transportation in MBA BM03	75	30	40	98

Table 3: Summary of the diversion analyses.

Considering the misuse, the measures have been estimated by answering the set of questions collected in the Example Sodium Fast Reactor case study [14].

The same set of questions has been applied to the BR2, to allow a comparison between the two installations according to the PR&PP methodology. Table 4 summarizes the results from the misuse analyses.

Misuse strategy	TD	PC	PT	MT	DP
Plutonium breeding in the positions of Fuel Assemblies (FA) or Reflector Assemblies (RA)	75	30	40	50	85
Plutonium breeding in the In-Vessel Fuel Storage (IVFS)	75	30	40	30	85
Plutonium breeding in the position of In-Pile Sections (IPS)	75	50	40	50	25
Plutonium breeding in the BR2 reactor	75	50	30	30	50

Table 4: Summary of the misuse strategies.

6. Discussion

6.1 Fresh fuel diversion

Considering first the diversion scenarios, the four material targets can be grouped in two broad groups, considering the fresh fuel separated from the spent fuel.

Fresh fuel (either single assemblies or entire transport casks) is a very attractive material for proliferators because of its high plutonium content and its low radiation level. Although further manipulations are needed to obtain weapon usable material, every scenario involving fresh fuel scores quite low proliferation resistance characteristics in terms of cost and time.

On the other hand, the same scenarios show very high detection probability, thanks to the safeguards measures implemented in the facility. For the fresh fuel, these include weight measurements of the incoming cask and NDA techniques to verify the single assembly. In addition, several cameras and seals will be employed to verify the material.

The Safeguards measures implemented in the facility are used to determine the detection probability of each scenario. They are very important in the case of fresh fuel, because they are the only PR measures in place, since the other parameters do not show very good PR characteristics.

The technical difficulty is lower in the case of cask diversion because the fuel assemblies do not have to be manipulated. However, the detection probability is higher in the same case because it has been judged easier to detect a missing cask or the switch between two casks.

Diversion occurring during core reshuffling has higher technical difficulty because the fuel is inserted in the LBE and therefore requires cleaning process afterwards.

6.2 Spent fuel diversion

A similar discussion can be done for the scenarios concerning spent fuel. Diversions of single assemblies or of entire casks have been considered.

In all scenarios, the fuel has to be reprocessed and this increases the technical difficulty, proliferation cost and time of all scenarios. All these three measures are constant over all cases because they all require reprocessing of the spent fuel and this is the determining segment for these three measures. In the case of spent fuel diversion therefore the only parameter that can vary is the detection probability. The most critical scenarios are the replacement of one spent fuel assembly with a dummy, and the introduction of one spent fuel assembly in the waste or experiments hot cell (HW or HE). Whereas the large uncertainties associated with spent fuel verifications play the same role for all scenarios with spent fuel since a dummy replacement is always assumed, the differences in DP for these scenarios lay in the fact that verifications on waste or samples associated to experiments going out from the reactor hall may be not as strict as the ones devoted to spent fuel assemblies.

For instance in the case of experiments once the irradiation is completed the In-Pile Section is removed and directly put in the hot cell. There it is dismantled and the sample used for the irradiation experiment is sent to the customer that ordered it. All the remaining parts of the IPS are sent away as waste material. Given all these manipulations the detection probability for a diversion has been judged lower than in the other scenarios.

Like in the case of fresh fuel diversion, the replacement of entire casks has been judged the easiest scenario to detect, scoring the highest detection probability.

In the last scenario concerning fresh/spent fuel (strategy: PS), the fuel needs to enter the reactor core for at least one cycle. This increases the proliferation cost and time because reprocessing is likely to be needed also in the case of short irradiation time. Also the technical difficulty is higher because of the radiation level from the assembly coming out from the core.

6.3 Misuse strategies

Considering the misuse scenarios, as in the case of the diversion analyses, the Detection Resource Efficiency (DE) is the same for each strategy, because they do not involve any major modification to the facility and to the safeguards measures. However, within a single misuse strategy, the estimation of the value attributed to the DE varies along the misuse segments. This is because this metric considers both MYRRHA and the host State in the broad sense (e.g. import-export controls are used for the detection of illicit procurement).

The plutonium production capability of MYRRHA is rather high because each scenario can produce some kilograms of Pu each year, while the IPS replacement has the lowest production capability (in the range of 100 grams per year).

All the three misuse strategies have about the same proliferation resistance; the only major difference is that irradiation in the IVFS is capable of producing WG-Pu (assuming a fluence of about 10^{20} n/cm^2 [13]). Irradiation in the core leads to a value of fluence that is too high (~10^{22} n/cm^2, [13]) to obtain a good weapons quality of plutonium. The irradiation time has been considered equal to one operational cycle (i.e. 90 days). A period of 30 days is foreseen between two operational cycles and within one cycle the reactor hall would not be accessible.

Table 4 summarizes the values of the metrics used in the analysis for the misuse strategies.

The irradiation in the positions of fuel assemblies (FA) or reflector assemblies (RA) has been considered together because the geometry of FA and RA and the fluence in their positions are the same, with the only difference in the composition of the internal pins.

The irradiation in the IVFS requires the replacement of blank assemblies, which are made of a thin stainless steel clad and do not contain pins in the internal region. They are used only for the guiding of other assemblies and are not placed in the reactor during operation. Given the significant difference in weight between a fuel assembly and a blank assembly, the switch between the two can be easily detected with weight measurements. The integration of a weight measurement system in the fuel handling machine will increase the proliferation resistance of the facility.

The irradiation in the IPS positions scores the lowest detection probability because of the numerous types of experiments that can be loaded in MYRRHA. Each IPS channel can load only a small amount of target material and several loadings are needed to produce at least one

Significant Quantity. This allows the relaxation of the safeguards measures for this scenario, lowering its detection probability.

Considering the high number of target assemblies that has to be manipulated in every scenario [13], it is likely that the normal neutron flux will be somehow distorted.

Additional fuel assemblies may be loaded in several positions to try and conceal this fact. This is why additional assemblies in the reactor can be an indication of possible misuse of the facility.

6.4 Comparison between MYRRHA and the BR2

The previous study with the TOPS methodology [2] considered the overt diversion of fissile material by a subnational group and the covert diversion of material for the construction of 10-20 nuclear weapons.

The comparison with the PR&PP methodology extends this comparison, taking into account the misuse of both facilities for the unreported plutonium production.

In order to evaluate this threat the Binford study [12] has been used to estimate the Pu breeding capability in both facilities. The study gives the Pu production and percentage of non-fissile isotopes as a function of the neutron fluence.

According to the calculations reported in [13], MYRRHA proved to be more proliferation resistant than the BR2, because of the less attractive material that can be bred in MYRRHA, and its lower production capability.

In addition to the calculation according to the Binford study, the comparison between the two facilities has been performed using the same technique proposed in the PR&PP example case study [14]. In the case study of the Example Sodium Fast Reactor, the authors identified a set of more than 80 questions to be answered in order to estimate the parameters of the PR&PP methodology. The definition for the parameters is the same of the one used for the analysis of the diversion scenarios.

The same set of questions has been applied for both the MYRRHA and BR2 case; detailed information about the analysis can be found in [13].

Each question is answered using the linguistic values determined before (ranging from Very Low to Very High). Once all the questions related to one measure have been answered, the analyst can group the answers to obtain the representative value for the measure. The methodology to obtain the representative value is similar to one used in the diversion scenarios: the final value is the most limiting case evidenced by the single answers.

By looking at Table 4, the irradiation in the BR2 can be compared to the case of irradiation in IPS channels inside MYRRHA. The Technical Difficulty is the same in the two cases because of the difficulty to reprocess and to handle irradiated materials. Also the cost associated to the two scenarios is similar because they imply the loss of income from the experiments performed in the reactors.

The Proliferation Time is lower in the case of the BR2 because of the higher number of positions that can be used for irradiation, and the Material Type produced is WG-Pu.

In the case of the irradiation in the IPS positions it is possible to lower the detection probability of the misuse because of the small amount of Pu that can be produced; this is not the case for the BR2, which requires a higher inspection effort and detection probability for the misuse.

7. Design variations

Another role of the Proliferation Resistance analysis is the support to the design team in order to show the positive and negative safeguards characteristic of the possible design variations.

Since the types of the fresh fuel storage and of the spent fuel storage are not fixed yet in the design, this Proliferation Resistance analysis can give a support to the decision.

7.1 Fresh fuel storage

The reference case assumed the fresh fuel storage inside a specific room with adequate radiation shielding. Two design variations foresee the storage in the transport containers in which the assemblies arrive at the MYRRHA site (DV1), or in another type of containers (with the consequent switch of the assemblies from the transport cask to the storage cask, DV2).

If the first design variation is applied (DV1), the incoming cask can be diverted during the interim storage, following the same diversion path of the case defined for fresh fuel assemblies stored according to the reference design.

Target	Strategy	Diversion point	TD	PC	PT	DP
Cask of fresh fuel	RE; SB	During transportation in MBA BM01	2	2	10	98
Fresh fuel assembly	RD	During transfer in BM02	10	2	10	95
	S	During core reshuffling	30	5	10	75

Table 5: first design variation (DV1). Changes in the evaluation of the diversion scenarios.

Comparing the reference case with DV1 (Table 3 and Table 5 respectively), the replacement of a fuel dummy in the first MBA (BM01) is considered now in the strategy for full cask diversion.

With this target variation, the technical difficulty has been assumed to decrease because it is not necessary to insert assemblies into another cask, but the actor has just to move the transport cask to the concealed facility.

This change in technical difficulty is compensated by an increase of the detection probability, because in general it is easier to detect with cameras the movement of an entire cask and a missing container in the fresh fuel storage. Camera surveillance however is not the only way to maintain the continuity of knowledge of the material and to detect the diversion. Item counting and random NDA measurements will ensure the effective safeguards of the material and can be used in case of loss of continuity of knowledge on any item. The attachment of seals to the storage casks decreases the inspection effort requested to the IAEA, which has only to verify the integrity of the seals without other verification measures. Considering all the safeguards activities in the facility the reference case and the first design variation (DV1) has been judged fairly equal from the safeguards point of view.

Target	Strategy	Diversion point	TD	PC	PT	DP
Original cask	RE; SB	During transportation in MBA BM01	2	2	10	98
Storage cask	RE; SB	During transportation in MBA BM01	2	2	10	98
Fresh fuel assembly	RD	During transfer in BM02	10	2	10	95
	S	During core reshuffling	30	5	10	75

Table 6: second design variation (DV2). Changes in the evaluation of the diversion scenarios.

According to the second design variation (DV2) a new target is identified, splitting the pathway analysis in the scenarios regarding the transport cask and in the scenarios regarding the storage cask.

The cask arriving in the system can be replaced or can be sent back full to the unloading point, the container used for storage can be again replaced or sent back to the storage area, while single fuel assemblies can be replaced during the transfer between the two casks or before going to the reactor.

Thus, several new acquisition paths have been identified in this last case. For this reason, although all these new scenarios score quite good proliferation resistance measures, it has been judged that this second design variation is the worst option from the safeguards point of view.

7.2 Spent fuel storage

The reference case assumed the storage of the spent fuel according to the wet-type storage.

The dry-route storage has been considered with two variations. According to the first option the fuel assemblies remain inside the cask used for the transportation from the reactor building to the spent fuel building. The cooling the cask is assured by air circulation).

The second option is the storage in vault-like rooms where the fuel assemblies are placed in a metal-sealed container that will be transported to the spent fuel building. Here the casks are lowered in a sort of vault (that could be a series of shaft in the concrete basement) and cooled there by air circulation.

Going from a wet-route to the dry-route storage, the acquisition paths change in a considerable way.

From the safeguards point of view the dry-route has some advantages and drawbacks compared to the wet-route:

1. the cleaning process is not necessary anymore, leading to the simplification of the design of the hot cell and avoiding all acquisition paths related to that procedure;
2. the spent fuel is not manipulated anymore once it has been placed in the cask, with a further simplification of all the processes regarding the spent fuel and eliminating other possible diversion paths;
3. the insertion of the spent fuel in the cask would require a complete characterization of the assembly at the moment of their loading. This would likely take place in a not-accessible area and would complicate the measurement.
4. the inspectors must be on site to supervise the whole process and to seal the cask just after its loading.

From the comparison it is evident that both design solutions show positive and negative aspects for the verification activities. Only general calculations have been performed so far and more detailed assessments have to be completed to investigate the technical feasibility of all the design variations and to identify the best design configuration.

7.3 Comparison of the design variations

The design variations described in sections 6.1 and 6.2 have been discussed only in a qualitative way since a quantitative discussion would pretend more precision than there is in reality. Having said this, in this section it is nevertheless attempted to discuss and quantify a new definition of the "Detection Resources Efficiency".

In order to compare the different design variations, a new definition of the metric "Detection Resources Efficiency" has been proposed in section 3.

According to the 2010 Safeguards Implementation Report [15], the total resources assigned to Belgium are 1.717 M$. In the Country there are 31 nuclear facilities and Locations Outside Facilities (LOF, e.g. hospitals), which required 130 inspections, 219 Person Days of Inspection (PDI), and a total of 362 Calendar Days in Field for Verifications (CDFV).

Two types of inspection will be required in MYRRHA: the Physical Inventory Verification (PIV) is an inspection performed every year following the Safeguards Criteria, while Interim Inspections (II) are required on a monthly-basis and they involve book auditing, C/S verification, and item counting.

In the recent years, SCK•CEN underwent about 5 PDI per year during the PIV and additional 2 PDI at every II. Therefore, a total of 27 PDI are requested now at the centre that will host the new facility.

Basing the consideration on the current situation, it has been assumed that MYRRHA will likely require 2-3 PDI for the annual inspection and about 1 PDI for each monthly inspection.

Fresh fuel storage	Spent fuel storage	Calendar Day in Field for Verifications			CDFV increase (Belgium)
		P. I. V.	I. I.	Total	
Room with shielding	Wet-route	2.5	1 x 11	13.5	3.7 %
	Dry-route	2	0.5 x 11	7.5	2.1 %
	Vault structure	2	0.5 x 11	7.5	2.1 %
Transport cask	Wet-route	2.5	1 x 11	13.5	3.7 %
	Dry-route	2	0.5 x 11	7.5	2.1 %
	Vault structure	2	0.5 x 11	7.5	2.1 %
Other cask	Wet-route	3	1.5 x 11	19.5	5.4 %
	Dry-route	2.5	1 x 11	13.5	3.7 %
	Vault structure	2.5	1 x 11	13.5	3.7 %

Table 7: Comparison of the design variations in terms of Detection Resource Efficiency.

Considering both type of verifications, the fresh fuel storage in the special room with proper radiation shielding and the storage into the transport containers is assumed to require the same amount of effort.

Extensive use of seals can save a lot of inspection resources because the inspectors only have to check the integrity of the C/S system.

The storage inside other type of cask requires an additional half day of inspections (both in the PIV and in each II) to check the transfer between the different casks.

Considering the options for the spent fuel storage, the dry-route (whether in containers or in a vault-like structure) is assumed to be the best option in terms of resources efficiency, while the wet-route storage requires another additional half day of inspections.

This is due to the checking of the transfer of the fuel assemblies in the cleaning process and to the verification of the movements inside the spent fuel pool.

The additional effort required to the IAEA should be in the order of 10 to 20 CDFV, equal to an increase of 2 to 6 % of the current resources devoted to Belgium (Table 4).

However, the numerical values of these calculations are purely qualitative measures to list the possible design variations and should not be considered as accurate in the absolute scale. Also the magnitude of difference between the different design options has been assumed by the analyst and does not follow any standard methodology.

8. Conclusions

This document offered an overview of the proliferation resistance analysis of MYRRHA according to the PR&PP methodology. The analysis considered as reference the "Conceptual Design" of August 2011 [5],[6].

Both diversion of nuclear material and misuse of the facility have been considered in the evaluation.

Considering the diversion scenarios, fresh fuel (either single assemblies or entire transport casks) is a very attractive material for proliferators because of its high plutonium content and its low radiation level. Each scenario involving fresh fuel scores low proliferation time and cost to complete a pathway, but a high or very high detection probability.

The most attractive scenarios involve the replacement of one reflector assembly with fresh fuel or the switch between a spent fuel assembly and a fresh fuel one. This is because the verifications on reflector assemblies may be not as strict as the ones devoted to spent fuel, and because verification on spent fuel still has quite large measurement uncertainties, especially in the case of MYRRHA with high Pu content MOX assemblies where it will be very difficult to distinguish spent fuel assemblies with various irradiation histories.

In the case of scenarios involving spent fuel, the technical difficulty, proliferation cost and time are quite high because of the needed reprocessing activities. In addition, the fact that the fuel has been inside LBE complicates the required processing.

The most critical scenario is the introduction of one spent fuel assembly in the experiments hot cell or in the waste hot cell. This is because of the large uncertainties associated with spent fuel verifications, and because verifications on waste going out from the reactor hall may not be as strict as the ones devoted to spent fuel assemblies. All material declared as experiment or waste will not be stored at the MYRRHA facility and will be very difficult to track the material once it has left the facility.

Since the design has not been entirely fixed, this work analyzed different design variations for both fresh fuel and spent fuel storage, implementing the Safeguards-by-Design concept to the facility.

As a result of this analysis, the best solution identified for the fresh fuel is the storage into the transfer casks or in a specific room with adequate radiation shielding. This is because the extensive use of seals in these design options lowers the inspection effort required to the IAEA.

Concerning the spent fuel storage, the best design variation is not so obvious because all configurations have positive and negative aspects that balance each other. More detailed studies will investigate in depth all design variation and will identify the best solution.

Starting from these considerations, the inspection efforts should focus on increasing the detection probability of the scenarios that involve reflector assemblies and waste coming out of the reactor.

Considering the misuse of the facility, this analysis identified two different locations where plutonium breeding can happen. Irradiation could occur both inside the reactor core and in the In-Vessel Fuel Storage. Three items can host targets for the unreported Pu production: fresh fuel assemblies, reflector assemblies, and In-Pile Sections.

Radiation level in the core is too high to lead to the production of weapons usable material, while in the case of the IVFS Weapons-Grade Pu can be produced.

Due to this consideration, irradiation inside the core leads to higher production of plutonium, but of a lower quality compared to the one produced in the IVFS.

However, due to the very high number of targets that has to be introduced in the facility, all the scenarios score a medium or high detection probability. In the case of irradiation in the IPS positions, the probability is lower because of the variety of experiments that can be introduced in the reactor during normal operation.

The misuse threat has been evaluated also for the BR2, the material testing reactor that MYRRHA is going to replace in the future. The comparison between the two facilities showed that MYRRHA will offer better proliferation resistance characteristics than the current reactor. It is necessary to point out that the comparison considered only the plutonium production capability and a complete comparison of the two facilities will be able to give a more accurate judgment.

The applied methodology considered also the location where the facility will be built. In the case of MYRRHA, Belgium ensures very good level of transparency and collaboration with the IAEA.

Therefore, no concerns are raised for the design and construction of the facility and the new facility can be an opportunity to develop other verification measures and it provided a good case study to apply the PR&PP methodology.

The methodology has been applied to the MYRRHA research reactor by adapting the definition of the metric “Detection Resource Efficiency”. The used definition reflects the characteristics of the system, since it estimates the additional effort required to the IAEA to apply safeguards to the new facility, considering all segments needed for the proliferation of nuclear weapons (e.g. procurement of material, irradiation).

At the same time, this study offered the MYRRHA team additional information about the design options considered from the Safeguards point of view.

9. Acknowledgments

The authors would like to thank the MYRRHA design team for their collaboration and in particular Dider de Bruyn, Diana Naidoo, and Rafael Fernandez for their comments and suggestions.

10. References

[1] MYRRHA: Multi-purpose hybrid research reactor for high-tech applications. http://myrrha.sckcen.be.

[2] K. van der Meer, C. Turcanu, R. Carchon; *“Non-Proliferation Assessment of the XT-ADS MYRRHA”*. ESARDA Bulletin, No. 44. June 2010.

[3] A. Verledens et al.; *"BR2 - Research reactor with multiple applications."* SCK•CEN. 2011

[4] K. van der Meer, A. Borella, R. Rossa; *"A Proliferation Assessment of the MYRRHA Accelerator Driven System Based on the PR&PP Methodology"*. INMM 52nd Annual Meeting, Palm Desert, CA USA. July 17-21 2011.

[5] R. Fernandez. *Private communication*. SCK•CEN. August 28 2011.

[6] M. Sarotto et al.; *"Critical core design of MYRRHA-FASTEF: refinement of shutdown system and neutronic characterisation of the equilibrium sub-cycle core."* UTFISSM-P9P0-011, ENEA - SCK•CEN. June 14 2011.

[7] International Atomic Energy Agency; *"Status and Advances in MOX Fuel Technology."* Technical Reports Series No. 45. 2003.

[8] G. van den Eynde. *Private communication*. SCK•CEN. August 11 2011.

[9] Generation IV International Forum; *"Evaluation Methodology for Proliferation Resistance and Physical Protection of Generation IV Nuclear Energy Systems"*, Revision 5. November 30 2006. Although the PR&PP expert group released in November 2011 a Rev.6 of the document, the main concepts of the methodology have not been changed significantly for the purposes of this study.

[10] Generation IV International Forum; *"Addendum to the Evaluation Methodology for Proliferation Resistance and Physical Protection of Generation IV Nuclear Energy Systems"*. January 31 2007.

[11] S. Benedetti; *"Neutronic Coupling between the MYRRHA core and In-Vessel Fuel Storage"*. Master Thesis at Politecnico di Torino and SCK•CEN. August 2011.

[12] F.T. Binford; *"Diversion Assumptions for High Powered Research Reactors"*. Oak Ridge National Laboratory, Oak Ridge, Tennessee. January 1984.

[13] R. Rossa; *"Study of some aspects of Proliferation Resistance of the MYRRHA facility"*. Master Thesis at Politecnico di Torino and SCK•CEN. October 2011.

[14] Generation IV International Forum; *"PR&PP Evaluation: ESFR Full System Case Study Final Report"*. 2009.

[15] International Atomic Energy Agency; *"The Safeguards Implementation Report for 2010."* 2011.

Applicability of Nonproliferation Tools and Concepts to Future Arms Control

Mona Dreicer[1], Gotthard Stein[2]

1. Lawrence Livermore National Laboratory - Livermore, California, United States
2. Consultant, Forschungszentrum Jülich GmbH
in der Helmholtz-Gemeinschaft 52425 Jülich, Germany

E-mail: dreicer1@llnl.gov, g.stein@fz-juelich.de

Abstract:

A Working Group on Broader Perspectives on Nonproliferation and Nuclear Verification (WG3) was organized by the ESARDA/INMM International Safeguards and Nonproliferation and Arms Control Technical Divisions, in October 2011. The group considered how nonproliferation tools and culture could facilitate verification of future nuclear treaties. Two of the key challenges identified were providing confidence by monitoring and verification of the warhead lifecycle and fissile materials in States with nuclear weapons. These issues are complicated by a lack of consensus on disarmament goals, complexity of the weapons complex in some P-5 States, the technical capacity in countries without nuclear weapons, restrictions on the sharing of sensitive information to prevent proliferation, and the level of confidence in verifying compliance that can be achieved. Following-on from this discussion, a state-level approach could offer approaches to overcoming the obstacles that exist for verifying possible future arms control agreements. Next steps and potential R&D for technical verification and analysis are outlined.

Keywords: nonproliferation; arms control; verification

1. Introduction

A Working Group on *Broader Perspectives on Nonproliferation and Nuclear Verification* was organized by the *INMM International Safeguards and Nonproliferation and Arms Control Technical Divisions* in the frame of the ESARDA/INMM conference Aix en Provence October 2011. The presentations focused on the technical topics related to international security and stability in global nonproliferation and arms control regimes, specifically asking how nonproliferation tools and culture might facilitate in the verification of future nuclear treaties with a focus on:

- Identifying existing tools and considering their applicability to the new challenges of verifying nuclear arms reductions?
- Modifications needed for this new context?
- Opportunities for use
- Existing gaps; and
- Needed R&D

The Working Group concluded[1] that a more systematic analysis of applying existing nonproliferation mechanisms might be useful, particularly for implementing international safeguards in weapons states, furthering the concept of remote monitoring, better understanding the implications of uncertainty in verification regimes, and the utility of applying a state-level approach, as currently being explored by the IAEA, to arms control. The group asked the following questions:

- "What is zero?" What will be accepted as "complete disarmament"?
- What would be an overarching framework for a network of verification regimes?
- Would verification standards change as reductions are implemented?
- Who are the Stakeholders: multilateral vs. bilateral parties, NWS vs. NNWS, or open society stakeholders such as NGOs, Industry, and the general public
- How can weapons-sensitive, proprietary, and classified information be protected?

Some of the challenges in verifying future arms control agreements might be addressed by various models for governance taking into account the questions highlighted above. Rather than aiming for a universal agreement, a step-by-step approach working to implement a web of complementary verification regimes is the most likely. This paper will not address the political aspects of this issue but focus on establishing technical mechanisms to increase transparency and verification. To build confidence in the ability to monitor and verify compliance, further development of the following concepts are needed: R&D for advancing technical capabilities, greater engagement with a wide variety of potential stakeholders (e.g P-5, IAEA, NNWS, United Nations, etc), and demonstration projects are needed. The ideas in this paper will be presented to the INMM Nonproliferation and Arms Control Division and the ESARDA Subgroup on Disarmament of the Novel Technology Subgroup and the VTM Group.

2. The Complexity

A weapons program is an interlinked complex of facilities and processes where materials (i.e. plutonium and/or uranium), components and weapons are produced, transported and stored (Figure 1). In some States, there are stages of the weapons lifecycle where civilian and military weapons activities are not clearly separated. There are various bilateral and multilateral programs that have worked to establish

materials control, accounting and safeguards systems in nuclear weapons and non-nuclear weapons states. Although not simple to achieve, comprehensive safeguards systems could be put into place in a State with nuclear weapons taking into account the protection of national security and proliferation-sensitive information[2].

The difficulty of designing a comprehensive warhead verification regime that could be verified with high-level of confidence has been debated since the 1960's (in the U.S. at least). If we assume that reductions of nuclear stockpiles will be accomplished by a network of different initiatives, a compatible set of continuity of knowledge regimes must begin by verifying baseline declarations and continue by monitoring movements of accountable items, any new production or dismantlement, transportation and storage for strategic, nonstrategic, deployed and stored warheads. It will also be necessary to monitor irreversible dismantlement of warheads and safeguarding of resulting material, as well as new civilian nuclear material production not currently safeguarded under IAEA safeguards in nuclear weapons states and states not party to the NPT.

A framework will be needed to make progress in such a complex political, security and technical situation. Given a common approach, it might be possible to take information and inspections from the network of different agreements and initiatives and draw conclusions regarding a State's compliance with arms control commitments. Taking stock and learning from existing initiatives is the first step.

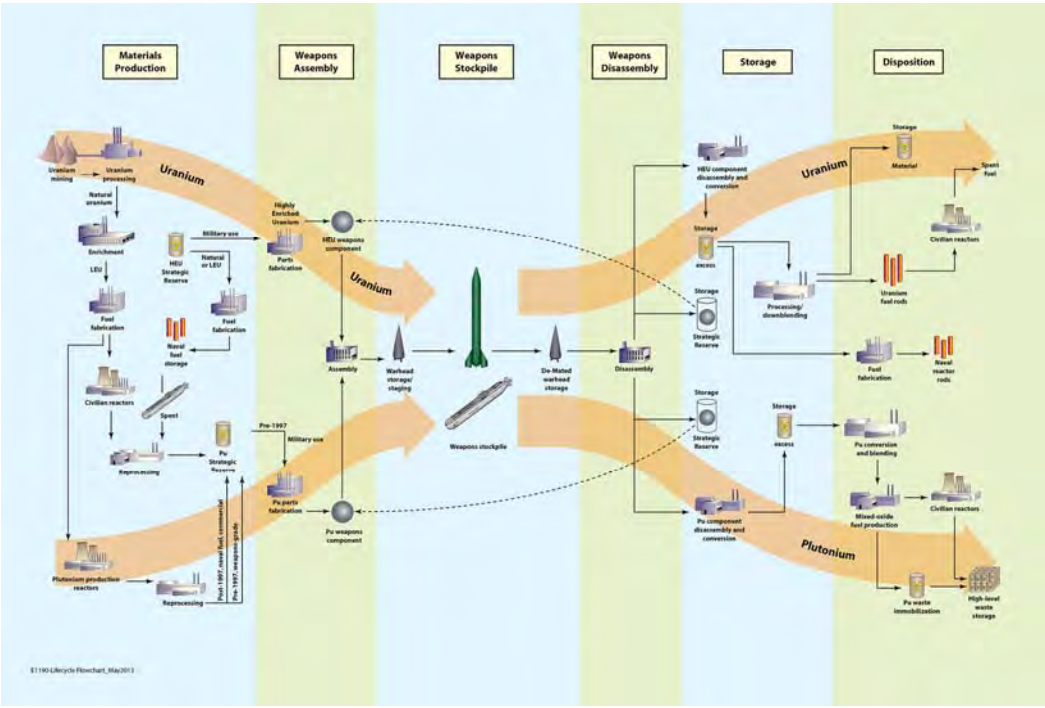

Figure 1: Nuclear materials and weapons lifecycle

3. Existing Mechanisms

There are many international nonproliferation programs that focus on nuclear security and/or material accountancy. IAEA Safeguards agreements and the Additional Protocol are the most prominent mechanism for verifying the peaceful uses of nuclear material in Non-Nuclear Weapons States. Negotiations to create some sort of fissile material control regime that would limit production of nuclear material for weapons in Nuclear Weapons States and States outside the Nuclear Nonproliferation Treaty has not yet been achieved but continues to be on the international security agenda. Initiatives undertaken bilaterally (U.S-Russia) and multilaterally (G8 Global Partnership) have worked to improve material accountancy in the Former Soviet Union and beyond. In addition, counterterrorism initiatives, not specifically nonproliferation-oriented, provide additional levels of assurances of responsible behavior or nonproliferation *bona fides*.

The U.S. and Russia have made some limited in-roads towards verifying parts of the nuclear weapons lifecycle. For example, transparency monitoring provisions under the 1993 United States-Russian Federation HEU Purchase Agreement allow for monitoring the down-blending of excess Russian weapons-origin highly enriched uranium to low enriched uranium; Plutonium Management and Disposition Agreement aims to dispose of excess weapons-grade plutonium monitored by inspectors, and the Plutonium Production Reactor Agreement allows for reciprocal monitoring of the 5 U.S. and 5 Russian shut-down plutonium production reactors. The START Treaty followed by New START, limits the numbers of strategic arms and provides verification and transparency via data exchanges/notifications and inspections/exhibitions in the U.S. and Russia. From 1996-2000, Russia, the U.S. and the IAEA worked to develop a system for verifying nuclear weapons disarmament and those who participated concluded that

there were no technical obstacles to being able to implement such a regime (Trilateral Initiative).

4. Possibility of a State Level Approach

The IAEA has been improving its processes for safeguards implementation to ensure it is objectives-based and information-driven. The IAEA State-Level Concept (SLC)[3,4] outlines three phases:

1. Developing State-level safeguards approaches
2. Planning & conducting safeguards activities, and
3. Establishing knowledge & drawing conclusions.

Decades of experience has taught the IAEA that integrating a wide variety of information in an objective way is the most effective way to analyze monitoring data and provide the information that States need to make their verification decisions.

To address the first phase, a methodology to implement a State-level Approach (SLA) allows State-specific approaches to nuclear safeguards, i.e. differentiation between States, taking into account all information available to the IAEA and being responsive to changes in risk assessment. It is not limited only to States with an Additional Protocol and it is applicable to all States with a safeguards agreement in force. This process is being implemented in three steps[5]:

– Identification of plausible acquisition paths,
– Specification and prioritization of State-specific technical objectives,
– Identification of safeguards measures to address the technical objectives.

The SLA outlines sequences of activities (acquisition paths, (AP)) that a State could consider to acquire weapons usable material. It analyzes all plausible APs aiming to determine whether a proposed set of safeguards measures will be sufficient. Mapping out the APs is essentially producing a state-specific network of process and material and flows with identified nodes for inter-connections[6]. The "relative attractiveness" of an AP, or usefulness in acquiring nuclear weapons, is considered in addition to the time it would take to implement such a process in a country. Currently, the IAEA is using this approach based on expert judgment, but a more transparent and reproducible method is needed[4].

A framework for collection and analysis of monitoring/verification information related to new arms control agreements could be formulated using the same characteristics being proposed for IAEA Safeguards[5]:

- objective – use the same method and criteria for all States;
- transparent – analysis should be open; understood methodologies;
- standardized – steps of the analysis have to be defined in detail;
- reproducible – conclusions not depending on who performs the analysis; and
- document – decisions made during the analysis have to be protocoled.

SLC Phases two and three would depend very much on the scope of the new agreements addressing the different parts of the nuclear weapons lifecycle. A common methodology cross the new agreements/initiatives could facilitate state-level analysis and conclusions. Table 1 presents steps that could be taken to developing such an approach and aid in design of a future program of research.

Phases		Focus & Questions
Develop approach	Analyze cheating pathways and level of risk	Taking into account governance, technology, cooperative measures, national technical means
	Monitoring & Verification Measures/technologies	Do stakeholders consider methods sufficient?
	Acceptable level of uncertainty	Bi-lateral, regional and/or global
Planning and conducting Activities	Existing treaties, agreements and regimes	Gaps in the network
	Identification of Verification Gaps	Existing technology
	Design new initiatives	Political feasibility
Establishing knowledge	Collection and analysis of data	Dealing with sensitive, classified and proprietary information
	Use of variety of data sources: NTM, unilateral, treaty-based and open source information	Managing types of data from different countries and regions in different time scales; data volumes
		Consultation & Clarification processes
Drawing conclusions	Influence of trust on data interpretation & objectivity	Lessons learned from the IAEA?
	Critical review/adjudication of varying interpretations	
	Presentation of data to analysts and decision-makers	

Table 1: Considerations on developing a state-level approach for achieving confidence, for possible future arms reductions.

5. Research and Development for Verification Technologies

Whatever governance and analytical framework is constructed, verification technologies are going to be needed for implementing any future regime(s). The R&D conducted to support IAEA safeguards and counterterrorism initiatives concentrate on materials detection and accounting. Most verification mechanisms needed to monitor and verify the complicated phases of a weapons lifecycle are at earlier stages of development. There has been some work conducted over the past 10 to 15 years but there is much more to be done. Table 2 provides a list of possible research, development and deployment needs for cooperative measures that might be used in future verification initiatives, with no indication of priority. Political will, availability of resources and the possibility of arms reductions negotiations will be drivers for R&D program decision-makers however, the length of time required to find viable technical solutions must be taken into account.

6. Summary

It does not seem likely that a global arms reductions agreement could be achieved. It is more practical to work on a step-by-step approach to implement a web of complementary regimes that might ultimately achieve this goal. When the political challenges are overcome, technical and analytical capabilities will be needed to maintain confidence via increased transparency and technical verification. To build confidence in the ability to monitor and verify compliance, a consistent analytical framework, R&D advances, and demonstration projects will be needed. We have proposed a state-level analytical approach be considered in developing future arms reductions initiatives, which has been based on the IAEA's State-Level Approach, and technical R&D needed to support implementation.

Monitoring Objective	Possible Cooperative Measures	Research, Development & Deployment Needs
Non-deployed Monitored storage	Counting/Transparency Declarations Continuity of knowledge Routine inspections Remote monitoring	RDE – confirmation of warhead contained in container (attributes, imaging) (HEU, Pu) Information barriers/Managed Access; authentication Tags/unique identifiers for containers Remote monitoring
• Production • Weaponization	• Multiple steps with increasing intrusiveness • Declarations and Accountancy • Routine to short notice inspections • Continuity of knowledge	• Tags for warheads & components • Information barriers • Managed Access • Satellite Imagery • Environmental Monitoring • Forensics
• Dismantlement	• Done in multiple steps with increasing intrusiveness • Declarations • Transparency to counting to accounting • Continuity of knowledge • Routine to short notice inspections	• Tagging components & materials (to track from dismantled components to fissile material) • Managed Access Satellite Imagery • Warhead measurements using RDE
• State-level	• Cradle-to-grave tracking (State-level continuity of knowledge) • Inspections	• Information analysis • Sampling Statistics • Propagation of Uncertainty • Game theory • Societal Monitoring

Table 2: Proposal for the development of verification technologies

7. References

[1] M. Dreicer, G. Stein, *Broader Perspectives on Non-proliferation and Nuclear Verification*, INMM/ESARDA Conference Working Group 3, Aix en Provence, 2011.

[2] C. Listner, M.J. Canty, G. Stein, A. Rezniczek, *Can State-level Safeguards be applied to Nuclear Weapon States?* presented at DPG Conference, Dresden 2013.

[3] J. Cooley, *Conceptual Framework for IAEA Safeguards Implementation*, presented at the INMM Workshop on Evolving the State-Level Concept, Charlottesville, Virginia, 2012.

[4] J. Cooley, *The State-level Approach to International Safeguards*, JNMM, 2009,

[5] C. Listner, M.J. Canty, G. Stein, A. Rezniczek, I. Niemeyer, *A Concept for Handling Acquisition Path Analysis in the Framework of IAEA's State-level Approach*, INMM Annual Meeting Proceedings, Orlando, 2012.

[6] C. Reynolds, *Developing State-level Safeguards Approaches: Reflections from Select Country Case Studies* INMM Annual Meeting Proceedings, Orlando, 2012.

This work performed under the auspices of the U.S. Department of Energy by Lawrence Livermore National Laboratory under Contract DE-AC52-07NA27344. LLNL-CONF-636653

Development of an Advanced Ceramic Seal for Maintaining Continuity of Knowledge in Treaty Verification and Safeguards Applications

Heidi A. Smartt, Juan A. Romero, Maikael Thomas, Billy Cunningham
Sandia National Laboratories - P.O. Box 5800 MS1371 - Albuquerque, New Mexico 87185 USA
E-mail: hasmart@sandia.gov

Abstract:

Sandia National Laboratories and the Savannah River National Laboratory are collaborating on research and development of technologies for an advanced capability prototype tamper-indicating device known as the Ceramic Seal. Advanced capabilities include multiple levels of tamper indication such as a frangible seal body, surface coatings, and an active detection of seal status; and unique identification via electronics as well as non-reproducible surface features. The innovation of the Ceramic Seal is the inclusion of multiple advanced capabilities in a volume comparable to the ubiquitous metal cup seal. Our advanced capability small volume seal has application in treaty verification and safeguards regimes for maintaining continuity of knowledge. Once attached to a monitored item, the seal's identity and status can be verified in-situ rather than requiring removal and analysis at an inspectorate location.

The Ceramic Seal has evolved from a first generation prototype constructed of alumina to a second generation prototype manufactured from low-temperature co-fired ceramic (LTCC). LTCC allows integration of passive electronic components into the seal construction material. Vulnerability reviews have been conducted periodically throughout the project and results used to guide the design. This paper will describe the capabilities of the current generation Ceramic Seal.

Keywords: Tamper-indicating devices; seals; Containment and Surveillance

1. Introduction

Containment/surveillance (C/S) measures aim to ensure Continuity of Knowledge (CoK) or Chain of Custody (CoC) during inspector absence on the movement of nuclear or non-nuclear material, weapons throughout their lifecycle, equipment and samples, and preserving the integrity of relevant data. Viewed as complementary to nuclear material accountancy, C/S is a critical element of many non-proliferation regimes. C/S equipment and approaches require continuous improvements because (1) the adversary continues to technically advance (which could render C/S equipment obsolete with a single technical advancement), (2) requirements could change based on the introduction of new procedures or approaches, and (3) as technology advances there may be new options for C/S equipment, including options that provide efficiency gains.

TheCeramic Seal [1,2], a collaborative effort between Sandia National Laboratories (SNL) and the Savannah River National Laboratory (SRNL), integrates multiple advanced technologies into a prototype next generation loop seal with various technical options available depending on the deployment. One possible deployment is as a replacement for the ubiquitous metal cup seal (Figure 1) used by various organizations. The metal cup seal, although environmentally robust, inexpensive, and small in size, is operationally burdensome and its integrity is not able to be verified in-situ. The Ceramic Seal addresses issues with the metal cup seal and makes additional security advancements (tamper indication and unique identification) and efficiency improvements (in-situ verification and ease of application). Its innovation is the integration of these advanced capabilities in a small volume, including a self-securing wire feature; multiple levels of tamper indication via a frangible seal body, surface coatings, and active detection of state through low power electronics; electronic identification number verified in-situ through a contact reader, and physical identification via non-reproducible surface features. This paper will discuss the status of the research and development of the various technologies and integrated prototype loop seal.

Figure 1: Size comparison of a metal cup seal (left), rapid prototype of an early model of the Ceramic Seal (right), and a U.S. quarter (bottom).

2. Advanced security

The most critical element of a seal applied in a treaty verification regime is its tamper-indicating features. A loop seal will employ a wire or fiber-optic cable (FOC) threaded through a monitored item's hasp or otherwise secured, and the wire

or FOC will terminate within the seal body. In single use seals such as the Ceramic Seal and metal cup seal (versus multiple use seals in which the seal wire can be removed and reattached), confidence must be maintained that the wire is unable to be removed from the seal body once secured without detection and that the seal body has remained intact such that the seal body has not been opened and the wire removed/replaced. Tamper-indicating features on the seal body serve the role of providing this confidence. The following subsections describe the advanced tamper-indicating features in use by the Ceramic Seal.

2.1 Seal body

The body of the Ceramic Seal is fabricated using a low-temperature co-fired ceramic (LTCC) process. With LTCC, passive components such as resistors, capacitors and inductors along with conductive line traces can be integrated into a monolithic package, thereby freeing valuable space for active components and the battery. Furthermore, LTCC packaging can reduce electronic noise and radiated emissions from the device [3].

The properties of the material used in LTCC meet the requirements of "frangibility" – that is, upon deformation it tends to break into fragments rather than retaining cohesion, yet the material is strong enough to withstand the operational environment. Frangibility is important so that a tamper attempt might result in difficult-to-reassemble fragments. Other materials also meet these requirements; however, they do not have the added benefits of LTCC, namely the ability to integrate electronics. The first prototype of the Ceramic Seal was constructed of 99.8% Al_2O_3. The current version, using DuPont 951 LTCC Green Tape™ material, is manufactured using, by weight, 50.3% Al_2O_3, 31.3% SiO_2, 11.9% PbO, 1.1% K_2O, and 5.4% CaO [3].

The LTCC manufacturing process involves punching unfired or green ceramic sheets with via holes, screening with a conductor, stacking with excellent precision, laminating the result into a monolithic three-dimensional structure, and firing in a furnace. Figure 2, Figure 3, and Figure 4 show the Ceramic Seal during the LTCC process.

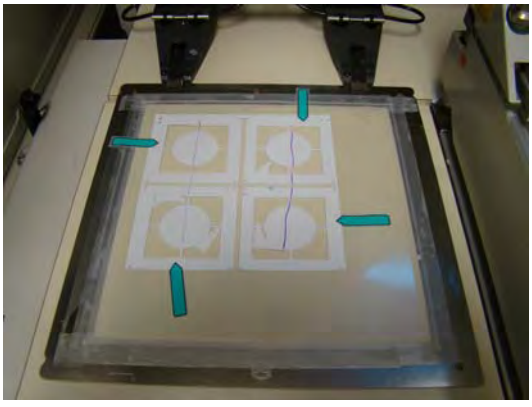

Figure 2: LTCC Green Tape™ punching process.

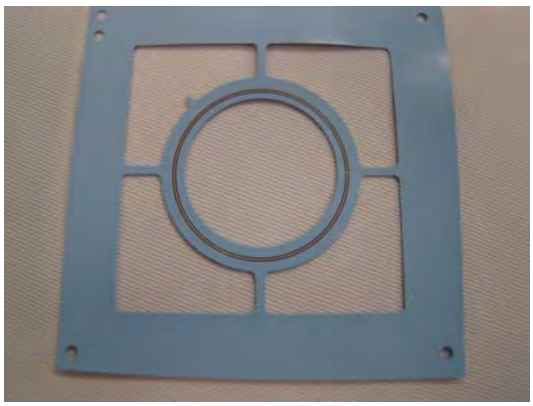

Figure 3: Conductive trace screen printing.

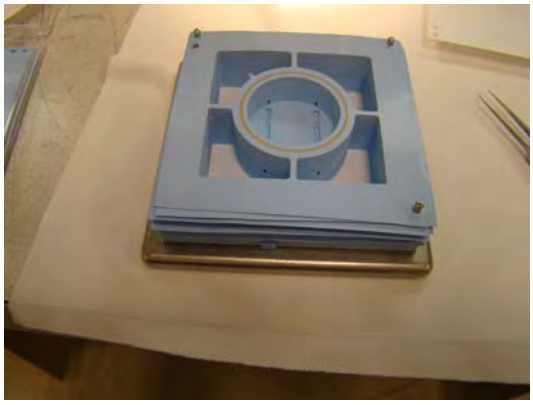

Figure 4: Green Tape™ stacking prior to lamination.

2.2 Tamper planes

As mentioned above, conductive line traces can be integrated into the LTCC – some are used to connect electronic components and a separate set are embedded throughout the body of the seal for tamper indication (tamper planes). These tamper planes are connected to the electronics and if disrupted, i.e., signals cannot pass, software within the electronics impacts performance.

2.3 Active tamper indication

The Ceramic Seal provides active tamper indication. Physically, the electronic components are attached to the embedded line traces in the seal cap (see Figure 6 for electronics housing). The Ceramic Seal utilizes a single microcontroller. Two battery springs make contact with a battery directly below the electronics.

Seal firmware is programmed prior to deployment; however, the Ceramic Seal requires "personality programming" in-situ, meaning configuration must happen via the RS232 serial communication vias located on the cap of the seal. Personality programming loads the secret keys onto the seal, sets message creation interval, and sets absolute time. The electronics will not be powered until the seal cap and base is connected, so personality programming the seal must happen after it has been closed. However, for

added security, we have designed the seal to accept personality programming only one time, i.e. cryptographic keys can only be loaded a single time.

The seal creates several message types – state-of-health (configurable), anomalous events, and the seal interrogation history. As messages are created, we append a message authentication code (MAC) using the 128-bit CMAC algorithm with AES cipher (and optionally encrypted using 128-bit AES) before storing in flash memory. The MAC derives its uniqueness from the secret key, the seal's 8 byte ID, a non-repeating message count and a clock. The 8 byte ID is assigned during firmware programming and can be a unique number by procedure. The MAC ensures that the seal itself can be uniquely identified due to the combination of the 8 byte ID with the cryptographic key.

A seal reader, which will also have the secret keys, will be able to send an authenticated command to the seal (over the serial port), receive the requested message(s), and authenticate them using its copy of the secret key.

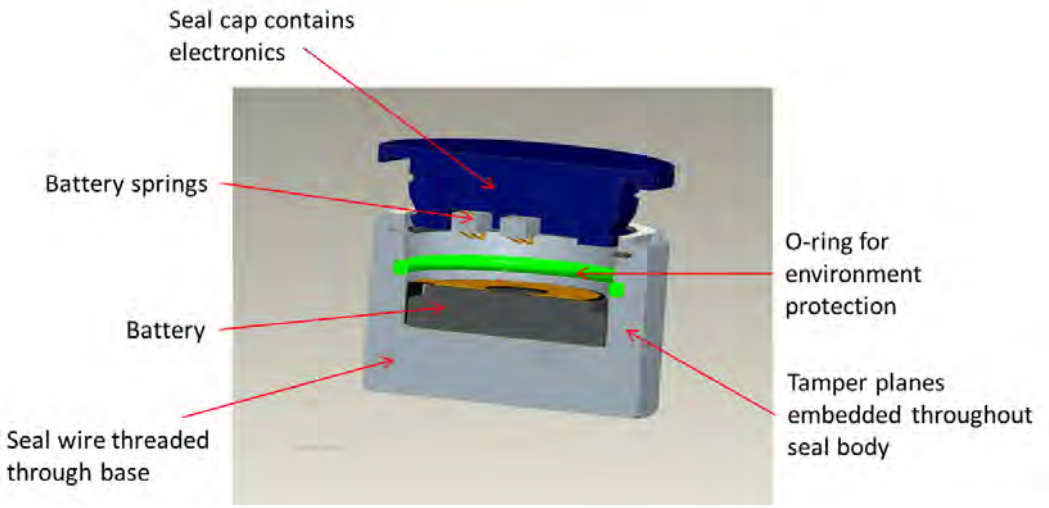

Figure 5: Seal concept. Image courtesy SRNL.

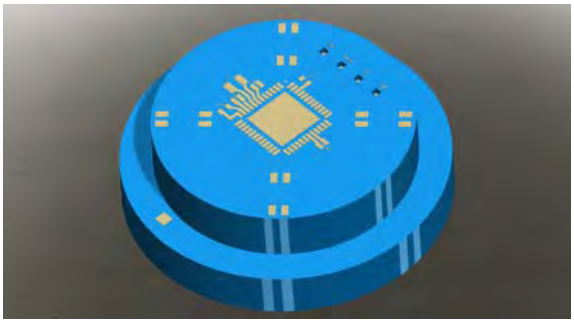

Figure 6: Seal cap, fabricated using LTCC, with electronics underside.

2.4 Coatings

SRNL is developing coatings [4,5] for application to the outer surface of the seal body. Modification to the seal body will be noticeable under a fluorescent light. As the coatings are in development, they will not be discussed in this paper.

3. Improved efficiency: self-securing wire

The capability of self-securing wire not only improves efficiency but touches upon security as well. The wire ends must securely terminate in the seal body in such a manner that they cannot be easily removed, and must do so in an efficient manner. In the Ceramic Seal design, the wire is routed through the monitored item and into the seal base, where it is secured by a tortuous path. The design team and SNL vulnerability review (VR) team iterated on several designs before choosing the method shown in Figure 7.

Figure 7: Rapid prototype of seal base highlighting self-securing wire mechanism. Image courtesy SRNL.

The wire itself is important as well. Active research in identifying appropriate wires is on-going and commercial candidates have been identified. The current seal prototype does not have the capability to monitor the integrity of the wire using the internal electronics; however, such a capability is anticipated in future research. There are instruments available to externally connect to the wire after initial deployment and subsequently during verification to determine if the wire has been tampered with.

4. Improved efficiency: in-situ verification

The Ceramic Seal allows in-situ verification with a contact reader to verify its integrity. Currently, the reader is implemented using a serial connection and a laptop computer. As described in section 2.3, the seal reader will contain the same secret keys as the seal. It will be able to send an authenticated command to the seal over the serial port, receive the requested message(s), and authenticate them using its copy of the secret key. The reader supports the following commands: request latest sensor state of health, request a specific message number from the seal, request that the seal send the latest anomalous/tamper message, request that the seal send all anomalous/tamper messages stored on the seal, and personality programming.

5. Next steps

The next step in the design is to complete development of the Ceramic Seal software. Once complete, the VR team will review the electronics and software and provide guidance for any modifications, if any, to the electronic and software design team.

The seal prototype will be fabricated and assembled using LTCC and will consist of tamper planes, the electronics, battery, and coatings from SRNL. The completed prototype will undergo functional testing, and then a comprehensive VR. Final modifications will be made to the seal based on guidance from the VR team.

6. Acknowledgements

The authors thank the Office of Defense Nuclear Nonproliferation Research & Development for funding this effort.

Unless otherwise noted, all pictures or images have been taken or created by Sandia National Laboratories.

Sandia National Laboratories is a multi-program laboratory managed and operated by Sandia Corporation, a wholly owned subsidiary of Lockheed Martin Corporation, for the U.S. Department of Energy's National Nuclear Security Administration under contract DE-AC04-94AL85000.

7. References

[1] Smartt, H.A., et al; *First Prototype of the Intrinsically Tamper Indicating Ceramic Seal; Proc. Institute Nuclear Materials Management*; Orlando, FL; 2012.

[2] Smartt, H.A., et al; *Intrinsically Tamper Indicating Ceramic Seal (ITICS); Proc. Institute Nuclear Materials Management*; Palm Desert, CA; 2011.

[3] Chan, Y.C., Li, G.Y.; *Fabrication and Characterization of Multilayer Capacitors Buried in a Low Temperature Co-Fired Ceramic Substrate; Active and Passive Elec. Comp.;* Vol. 20; 1998; pp. 215 – 224.

[4] Mendez-Torres, A.E., et al; *Synthesis and Characterization of Smart Functional Coatings by Chemical Solution Deposition Methods; Proc. Institute Nuclear Materials Management*; Palm Desert, CA; 2011.

[5] Krishna, R.M., et al; *Characterization of Transparent Conducting Oxide Thin Films Deposited on Ceramic Substrates; Materials Letters;* Vol. 65 no. 1; 2011.

Societal Verification: Intellectual Game or International Game-Changer

Kelsey Hartigan, Corey Hinderstein
Nuclear Threat Initiative - 1747 Pennsylvania Avenue, NW - Washington, DC 20009
E-mail: hinderstein@nti.org, hartigan@nti.org

Abstract:

Within the nuclear nonproliferation and arms control field, there is an increasing appreciation for the potential of open source information technologies to supplement existing verification and compliance regimes. While clearly not a substitute for on-site inspections or national technical means, it may be possible to better leverage information gleaned from commercial satellite imagery, international trade records and the vast amount of data being exchanged online and between publics (including social media) so as to develop a more comprehensive set of tools and practices for monitoring and verifying a state's nuclear activities and helping judge compliance with international obligations.

The next generation "toolkit" for monitoring and verifying items, facility operations and activities will likely include a more diverse set of analytical tools and technologies than are currently used internationally. To explore these and other issues, the Nuclear Threat Initiative has launched an effort that examines, in part, the role that emerging technologies and "citizen scientists" might play in future verification regimes. This paper will include an assessment of past proliferation and security "events" and whether emerging tools and technologies would have provided indicators concurrently or in advance of these actions. Such case studies will be instrumental in understanding the reliability of these technologies and practices and in thinking through the requirements of a 21st century verification regime.

Keywords: Verification, social media, open-source information, arms control, disarmament

1. The "Datafication" of Society

The ability to communicate and exchange information globally has changed the way publics interact, businesses operate and governments function. Private citizens can now access high resolution commercial satellite imagery, small business owners can market and ship to consumers all over the world and publics can demand more of their government with a mere 140 characters. Facebook has now exceeded 1 billion users, and every minute, over 100,000 tweets are sent and more than 3,000 photos are uploaded on Flickr.[1]

By tapping into these diverse sources of information, governments and engaged publics are leveraging "big data" to open up new areas of analysis. As the Economist's Kenneth Cukier and Oxford's Viktor Mayer-Schoenberger explain:

> Today, less than two percent of all stored information is non-digital. Given this massive scale, it is tempting to understand big data solely in terms of size. But that would be misleading. Big data is also characterized by the ability to render into data many aspects of the world that have never been quantified before; call it "datafication." For example, location has been datafied, first with the invention of longitude and latitude, and more recently with GPS satellite systems. Words are treated as data when computers mine centuries' worth of books. Even friendships and "likes" are datafied, via Facebook. This kind of data is being put to incredible new uses with the assistance of inexpensive computer memory, powerful processors, smart algorithms, clever software, and math that borrows from basic statistics. [2]

This "datafication" of society, combined with novel tools and technologies that sort, analyze and even predict certain outcomes, have powerful implications for how states and publics might address the most pressing international security challenges of the 21st century.

1.1 Arms Control and Nonproliferation Applications

Within the nuclear arms control and nonproliferation arena, the greater connectivity of people in previously isolated areas, improvements in data mining and filtering techniques, and open source information technologies have the potential to increase government transparency, empower non-traditional actors to monitor and report illicit acts, and even assist with verifying a state's compliance with international obligations. As the U.S. State Department's Acting Under Secretary for Arms Control and International Security, Rose Gottemoeller, has explained:

> Our new reality is a smaller, increasingly networked world where the average citizen connects to other citizens in cyberspace hundreds of times each day. Today, any event, anywhere on the planet, could be broadcast globally in seconds. That means it is harder to hide things. When it is harder to hide things, it is easier to be caught. The neighborhood gaze is a powerful tool, and it can help us to verify the treaties and agreements we've created.[3]

Nontraditional stakeholders can increase the likelihood that violations of international commitments are detected. To be effective, the first task is to define the detection goals. In some rare cases, societal data and devices might

be directly relevant to treaty limited items. In other instances, these tools might convey information that is only indicative of potential violations or misuse. Pinpointing the detection tasks is a crucial first step, and can include a range of objectives:

- Defining **patterns** (e.g. of behavior, activities, movements of people and things)
- Looking for **shifts** (e.g. changes of behavior, activities, movements either from the norm or from the expected)
- Identifying **outliers** (a single activity, person or pursuit that doesn't match the expected or predicted)
- Filling in **blind spots** (e.g. where are there gaps in knowledge from traditional verification systems)
- Detecting **signals** (e.g. something which may indicate something else but which is not itself a proscribed activity)[4]

Open source information derived from societally generated sources is already included in national all source intelligence gathering and analysis. For example, in the United States, the Central Intelligence Agency runs the Open Source Center on behalf of the Director of National Intelligence. The Open Source Center gathers data from a variety of sources, including publicly available information that is posted on new media platforms such as YouTube, Facebook, Twitter and LinkedIn. These collection efforts are in the early stages, however, and this type of information is not yet integrated into treaty compliance monitoring and verification efforts.

To study these and other issues, in 2012, the Nuclear Threat Initiative launched a Societal Verification Working Group as part of its Verification Pilot Project. NTI assembled a group of ten experts from multidisciplinary backgrounds to systematically review the potential for open source information technologies to supplement existing nuclear verification and compliance regimes.

For the past year and a half, NTI's Societal Verification Working Group has been examining the opportunities and challenges that accompany a greater public role in verification. While the group is exploring the utility of social media platforms like Twitter and Facebook, the focus extends beyond this to include data gathered through other non-traditional, commercial sources and analysis from nongovernmental organizations, independent scientists and other nonstate actors.

While the working group's findings and recommendations are not yet complete, the group is working to define a framework for how states might integrate various societal contributions within existing and future verification regimes. When the project began, the central challenge appeared to be one of data validation and management – how is the information captured and sorted, and what tools are necessary to overcome language barriers and validate the authenticity of the information. It is now clear, however, that the primary challenges are not necessarily technical, but operational and political. The ability to craft an information architecture that takes advantage of the amount of information that is now available and organizes data in a coherent, accessible manner will largely determine the extent to which new forms of commercial and open source information might be successfully collected and integrated with future arms control verification regimes. How this information is communicated with the public is equally important given the ongoing debate on online privacy, civil liberties and the role of government.

2. Future Verification Needs

Today, existing verification tools and systems are largely effective given the tasks at hand. Yet as future agreements become more complex and involve a greater number of parties, future verification regimes will likely require new and enhanced tools for monitoring and verifying compliance.

2.1 Verification Methods and Tools

The two primary methods for verifying existing treaties and agreements are National Technical Means (NTM) and cooperative monitoring measures. National Technical Means (NTM) refers to those measures deployed by states parties independently, including reconnaissance satellites, signals intelligence and electronic intelligence. Cooperative monitoring measures include a variety of systems, devices and technologies that parties jointly agree to within the context of a treaty or agreement. For instance, in 1987, the United States and Soviet Union first agreed to allow cooperative on-site inspections to verify the Intermediate Nuclear Forces (INF) Treaty. The treaty included a detailed set of carefully scripted ground rules for on-site inspections. U.S. and Russian experts have since developed and agreed to use portal perimeter monitoring, tags and seals and other cooperative measures to verify compliance. Similarly, IAEA inspectors utilize a variety of tools, including containment and surveillance and environmental monitoring to confirm facility accounting and operating records.

Future verification regimes are likely to become even more rigorous and intrusive as states move to lower numbers of nuclear weapons and parties need the ability to detect and monitor smaller items and quantities of nuclear material. It will no longer be enough to count and monitor delivery vehicles, especially as states begin to address non-strategic and non-deployed systems. Warheads held in containers in storage facilities will likely need to be monitored and accounted for. In fact, future arms control agreements may require the exact number of warheads to be counted, a metric that inspectors have not used in past agreements. It may even be necessary to monitor the cradle to grave lifecycle of individual warheads and materials, particularly as

nuclear power programs expand, and additional facilities and material flows need to be safeguarded.

2.2 The Growing Gap

While important progress and technical achievements have been made, parties are likely to encounter strains on existing NTM and other cooperative monitoring measures going forward. Given the likely demands of future verification requirements, states will need to take advantage of all possible tools and sources of knowledge about compliance. Societal verification has a role to play. Nontraditional tools and data sources can add to the verification process, and provide additional information or context to intelligence gathered through other means. For example, data gleaned from open source information might provide details on daily routines such as when a facility operates or employees report to work, flag sudden upticks of activity at certain military installations or facilities, or reveal connections or sudden drops in activity among scientists or engineers with specialized training and expertise. Societal verification contributions will always be fundamentally unreliable as a stand-alone source given the prospects for government intervention and manipulation, but this is why societal verification is intended to be a supplement to traditional tools and methods, not a replacement.

A larger framework for incorporating societal verification mechanisms with existing all source intelligence efforts in the near term, and phasing in more complex tools and resources over the longer term, will be required if states are to take full advantage of the new forms of societal verification available today.

3. Societal Verification

The societal verification concept is not new. In fact, such a theory was first introduced in the 1950's as "inspection by the people." Seymour Melman and Lewis Bohn were among the early theorist who outlined provisions for such a concept. Agreements were expected to require participating governments to criminalize violations, develop assurances and protection for individuals reporting on their country, and socialize the public to place international concerns over domestic loyalties.[5]

During the 1990's societal verification gained renewed attention, including when Joseph Rotblat picked up many of the same themes Melman, Bohn and others developed early on, such as legal protections for reporting, the need for broad participation, and the "deeply felt moral obligation" to report violations of a treaty to eliminate nuclear weapons.[6] He also suggested that scientists and technologists in relevant industries could act as watchdogs, both of their organizations and of their colleagues. These early concepts outlined many of the fundamental issues that still need to be addressed today in order to integrate new tools and systems into future verification regimes.

Modern day concepts of societal verification can take on many forms. While the "whistleblowing" component is still an area for examination, technical growth in both data sources and data analysis make more advanced uses of societally generated data more interesting. A multitude of online platforms and the spread of smart phones and other information and communication technologies make it possible to collect and analyze massive amounts of publicly generated data. Public-private partnerships can also provide additional insight into information collected by companies about attempted procurements and activities of potential treaty violators. Outside experts also have increasingly sophisticated tools to perform their own analysis and disseminate their findings and recommendations to a broad, international audience which acts as a check on government conclusions. These resources can provide additional windows of insight and provide increased confidence over the long run that a state is living up to its obligations.

3.1 The Societal Verification Spectrum

Given the range of tools and data available, it is helpful to think about societal verification as a continuum where some efforts fall on the passive end of the spectrum, and others on the active end. Passive and active "sensing" have unique characteristics, which are particularly important to distinguish as states begin to utilize such analysis and tools and parties build a framework for future use. Whether and how to connect the entities that utilize different types of societal verification – governments and private citizens or corporations – will be an important challenge to consider since such analysis currently takes place in separate silos.

3.1.1 The Passive End of the Societal Verification Spectrum

Passive forms of societal verification center on data collection and analysis, and serve a "listening" function. Content from social networking sites, blogs, microblogs and photo sharing sites can be harnessed to better understand public perception and responses to evolving situations. For example, experts at the Pacific Northwest National Laboratory recently analyzed a ten percent sample of tweets to determine the social media footprint of India's April 19, 2012 Agni-V long range missile test. The PNNL team was able to isolate a set of tweets (some in Hindi) focused on the test, which provided some insight into the public reaction and regional security implications of the missile firing. Further analysis of such information might be able to identify whether test preparations would have been visible in the days and weeks prior, particularly if combined with other data streams.

Social media analytics can pinpoint the topic, sentiment and mood of selected conversations, posts or chats, and experts are increasingly able to add a predictive component to such analysis.[7] This data can be harvested and integrated with data from other sources, so as to include other spatial and temporal characteristics which may provide additional insight.

There are several challenges for passive types of societal verification. While the sheer quantity of information can allow for less precision overall, it is still difficult to decipher signals from the noise, particularly in the arms control and nonproliferation context if it is unclear what signals one is hoping to detect. On the other hand, the sheer volume of data has the advantage of quickly isolating outliers – those individual messages or pieces of information that are either in conflict with what the vast majority is reporting or stands out as providing a unique piece of data. This helps to dismiss an anomalous source or narrow attention to a smaller set of data points worth deeper investigation. Language, cultural and socioeconomic barriers, timeliness of collection and analysis and legal questions regarding privacy and data ownership also need to be further explored.

3.1.2 The Active End of the Societal Verification Spectrum

Active forms of societal verification rely on public "mobilization." Rather than simply collecting data that already exists, active sensing requires the tasking of specific actions to individuals or groups who are otherwise generating unspecific information. For instance, DARPA's 2009 "Red Balloon" Challenge and the State Department's follow-on TAG Challenge asked the public to help identify and report certain items (red balloon and jewel thieves, respectively) that were located throughout the U.S., North America and Europe. [8] The runner-ups of a separate, more recent State Department challenge took this concept a step further and proposed creating online treaty relevant games such as a "Where's Waldo" inspired challenge where individuals, using avatars to mask their identity, would be given points when they identify treaty relevant objects; another game invited users to use geocaching and QR codes to accept and complete challenges from treaty experts.[9] Other forms of active sensing could include engaged citizens purchasing personal technologies, such as a smart phone equipped with an accelerometer, which would allow the user's phone to constantly collect data and send alerts when abnormalities are detected.[10]

Crowdsourcing, ubiquitous sensing, and games or challenges can provide an excellent opportunity to tap into the insight of engaged publics, but data verification, legal and political issues and incentives for continued participation complicate such methods. While mobilization structures hold promise, such forms of societal verification also present the most challenges which may in some cases be insurmountable absent careful and rigorous concept development and implementation.

3.2 The Role of Outside Experts

Nongovernmental organizations, independent scientists and other nonstate actors can utilize the full range of passive and active societal verification activities. Indeed in many instances, outside experts self-mobilize as certain events arise. As access to commercial satellite imagery expands, for instance, nontraditional actors are providing additional insight and expertise by using this imagery to give the public a better understanding of what is happening in certain countries. For example, the Institute for Science and International Security (ISIS) utilizes satellite imagery to analyze nuclear sites and facilities in Iran, Syria, Israel, Pakistan, India and North Korea. Citizen "scientists" have also proven highly effective and accurate in projects coordinated by the National Archives, Galaxy Zoo, and National Geographic, to name a few.

How such analysis is corroborated and integrated with existing information structures and how outside experts are cultivated and connected will be important issues to consider if third party analysis is formally integrated in future frameworks. Alternatively, it might prove valuable to leave these communities separate from formal verification systems and allow them to act as both a check and balance to state-level analysis and a canary in the coal mine to identify areas requiring further attention by national authorities.

4. Framework for Leveraging Societal Data and Tools

When making compliance determinations, states can integrate passive forms of societal verification with all source intelligence and National Technical Means at any point, but over the long-term, states may consider codifying societal verification contributions in future treaties, better integrating outside expert analysis, and assessing the role of more active methodologies.

4.1 Incorporating Passive Sensing with All Source Intelligence

As a mere data collection tool, states can more easily integrate societal verification mechanisms on the passive end of the spectrum with existing all source intelligence efforts. In some cases, national intelligence systems are already using some of these data sources and developing advanced analytics. These efforts are almost exclusively focused on other issue areas, however, and have not yet been folded into treaty verification efforts.

In 2010, the Nuclear Threat Initiative published *Cultivating Confidence*, a study focused on verification, monitoring and enforcement for a world without nuclear weapons, which also laid the groundwork for NTI's ongoing

Verification Pilot Project. One area of focus included on how states might verify the nonproduction and elimination of fissile material for weapons. Here, Annette Schaper emphasized the contribution engaged citizens can make through societal verification. Schaper suggested states incorporate societal verification with National Technical Means since NTM is broadly understood as "collecting any information that could help draw conclusions regarding a treaty partner's compliance." Schaper explains:

> National technical means is a well-accepted additional tool of verification that is carried out by states, initially without visible international cooperation. The term is officially included in many arms control treaties and denotes various monitoring technologies, especially satellite observation, or other additional verification measures. Examples are the collection of and analysis of environmental samples, or the monitoring of international trade of a country. More broadly, it is understood as collecting any information that could help draw conclusions regarding a treaty partner's compliance, including potential societal verification. Although not officially acknowledged in diplomatic communities, NTM in fact means typical intelligence measures. Societal verification, and more broadly, NTM increases the probability of the detection of noncompliance and therefore constitute an important deterrent.

The Director of the International Data Centre (IDC) of the Comprehensive Nuclear Test Ban Treaty Organization, *Lassina Zerbo*, has also suggested that such methods be incorporated with national analysis and decision making: "When, for example, nations make a case to the commission that an on-site inspection should be launched, they would be free to supplement the information that they gather through national technical means with data collected via societal verification."

As governments continue to develop additional tools, programs and systems for passive data analysis, key questions regarding access and information flow remain:

- What legal and privacy issues need to be addressed to access data?
- How is the data integrated with other data streams?
- How should states incorporate data identified and analyzed by outside experts?

In order to successfully integrate societal verification contributions with other data streams, states will need to clearly define the scope of work, and allocate the necessary resources for collecting, analyzing and fusing future analysis with other verification activities. It is not yet clear how, and if, outside analysis is considered when states make compliance determinations. The nonproliferation community has been more successful at incorporating outside expert analysis, but input into treaty verification has not been equally established or accepted. The incorporation of active sensing also presents serious challenges if citizens from different countries participate in games, challenges or sensing that their home government may not support. Integrating societal verification data with national intelligence systems could also exacerbate public mistrust and "big brother" fears if governments fail to explain what types of information might be collected, and for what purpose. Given the international character of the data and tools, international norms and arrangements are more likely to foster understanding and trust, since contributing to another state's intelligence gathering may be perceived as espionage. A framework that clearly establishes the role and responsibilities of citizens, technology holders, states and international bodies is more likely to address legal concerns surrounding espionage and treason, but this will require much greater acceptance of the value of societal verification than currently exists.

4.2 Future Collaboration and Treaty Regimes

Treaties might eventually explicitly allow for societal verification as part of, or in addition to NTM and other cooperative monitoring measures. Such provisions would facilitate the broader incorporation of both passive and active forms of societal verification, as well as a better defined role for outside experts. The ability to successfully integrate these tools and activities into future verification regimes will largely depend on the degree of international cooperation and collaboration early on. Such collaboration will facilitate trust and confidence in both the tools and the processes such that future agreements acknowledge an already established and proven role of society and provide for appropriate legal protections.

This type of framework will take time to establish. Participation from non-democratic and less transparent governments will be very challenging, but is critical to the overall success of any future arrangement. Societal data and participation is inherently international in nature, and thus more likely to be effective if international norms are established.

5. Shifting the Societal Verification Conversation

The issues and opportunities outlined above provide a very general overview of the inquiry in to the value of societal verification for arms control and nonproliferation treaty verification. How to integrate information gleaned from such tools and sources into larger framework for monitoring and verifying a state's nuclear activities is a long term challenge. By clearly articulating the responsibilities of all stakeholders and establishing global norms for use and conduct, states can start to leverage the power of new information and communication technologies in a more effective and systematic manner. As a first step, the societal verification conversation needs to shift from *whether* states should take advantage of such tools and insight, to *how* they should do so.

6. Acknowledgements

The authors wish to thank NTI's Societal Verification Working Group and the Verification Pilot Project principals from the U.S. Departments of Defense, Energy and State, Sweden, UK and Norway for their enthusiasm and in-kind support for this effort. The authors also wish to thank Jessica Bufford and Jim Fuller for their contributions to this paper.

7. References

[1] *Internet 2012 in Numbers;* Royal Pingdom Tech Blog; January 16, 2013 and DOMO; *Data Never Sleeps, June 8, 2012.*

[2] Cukier K and Mayer-Schoenberger V; *The Rise of Big Data; Foreign Affairs; May/June 2013*; http://www.foreignaffairs.com/articles/139104/kenneth-neil-cukier-and-viktor-mayer-schoenberger/the-rise-of-big-data?page=show

[3] Gottemoeller R; *Mobilizing Ingenuity To Strengthen Global Security; South by Southwest Conference (SXSW); Austin, TX; March 8, 2013;* http://www.state.gov/t/us/205933.htm

[4] Hinderstein C and Hartigan K; *Societal Verification: Leveraging the Information Revolution for Arms Control Verification;* INMM Annual Conference, July 2012.

[5] Melman, S; Inspection by the People: Mobilization of Public Support, *Excerpts from Inspection for Disarmament*. Columbia University Press, New York, 1958, p. 41.

[6] Rotblat, J; *Toward a Nuclear Weapon-Free World: Societal verification*, Security Dialogue, Vol. 23, No. 51, 1992, p. 57.

[7] See for example, Whattams K and Gastelum Z, *State-of-the-Art of Social Media Analytics Research;* PNNL; January 2013; http://www.pnnl.gov/main/publications/external/technical_reports/PNNL-22171.pdf

[8] *DARPA Network Challenge Project Report*; Feb 16, 2010; http://www.eecs.harvard.edu/cs286r/archived/fall10/papers/ProjectReport.pdf

[9] Childers A and Mappus R; *Innovation in Arms Control Challenge;* March 4, 2013; http://www.state.gov/t/us/205680.htm

[10] Stubbs C and Drell S; *How to Detect a Nuclear Test on Your iPhone;* Foreign Policy; April 9, 2013; http://www.foreignpolicy.com/articles/2013/04/09/how_to_detect_a_nuclear_test_on_your_iphone

Closing Plenary

J. Tushingham, ESARDA Vice-President
National Nuclear Laboratory, Harwell Science Campus Didcot, Oxfordshire OX11 0QT United Kingdom

Ladies and Gentlemen,

Welcome to the final session of the 35th ESARDA Symposium, in which I will attempt to summarise the key points from the week's meeting. I will try not to be too long, as I am sure that you would like to commence your journey home; or enjoy a final evening in this beautiful city.

For many of us, the week commenced with a series of meetings of the Working Groups, the details of which I hope will be available to those unable to attend via ESARDA's information repository of CIRCABC.

In addition to the technical working groups, the Editorial Committee discussed at length raising the visibility of the ESARDA Bulletin. We see this increasingly as a scientific journal, whilst the improved ESARDA website provides the opportunity for working groups to report on a range of activities on a shorter timescale. The Editorial Committee encourages authors to reference appropriate papers from within the ESARDA Bulletin, to promote the Bulletin to the wider scientific community as a free resource available via the ESARDA website.

The Steering Committee encourages organisations, active in research and development associated with the aims of ESARDA, to seek membership of the Association. During the meeting, the Steering Committee was pleased to approve an application for membership from Uppsala University: the University is particularly active in the area of non-destructive analysis and has worked with the IAEA through the Swedish Support Programme. At the same time, Michel Richard was accepted as an individual member following a distinguished career in safeguards and a number of roles within ESARDA.

The evening commenced with a meeting of the International Safeguards Division of INMM, during which Mr M Whitaker presented an excellent overview of US technology development under the Next Generation Safeguards Initiative (NGSI). The NGSI has brought about a high level of collaboration between US laboratories, capitalising on field trials with domestic and international partners, to bring about near-term testing and deployment. Ultimately, the initiative will provide practical support to the IAEA Department of Safeguards, including development of the State Level Concept.

Following an enjoyable reception, the first day of the 35th Symposium commenced with two plenary sessions. Our ESARDA President, Klaas van der Meer, opened the symposium, noting ESARDA's role in enhancing peace and identifying a number of threats and opportunities. 'On the bright side': disarmament verification and a broader interest in non-proliferation, with European Actions such as the Instrument for Stability. These contrast with threats from terrorist activity and the actions of States non-compliant with their safeguards obligations. There were also neutral challenges, such as implementation of the Additional Protocol and the safeguards requirements on new facilities. An improved relationship between political and technical sciences was advocated.

We were honoured to receive an opening presentation from Mr W Bauwens, Special Envoy for Disarmament, on behalf of the Belgian Minister of Foreign Affairs. Belgium shares the vision of a world without nuclear weapons, but with effective security assurances. Disarmament and non-proliferation go hand-in-hand, with a call on India, Pakistan and Israel to join the NPT as Non-Nuclear Weapon States. However, we will not achieve universality of the NPT if we cause doubts ourselves.

On the subject of disarmament, Belgium welcomed and supported continued progress between the US and Russian Federation, whilst NATO membership and the newly-created nuclear non-proliferation and arms control committee enabled and promoted nuclear arms reduction.

Belgium strongly supports IAEA work in verification and implementation of an additional protocol, and welcomes improved efficiency and effectiveness of safeguards implementation. Mr Bauwens called on all Member States to meet the standards set by the EU, with a comprehensive safeguards agreement and additional protocol. He concluded by describing some of the safety and security challenges in the peaceful use of nuclear energy and urged Member States to uphold the NPT and not be distracted from it.

Mr N Whiting addressed the symposium on behalf of IAEA DDG Mr H Nackaerts. He described current challenges, including:

how to continue to implement safeguards effectively; and the importance and limitation, in terms of its voluntary nature, of the Additional Protocol;

how to deal with non-compliance, with the examples of DPRK, Syria and Iran; and

rising demand for services, particularly with the growth in sensitive nuclear technologies.

Meeting these challenges required application of a holistic approach to the State as a whole – the State Level Concept – with increased safeguards-relevant information combined with State-specific factors, to be used in planning, implementation and evaluation, to seek credible assurance.

Cooperation between the Agency and State Authority was considered essential. The Agency will not discriminate – all States are equal with the law – but State cooperation will input into the implementation of safeguards.

Clandestine operations at undeclared facilities are seen as the main threat. More strategic targeting of resources is essential. Implementation must be focussed on areas of higher safeguards significance, changing working practices and deploying new technologies. The Department of Safeguards has published its first long-term plan, to invest in the best possible technologies. For the future, the Agency will persist with efforts for universal acceptance of the Additional Protocol, with collaboration from States and increased focus on non-collaboration. More focused safeguards are foreseen, utilising all safeguards-relevant information, with robust measures for non-compliance.

The third presentation, by Mr Szymanski, EC ENER E, described current and mid-term developments within Euratom. He noted the challenge of additional requirements for resources, associated with new Member states, against a background of a reduction in resources of 5% over five years. An integrated management system was intended to improve efficiency, and to ensure internal compliance, whilst adopting ISO standards.

Euratom was reinforcing ties with Member States through annual bilateral meetings, meetings of all Member States and training events. Collaboration with the IAEA is intended to enable the drawing of independent conclusions whilst minimising duplication of effort. The EC and IAEA had agreed to establish a reflection group, to identify new areas for the Partnership Approach, following the production of facility-specific documents. The EC seeks swift implementation of improvements identified by the reflection group.

In his conclusions, Mr Szymanski noted that modern techniques and efficient approaches were required. Continued cooperation was essential, and ESARDA was seen as a unique vehicle for support.

The session concluded with Mr Fanghänel of the EC JRC ITU demonstrating the importance of nuclear security through the Seoul Security Summit; and the importance of safeguards and a reinforced role for the JRC through the 2013 symposium 'Benefits and limitations of nuclear fission in a low carbon economy'.

The Euratom 2014-2018 Programme includes at least three objectives related to safeguards. The JRC operates the On-Site Laboratories at La Hague and Sellafield, and also contributes through the European Commission Support Programme to IAEA Safeguards. A number of specific developments were described, including:

- liquid scintillator-based neutron measurements;
- sealing technologies;
- design information verification;
- strengthened safeguards (e.g. application of Large Geometry Secondary Ion Mass Spectrometry, LG-SIMS); and
- trade analysis and open source information.

Other activities included combating illicit trafficking through source attribution; support through the EU CBRN action plan; and education and training, through a European Nuclear Safety and Security School and events including an Additional Protocol training exercise for the IAEA.

The second plenary session welcomed the President of INMM, Mr Sorensen, who described recent developments within INMM, with a workshop on nuclear security scheduled for October 2013 and participation encouraged in PATRAM 2013. A close ESARDA-INMM relationship is seen as critical to impact effectively on the issues associated with nuclear material management. Both parties are working to strengthen this relationship, with a letter of intent signed in 2011 and appointment of Wilhelm Janssens as the first non-US chair of the Chapter relations Standing Committee. There are currently 29 chapters, with strong international growth. In preparing for the future, INMM continues to engage with the IAEA, ESARDA and WINS, primarily through regional chapters. In conclusion, INMM was viewed as operating in a dynamic environment, filled with uncertainty and opportunity. A strong collaborative relationship between ESARDA and INMM is as important as ever.

Mr Meylemans, EC ENER, provided an overview of the state of play of Euratom Safeguards: adapting to new challenges. The Commission required transparency alongside efficient and effective use of resources. To this end, in 2011, the Directorate decided to implement an Integrated Management System, with clear objectives and risk management complemented by additional ISO standards for inspection, measurement and audit.

The evolution of cooperation with the Agency was explained, with Partnership Approach documents subject to update and incorporation of new technical developments into the Joint Use Agreement.

At the conceptual level, concern was raised that near-exclusive use of acquisition path analysis excludes some factors, such as a proven commitment of the State to non-proliferation.

The reflection group formed in 2011 had identified strategic areas for enhanced cooperation, and reported on how

better to use the Euratom safeguards system. In summary, Euratom was looking for new opportunities to improve safeguards in the EU through partnerships and collaboration.

For the Agency, Mr Tsvetkov reviewed the history of co-operation with Euratom, and the improved efficiency under the new Partnership Approach of 1992. The 2011 reflection group identified underlying foundations and strategic areas of maximum impact, including more efficient management and use of common instruments, processes and procedures. Cooperation was strengthened with:

- introduction of the EC Quality Management System, with common elements to facilitate exchange of information;
- broader application of the principle 'one job, one person'; and
- exchange and utilisation of safeguards information.

Enhanced cooperation in the longer term would include joint training and channels of communication, to ensure that cooperation leads to real gains in efficiency. Enhanced cooperation brought real benefits, with the reflection group identifying specific areas for greater cooperation and where more can be done.

Mr Senzaki, JAEA, described the background to establishment of the Integrated Support Centre for Nuclear Non-Proliferation and Nuclear Security (ISCN) in 2010. Support was provided in three areas:

- capacity-building assurance;
- assistance for infrastructure development; and
- technology development and support for detection and measurement of nuclear material.

Over two years, the first of these areas included:

- 16 courses or workshops on nuclear security;
- 9 courses on safeguards and State Systems of Accountancy and Control; and
- 8 courses on international non-proliferation.

A total of 679 international participants had attended these and four additional courses.

Support was also described to the research and development of technologies, with international collaboration from the US, IAEA and JRC. Overall, a range of international collaborations were in progress, with an ISCN workshop planned in conjunction with the IAEA conference on nuclear security.

Michel Richard brought the plenary session to a close with a review and vision for the future of ESARDA. The Association's historic objectives within research and development, and education, were successfully progressed, with working groups established, amalgamated or closed in response to changing requirements. A number of questions were put to the audience, associated with extending membership and collaborating with other think tanks.

...which brought nicely to a close a plenary session with a recurring theme for everyone to take forward of partnerships, cooperation and collaboration.

Of course, the major formal component of the ESARDA symposium is the technical sessions. It is impossible to do justice to the quality of the work presented by the authors within this closing plenary, but abstracts of the presentations and posters are available and papers will be published shortly on the ESARDA website.

Over 130 papers and posters were submitted to the Organising Committee, with over 60 organisations represented by the symposium participants. There were 21 technical sessions, with a dedicated poster session and, for the first time, a panel discussion: on disarmament verification.

There were 17 main themes, covering:

- Knowledge management and training;
- Safeguards by design;
- Implementation of safeguards;
- Fuel cycle back-end;
- Information management;
- Containment and surveillance;
- Integrated measurement and monitoring systems;
- Post-Fukushima: NDA techniques for molten fuel debris;
- Spent fuel verification;
- Neutron detection;
- NDA measurements;
- DA measurements; and
- Nuclear forensics.

Additional sessions dealt with synergies, partnerships and emerging technologies where ESARDA is increasingly working with other groups, covering:

- Non-proliferation, arms control & export control;
- Safeguards, safety and security;
- Disarmament verification; and
- Novel technologies.

A poster session gave an extended opportunity to present and discuss recent developments whilst, as already referenced, a panel discussion on disarmament verification highlighted technical challenges to the scientific community.

The Symposium benefitted from the support of a range of individuals and organisations, including:

- Staff of SCK-CEN, for organisation and administration;
- Staff of the Congrescentrum Oud St Jan, for their support and use of the Congrescentrum facilities;

- Commercial sponsors, for their financial support and provision of technical displays:
  - Nucleco
  - Urenco
  - Baltic Scientific Instruments
  - Canberra
  - Ortek
  - Ametek
  - Scannix
- Authors and speakers, for the high standard of papers and posters;
- Session chairs, for ensuring the smooth running of technical sessions;
- The Symposium Organising Committee; and
- All participants, for their attention and interactions throughout the symposium.

Papers presented at the 35th ESARDA Symposium will be made available to all participants via the ESARDA website, whilst a selection of papers will also be published in the ESARDA Bulletin. The Editorial Committee seeks volunteers to assist with the peer review of these papers.

Subject to confirmation, we expect the next annual meeting to continue the sequence of closed meetings in Luxembourg. Then, for 2015, we hope to secure a venue to follow on from the successful recent symposia, encouraging participants to leave their work in their hotel rooms and to meet informally to discuss and promote continuing developments in nuclear safeguards in an atmosphere of collaboration and cooperation.

And with that, I have the honour officially to close the 35th ESARDA Symposium. On behalf of the Symposium Organising Committee, I thank you all for your participation. Have a safe journey home, and goodbye for now.